Development of Dual-Location Acid and Glutathione Cleavable Block Copolymers for Drug Delivery

Arman Moini Jazani

A Thesis
In the Department
of
Chemistry and Biochemistry

Presented in Partial Fulfillment of the Requirements
For the Degree of
Doctor of Philosophy (Chemistry) at Concordia University
Montreal, Quebec, Canada

July 2021

© Arman Moini Jazani, 2021

CONCORDIA UNIVERSITY

SCHOOL OF GRADUATE STUDIES

This is to certify that the thesis prepared

By: Arman Moini Jazani

Entitled: Development of Dual Location Acid and Glutathione Cleavable Block Copolymers for Drug Delivery

and submitted in partial fulfillment of the requirements for the degree of

Doctor Of Philosophy (Chemistry)

complies with the regulations of the University and meets the accepted standards with respect to originality and quality.

Signed by the final examining committee:

_____ Chair
Dr. David Mumby

_____ External Examiner
Dr. Ali Nazemi

_____ External to Program
Dr. Sana Jahanshahi Anbuhi

_____ Thesis Supervisor
Dr. Jung Kwon Oh

_____ Examiner
Dr. Pat Forgione

_____ Examiner
Dr. Xavier Ottenwaelder

Approved by _____
Dr. Yves Gélinas, Graduate Program Director

7/28/2021 _____
Dr. Pascale Sicotte, Dean
Faculty of Arts and Science

Abstract

Development of Dual-Location Acid and Glutathione Cleavable Block Copolymers for Drug Delivery

Arman Moini Jazani, Ph.D.
Concordia University, 2021

The efficiency of chemotherapeutic drugs has been drastically compromised by their undesired side effects. Drug delivery via amphiphilic block copolymer (ABP)-based nanoassemblies has received considerable attention as a new therapeutic method to selectively deliver chemotherapeutic drugs to tumors. Nevertheless, one of the persisting challenges for this therapeutic method is the slow degradation of the nanoassemblies and the sluggish release of encapsulated drugs in the cancer cells. To circumvent this problem, a variety of cleavable linkages have been integrated in the nanoassemblies that can be degraded in response to endogenous stimuli found in tumor environments. Particularly, tumors are known to be acidic and have higher concentrations of cytosolic glutathione (GSH) compared to normal cells.

This thesis describes the investigation of novel strategies for the synthesis of dual location acid- and dual acid/GSH-degradable ABPs for intracellular drug delivery. Various ABPs were synthesized via atom transfer radical polymerization (ATRP), reversible addition fragmentation chain transfer (RAFT) polymerization and concurrent ATRP/RAFT polymerization to study their structure-property relationships for effective intracellular drug delivery. These copolymers were designed to have acid-labile acetal or ketal groups and GSH-cleavable disulfide linkages at a junction of hydrophilic and hydrophobic blocks and in hydrophobic blocks. They self-assembled to spherical micelles with cleavable linkages at the hydrophobic core or the interface. The studies of acid or/and GSH-responsive degradation and disassembly revealed that the cleavage of acid- and GSH-cleavable linkages results in disassembly of nanoassemblies through the synergistic shedding of hydrophilic corona as well as the loss of the hydrophobic/hydrophilic balance of micelles core. The nanoassemblies were successfully loaded with Doxorubicin (a clinically used anti-cancer drug) and exhibited enhanced drug release in the presence of acidic or/and GSH stimuli. Promisingly, dual-location acid and acid/GSH degradable nanoassemblies showed biocompatibility, anti-cancer activity and cellular uptake in HeLa cancer cells.

Acknowledgment

First, I would like to express my deepest gratitude to my supervisor, Prof. John Oh for offering me the opportunity to work in his lab as well as his enormous support and patient guidance throughout my graduate studies. I would like to thank him for giving me the freedom to work on my ideas and providing me with opportunities to collaborate with other researchers, with whom I have been able to publish many collaborative works.

I am grateful to two very knowledgeable committee members, Prof. Pat Forgione and Prof. Xavier Ottenwaelder for their constructive feedback in the committee meetings. Special thanks to Prof. Louis Cuccia for editing my review paper, Prof. Ali Nazemi and Prof. Sana Jahanshahi Anbuhi for accepting to be my defense examiners.

I am grateful to Prof. Xiantgto Wang and all his lab members specially Haowen Li in the institute of medicinal plant development (IMPLAD) in Beijing China for welcoming me to their beautiful country and their research lab. I appreciate their collaboration on *in vivo* investigation of dual location acid/GSH-cleavable nanoassemblies.

I would like to extend my appreciation towards Prof. Mathew Moffit and Yuhang Huang at the university of Victoria for their collaboration on microfluidic self-assembly of dual location GSH-degradable block copolymers.

I would also like to thank my collaborators in Oh's group for their contributions to my thesis projects including Chaitra Shetty for performing cells experiments on my synthesized polymers, Newsha Arezi for her polymer characterization studies, Keaton Maruya Li for his contribution to the thermoresposive polymer project, and Kamal Bawa for her collaboration works on PLA projects. My deepest gratitude also goes to other current and former Oh members with whom I have had unforgettable memories including Dr. Arun, Dr. Xiao, Dr. Liu, Dr. Sungmin, Dr. Gandhi, Kaywan, Soyoung, Dipa, Sunghwa, Bhupinder, Peter, Xiaolei, Twinkal, Ge, Bakr, Yuqing, Kadambari, Yuanfeng and Jun-ray.

I am also grateful to the technical staff who keep our facilities running: Dr. Alexy Denisov and Dr. Constantin Yannopoulos at Concordia NMR facility, Dr. Chris Law at Centre for Microscopy and Cellular Imaging (CMCI), and Dr. David Liu in FEMR at McGill University.

This work could not be done without funding from the funding agencies, including NSERC, FRQNT, Mitacs, and Faculty of arts and science at Concordia University who generously offered numerous scholarships and financially supported my Ph.D.

Finally, I would like to thank my parents for enduring the agony of living away from me to see me thriving in life. Thanks to my brother Ali who has always tried to fill my gap at home and my wife, Mitra, who has been the loveliest thing that happened to me during my Ph.D. Not to forget that my grandpa's spirit has always inspired me in life even now that he is not among us anymore.

Dedication

This thesis is dedicated to my parents, Homa Kabirsoltani and Nematollah Moini Jazani

For their endless love, support and encouragement

Contribution of Authors

This thesis is an original work by Arman Moini Jazani under the supervision of Prof. Jung Kwon (John) Oh. The chapters 2, 3, 4, 5 and 6 are reproduced in part or in whole, with permission from the publishers, from the original articles. Arman Moini Jazani has conducted experimental design, data collection and analysis, and manuscript preparation and revision for all the chapters. The detailed contributions for each chapter are as follows:

Chapter 2: Development and disassembly of single and multiple acid-cleavable block copolymer nanoassemblies for drug delivery

The entire chapter 2 has been published as: A. M. Jazani and J. K. Oh, Polymer Chemistry, **2020**, *11*, 2934-2954.

Contributions: The work was written by Arman Moini Jazani and edited by Prof. John Oh.

Chapter 3: Imidazole-mediated dual location disassembly of acid-degradable intracellular drug delivery block copolymer nanoassemblies

The entire chapter 3 has been published as: A. M. Jazani, C. Shetty, H. Movasat, K. K. Bawa and J. K. Oh, Macromolecular Rapid Communications, **2021**, 2100262.

Contribution: Chaitra Shetty conducted cytotoxicity with Alamar blue assay and cellular uptake by fluorescence microscopy for Dox-NPs. Hourieh Movasat carried cytotoxicity for empty micelles. Kamal Bawa assisted in data collection.

Chapter 4: Dual location dual acidic pH/reduction-responsive degradable block copolymers prepared via ATRP

The entire chapter 4 has been published as: A. M. Jazani and J. K. Oh, Macromolecules, **2017**, *50, 9427-9436.*

Chapter 5: Tumor-targeting intracellular drug delivery based on dual acid/reduction-degradable nanoassemblies with ketal interface and disulfide core locations

The portion of chapter 5 has been published as: A. M. Jazani, N. Arezi, C. Shetty, S. H. Hong, H. Li, X. Wang and J. K. Oh, Polymer Chemistry, **2019**, *10, 2840-2853.*

Contribution: Newsha Arezi conducted parts of Acid/GSH-responsive degradation, Dox loading, size and morphology studies, and acid/GSH-responsive drug release. Sung Hwa Hong conducted cell culture studies including cytotoxicity using MTT assay as well as cellular uptake by fluorescence microscopy and flow cytometry. Chaitra Shetty performed additional cytotoxicity with MTT and live/dead cell assays of Dox-NPs. Haowen Li in Dr. Xiangtao Wang (China) assisted in data collection and *in vivo* experiments.

Chapter 6: Facile strategies to synthesize dual location dual acidic pH/reduction-responsive degradable block copolymers bearing acetal/disulfide block junctions and disulfide pendants

The entire chapter 6 has been published as: A. M. Jazani, N. Arezi, K. Maruya-Li, S. Jung and J. K. Oh, ACS Omega, **2018***, 3, 8980-8991.*

Contribution: Newsha Arezi conducted acid/reduction-responsive degradation studies of block copolymers by GPC and ^{1}H-NMR. Keaton Maruya-Li assisted in data collection.

Table of Contents

List of Figures……xv

List of Schemes……..xx

List of Tables……xxi

List of Abbreviations……...xxii

Chapter 1 Introduction……1

1.1 Drug delivery and cancer treatment ……...……....1

1.2 Block copolymer-based nanoassemblies ……...……....1

1.3 General strategies of drug release……...3

1.4 Stimuli-responsive degradation (SRD) platform……....3

1.5 Synthesis of SRD-based ABPs…….…..4

1.6 Objectives and scopes of my PhD thesis……...….5

Chapter 2 Development and disassembly of single and multiple acid-cleavable block copolymer nanoassemblies for drug delivery …….……..8

2.1 Introduction ……..……..... 8

2.2 Single acid-cleavable nanoassemblies……...…...10

2.2.1 General synthetic approaches ……..……....10

2.2.2 Backbone acid-cleavable nanoassemblies ……..……...……..12

2.2.3 Pendant acid-cleavable nanoassemblies ……..……....15

2.2.4 Crosslinked acid-cleavable nanoassemblies (nanogels) ……..……..…..17

2.2.5 Shell-sheddable nanoassemblies ……..…….……..18

2.2.6 Acid-degradable non-hydrophobic supramolecular nanoassemblies ……..21

2.2.7 Strategies to accelerate degradation of acid-degradable nanoassemblies ……....…..22

2.3 Dual/multiple acid-cleavable nanoassemblies ……..…24

2.3.1 Single-location acid/reduction-degradable systems ……..……..25

2.3.2 Dual-location acid/reduction-degradable systems ……..28

2.3.3 Acid/light-degradable systems ……...……..…32

2.3.4 Acid/enzyme-degradable systems..…….....34

2.4 Summary and outlook……...34

Chapter 3 Imidazole-mediated dual location disassembly of acid-degradable intracellular drug delivery block copolymer nanoassemblies…….....…38

3.1 Introduction …….....38

3.2 Experimental …….....41

3.2.1 Instrumentation……..……..41

3.2.2 Materials. …….....41

3.2.3 Synthesis of ACMA. ……...42

3.2.4 Synthesis of carbonyl imidazole methacrylate (CIMA). . ……...…42

3.2.5 Synthesis of P1 and P2 block copolymers by ATRP.. …….…...42

3.2.6 Determination of critical micellar concentration (CMC) using a NR probe.. ...……..43

3.2.7 Aqueous micellization by nanoprecipitation method. ……....43

3.2.8 Investigation of acidic pH-responsive degradation……...……...43

3.2.9 Preparation of aqueous Dox-loaded micelle dispersions (Dox-NPs)…..…….44

3.2.10 Acidic pH-responsive Dox release from aqueous Dox-NPs….…….……44

3.2.11 In vitro cytotoxicity by Alamar Blue assay....……..……..44

3.3 Results and Discussion …….45

3.3.1 Synthesis of P1 and P2 block copolymers.. ……...……..…45

3.3.2 Aqueous micellization and colloidal stability.. …….……..…47

3.3.3 Acid-catalyzed degradation of P1. ……...…48

3.3.4 Acid-catalyzed degradation and crosslinking of P2-based nanoassemblies….……...…50

3.3.5 Encapsulation of drug molecules...…….….51

3.3.6 Acid-responsive Dox release. …….....…52

3.3.7 In vitro anti-tumor activity and intracellular trafficking of Dox-NPs…….…….54

3.4 Conclusion …….....55

Chapter 4 Dual location dual acidic pH/reduction-responsive degradable block copolymers prepared via ATRP ……...……57

4.1 Introduction ……..…....57

4.2 Experimental …….....59

4.2.1 Instrumentation. ……59

4.2.2 Materials. ……59

4.2.3 Synthesis of PEG-ketal-Br initiator ……59

4.2.3.1 AC1……60

4.2.3.2 AC2……60

4.2.3.3 AC3……60

4.2.3.4 AC4……61

4.2.3.5 PEG-DSC……61

4.2.3.6 AC5……61

4.2.3.7 AC6……62

4.2.3.8 PEG-ketal-Br (AC7)……62

4.2.4 Synthesis of DLDSRD block copolymers by ATRP. ……62

4.2.5 ATRP to synthesize PEG-b-PHMssEt block copolymer (control). ……63

4.2.6. ^{1}H-NMR investigation of ketal cleavage under ATRP conditions ……63

4.2.7 Dual stimuli-responsive cleavage of DLDSRDs……63

4.2.8 Aqueous micellization using dialysis method. ……63

4.3 Results and Discussion ……64

4.3.1 Synthesis of PEG-ketal-Br ATRP initiator. ……64

4.3.2 Synthesis of PEG-ketal-PHMssEt and kinetic investigation. ……68

4.3.3 Stability of ketal linkages during ATRP. ……71

4.3.4 Aqueous micellization and preliminary investigation of dual stimuli response of DLDSRDs……73

4.4 Conclusion ……74

Chapter 5 Tumor-targeting intracellular drug delivery based on dual acid/reduction-degradable nanoassemblies with ketal interface and disulfide core locations……76

5.1 Introduction ……76

5.2 Experimental ……78

5.2.1 Instrumentation. ……78

5.2.2 Materials. ……79

5.2.3 Synthesis of a PEG-labeled macro-RAFT agent (P4). ……....79
5.2.4 Synthesis of P5 block copolymers by RAFT...……79
5.2.5 Determination of critical micellar concentration (CMC) using a NR probe……....79
5.2.6. Aqueous micellization by dialysis method.……....80
5.2.7 Investigation of dual acid/reduction-responsive degradation……..……80
5.2.8 Preparation of aqueous Dox-loaded micellar dispersions (Dox-NPs).....81
5.2.9 Dual acid/reduction-responsive Dox release from aqueous Dox-loaded micelles.....81
5.2.10 Cell culture... ……...……..81
5.2.11 Flow cytometry... ……..81
5.2.12 Live cell imaging by epifluorescence microscopy……82
5.2.13 Cell viability using MTT assay……..…82
5.2.14 Cell viability using live dead cell assay…….....82
5.3 Results and Discussion ……..……...83
5.3.1 Synthesis of P5. ……..83
5.3.2 Aqueous micellization and colloidal stability…….....85
5.3.3 Investigation of dual acidic pH/reduction-responsive degradation…….86
5.3.4 Preparation of Dox-loaded micelles……....89
5.3.5 Dual location dual acidic pH/reduction-responsive release of encapsulated Dox…….90
5.3.6 Intracellular trafficking and anti-tumor activity of Dox-NPs…….....92
5.4 Conclusion ……...95
Chapter 6 Facile strategies to synthesize dual location dual acidic pH/reduction-responsive degradable block copolymers bearing acetal/disulfide block junctions and disulfide pendants...97
6.1 Introduction ……..97
6.2 Experimental …….....99
6.2.1 Instrumentation. ……..99
6.2.2 Materials. …….....99
6.2.3 Synthesis of vinyl ether-Br (A1)…….....99
6.2.4 Synthesis of Br-AC-SS-OH (A2).. ……100
6.2.5 General procedure for ATRP...……...…...100

6.2.6 General procedure for RAFT polymerization……...101
6.2.7 Synthesis of P2...……101
6.2.8 Synthesis of P4...…….……...101
6.2.9 Synthesis of P5..……..…...102
6.2.10 Synthesis of P8. …….……..102
6.2.11 Acidic pH-responsive degradation...……..……..102
6.2.12 Reduction-responsive degradation...……..……..102
6.3 Results and Discussion ……...103
6.3.1 Synthesis of Br-AC-SS-OH initiator (A2)...……..…103
6.3.2 Strategies to synthesize diblock copolymers...……...…104
6.3.2.1 Synthesis of P1 and investigation of ATRP kinetics.. ……..…….……105
6.3.2.2 Strategy I (ATRP-RAFT)...……107
6.3.2.3 Strategy II (ATRP-ATRP)...……..…110
6.3.3 Strategy III exploring concurrent ATRP/RAFT to triblock copolymer…...…….112
6.3.4 Stimuli-responsive degradation and structural investigation of block copolymers.....114
6.4 Conclusion ……..……...116
Chapter 7 Conclusion and future works……..……..117
7.1 Conclusion ……...……...117
7.2 Future works ……...……...…….……....119
7.2.1 SRD micelles drug delivery……..……..…...119
7.2.2 Dual location acid-cleavable nanoassemblies ……..…….....120
7.2.3 Structural designs ……..122
References……....126
Appendix A……...139
Appendix B……..……....144
Appendix C……..……....158
Appendix D……..……....165
Publications……..….178

Oral poster and presentations……..…….....180
Award and honours…….……..182

List of Figures

Figure 1.1 Illustration of structural designs for the synthesis of acid degradable ABPs and their nanoassemblies.....…….....5

Figure 2.1 Chemical structures and acid-catalyzed hydrolysis of typical acid-labile linkages. Note that R1 and R2 denote polymeric chains.…….…….10

Figure 2.2 Schematic illustration of general approaches for the development of acid-degradable block copolymers exhibiting single location acid-response and their nanoassemblies based on the number and location of acid-labile linkages: a) backbone acid-cleavable, b) pendant acid-cleavable, and c) acid-shell-sheddable nanoassemblies. ……..…….…..12

Figure 2.3 Schematic illustration of the synthesis, vesicular assembly, and pH-responsive disassembly of a triblock copolymer bearing β-thiopropionate linkages on the backbones…….13

Figure 2.4 Acid-degradable PEG-b-PAU-b-PEG triblock copolymer micelles for pH-triggered intracellular Dox delivery……..…….…...15

Figure 2.5 Typical monomers bearing pendant acid-labile linkages for the synthesis of pendant multi-cleavable block copolymers by the direct polymerization approach.……...…...…....15

Figure 2.6 Schematic illustration of two major strategies to synthesize acid-cleavable core-crosslinked nanoassemblies. ……...…….…18

Figure 2.7 Synthetic route towards an acid-degradable PCL-acetal-PEG-acetal-PCL triblock shell-sheddable block copolymer via a copper-mediated azido-alkyne click reaction……..19

Figure 2.8 Synthetic route to an acid-labile PEG-based shell-sheddable block copolymer bearing a cyclic acetal linkage by RAFT polymerization……..……...…..20

Figure 2.9 Schematic illustration for (a) the synthesis of PEG-Dlink$_m$-PLA acid-shell-sheddable block copolymer and its cleavage under tumor acidity and (b) enhanced cellular uptake of its nanoassemblies……..……...…….……...….21

Figure 2.10 Schematic illustration to prepare acid-shell-sheddable nanoassemblies by supramolecular self-assembly of 6-OH orthoester-modified β-CD derivatives and an adamantane-modified PEG……..……..…...….22

Figure 2.11 Schematic illustration to ketal hydrolysis in poly-β-aminoester ketal-2 via protonation of the tertiary amine groups in the backbones. ……...……..…….24

Figure 2.12 Schematic illustration of dual stimuli/acid-degradable nanoassemblies to explore single and dual location approaches. Note that the red crosses and black spheres denote different stimuli-cleavable linkages.…….……...…….25

Figure 2.13 Schematic illustration of the synthesis, crosslinking, and dual acid/reduction-responsive disassembly of acrylamide-based linear copolymers having pendant pyridyldisulfide groups and either aldehyde or amine groups by RAFT polymerization..……..26

Figure 2.14 Synthetic route and dual acid/reduction-responsive release of polydoxorubicin prodrug……...……..…….……...…….27

Figure 2.15 (a) Synthetic scheme and (b) illustration of aqueous micellization and dual acidic pH/reduction-responsive degradation of a PLA-based triblock copolymer consisting of a hydrophilic polymethacrylate and PLA blocks with a ketal linkage in the center of PLA block and disulfides at the polymethacrylate/PLA block junctions, thus exhibiting dual response at dual location…….29

Figure 2.16 Synthesis of a polypeptide block copolymer composed of a hydrophilic PEG block connected via a DMMA linkage with a thiol-pendant poly(L-cysteine) by ROP of α-amino acid N-carboxyanhydride initiated with an amine-terminated PEG derivative and a subsequent photo-cleavage reaction to generate pendant thiol groups.……...……...30

Figure 2.17 (a) Synthesis of a new dual acid/reduction-degradable block copolymers labeled with a ketal linkage at the block junction and disulfide pendants in the hydrophobic block, (b) DLS diagram, digital (inset), and TEM (inset) images of Dox loaded nanoassemblies, and (c) % Dox release from Dox-loaded nanoassemblies incubated at pH = 5.3 and 7.4 with and without 10 mM GSH…….…….…….…….31

Figure 2.18 Synthetic route to a PEG-based polyaspartamide conjugated through hydrazone linkages with coumarin groups by a combination of ROP and post modifications..…….32

Figure 2.19 (a) Schematic representation of polymer-drug nanovesicle cellular uptake and their degradation in endocytic compartments and (b) structural engineering of dual acid/enzyme-degradable polysaccharide vesicles……..…….34

Figure 3.1 Schematic illustration of intracellular drug delivery of Dox-loaded acid-cleavable nanoassemblies with acetal linkages located at interfaces and in micelles core……..40

Figure 3.2 Synthesis of P1 and P2 by ATRP……46

Figure 3.3 ^{1}H-NMR spectra in $CDCl_3$ for P1 (a) and P2 (b)…….47

Figure 3.4 For P1, schematic illustration of acidic-responsive degradation (a), GPC diagrams before and after treatment with HCl (20 μL) in DMF, compared with that of the PEG-AC-Br macroinitiator (b), and ^{1}H-NMR spectra before and 19 hrs after treatment with DCl (10 μL) in DMSO-d6 (c)..……..….49

Figure 3.5 Acid-catalyzed degradation of P1 and P2 nanoassemblies in aqueous acetate buffer solution at pH = 5.3. GPC diagrams of P1 before and after 72 hrs incubation at 1.7 and 0.06 mg/mL, compared with PEG-AC-Br precursor (a); GPC diagrams of P2 nanoassemblies at 1.7 mg/mL before and after 72 hr incubation, compared with PEG-AC-Br precursor (b); and schematic illustration of their crosslinking during acid-catalyzed degradation (c)...……...….51

Figure 3.6 DLS diagram and TEM image of Dox-NPs of P1 (a) and P2 (b) and %Dox release at pH = 7.4 and 5.4 in 70 μg/mL (c) and 20 μg/mL (d) for Dox-NPs of P1 and P2..……54

Figure 3.7 For P1 and P2 copolymers, viability of HeLa cells incubated with empty micelles (a) and Dox-NPs (b), compared with free Dox for 48 hrs, determined by Alamar Blue Assay; time-lapse fluorescence microscopy images of HeLa cells incubated with Dox-NPs (encapsulated Dox = 2.5 μg/mL), compared with free Dox (2.5 μg/mL), for 4 hrs (c). Scale bar = 20 μm.…….55

Figure 4.1 ^{1}H-NMR spectra of AC3 (a) and AC4 (b) in CDCl3. Note that the values under each spectrum are integrals..…….65

Figure 4.2 ^{1}H-NMR spectra of PEG-DSC (a), AC5 (b), AC6 (c), and AC7 (d, PEG-ketal-Br) in CDCl3. Note that the values under each spectrum are integrals. x denotes impurities including water...67

Figure 4.3 Scheme to synthesis DLDSRD block copolymers by ARGET ATRP and ^{1}H-NMR spectrum of DLDSRD-1 in $CDCl_3$ as an example 69

Figure 4.4 GPC diagrams of DLDSRD block copolymers, compared with PEG-ketal-Br initiator.....69

Figure 4.5 First-order kinetic plot over polymerization time for ARGET ATRP of HMssEt in the presence of PEG-ketal-Br in anisole at 40 °C.....71

Figure 4.6 DP determined by ^{1}H-NMR analysis for the samples taken during ATRP over conversion. The theoretical DP values are calculated with the targeting DP = 50 over conversions.....72

Figure 4.7 Evolution of ^{1}H-NMR spectra and extent of ketal cleavage for a mixture of PEG-ketal-Br in the presence of CuBr2 in DMSO-d_6 over time at room temperature.....72

Figure 4.8 Schematic illustration of dual-stimuli acidic pH and reduction-responsive cleavage of a ketal linkage and disulfide pendants of DLDSRD (a), 1H-NMR spectrum of DLDSRD-1 treated with a trace amount of HCl (b), and GPC diagrams of DLDSRD-1 in the absence and presence of excess DTT (1.2 equivalent to pendant disulfides) and HCl (0.63 mmol) in DMF (c).....74

Figure 5.1 Illustration of tumor-targeting intracellular drug delivery of doxorubicin-loaded dual acid/reduction-degradable nanoassemblies with ketal linkages at interfaces and disulfide pendants in micellar cores self-assembled from a well-controlled ketal-linked diblock copolymer composed of hydrophilic PEG block connected through a ketal linkage with a hydrophobic methacrylate having pendant disulfide linkages (PEG-ketal-PHMssEt, P5) synthesized by RAFT polymerization.....78

Figure 5.2 Synthetic scheme by RAFT polymerization (a) and 1H-NMR spectrum in CDCl3 (b) for dual acidic pH/reduction-responsive P5-A as an example, compared with P4, its macro-RAFT agent. Conditions for RAFT polymerization: [HMssEt]o/[P4]o/[AMBN]o = 50/1/0.3 in anisole at 73 °C, HMssEt/anisole = 0.6 wt/wt.....85

Figure 5.3 Overlaid fluorescence spectra (inset) and fluorescence intensity at maximum wavelength for aqueous mixtures consisting of NR with various amounts of P5 to determine CMC.....86

Figure 5.4 Schematic illustration of dual acidic pH/reduction-responsive degradation (a) and GPC traces of P5 before and after treatment with dual stimuli in DMF, compared with that of P4 macro-RAFT agent (b).....87

Figure 5.5 Schematic illustration of dual acidic pH/reduction-responsive degradation (a), typical examples of DMS diagrams after 6 hrs (b), and evolution of z-average diameter of micelles over time (c) incubated at acidic pH = 5.4 and physiological pH = 7.4 with and without 10 mM GSH.....89

Figure 5.6 DLS diagram and digital image (inset) (a) and TEM images at high (b) and low (c) magnifications of Dox-NPs. For TEM analysis, >80 micelles were selected randomly to manually calculate the average diameter...90

Figure 5.7 %Dox release from Dox-NPs being incubated at pH = 5.4 and 7.4 with and without 10 mM GSH...92

Figure 5.8 Flow cytometric histograms of HeLa cells incubated with Dox-NPs (encapsulated Dox = 2.5 μg/mL), compared with free Dox (2.5 μg/mL), for 4 hrs...93

Figure 5.9 Time-lapse fluorescence microscopy images of HeLa cells incubated with Dox-NPs (encapsulated Dox = 2.5 μg/mL), compared with free Dox (2.5 μg/mL), for 4 hrs. Scale bar = 100 um...93

Figure 5.10 Viability of HeLa cells incubated with empty micelles (a) and Dox-NPs and free Dox at physiological pH = 7.4 (b), determined by MTT assay; fluorescence microscopy images of live cells (c) and their viability (d) incubated with and without the various amounts of Dox-NPs (as encapsulated Dox) in the presence of dual acidic pH = 6.8/GSH-OEt, compared with the control at pH = 7.4, determined by Live/Dead Cell Assay...95

Figure 6.1 ^{1}H-NMR spectra of A1 (a) and A2 (b) in $CDCl_3$...104

Figure 6.2 First-order kinetic plot over time (a) and evolution of molecular weight and molecular weight distribution over conversion (b) for ATRP of OEOMA in the presence of A2 initiator, with various initial mole ratios of [OEOMA]o/[A2]o = 20/1, 50/1, and 100/1. The straight lines in (b) are theoretically calculated Mn values at conversion. Conditions for ATRP: [A2]o/[Cu(II)Br2]o/[TPMA]o/[Sn(II)EH2]o = 1/0.05/0.15/0.4 in anisole at 40 °C, OEOMA/anisole = 0.23 wt/wt...106

Figure 6.3 ^{1}H-NMR spectra of P1 (a), P2 (b), and P3 (c) in CDCl3. Note that x denotes impurities including water and acetone...109

Figure 6.4 First-order kinetic plot over time (a) and evolution of molecular weight and molecular weight distribution over conversion (b) for RAFT polymerization of HMssEt, initiated with AMBN in the presence of P2 macro-RAFT agent. Conditions for RAFT polymerization: [HMssEt]o/[P2]o/[AMBN]o = 50/1/0.3 in anisole at 70 °C, HMssEt/anisole = 0.6 wt/wt.....109

Figure 6.5 FT-IR spectrum of P4, compared with P1. The spectrum of P1 is shifted for better visualization...111

Figure 6.6 ^{1}H-NMR spectra of P7 (a), P8 (b), and P9 (c) in $CDCl_3$...113

Figure 6.7 Schematic illustration of degradation (a) and GPC traces (b) of P3 before and after treatment with acid and DTT, compared with P1 precursor (POEOMA homopolymer) (b).....115

Figure 6.8 Schematic illustration of degradation (a) and GPC traces (b) of P9 before and after treatment with acid and DTT, compared with P7 precursor...116

Figure 7.1 Schematic illustration of a new design of dual location acid-cleavable nanoassemblies with benzylic acetal linkages located at interfaces and in disulfide bonds in micellar cores with potential ability to sequentially degrade in tumor tissues and intracellular environments.....121

Figure 7.2 Schematic illustration of a new approach to synthesize a triblock copolymer with acetal and disulfide junctions without post-polymerization modification..…….124

List of Schemes

Scheme 4.1 Synthetic route to AC3……..….....64

Scheme 4.2 Synthetic route (I) to PEG-ketal-Br initiator, starting with AC3. ……66

Scheme 6.1 Synthetic route to Br-AC-SS-OH (A2).……...103

Scheme 6.2 Strategies I and II to synthesize well-defined diblock copolymers composed of POEOMA and PHMssEt blocks……..105

Scheme 6.3 Synthetic approach III to synthesize triblock copolymer consisting of POEOMA and PHMssEt blocks..…….112

Scheme 7.1 Proposed reaction scheme to optimize the synthesis of ketal-labeled ATRP macroinitiator……...123

List of Tables

Table 4.1 Characteristics and properties of DLDSRD block copolymers synthesized by ARGET ATRP of HMssEt in the presence of PEG-ketal-Br..……...……..68

Table 5.1 Characteristics and properties of P5 block copolymers synthesized by RAFT polymerization of HMssEt in the presence of P4 macro-RAFT agent**.**…….84

Table 6.1 Characteristics and properties of P1 homopolymers synthesized by ATRP of OEOMA in the presence of A2..…….107

Table 6.2 Characteristics and properties of block copolymers..…….110

List of Abbreviations

ABP	Amphiphilic block copolymer
ACVE	Acetyl vinyl ether
ACMA	Acetyl methacrylate
ADH	Adipic dihydrazide
AMBN	2,2'-Azodi(2-methylbutyronitrile)
ARGET	Activators regenerated by electron transfer
ATRP	Atom transfer radical polymerization
Br-iBuBr	Bromoisobutyryl bromide
$CDCl_3$	Deuterated chloroform
CDI	Carbonyl diimidazole
CMC	Critical micellar concentration
CPT	Camptothecin
CPTP	4-Cyano-4-(phenylcarbonothioylthio)pentanoic acid
CRP	Controlled radical polymerization
DCl	Deuterium chloride
DCM	Dichloromethane
DLDSRD	Dual location dual stimuli responsive degradable
DLS	Dynamic light scattering
DMAP	4-(Dimethylamino)pyridine
DMEM	Dulbecco's modified Eagle's medium
DMF	Dimethylformamide
DOX	Doxorubicin

DOX-NPs	Doxorubicin loaded nanoparticles
DP	Degree of polymerization
DTT	DL-dithiothreitol
DTDEA	Dithiodiethanonic acid
DMMA	2,3-dimethylmaleimidic acid
DMSO-d_6	Deuterated dimethyl sulfoxide
DSC	Disuccinimidyl carbonate
EDC	1-Ethyl-3-(3-dimethylaminopropyl)carbodiimide
EPR	Enhanced permeability and retention effect
Et_3N	Triethylamine
EA	Ethyl acetate
FBS	Fetal bovine serum
FT-IR	Fourier-transform infrared spectroscopy
GPC	Gel permeation chromatography
GSH	Glutathione
HCl	Hydrogen chloride
HE	Hexane
HEMA	2-Hydroxyethyl methacrylate
HI	Hydrogen iodide
HMssEt	Methacrylate having a pendant disulfide linkage
IUPAC	International union of pure and applied chemistry
IV	Intravenous
LCST	Lower critical solution temperatures

MeOH	Methanol
M_n	Number average molecular weight
MWCO	Molecular weight cut off
MTT	3-(4,5-dimethylthiazol-2-yl)-2,5-diphenyl-2H-tetrazolium bromide
NaOH	Sodium hydroxide
NMR	Nuclear magnetic resonance spectroscopy
NR	Nile red
OEOMA	Oligo(ethylene glycol) monomethyl ether methacrylate
PAU	Poly(acetal-urethane)
PBS	Phosphate buffered saline
PCL	Polycaprolactone
PDOX	Polydoxorubicin
PEG	Poly(ethylene glycol)
PEI	Poly(ethylene imine)
PES	Polyethersulfone
PHMssEt	Polymethacrylate having multiple disulfide pendants
PLA	Polylactide
POEOMA	Poly(oligo ethylene oxide methacrylate)
POSS	Polyhedral oligomeric silsequioxanes
PPG	Poly(propyl glycol)
PPTS	Pyridinium p-toluenesulfonate
PEG-Br	PEG-functionalized bromide
PTFE	Polytetrafluoroethylene

RAFT	Reversible addition fragmentation chain transfer
rROP	Radical ring opening polymerization
ROP	Ring opening polymerization
RDRP	Reversible deactivation radical polymerization
$SnEH_2$	Tin(II) 2-ethylhexanoate
SRD	Stimuli responsive degradable
TDA	Terephthaldicarboxyaldehyde
TEM	Transmission electron microscopy
THF	Tetrahydrofuran
TPMA	Tris(2-pyridylmethyl)amine
UV/vis	Ultraviolet/visible

Chapter 1: Introduction

1.1 Drug delivery and cancer treatment

Cancer is a common cause of death, accounting for almost half of deaths in Canada together with heart disease in 2018.[1] Several types of cancer treatment modalities, including chemotherapy and radiotherapy, have been used in the last decades. Nevertheless, the efficiency of marketed chemotherapeutic medications has been drastically compromised by their unwanted and uncomfortable side effects including alopecia, hepatotoxicity, cardiotoxicity, myelosuppression, nephrotoxicity, and mucositis.[2] Drug delivery via nano-sized delivery vehicles has received considerable attention as a new therapeutic method to treat cancer due to their safety and ability to selectively deliver chemotherapeutic drugs to tumors. Micelles, polyplexes, crosslinked gels, dendrimers, liposomes, nanospheres, metal oxide nanoparticles, and metal-organic frameworks (MOFs) are just some of the examples of delivery vehicles that have been reported in the literature.[3, 4] This method, which works by encapsulating or conjugating pharmacologically active agents into the nanostructures, cannot only reduce the toxicity of chemotherapeutic agents by limiting off-target side effects but can also affect the pharmacokinetics of drugs by improving their absorption, distribution, metabolism, and excretion (ADME).[5] These advantages of drug delivery systems are merely granted to them by their nano-metered size which allows them to passively accumulate in the tumor tissues via enhanced permeability and retention (EPR) effect while circumventing clearance by the reticuloendothelial system.[6, 7] The journey of drug delivery nanoparticles for cancer treatment begins with intravenous (IV) injection into the bloodstream. After exiting the large gaps between the endothelial lining of the blood vessels, they access the tumor tissue where they penetrate the tumor and enter the cells via different cell-entry mechanisms.[8] In the cells, they release their therapeutic cargo and will subsequently exit the cells and are excreted from the body.

1.2 Block copolymer-based nanoassemblies

Among the various drug delivery vehicles mentioned above, nanoassemblies of amphiphilic block copolymers (ABP) are of particular interest due to their biocompatibility, colloidal stability at high dilution, and facile functionalization.[9, 10] They have seen promising success in clinical trials with one example that is approved by regulatory bodies worldwide (Genexol approved in

South Korea, 2007) and at least seven ABP nanomedicine are in clinical trials for the treatment of different types of cancer.[11-13]

The ABPs are composed of a hydrophilic block covalently connected to a hydrophobic block. Generally, AB diblock and ABA triblock copolymers, where A is hydrophilic and B is the hydrophobic block, are used for the development of nanoassemblies for anti-cancer drug delivery. BAB and ABC block copolymers as well as more complicated architectures such as graft, star, dendritic, cyclic, and branched polymers are also studied.[14-16] Poly(ethylene glycol) (PEG) is a common choice of hydrophilic blocks due to its stealth properties and low immunogenicity.[17] Zwitterionic polymers, poly(vinyl alcohol), polyoxazolines, and polysaccharides are also widely used. Polypeptides and polyesters (e.g. polylactides (PLA) and polycaprolactones (PCL)) are the most common examples of hydrophobic blocks. Polymethacrylates are also frequently used, thanks to their biocompatibility and facile synthesis.[18, 19]

In an aqueous environment, ABPs can self-assemble into micelles (nanoassemblies), where hydrophobic block is positioned inside the core, which can encapsulate the hydrophobic drugs, and hydrophilic block forms the corona. Self-assembly can reduce the interfacial energy and the interfacial area of the insoluble blocks,[20] and allow the formation of nanoassemblies of various morphologies (e.g. vesicles, spherical micelles, or cylindrical micelles), size, and dispersity.[21] The self-assembly happens above the critical micellar concentration (CMC), which is extremely important for the delivery of drug molecules as it determines the stability of nanoparticles in the blood circulation. In addition to the structure of hydrophobic and hydrophilic blocks, the degree of polymerization (DP) and molecular weight of block copolymers play a critical role in self-assembly, drug loading and release.[20, 22] Other parameters, such as crystallinity, dispersity (Đ), and preparation process also have an impact on particle size and morphology of nanoassemblies which subsequently affect the particle-cell interactions.[8, 20, 23]

1.3 General strategies of drug release

Conventionally designed block copolymer-based nanoassemblies can release drugs through three mechanisms: 1) diffusion through water-filled pores, 2) diffusion through the polymer matrix, and 3) erosion.[24] These mechanisms are passive and show the slow release of

encapsulated drug molecules. They normally exhibit a triphasic diagram, which starts from a burst drug release due to the diffusion of drugs attached to the surface of nanoparticles, followed by slower release due to the diffusion through the polymer matrix, and finally a faster release phase is induced by erosion.[25] Many factors influence drug release including polymer morphology, size, hydrophobicity, polymer-drug interaction, method of preparation, and method of drug purification.[24] Other experimental factors such as the method of release experiment, the concentration of polymer, size of dialysis bag, stirring speed and temperature are also very important.

1.4 Stimuli-responsive degradation (SRD) platform

Despite promises, one of the persistent challenges in drug delivery using polymeric nanoassemblies is the slow-release profile of drugs from ABP nanoassemblies. To enhance the drug release from ABP nanoassemblies, stimuli-responsive linkages have been incorporated into the design of the block copolymers and their nanoassemblies. Upon the cleavage of labile linkages, the SRD-exhibiting nanoassemblies display noticeable changes in their properties after exposure to endogenous or exogenous stimuli.[26] The response to the stimuli could be in terms of chemical changes such as degradation of covalent bonds or it can be in the form of physical changes such as a change in hydrophobicity.[27, 28] ABP nanoassemblies undergo degradation at the interface of hydrophilic corona or in their hydrophobic core. The degradation of the cleavable chemical linkages eventually results in a change in hydrophilic-hydrophobic balance, swelling, aggregation, dissociation, disintegration, or disassembly of colloidal particles.[27, 29] Stimuli that can induce the degradation of covalent chemical linkages are generally sorted into 1) endogenous (internal) stimuli, which are present in the tumor microenvironments such as glutathione (GSH), matrix metalloproteinase, esterase, acidic pH and reactive oxygen species (ROS),[30-32] and 2) exogenous (external) stimuli, which are applied from outside of the body such as light, temperature, ultrasound, magnetic field and electric field.[33, 34]

GSH and acidic pH are among the most studied examples.[31, 35-37] The higher cytosolic GSH concentration of tumor tissues, which is at least 4 times higher than normal tissues, and higher concentration of intracellular GSH, which is 100-1000 times greater than human plasma and blood, is utilized extensively to trigger destabilization of nanocarriers and selectively release drugs.[38, 39] A great deal of work has been done to study disulfide labeled polymeric

nanoassemblies as the main linkage that endows nanoparticles with GSH responsive property. The degradation of disulfide bonds in the presence of GSH leads to the formation of two thiols groups. Such events can be hampered to disassemble nanoassemblies by shedding the corona and/or causing a drastic change in the hydrophobic balance of nanoassemblies cores. The plethora of GSH-cleavable polymeric nanoparticles have been reviewed extensively.[36, 37, 40] Particularly, Dr. Oh's group has significantly contributed to this area and has reported numerous examples of nanoassemblies with disulfide bonds at the junction,[41, 42] pendant chain,[43, 44] and backbone[45] of ABPs. Advanced GSH responsive nanoassemblies labeled with disulfide bonds in dual locations were also explored.[46, 47] Acidic pH is a promising endogenous stimulus because of the acidic property of tumor tissues (pH = 6.7-7.0) and endosomes and lysosomes (pH= 4.0-6.0).[31, 48] The details on acid cleavable polymeric nanoassemblies are discussed thoroughly in chapter 2.

1.5 Synthesis of SRD-based ABPs

Generally, the stimuli responsive degradable ABPs are synthesized using a combination of synthetic polymerization methods and require meticulous incorporation of degradable linkages into the initiators or monomers. Figure 1 shows some common structural designs of SRD block copolymers and their nanoassemblies. The linkages can be positioned in the 1) backbone of hydrophobic blocks, 2) pendant chains, 3) between the hydrophobic blocks, and 4) at the junction of hydrophilic and hydrophobic blocks. Ultimately, the nanoassemblies from these ABPs will have degradable linkages in the core or at the interface of nanoassemblies. The backbone degradable ABPs are commonly synthesized by step-growth polymerization.[49-51] Ring opening polymerization (ROP) using a degradable initiator is used to synthesize ABPs with the degradable linkage between two hydrophobic blocks or at the junction of hydrophilic-hydrophobic block.[52, 53] The synthesis of SRD ABPs has witnessed significant progress during the past 25 years due to the advances of controlled radical polymerization (CRP), which is also named "reversible-deactivation radical polymerization (RDRP)" by the international union of pure and applied chemistry (IUPAC). The most prominent examples are atom transfer radical polymerization (ATRP),[54] reversible addition fragmentation (RAFT) polymerization,[55, 56] and nitroxide mediated polymerization (NMP).[57] Pendant multi-cleavable micelles are predominantly synthesized by RDRP.[43, 58] In addition, a plethora of click type reactions have been investigated

for synthesizing SRD block polymers, some of which include alkyne-azide, thiol-ene, thiol-eyne, oxime, and so on.[59, 60]

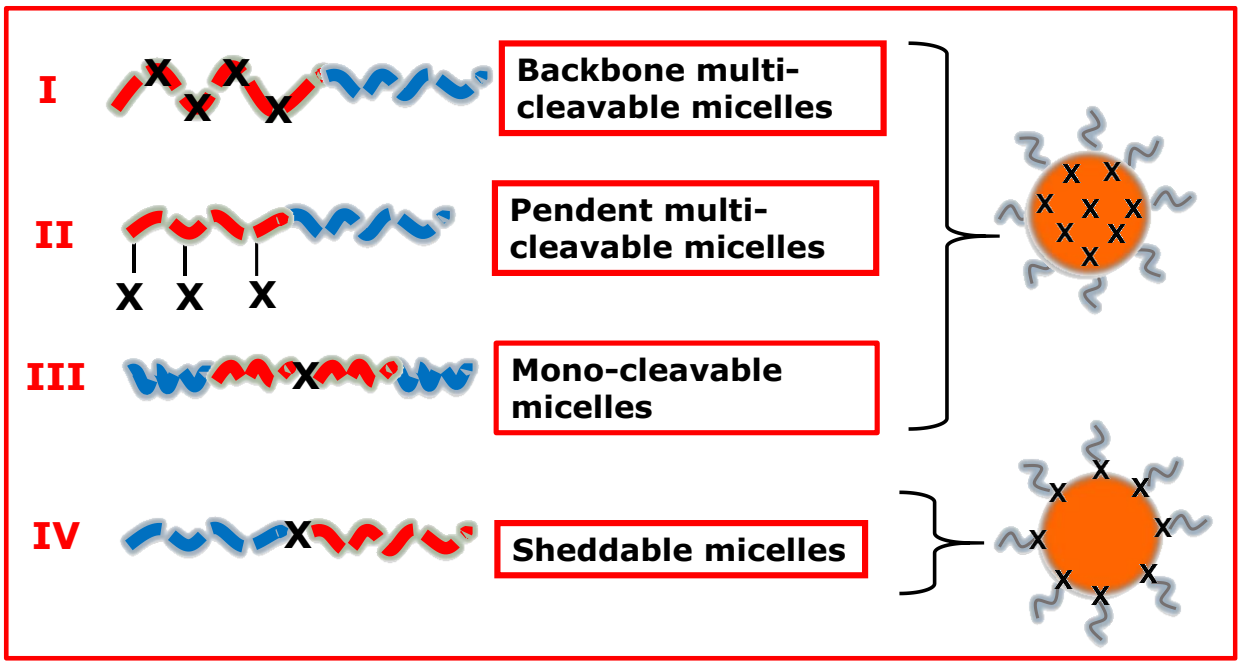

Figure 1.1 Illustration of structural designs for the synthesis of acid degradable ABPs and their nanoassemblies.

1.6 Objectives and scopes of my PhD thesis

My PhD thesis focuses on the exploration of dual location acid- and dual acid/GSH-responsive degradation platform for advanced intracellular drug delivery and enhanced/controlled release of encapsulated chemotherapeutics. We have developed various strategies utilizing RDRP and facile coupling reactions that allow for the synthesis of novel ABPs. These copolymers were designed to have acid-labile acetal or ketal groups and GSH-cleavable disulfide linkages at a junction of hydrophilic and hydrophobic blocks and in a hydrophobic block. The synthesized copolymers were characterized for aqueous micellization driven by self-assembly, acidic pH-responsive degradation and disassembly, drug loading and release, and biological activities toward cancer cells. Furthermore, we studied the structure-property relationship in the design and synthesis of effective nanoassemblies for on-demand and synergistic drug release.

In chapter 2, recent advances in the synthesis and disassembly of acid-cleavable block copolymers for controlled drug delivery are comprehensively reviewed. Various strategies to integrate acid-labile linkages in the block copolymers at different locations, as in micelle cores and core/corona interfaces are particularly focused. Additionally, elegant strategies that allow for the synthesis of dual acid/reduction, acid/light, acid/enzyme-degradable block copolymer systems with cleavable linkages in single or dual locations are discussed.

In chapter 3, a facile strategy is reported that enables the synthesis of an acid-cleavable ABP that is labeled with acetaldehyde acetal groups in the junction and pendant chains (PEG-Acetal-PACMA). The block copolymer forms nanoassemblies with acid-cleavable linkages in hydrophobic cores and at core/corona interfaces. Moreover, the effect of incorporation of acid-ionizable imidazole pendants in hydrophobic cores on the encapsulation of doxorubicin (Dox), acid-catalyzed hydrolysis of acetal linkages, drug release, *in vitro* cells toxicity, and cellular uptake are investigated.

In chapter 4, a new strategy utilizing ATRP is used to synthesize a dual location acidic pH/GSH-responsive degradable block copolymer (PEG-Ketal-PHMssEt) labeled with an acidic pH-labile ketal linkage at the block junction and pendant reductively cleavable disulfide groups in the hydrophobic block at dual locations. Here, we focus on studying different routes to synthetize a ketal labelled PEG macroinitiator and investigating ketal stability in ATRP conditions.

In chapter 5, a robust approach, which involves the synthesis of a new RAFT macro chain transfer agent followed by RAFT polymerization, is reported to synthesize the PEG-Ketal-PHMssEt block copolymer introduced in chapter 4. This chapter focuses on the investigation of self-assembly, dual acidic pH/GSH degradation, drug release from the nanoassemblies as well as the studies of their anti-cancer cell activity and cellular internalization.

In chapter 6, we report a new dual acidic pH/GSH-responsive degradable ABPs featured with dual acidic pH-labile acetaldehyde acetal linkage and reductively cleavable disulfide bond at the hydrophilic/hydrophobic block junction as well as pendant disulfide bonds in the hydrophobic block. Three strategies were explored to synthesize these block copolymers by utilizing the combination of ATRP and RAFT polymerization in a sequential or concurrent mechanism, along

with facile coupling reactions. Furthermore, the structural investigations by polymer degradation are conducted to study the polymer composition as diblock or triblock copolymer.

In chapter 7, conclusions from my four research projects are summarized and future research directions are proposed.

Chapter 2: Development and disassembly of single and multiple acid-cleavable block copolymer nanoassemblies for drug delivery

2.1 Introduction

Cancer nanomedicines centered on macromolecular approaches have been extensively explored to diagnose and treat cancer based on improved delivery of anticancer agents to tumors (*i.e.* improved biodistribution).[61, 62] The design and development of ABP exhibiting SRD through chemical transformations, in response to stimuli, is a promising platform to construct smart nanoassemblies (or nanocarriers) for tumor-targeting drug delivery.[26, 27, 63-65] SRD driven by chemical transformations involves the cleavage of labile covalent linkages incorporated in the block copolymers, causing the disintegration or destabilization of nanoassemblies.[28, 66-68] Compared with conventional non-degradable systems, SRD-exhibiting nanoassemblies offer the controlled/enhanced release profile of encapsulated therapeutics. Biodegradation is achieved *via* acidic pH as well as reductive, oxidative, and enzymatic reactions, which are characteristic stimuli inducing chemical transformations found in cellular environments.[32, 36, 40, 69-73] Among these, acidic pH is the most promising endogenous stimulus since the tumor microenvironment is known to be slightly acidic (pH = 6.5-6.9), compared to normal tissues (pH = 7.4).[74] Furthermore, endosomes and lysosomes in cells are more acidic (pH = 4.5-6.5). The acidity of tumor tissues is caused by increased lactic acid production due to the elevated glycolytic rate of tumor cells even under aerobic condition, commonly referred to as the Warburg effect. In addition, tumor cells are characterized by defective vasculature and vast hypoxic regions, which primarily rely on anaerobic glycolysis for energy generation, thus producing lactic acid as the main product of glucose breakdown. There is compelling evidence that acidity of tumor cells plays a critical role in tumor metastasis and drug resistance.[75, 76] In biological systems, drug-loaded acid-degradable nanoassemblies (nanocarriers) can be administered to the body through IV injection. While circulated in the blood, they target tumor tissues having typical irregular endothelial cells of vasculatures due to the Enhanced Permeability and Retention (EPR) effect. Once being extravasated into tumor tissues, drug-loaded acid-degradable nanoassemblies can subsequently undergo cellular uptake through various entry mechanisms.[77-84] Once inside tumor tissues and cells whose pH is acidic, acid-degradable nanoassemblies can dissociate to allow for the release of encapsulated therapeutics in a controlled/enhanced fashion.

Of two important classes of acidic pH-responsive block copolymers, acid-ionizable systems incorporate ionizable groups into the design of block copolymers. Widely-used ionizable groups include tertiary amines with pKa values lower than physiological pH, that tend to be neutral or even hydrophobic at pH = 7.4. Under acidic conditions, these amine groups are protonated and convert to their corresponding quaternary ammonium salts, thus becoming hydrophilic or water-soluble. Such physical transformations based on polarity change cause the disintegration or degradation of the nanoassemblies. This topic is covered in previous review articles.[35, 85] In addition to acid-ionizable systems, acid-cleavable systems were designed with ketal, acetal, orthoester, imine, oxime, hydrazone, 2,3-dialkylmaleamidic amide (DMMA), boronic ester, and β-thiopropionate groups as typical acid-labile linkages. As illustrated in Figure 1, these linkages can be cleaved under acidic pH conditions. Each linkage possesses distinct reactivities (or sensitivities) towards acid-catalyzed hydrolysis in an aqueous environment, thus presenting tunable cleavage rates. Evidently, the cleavage rate is faster at lower pH values due to a higher concentration of hydronium ions.[86] For the acetal/ketal family, the hydrolysis rate can be mainly determined by the stability of the carbocation intermediates that are formed through the elimination of alcohol species from the carboxonium after protonation of an oxygen atom of the acetal/ketal moieties. The carbocation stability is greatly affected by structural factors such as steric, resonance, and induction effects of attached substituents. Thus, their cleavage rate (hydrolysis rate) varies with the substituents attached on the central carbon atom of the acetal/ketal moieties. Detailed studies on the kinetics of acetal hydrolysis in the form of small molecules[87-89] and polymers[90-93] have been reported. Further to the acetal/ketal family, the hydrolysis rate for imines, including oximes and hydrazones, has also been studied.[94, 95] Exploring these features of acid-cleavable chemistries, numerous strategies have been developed to synthesize acid-degradable block copolymer nanoassemblies for tumor-targeting drug delivery.[31, 96]

This review article describes elegant strategies that allow for the synthesis of acid-degradable block copolymers reported in recent years. The strategies are summarized based on the nature, number, and location of acid-labile linkages positioned within the backbone, in pendant chains, at hydrophilic/hydrophobic block junctions in block copolymers or as crosslinks. Consequently, they self-assemble into nano-sized particles labeled with acid-cleavable linkages in a single location: (*i*) in the hydrophobic core or (*ii*) at core/corona interface. Furthermore, this review

summarizes dual acid/stimulus-degradable systems, responsive to other stimuli such as reduction, light or enzymes along with acid-cleavable linkages in single and dual locations.

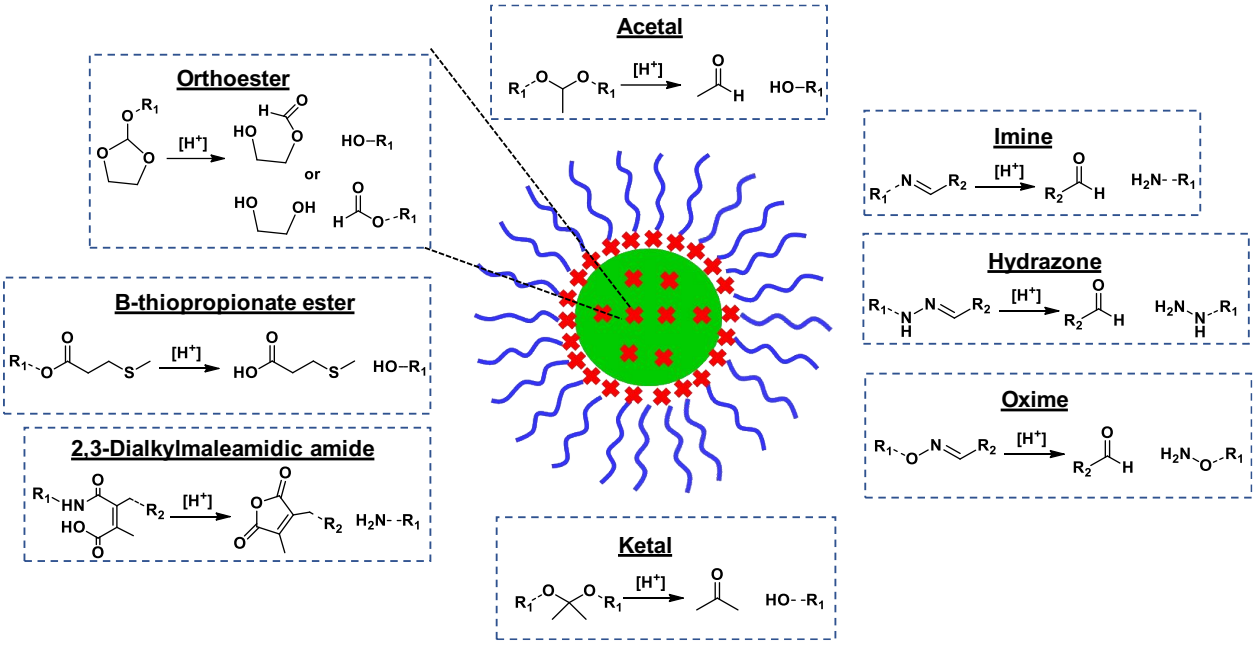

Figure 2.1 Chemical structures and acid-catalyzed hydrolysis of typical acid-labile linkages. Note that R_1 and R_2 denote polymeric chains.

2.2 Single acid-cleavable nanoassemblies

2.2.1 General synthetic approaches

Four general approaches to synthesize single location acid-responsive block copolymers have been explored for the development of acid-degradable block copolymer nanoassemblies. Based on the number and location of acid-labile linkages in acid-degradable block copolymers, these approaches include backbone acid-cleavable, pendant acid-cleavable, acid-cleavable crosslinked, and acid-shell-sheddable nanoassemblies. The acid-cleavable linkages are located in hydrophobic cores for backbone, pendant, and crosslinked nanoassemblies, while at core/corona interfaces for shell-sheddable nanoassemblies. This section describes general synthetic strategies to integrate acid-cleavable linkages (shown in Figure 2.1) in the synthesis of block copolymers, as schematically illustrated in Figure 2.2. Furthermore, their advantages and drawbacks with respect to tumor-targeting drug delivery are briefly discussed.

Backbone acid-cleavable assemblies shown in Figure 2.2a are formed by aqueous micellization though self-assembly of block copolymers labeled with acid-labile linkages on

hydrophobic backbones. Step-growth polymerization through polycondensation and polyaddition is a general means to synthesize backbone multi-cleavable block copolymers. In this approach, nucleophilic monomers such as diamines, dialcohols and dithiols are reacted with electrophilic monomers, such as aldehydes, ketones and vinylethers to link polymeric units *via* acid-degradable linkages. Promisingly, drug molecules bearing difunctional groups can also be used as monomers for step-growth polymerization for covalent incorporation into copolymer backbones, along with the acid cleavable linkages.[97] In acidic environments, they are fully degraded to smaller fragments upon cleavage of the backbone acid-labile linkages through a main chain degradation mechanism. The resulting small fragments can subsequently be more readily excreted from tissues, thus imparting lower systemic toxicity. Pendant acid-degradable nanoassemblies (Figure 2.2b) are fabricated from block copolymers having pendant acid-labile linkages in the hydrophobic blocks (*i.e.* acid-degradable cores). They are generally degraded through a change in hydrophobic/hydrophilic balance of the core upon cleavage of the pendant acid-labile linkages in the block copolymers. Despite these features, this approach suffers from several drawbacks that hamper drug delivery. One drawback involves slow and incomplete cleavage of pendant acid-degradable linkages such as acetaldehyde acetal groups at biological pH, which leads to slow drug release. Another drawback is associated with the degraded products, most of which are not fully water-soluble. As a consequence, they tend to form micron-sized aggregates that could be toxic due to bioaccumulation. Acid-shell-sheddable nanoassemblies (Figure 2.2c) dissociate by degradation of acid-cleavable linkages located at the interface of the hydrophilic corona with the hydrophobic core. When exposed to acidic pH, the corona is shed from the core, causing a destabilization of the nanoassembly. Detachment of the hydrophilic shell could lead to the aggregation of hydrophobic cores which may impede drug release. However, this approach is a promising route to defuse the conflict of favorable prolonged blood circulation and poor cellular uptake of PEG, commonly referred to as the "PEG dilemma". This can be addressed by choosing suitable acid-labile junction that can be cleaved in tumor tissues (pH ≈ 6.5-6.9).[2, 98] Crosslinked nanoassemblies are detailed in Section 2.4.

In addition to acid-degradable ABPs, the synthesis of thermoresponsive copolymers bearing acid-labile linkages has been explored. Their thermoresponsive properties at lower critical solution temperatures (LCST) were adjusted with changes in molecular weight[99] and hydrophobic/hydrophilic balance,[100, 101] upon acid-responsive cleavage. In addition to acid-

degradable nanoassemblies exhibiting single response, a combination of acid sensitivity with an additional stimulus result in degradable nanoassemblies exhibiting dual response.[29, 102-106]

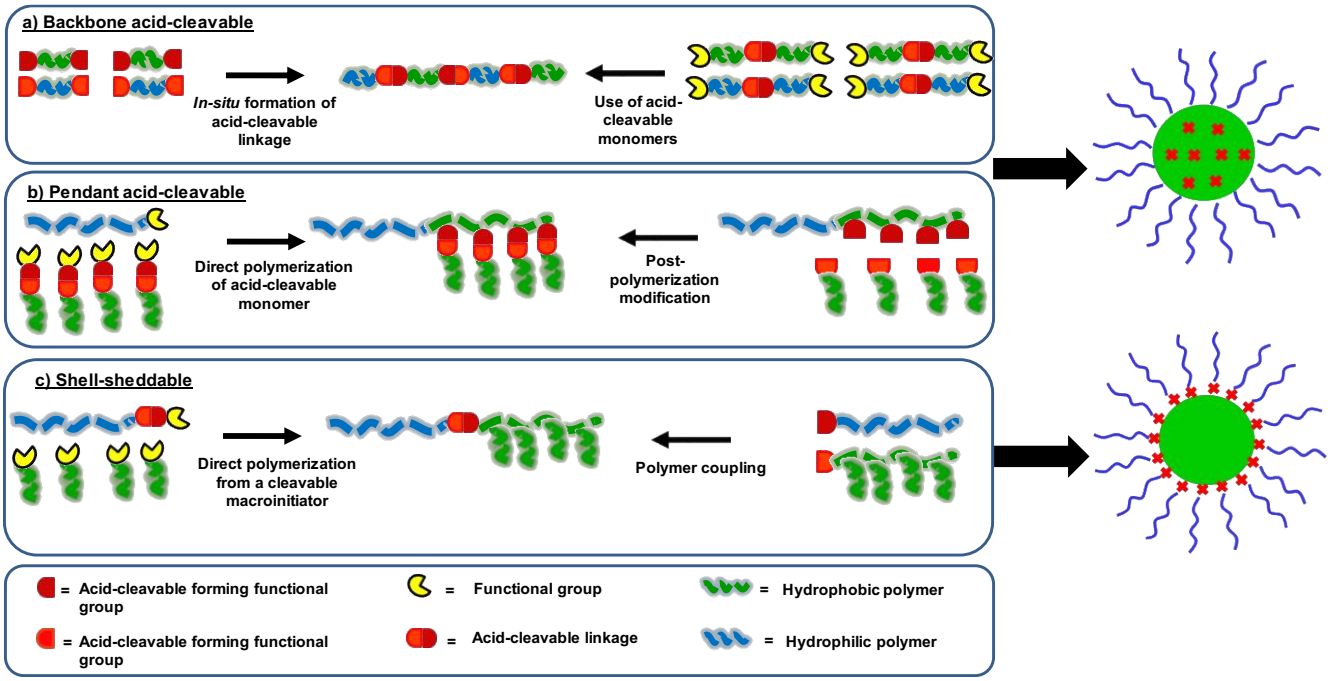

Figure 2.2 Schematic illustration of general approaches for the development of acid-degradable block copolymers exhibiting single location acid-response and their nanoassemblies based on the number and location of acid-labile linkages: a) backbone acid-cleavable, b) pendant acid-cleavable, and c) acid-shell-sheddable nanoassemblies.

2.2.2 Backbone acid-cleavable nanoassemblies

Polycondensation through *in situ* formation of acid-labile linkages as building blocks is used for the synthesis of acid-degradable copolymers with backbone acid-cleavable linkages. Polyacetals were synthesized by catalytic polycondensation of a divinyl ether and a diol. The catalyst is typically pyridinium p-toluenesulfonate (PPTS).[107] Incorporation of functional diols into the polyacetal synthesis found various applications, including HIF-1 inhibitor diols,[97] alkyne- or activated ester-labeled diols[108] for drug delivery and Fmoc-serinol for protein therapy.[109]

A similar strategy was utilized for the catalytic synthesis of polyorthoesters using air/moisture-stable vinyl acetal precursors[110] and a triblock copolymer comprised of PEG and oxime-tethered polycaprolactone (PCL) blocks.[111] A copolymer labeled with β-thiopropionate linkages on the backbones was synthesized by polycondensation of a divinyl ether with a dithiol. As seen in Figure 2.3, the following reaction of terminal thiol groups in the copolymer with a

PEG bearing a terminal vinyl ether allows for the synthesis of an ABA-type triblock copolymer bearing backbone β-thiopropionate linkages in the central B block. The formed triblock copolymer was amphiphilic and thus self-assembled to form nanoassemblies which degrade at pH = 5.5.[112]

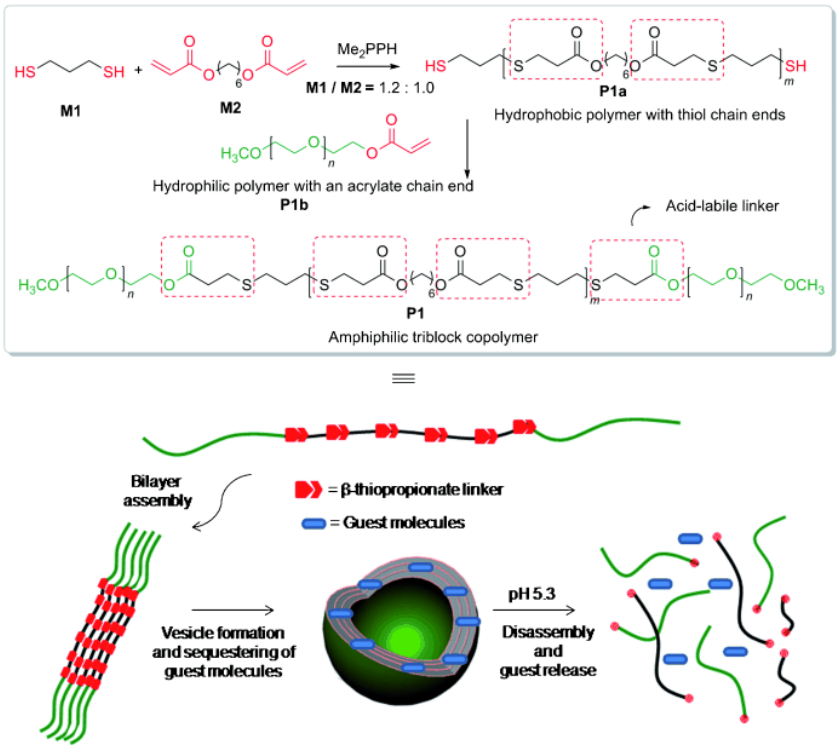

Figure 2.3 Schematic illustration of the synthesis, vesicular assembly, and pH-responsive disassembly of a triblock copolymer bearing β-thiopropionate linkages on the backbones. Copyright 2013 Wiley.

Step-growth polymerization of reactive monomers bearing acid-labile linkages has also been extensively explored for the synthesis of a variety of acidic pH-degradable step-growth copolymers. Click-type reactions were preferably employed. Aza-Michael addition of various diamines with divinyl precursors (bearing ketal or acetal linkages) enabled the synthesis of polyamidoamines bearing backbone acetal or ketal linkages. A diacrylamide, a diacrylate, or a dimaleimide reacted with various diamines such as dipiperidine for linear copolymers,[91] poly(ethylene imine) (PEI) for branched copolymers,[35, 113] and octaamine polyhedral oligomeric silsequioxanes (POSS) for dendritic copolymers.[114] Atom transfer radial polyaddition of a ketal dibromine to a divinyl precursor yielded a PEG-grafted polyester bearing ketal linkages on the backbone.[99] In addition to click reactions, conventional step-growth polymerization methods have also been utilized to synthesize polyurethane, polyether, and polyester bearing backbone

acetal, ketal, and orthoester linkages. Several reports describe the synthesis of acid-cleavable polyurethanes through carbamate bond formation by reaction of diols labeled with acetal or orthoacetal linkages with diisocyanates.[90, 115-117] Other reports also show the synthesis of acid-degradable dendritic polyethers by polyaddition of α-epoxy-ω-hydroxyl-functionalized AB_2-type monomers bearing ketal[118] and acetal[119] groups and a ketal-labeled polyester synthesized by reaction of a ketal-labeled diol with a diacylchloride.[120]

Most of the formed polyacetals and polyketals were designed to be either hydrophilic or hydrophobic (not amphiphilic), thus forming submicron-sized nanoparticles in aqueous solution *via* nanoprecipitation. Figure 2.4 illustrates an acidic pH-degradable PEG-based poly(acetal urethane) (PAU) triblock copolymer (PEG-b-PAU-b-PEG) synthesized by polyaddition to allyl-terminated PAU, followed by a thiol-ene click reaction with PEG-SH. The copolymer was designed to be amphiphilic and thus formed self-assembled micelles in aqueous solution. They displayed fast swelling and disruption under acidic pH = 4-5, while being stable at pH = 7.4. The micelles exhibited controlled and pH-dependent release of encapsulated Dox.[121]

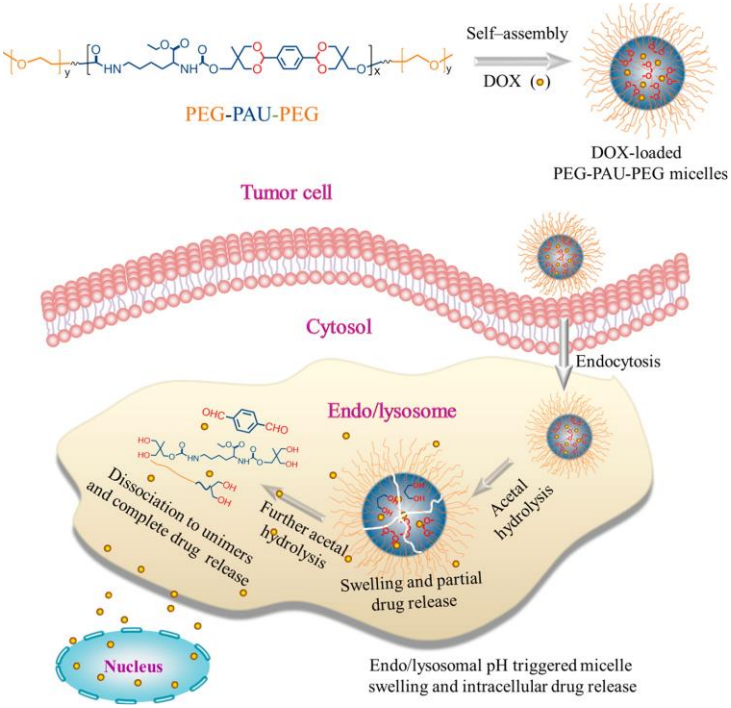

Figure 2.4 Acid-degradable PEG-b-PAU-b-PEG triblock copolymer micelles for pH-triggered intracellular Dox delivery. Copyright 2015 American Chemical Society.

2.2.3 Pendant acid-cleavable nanoassemblies

Two strategies have been explored to synthesize pendant multi-cleavable block copolymers: (*i*) direct polymerization of acid-degradable monomers and (*ii*) post-modification of functional precursor polymer.

Direct polymerization utilizes controlled polymerization techniques to synthesize acid-degradable random and mostly block copolymers. As shown in Figure 2.5, this strategy requires the design of novel functional monomers bearing pendant acid-labile groups. Controlled radical polymerization (CRP) techniques have been widely explored. ATRP has been examined using PEG-based macro-initiators with various acid-labile monomers bearing cyclic orthoesters (M1,[122, 123] M2,[124] and M3[125]), acetals (M4[126]), and ketals (M5[127]) to synthesize a variety of well-controlled PEG-based block copolymers. In addition to ATRP, RAFT polymerization was examined with a RAFT mediator for copolymerization with (meth)acrylate and (meth)acrylamide bearing pendant cyclic acetals (M6[128]), β-thiopropionates (M7[129]), and tetrahydropyran (M8[130]) to synthesize well-controlled acid-degradable random or block copolymers. ROP has also been explored. PEG was used as a macroinitiator with a cyclic acetal carbonate monomer (M9[131]) to synthesize PEG-based polycarbonate block copolymers and a typical acetal-bearing epoxide monomer (M10 and M11)[132, 133] to synthesize PEG-based polyethers. These synthesized amphiphilic copolymers formed self-assembled micelles with acid-degradable hydrophobic cores, surrounded with hydrophilic PEG coronas. These copolymers were degraded under acidic pH conditions through a change in the hydrophobic/hydrophilic balance of core blocks.

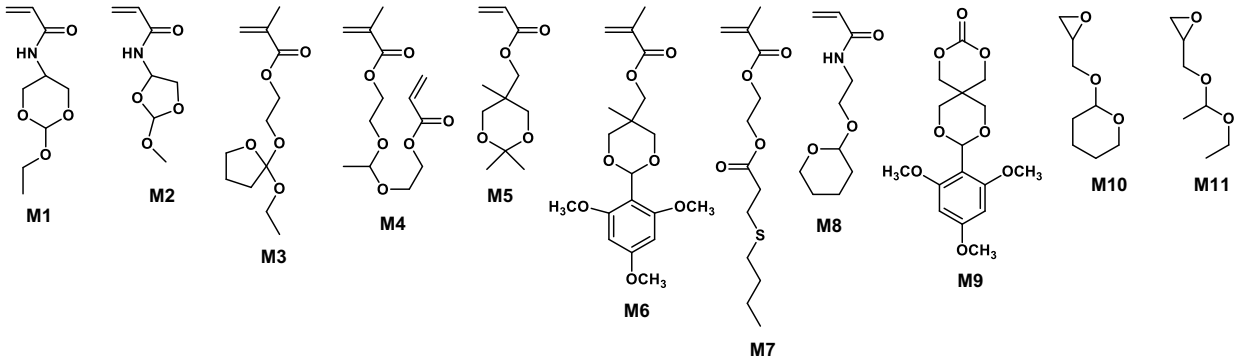

Figure 2.5 Typical monomers bearing pendant acid-labile linkages for the synthesis of pendant multi-cleavable block copolymers by the direct polymerization approach.

A post modification strategy has been explored to synthesize acid-degradable block copolymers. Particular examples explore a facile coupling reaction through *in situ* formation of hydrazone,[134-137] imine,[138-140] and acetal[141] linkages to form drug-conjugated block copolymers, thus prodrug nanoassemblies. Dox contains carbonyl and amino groups that can react with pendant hydrazine or carbonyl in block copolymers and form Dox-polymer prodrugs *via* imine or hydrazone linkage. In other examples, amidation of Dox with the DMMA side chains of a poly(β-L-malic acid)[142] and a thiol-ene reaction to conjugate β-lapachone (anticancer drug) functionalized with an imine group,[143] were reported. In addition to the conjugation of anticancer drugs, other reactions were employed to modify hydrophilic copolymers with pendant acid-cleavable species. Typical examples include dextran protected with a dimethyl ketal group,[144, 145] poly(vinyl alcohol) conjugated with vinyl ether acrylate through an acetal linkage,[146] and PEG-b-PCL conjugated with DMMA.[147]

2.2.4 Crosslinked acid-cleavable nanoassemblies (nanogels)

A challenge for self-assembled micelles formed by physical aggregation of polymeric chains is the undesired dissociation to unimers upon dilution in blood (4L). This occurs when the concentration of micelles in blood is below the CMC of the block copolymer. To circumvent this challenge, a promising solution is to introduce acid-labile crosslinks to the corresponding ″acid-cleavable crosslinked nanogels″. This approach offers not only enhanced colloidal stability during circulation in the blood, but also acid-responsive cleavage of labile crosslinks for enhanced/controlled release of encapsulated drugs.

This approach has mainly been explored to synthesize core-crosslinked nanoassemblies. Figure 2.6 schematically illustrates two major strategies. Strategy I involves *in situ* formation of acid-labile crosslinks. One report described the use of terephthaldicarboxyaldehyde (TDA, a difunctional aldehyde) as a crosslinker for a block copolymer bearing pendant hydrazide groups (NH_2-NH-C(O)-) to yield core-crosslinked nanogels through reversible acylhydrazone linkages. Excess hydrazine groups in the copolymer were subsequently used for bioconjugation with biotin and fluorescein isothiocyanate.[148] Other reports utilized TDA with block copolymers having pendant amine groups for the fabrication of acid-degradable nanogels through the formation of benzylimine linkages.[149] As an extension to small molecule crosslinkers, the synthesis of a polymeric pendant aldehyde and a polymeric pendant amine by RAFT polymerization have also

been explored. The co-micellization of the mixed block copolymers yielded acid-cleavable crosslinked nanogels *via* the formation of reversible benzimine linkages.[28, 150-152] Strategy II involves conjugation with crosslinkers bearing an acid-labile linkage. An example includes linking a diazide, bearing an acetal linkage for crosslinking, with a polyphosphoester, bearing pendant alkyne groups, through a copper-mediated azido-alkyne reaction.[153] Also, a diamine bearing a ketal linkage was used to prepare vinyl polymers bearing pendant pentafluorophenyl groups through a facile coupling reaction.[89, 154, 155]

Similar strategies have been further explored to synthesize shell-crosslinked nanoassemblies. Examples include the use of TDA with a PEG-based vinyl copolymer bearing pendant amino groups through *in situ* formation of benzimine linkages (Strategy I)[156] and the use of a ketal-bearing diamine with a PEG-based poly(amino acid)s bearing pendant carboxylic acids *via* the formation of amide linkages (Strategy II).[157]

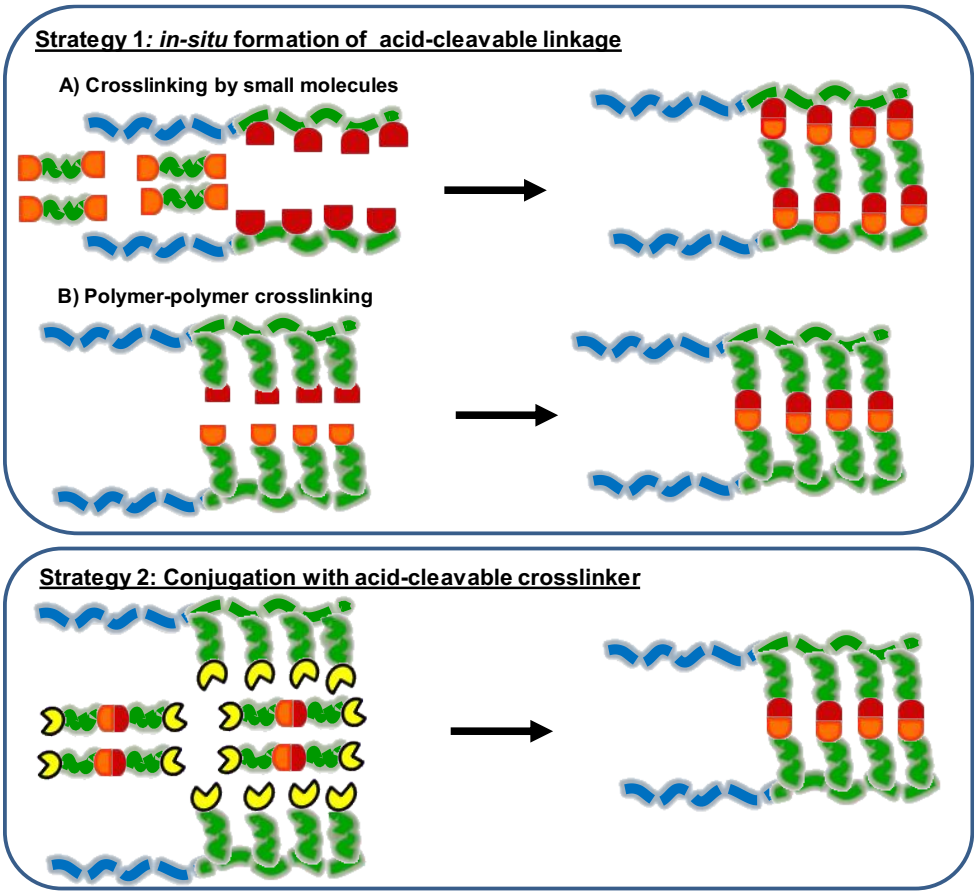

Figure 2.6 Schematic illustration of two major strategies to synthesize acid-cleavable core-crosslinked nanoassemblies.

2.2.5 Shell-sheddable nanoassemblies

Acid-degradable shell-sheddable block copolymers consist of acidic pH-labile groups at the junction of the hydrophilic and hydrophobic blocks. Linear, star-shaped, and grafted di- and tri-block copolymer chain architectures are possible. Two approaches have been explored: (*i*) conjugation and (*ii*) direct polymerization.

The conjugation approach utilizes mainly click-type reactions of two or more reactive homopolymers bearing acid-labile linkages, typically acetal, to synthesize various shell-sheddable block copolymers or prodrugs. Azide-alkyne click reaction using an azido-terminated PEG labeled with an acetal linkage (PEG-acetal-N_3) was the focus of some studies. PEG-acetal-N_3 was synthesized in two steps: (*i*) reaction of PEG with 2-chloroethyl vinyl ether and (*ii*) azidation of the formed PEG-acetal-Cl with sodium azide.[158] As illustrated in Figure 2.7, the formed PEG-acetal-N_3 reacted with an alkyne-terminated PCL, synthesized by ROP, to yield a liner shell-sheddable triblock copolymer, PCL-acetal-PEG-acetal-PCL.[159] This block copolymer self-assembled to form flower-like nanoassemblies with acetal linkages at the PCL core/PEG corona. When exposed to acidic solution, the acetal linkages were cleaved, thus shedding the PEG coronas from the PCL core, leading to enhanced release of encapsulated Dox. Similarly, a PEG-acetal-N_3 precursor was used to synthesize acid-degradable shell-sheddable copolymers with various architectures, including a three-arm star PEG-acetal-PCL diblock copolymer[160] and a Dox prodrug.[161] Other reports also explored the azido-alkyne click reaction to synthesize a PEG-grafted polyester[162, 163] and PCL-based vinyl-type copolymers.[164, 165] In addition to click chemistry, a facile coupling reaction through *in situ* formation of pH-cleavable linkages was explored to synthesize shell-sheddable block copolymers and prodrugs. Typical examples include: imine[166-169], tetrahydropyran[170] and DMMA.[171] However, the coupling of two reactive homopolymers has imposed a challenge in the purification of the target block copolymers from excess homopolymers and low coupling efficiency due to increased steric hindrance.

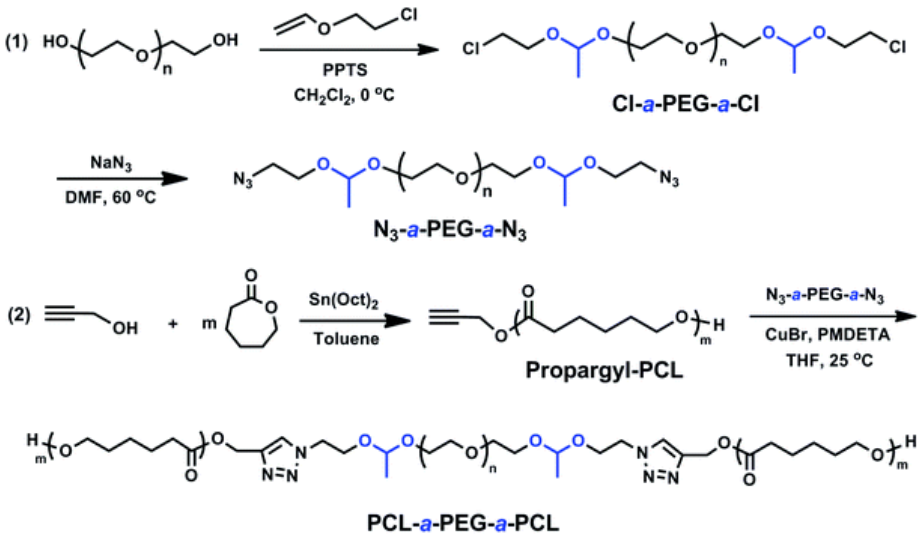

Figure 2.7 Synthetic route towards an acid-degradable PCL-acetal-PEG-acetal-PCL triblock shell-sheddable block copolymer *via* a copper-mediated azido-alkyne click reaction. Copyright 2013 Royal Society of Chemistry.

A direct polymerization approach has been explored to synthesize acid-shell-sheddable block copolymers. This approach requires the design and synthesis of novel (macro)initiators for ATRP and ROP or (macro)RAFT-mediators for RAFT polymerization. For CRP techniques with vinyl monomers, including (meth)acrylates, a typical example is the synthesis of an acid-labile PEG-based macro-RAFT agent bearing a cyclic acetal linkage.[172] As illustrated in Figure 2.8, PEG was functionalized with a benzylaldehyde group by a carbodimiide coupling using 4-formylbenzoic acid. The formed precursor (1) was used for the reaction with 1,1,1-tris(hydroxylmethyl)ethane and 4-(cyanopentanoic acid)-4-dithiobenzoate (CPADB). The resulting macro-RAFT agent (3) successfully mediated RAFT polymerization of various methacrylates, including a cholesterol-bearing methacrylate (Mchol) to synthesize a PEG-cyclic acetal-PMchol. Subsequently, the terminal dithioester group was aminolyzed to the corresponding thiol, followed by disulfide-thiol exchange with 2,2-dithiopyridine to the corresponding pyridiyldisulfide. Other examples include a double-head iniferter having both terminal bromine and RAFT moieties for both ATRP and RAFT polymerization[173] and a PEG-based bromine labeled with an orthoester linkage for ATRP.[174]

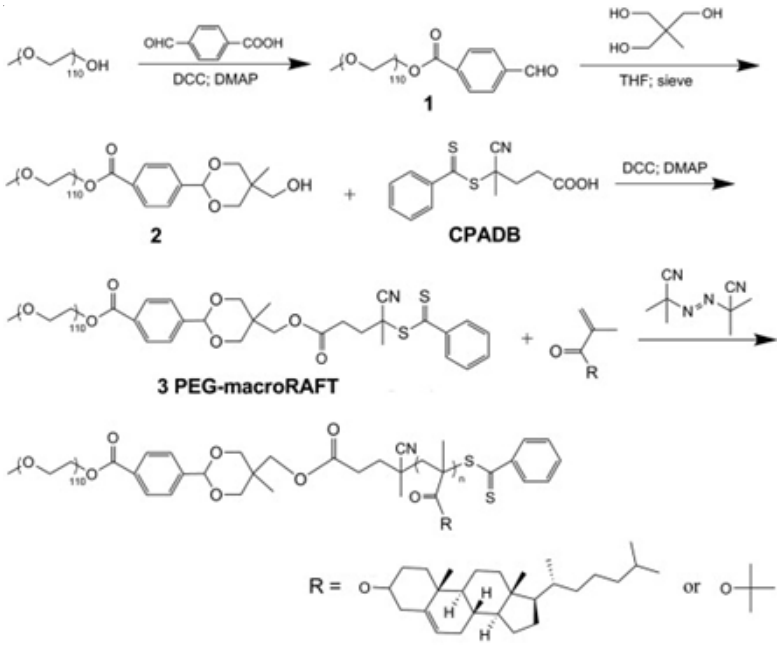

Figure 2.8 Synthetic route to an acid-labile PEG-based shell-sheddable block copolymer bearing a cyclic acetal linkage by RAFT polymerization. Copyright 2013 Elsevier.

For the ROP technique of cyclic monomers, a typical example involves the synthesis of an acid-labile PEG initiator having a methylmaleimic acid bridge and a hydroxy terminus (Figure 2.9). The resulting PEG-Dlink$_m$-OH was used as a macro-initiator for the ROP of lactide (LA) to yield a PEG-Dlink$_m$-PLA shell-sheddable block copolymer. Upon arriving at a tumor site, the PEG layer was shed to increase zeta potential by responding to tumor acidity. This significantly enhances cellular uptake and improves the i*n vivo* tumor inhibition rate.[175] Reports also describe the synthesis of a PEG-acetal-OH, for the synthesis of a PEG-acetal-PLA[176] and PEG-acetal-polycarbonate diblock,[177] a PEG-ketal-OH, for a PEG-ketal-PCL diblock,[178] and a HO-acetal-poly(propylene glycol)-acetal-OH for a PEG-acetal-poly(propyl glycol) (PPG)-acetal-PEG triblock copolymer.[179]

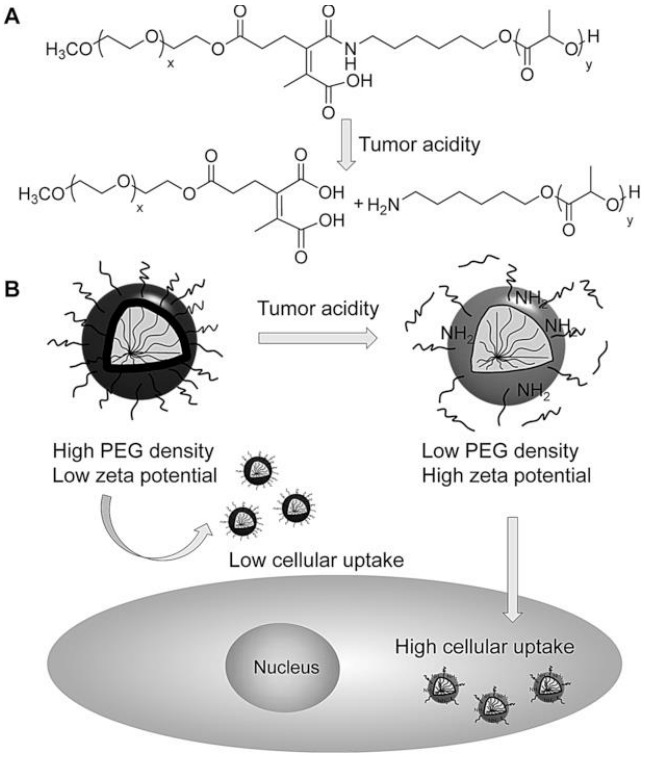

Figure 2.9 Schematic illustration for (a) the synthesis of PEG-Dlink$_m$-PLA acid-shell-sheddable block copolymer and its cleavage under tumor acidity and (b) enhanced cellular uptake of its nanoassemblies. Copyright 2016 Wiley.

2.2.6 Acid-degradable non-hydrophobic supramolecular nanoassemblies

Most of the acid-degradable nanoassemblies described above are formed by the synthesis of covalently-conjugated ABPs and their self-assembly through hydrophobic interactions. In contrast, non-hydrophobic supramolecular interactions have also been explored to fabricate a variety of acid-degradable supramolecular nanoassemblies.[180] Hydrogen-bonding interactions were used to develop supramolecularly-crosslinked nanogels. A block copolymer having pendant adenine groups, synthesized by RAFT polymerization, self-assembled with a hydrophobic uracil-containing crosslinker (diuracil) through adenine-uracil nucleobase pairing. In response to acidic pH, the base pairs were disrupted, causing dissociation of the nanogel. Host-guest interactions were used to prepare shell-sheddable nanoassemblies[181, 182] and polyrotaxanes.[183] As an example, Figure 2.10 illustrates the fabrication of an acid-shell-sheddable nanoassembly. A family of 6-OH orthoester-modified β-cyclodextrin (β-CD) derivatives were synthesized by a facile coupling reaction of β-CD with a cyclic ketene acetal. The synthesized asymmetric acid-cleavable β-CD derivatives were used to form amphiphilic supramolecular nanoassemblies with adamantane-

modified PEG through host-guest interactions in water. Rapid dePEGylation occurred at acidic pH due to hydrolysis of the interfacial orthoester linkages.[182]

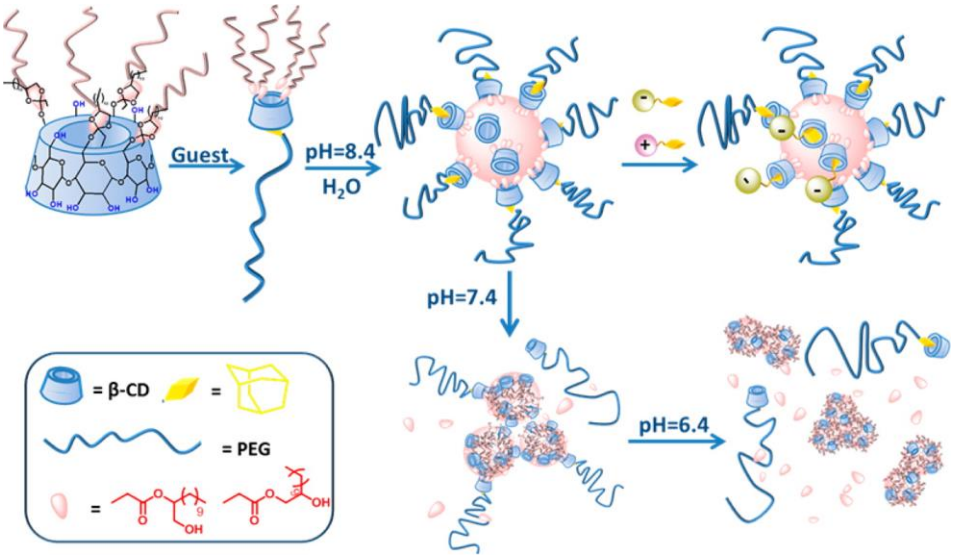

Figure 2.10 Schematic illustration to prepare acid-shell-sheddable nanoassemblies by supramolecular self-assembly of 6-OH orthoester-modified β-CD derivatives and an adamantane-modified PEG. Copyright 2014 American Chemical Society.

2.2.7 Strategies to accelerate degradation of acid-degradable nanoassemblies

Maintaining a satisfactory balance between high colloidal stability during blood circulation and rapid drug release at the site of action is an important consideration for designing acid-cleavable block copolymers. Particle dissociation during blood circulation and sluggish drug release in tumor tissues are undesirable consequences of incorporating inappropriate acid-cleavable chemistries into the block copolymers. In addition to efforts to fine tune acid-cleavable linkage hydrolysis to match with the acidic environment of tumors, several strategies have been explored to accelerate the hydrolysis rate of acid-cleavable linkages in block copolymers and their nanoassemblies. Three main strategies are summarized in this section.

Strategy I involves the integration of tertiary amine (t-amine) groups into acid-degradable copolymers. Figure 2.11 illustrates an example of the incorporation of a β-aminoester linkage into the backbone of a polyketal.[184] Protonation of t-amine groups allows for the facile penetration of hydronium ions into the hydrophobic core, consequently enhancing their hydrophilicity and thus promoting their degradation. Several reports also describe promoting hydrolysis of acid-cleavable linkages by copolymerization of methacrylates bearing pendant t-

amine groups such as 2-(dimethylamino)ethyl methacrylate), 2-(diethylamino)ethyl methacrylate, and 2-(diisopropylamino)ethyl methacrylate with acid-cleavable methacrylates bearing orthoester, benzylic acetal and solketal groups.[185-187] The incorporation of pendant t-amine groups can increase hydrophilicity and amplify acetal hydrolysis. However, it should be noted that protonation of t-amine groups with pKa = 6.4-7.4 in the vicinity of acid-cleavable linkages could convert t-amine groups to the positively-charged quaternary ammonium groups and thus reduce the hydronium concentration in aqueous media.

Strategy II utilizes a stimuli-responsive cleavage approach. For example, a recent report describes the synthesis of a polyketal with *o*-nitrobenzyl side chains to facilitate the degradation of the polymer backbone in a self-immolative manner.[188] Upon UV irradiation, *o*-nitrobenzyl groups were cleaved to generate the corresponding carboxylic acid moieties. Such photo-responsive cleavage consequently increased the acidity of the ketal environment and enhanced their hydrolysis rate. Another report shows that complexation *via* host-guest interactions with pillar[5] arenes containing carboxylic acid moieties accelerated the cleavage of pendant ketal groups in poly(N-[(2,2-dimethyl-1,3-dioxolane) methyl]acrylamide).[189]

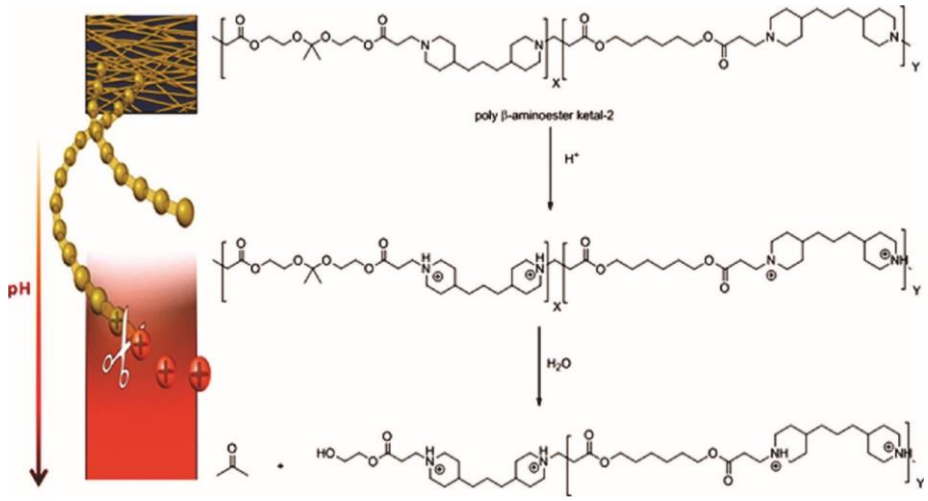

Figure 2.11 Schematic illustration to ketal hydrolysis in poly-β-aminoester ketal-2 *via* protonation of the tertiary amine groups in the backbones. Copyright 2010 American Chemical Society.

Strategy III explores self-amplifying acetal degradation through the formation of hydrogen iodide (HI). A polyacetal consisting of 3-iodopropyl acetal moieties undergoes β-elimination after acid hydrolysis, which generates aldehyde derivatives and releases HI (a strong acid), leading to rapid acetal degradation.[190]

2.3 Dual/multiple acid-cleavable nanoassemblies

In addition to decreased pH, GSH (a tripeptide containing cysteine) is found at elevated concentrations in cancer cells, and several enzymes (*e.g.* esterase or peptidase) are abnormally overexpressed in tumor tissues. In addition to these endogenous stimuli found in tumor environments, light has also been explored as a promising exogenous stimulus that can allow for the spatial and temporal control of drug release. These features have led to intense exploration of various strategies to synthesize smart nanoassemblies degradable in single stimulus response to reduction, enzyme, or light. Further efforts have been made to exploit the advantages of these stimuli in combination with acidic pH, *i.e.* dual acid/stimulus-responsive degradation, to achieve synergistic/accelerated micelle degradation and drug release.

For the development of dual/multiple stimuli/acid-degradable nanoassemblies, the combined cleavable linkages are generally incorporated in the micellar core and/or the core/corona interface as in single location and in dual location (*i.e.* single location or dual location stimuli-degradable nanoassemblies). General strategies that explore single and dual location approaches are schematically illustrated in Figure 2.12. In particular, the dual location approach can be envisaged to have superior propensity to degrade nanoassemblies induced with combined modules through the detachment of hydrophilic coronas and the dissociation of the hydrophobic core. The following sub-sections describe elegant strategies reported in the literature.

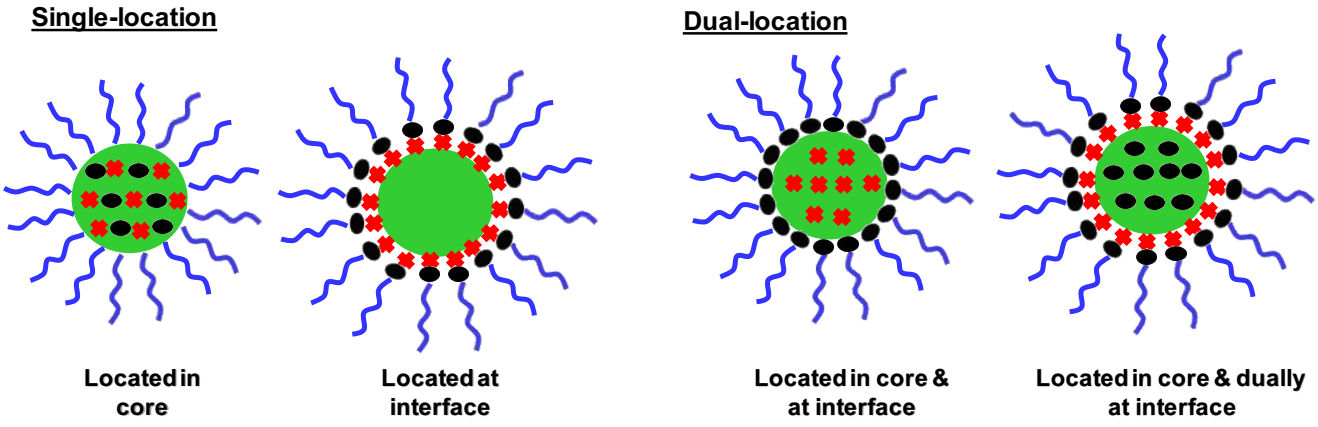

Figure 2.12 Schematic illustration of dual stimuli/acid-degradable nanoassemblies to explore single and dual location approaches. Note that the red crosses and black spheres denote different stimuli-cleavable linkages.

2.3.1 Single-location acid/reduction-degradable systems

In biological environments, GSH (a tripeptide containing a cysteine) is present at different concentrations between intracellular and extracellular compartments, and is also found at elevated concentrations in cancer cells.[38, 191, 192] Because disulfide bonds are cleaved to their corresponding thiols in a reducing environment or in the presence of GSH, disulfide chemistry has been extensively explored for the development of GSH-responsive degradable nanoassemblies for controlled/enhanced drug release.[193, 194] Note that diselenide chemistry has been also explored for reduction-responsive degradation.[195-198] Several approaches have been proposed to fabricate nanoassemblies constructed with acid-labile and disulfide linkages exhibiting dual acid/reduction responses in the micelle core, in the hydrophilic corona or at the core/corona interface.

For a dual acid/reduction response in the micelle core, both acid-cleavable and disulfide linkages are incorporated in pendant chains, on backbones of block copolymers, or as crosslinks in the nanoassemblies. Acrylamide-based linear copolymers having pendant pyridyldisulfide groups and either aldehyde or amine groups were synthesized by RAFT polymerization.[199] As illustrated in Figure 2.13, the copolymer chains were crosslinked through imine bond formation between the aldehyde and amine groups at pH = 8 and disulfide bond formation by disulfide-thiol exchange reaction. This yielded a dual-responsive crosslinked nanogels with acidic pH- and GSH- responsive properties. When exposed to tris(2-carboxyethyl)phosphine (a reducing agent) in acidic pH (5.5), the nanogels disassembled into their polymer chain components. Furthermore, grafting PEG into the nanogels demonstrates their potential to undergo post-assembly functionalization. ABPs of PEG-b-poly(2,4,6-trimethoxybenzylidene-pentaerythritol carbonate-*co*-5-methyl-5-propargyl-1,3-dioxan-2-one) (PEG-b-P(TMBPEC-*co*-MPMC)) with pendant reactive alkynyl groups as well as pH-sensitive acetal groups were synthesized by the ROP technique.[200] Their nanoassemblies were crosslinked through azido–alkyne click chemistry of at the pendant alkyne groups with bis(azidoethyl)disulfide (a disulfide-labeled diazido crosslinker), yielding disulfide-core-crosslinked nanogels labeled with both acetal and disulfide linkages in the core. The nanogels appeared to have good colloidal stability due to core-crosslinking. They also exhibited enhanced release of encapsulated Dox at pH = 5 with 10 mM DTT, compared with either pH = 5 or DTT alone. The on-demand drug release induced by acidic pH and reductive environment of cancer cells enhanced the cytotoxicity of nanogels to MCF-7/ADR cells.

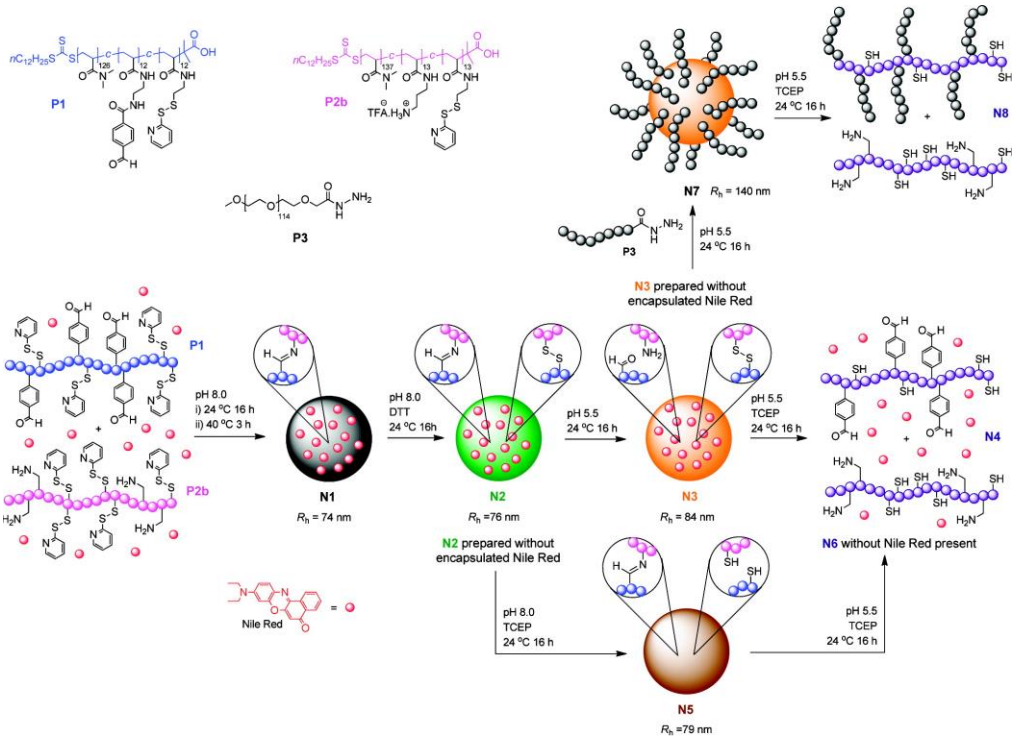

Figure 2.13 Schematic illustration of the synthesis, crosslinking, and dual acid/reduction-responsive disassembly of acrylamide-based linear copolymers having pendant pyridyldisulfide groups and either aldehyde or amine groups by RAFT polymerization. Copyright 2012 American Chemical Society.

Drug molecules (e.g. Dox) were conjugated onto polymeric chains through acid-labile hydrazone or imine linkages. Upon aqueous self-assembly of the formed block copolymer prodrugs, the resultant nanoassemblies were further subjected to core-crosslinking through amide formation with dithiodiethanonic acid (DTDEA) for PEG-b-poly(acrylic acid)[201] and *in situ* disulfide-core crosslinking through disulfide-thiol exchange for PEG-b-polyaspartate.[202] The formed nanogels functionalized with both hydrazone linkages and disulfide crosslinks responded to acidic pH for Dox release, *via* cleavage of hydrazone linkages, and to GSH for disassembly *via* cleavage of disulfide crosslinks. Another report describes the fabrication of nanoassemblies of PEG-b-poly(6-O-metacryloyl-D-galactopyranose) conjugated with Dox through disulfide and imine linkages.[203]

Recently, the synthesis of polydoxorubicin (PDOX) labeled with backbone disulfide and hydrazone linkages was reported.[204] Figure 2.14 illustrates the synthetic route to a disulfide-labeled Dox dimer (Dox-ss-Dox) by reaction of Dox with DTDEA through the formation of amide bonds, followed by step-growth polymerization with adipic dihydrazide (ADH). The

resulting polyDox particles with 78% Dox content could completely release DOX-SH within 1.5 days at the tumor microenvironment, but no measurable leakage in the physiological media was observed.

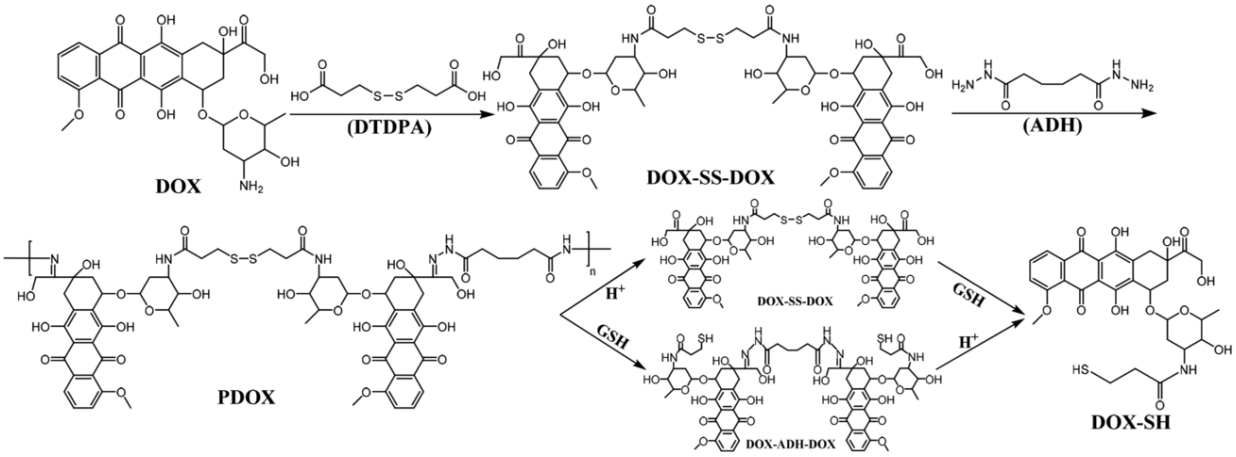

Figure 2.14 Synthetic route and dual acid/reduction-responsive release of polydoxorubicin prodrug. Copyright 2018 Wiley.

For dual responses at the core/corona interface, supramolecular block copolymers were prepared by molecular recognition of nucleobases between poly(2-(2-methoxyethoxy)ethyl methacrylate-co-oligo(ethylene glycol) methacrylate) (P(MEO_2MA-co-OEGMA))-SS-PCL-adenine labeled with a disulfide at the block junction and a uracil-terminated PEG (PEG-U). The copolymer self-assembled into micelles with PCL cores surrounded with both P(MEO_2MA-co-OEGMA) and PEG coronas, which were labeled with reduction-responsive disulfide linkages and pH-responsive nucleobase interactions at the core/corona interface. Upon cleavage of these linkages, controlled release of encapsulated Nile red (NR) was achieved.[205] Another report describes the development of galactosamine-modified polymeric micelles which were responsive to both reduction (*via* disulfide exchange) and acidic pH (*via* acetal cleavage) constructed from poly(ethylethylene phosphate)-acetal-PCL-SS-poly(2-dimethylaminoethyl methacrylate) for co-delivery of anticancer drugs and nucleic acids.[206]

For dual responses in coronas, dual acid/reduction-degradable shell-crosslinked nanoassemblies with disulfide and acid-labile linkages were prepared using ADH as a disulfide-labeled crosslinker. The terminal hydrazide groups of ADH were conjugated to pendant aldehyde groups of hydrophilic blocks in various block copolymers such as a linear[207] and a four-armed

star[208] polymethacrylate as well as chitosan,[209] yielding crosslinked shells with disulfide-labeled crosslinks through the formation of hydrazone bonds.

2.3.2 Dual-location acid/reduction-degradable systems

Dual location acid/reduction-degradable nanoassemblies are constructed from block copolymers labeled with acid-labile and disulfide linkages in different positions, (e.g. the hydrophobic block and at the hydrophilic/hydrophobic block junction). Their self-assembled micelles possess dual responses both in the micelle core and core/corona interface, thus attaining dual response at dual locations. One strategy to synthesize dual location dual acid/reduction-cleavable nanoassemblies involves the incorporation of disulfide linkage at the interface and acid-labile linkages in the micelle core, (*i.e.* disulfide (interface)/acid (core)). An ABA-type PLA-based triblock copolymer containing a disulfide linkage between the hydrophilic poly(oligoethylene oxide methacrylate) (POEOMA) and PLA blocks and a ketal linkage in the center of the PLA block (POEOMA-ss-PLA-ketal-PLA-ss-POEOMA) was synthesized by a combination of ROP, ATRP, esterification, and coupling reactions.[52] The self-assembled micelles have ketal linkages in the PLA cores and disulfide linkages at the core/corona interface. As illustrated in Figure 2.15, the cleavage of interfacial disulfide bonds in the presence of glutathione (GSH) resulted in shedding coronas from micelles, while the cleavage of the core ketal linkages under acidic conditions resulted in the disruption of the micelle cores. Compared with single response systems, dual response in the presence of GSH at acidic pH at dual locations (both core and interface) resulted in the synergistic regulation of micelle destabilization, ultimately leading to accelerated cargo release. The synthesis of nanoassemblies with disulfide (interface)/acid (core) based on polycarbonate,[210] PCL,[211] and polyvinyl[212] block copolymers has also been reported.

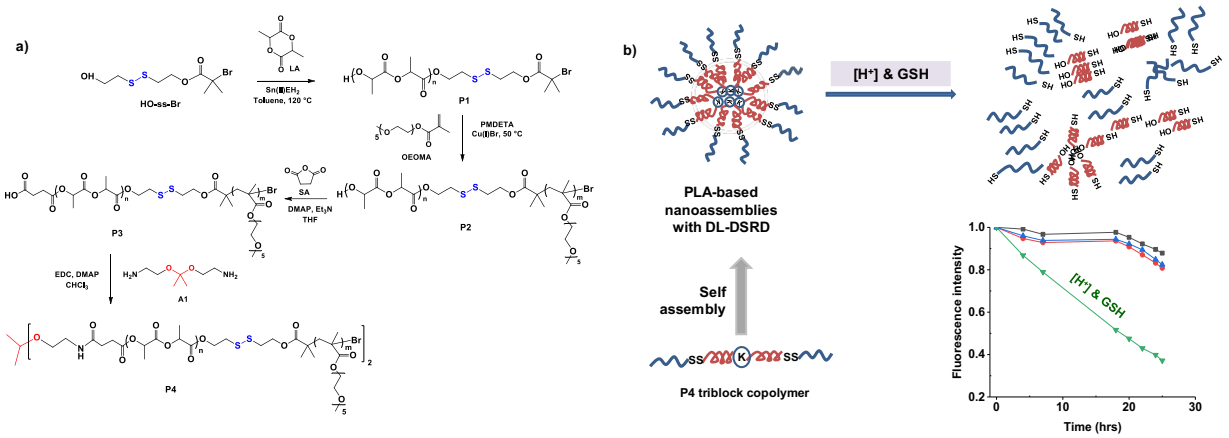

Figure 2.15 (a) Synthetic scheme and (b) illustration of aqueous micellization and dual acidic pH/reduction-responsive degradation of a PLA-based triblock copolymer consisting of a hydrophilic polymethacrylate and PLA blocks with a ketal linkage in the center of PLA block and disulfides at the polymethacrylate/PLA block junctions, thus exhibiting dual response at dual location. Copyright 2018 Wiley.

Another strategy explores the incorporation of acid-labile linkages at the interface and disulfide linkages in the micelle core, (*i.e.* acid (interface)/disulfide (core)). PCL-based grafted copolymers bearing an acetal linkage at the hydrophilic/hydrophobic block junction and a single disulfide linkage on the hydrophobic backbone were synthesized by a combination of ROP and RAFT polymerization techniques.[213-216] Furthermore, PCL-bearing polyurethane linear copolymers linked with hydrophilic PEG through benzoic imine[217] or hydrazone[218] linkages as well as a PCL labeled with a disulfide linkage connected with a PEG block through a hydrazone bond[219] was synthesized by ROP and facile coupling reactions. These copolymers self-assembled to form dual acid/reduction-degradable nanoassemblies with an acid-labile interface and a disulfide core.

Recently, a polypeptide block copolymer composed of a hydrophilic PEG block connected through an acid-cleavable DMMA linkage with a thiol-pendant poly(L-cysteine) was synthesized. The synthesis involved ROP of nitrobenzyl-bearing α-amino acid *N*-carboxyanhydride initiated with an amine terminated PEG derivative and a sequential photo-cleavage reaction to generate pendant thiol groups (Figure 2.16). Self-assembly and subsequent oxidation of thiol groups allowed for the formation of a new class of polypeptide copolymer nanoassembly with a sheddable PEG corona and a disulfide-crosslinked core. In response to acid and reduction, the resultant nanoassemblies exhibit dual-stimuli-triggered drug release profiles of the anticancer drug camptothecin (CPT). CPT-loaded nanogels facilitated cellular internalization and CPT was released inside the HeLa cells at pH 6.5, as

confirmed by flow cytometry and fluorescence microscopy.[220] Another polypeptide block copolymer with a benzimine linkage at the block junction was synthesized by a combination of ROP, a coupling reaction, and thiol-oxidation for core crosslinking. Its applicability to dual acid/reduction-degradable intracellular drug delivery to tumors was demonstrated with both *in vitro* and *in vivo* studies.[221]

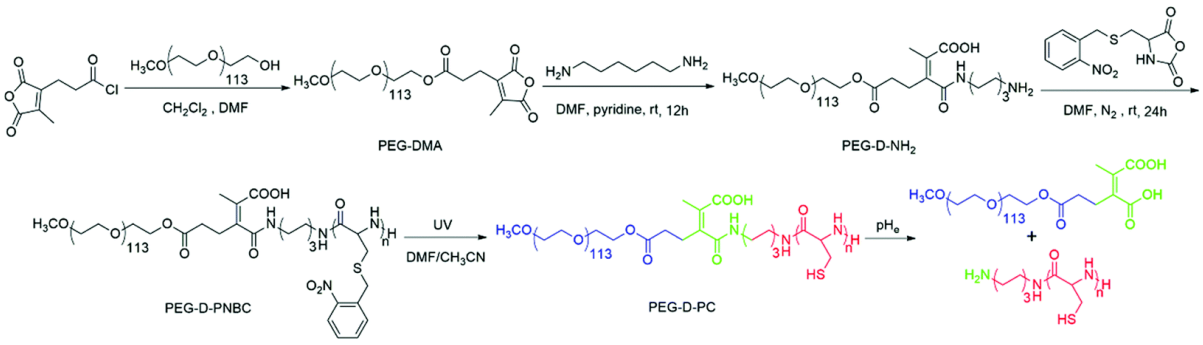

Figure 2.16 Synthesis of a polypeptide block copolymer composed of a hydrophilic PEG block connected *via* a DMMA linkage with a thiol-pendant poly(L-cysteine) by ROP of α-amino acid *N*-carboxyanhydride initiated with an amine-terminated PEG derivative and a subsequent photo-cleavage reaction to generate pendant thiol groups. Copyright 2018 Royal Society of Chemistry.

New strategies utilizing CRP techniques have been explored to synthesize a novel block copolymer having a ketal linkage at the block junction and multiple disulfide pendants in the hydrophobic block. The diblock copolymer comprises a hydrophilic PEG block covalently conjugated through a ketal linkage with a hydrophobic polymethacrylate block having pendant disulfide linkages (PHMssEt; *i.e.* PEG-ketal-PHMssEt block copolymer, P5). This approach is versatile as the number of pendant disulfide linkages in the micelle core is easily adjusted through controlled radical polymerization. An attempt using ATRP to synthesize the block copolymer was not straightforward due to the instability of ketal linkages at interfaces under ATRP conditions.[222] Promisingly, as illustrated in Figure 2.17, the RAFT polymerization in the presence of a newly-synthesized PEG-based macro-RAFT agent labeled with a ketal linkage (PEG-ketal-RAFT, P4) allows for the successful synthesis of a well-controlled block copolymer (P5).[223] P4 was synthesized using robust multi-step route utilizing carbamate chemistry to endow stability during protection/deprotection steps. Not only does the cleavage of the ketal linkages, under endosomal or lysosomal pH conditions, sheds coronas at the interfaces, but also the reductive cleavage of pendant disulfides to the corresponding thiols, in the presence of cellular GSH, causes a change in hydrophobic/hydrophilic balance in the micelle core. This dual

acid/reduction response leads to synergistic and accelerated drug release, compared with the single response at single location analogues. These results, combined with *in vitro* cell culture experiments including cell viability and cellular uptake, demonstrate the versatility of dual location dual acidic pH/reduction-responsive degradation in the development of tumor-targeting intracellular drug delivery vehicles for cancer chemotherapy.[223] This versatile strategy has recently been explored to synthesize a degradable double hydrophilic block copolymer for dual acid/reduction-responsive disassembly and thermoresponsive tunability.[224]

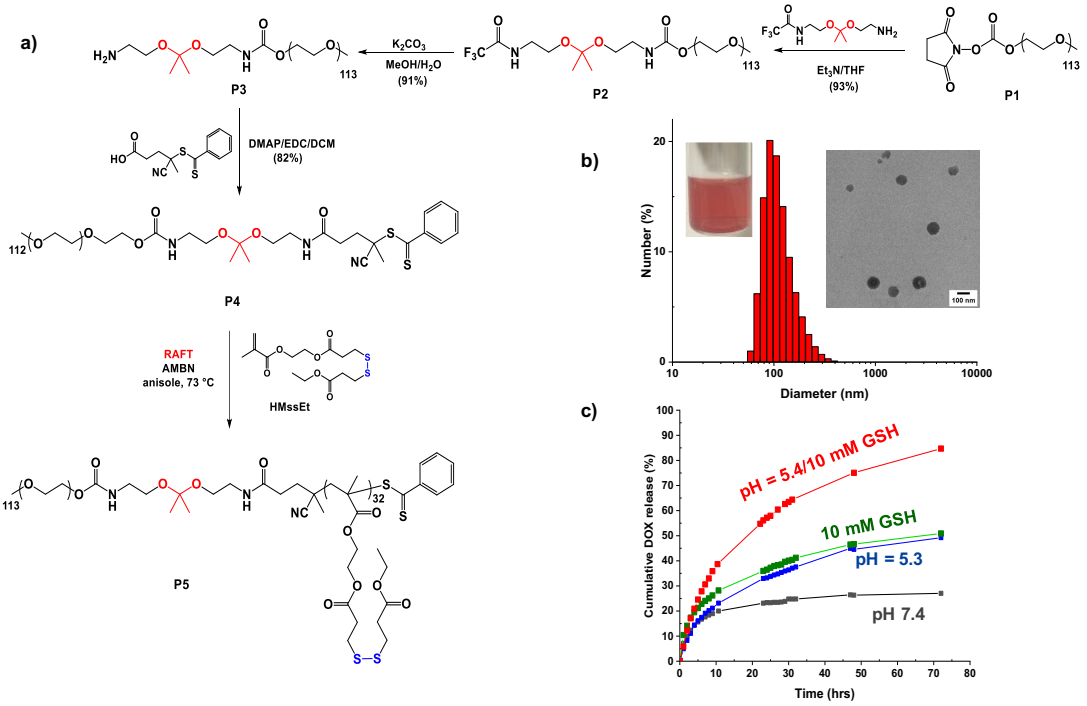

Figure 2.17 (a) Synthesis of a new dual acid/reduction-degradable block copolymers labeled with a ketal linkage at the block junction and disulfide pendants in the hydrophobic block, (b) DLS diagram, digital (inset), and TEM (inset) images of Dox loaded nanoassemblies, and (c) % Dox release from Dox-loaded nanoassemblies incubated at pH = 5.3 and 7.4 with and without 10 mM GSH. Copyright 2018 Royal Society of Chemistry.

The robust approach was further explored to synthesize a new dual acid/reduction-degradable block copolymer labeled with dual acetal and disulfide linkages at the block junction as well as pendant disulfide bonds in the hydrophobic block, POEOMA-AC-SS-PHMssEt (AC: acetal). This new approach utilizes the combination of ATRP and RAFT polymerization in a sequential or concurrent mechanism, along with facile coupling reactions. This study provides the first example of a block copolymer with a reductively and acidic degradable junction, and elucidates

the interplay of RAFT and ATRP for synthesizing dual location dual stimuli responsive nanocarriers.[225]

2.3.3 Acid/light-degradable systems

Dual acid/light-degradable nanoassemblies contain photo-cleavable linkages such as coumarin and o-nitrobenzyl groups, along with acid-labile linkages. Most systems were designed with the linkages located mainly in the micelle core. Coumarin-based light-crosslinkable and pH de-crosslinkable nanoassemblies were formed from amphiphilic copolymers such as poly(amino acid) [226] and polyurethane[227] conjugated through hydrazone linkages with the coumarin groups. Figure 2.18 illustrates an example of the synthesis of a PEG-based polyaspartamide having both hydrazone and coumarin groups by a combination of ROP and post modifications with hydrazine and 7((4-oxopentyl)oxy)-4-methylcoumarin. The resultant block copolymer self-assembled to form nanoassemblies that were stabilized *via* UV-induced crosslinking based on dimerization of the coumarin moieties. The formed nanogels were dissociated upon cleavage of the hydrazone linkages under mild acidic conditions, accelerating release of the encapsulated drug.

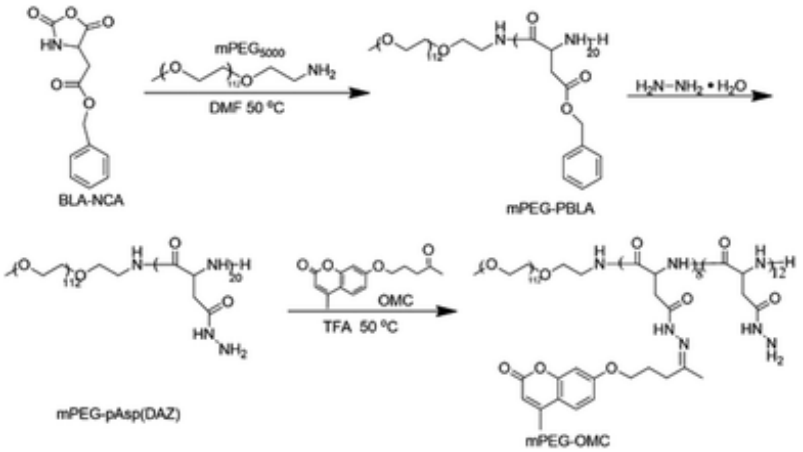

Figure 2.18 Synthetic route to a PEG-based polyaspartamide conjugated through hydrazone linkages with coumarin groups by a combination of ROP and post modifications. 2015 Copyright Royal Society of Chemistry.

In addition to coumarin, o-nitrobenzyl light-cleavable groups have been utilized for the fabrication of dual acid/light-cleavable nanoassemblies. Amphiphilic glycol chitosan grafted with o-nitrobenzyl succinate conjugates was synthesized by conjugating hydrophobic light-sensitive *o*-nitrobenzyl succinate (NBS) to the main chain of hydrophilic glycol chitosan. This copolymer was treated with glutaraldehyde to form core-crosslinked nanogels through imine linkages.[228] In fact, the synthesis of several PEG-conjugated block copolymers labeled with acid-

labile and o-nitrobenzyl linkages have been reported. Examples include a PEG-based polyacetal labeled with o-nitrobenzyl groups on the backbone[229] and a PEG-based triblock copolymer labeled with β-thiopropionate and o-nitrobenzyl linkages in the central hydrophobic block.[230] These copolymers self-assembled to form nanoaggregates with both o-nitrobenzyl groups and acetal or β-thiopropionate groups in the core. Dual pH/light-mediated degradation of these nanoassemblies increased therapeutic potency versus cancer cell lines *in vitro*.

For dual acid/light-cleavable nanoassemblies at the core/corona interface, linear dendritic copolymers were synthesized *via* connecting the hydrophilic PEG block to a hydrophobic dendron with o-nitrobenzyl and acetal groups as bridges between the two blocks. They self-assembled to form nanoassemblies displaying a dual acid and light responsive interface NR encapsulated in these nanoassemblies showed rapid release upon UV light exposure (35% in 60 min), while the sluggish NR release was observed at pH 5.4 (less than 20% in 70 hrs), which was attributed to the slow hydrolysis rate of the acetal groups and its shielding by the micelle's unique morphology.[231]

2.3.4 Acid/enzyme-degradable systems

Dual acid/enzyme-cleavable nanoassemblies have been synthesized via the incorporation of enzyme-responsive cleavable linkages along with acid-labile linkages. Polysaccharide-based vesicular nanoscaffolds were synthesized for the administration of Dox *via* physical loading and polymer–drug conjugation toward drug delivery for breast cancer cells.[232] As illustrated in Figure 2.19, dextran was modified with a renewable resource, 3-pentadecyl phenol, through both acid-labile imine and aliphatic ester linkages that can be cleaved in response to acid and an esterase enzyme. The formed dextran-based copolymer was amphiphilic and self-organized into nanovesicles with diameters of *ca.* 200 nm in water. Dox was conjugated to the copolymer through imine linkages as well as by physical encapsulation in hydrophilic pocket. At pH = 5-6 and in the presence of an esterase, both imine and ester linkages were cleaved to release 100% of the loaded Dox molecules. *In vivo* cell culture results suggest that the newly-developed acid/enzyme-cleavable polysaccharide vesicular assemblies are potential drug vectors for the administration of Dox, in both loaded and chemically conjugated forms, for the efficient killing of breast cancer cells.

High molecular weight dual acid/enzyme-cleavable branched copolymers were synthesized by RAFT polymerization through copolymerization with a dimethacrylate crosslinker bearing a GFLGK peptide linkage. The conjugation of Dox to the copolymer *via* the formation of a hydrazone linkage allows the synthesis of dual acid/enzyme-degradable polymer prodrug nanogels. They degraded to smaller fragments of 8.6 nm in the presence of papain at pH = 5.4 (dual stimuli), which lead to enhanced Dox release. *In vitro*, *in vivo*, hematological, and histological assays corroborated anti-tumor activity against 4T1 breast cancer cells and biological safety of this nanocarrier for Dox drug delivery.[233-235]

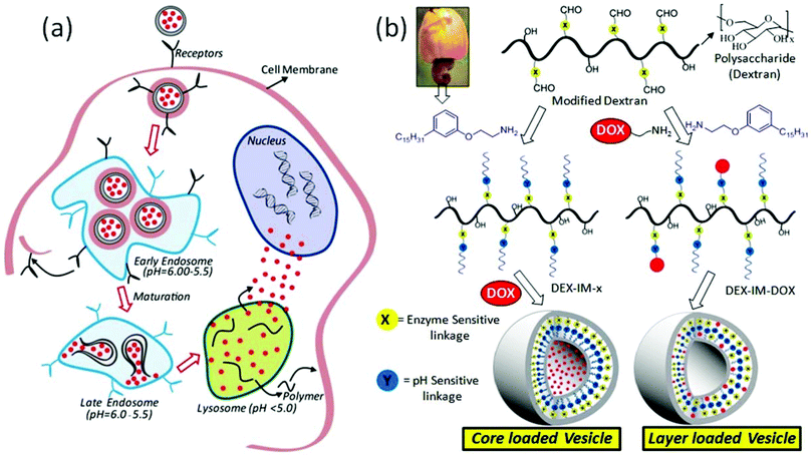

Figure 2.19 (a) Schematic representation of polymer-drug nanovesicle cellular uptake and their degradation in endocytic compartments and (b) structural engineering of dual acid/enzyme-degradable polysaccharide vesicles. Copyright 2015 Royal Society of Chemistry.

2.4 Summary and outlook

Acid-responsive block copolymers bearing cleavable linkages have become a formidable choice of building blocks for constructing effective nanoassemblies for tumor-targeting drug delivery. They are designed with acid-labile linkages that are stable under normal physiological pH conditions, but cleaved in acidic environments, particularly in tumor tissues and in endosomes/lysosomes. Various acid-cleavable linkages can be incorporated into acid-degradable block copolymers at various positions, as on hydrophobic block backbone, in pendant chains, or at the hydrophilic/hydrophobic block junctions. Their aqueous micellization enables the formation of self-assembled nanoassemblies at single location, as in the hydrophobic cores, shells, or at the core/corona interface. They are degraded or disintegrated upon the cleavage of

acid-labile linkages under acidic pH conditions, leading to controlled and enhanced release of encapsulated drugs.

Due to the acidic environment of cancer cells and the versatility of acid-cleavable chemistries, acid-cleavable block copolymers have been explored extensively for biomedical applications in the past decades. Despite numerous examples of block copolymers reported in the literature, only a few examples of acid-cleavable block copolymers have entered clinical trials (*e.g.* NC-6300 from Nanocarrier is in phase 1 clinical trial).[13] In addition to the general shortcomings pertaining to polymeric nanocarriers, transforming acid-cleavable block copolymers from "bench-top to bed-side" requires a more comprehensive understanding of the acid-cleavable chemistry and degradation kinetics in the macromolecular form. With advances of research in cancer cell biology, our understanding of the importance in controlling acidity of the cancer microenvironment in regulating tumor metastasis and drug resistance is mounting.[236] In addition to activating lysosomal enzymes, the acidity of the tumor microenvironment can induce pro-metastatic factors.[75] The future design of acid-cleavable block copolymers should be tailored to not only be applied for increasing anti-cancer drug release but also to tune the acidity of the tumor environment for reducing tumor progression. Other intriguing and emerging applications of acid-cleavable block copolymers, such as their use for drug delivery to inflammation,[237] corrosion inhibitors release,[238] self-healing networks,[239] biodegradable gels for tissue engineering,[240] and porous materials[241] are now attracting the attention of other researchers to this diverse family of polymers.

Along with single acid-responsive degradation, dual and multiple stimuli-responsive degradation has been explored for acid/reduction, acid/light and acid/enzyme responses to improve drug release profiles. In particular, dual location the dual acid/reduction degradation strategy has been proposed in the form of block copolymers with an acid-labile linkage at the block junction and pendant disulfide linkages in hydrophobic block. Their self-assembled micelles exhibit a dual response both in the micelle core and core/corona interface. The encouraging results demonstrate that this new strategy can not only facilitate the synergistic/accelerated release of drugs but can also enhance the precision of degradation of nanocarriers and thus generate functional multifaceted behavior. Each degradable linkage, positioned at different locations, can be independently stimulated to allow for more precise control over dissociation and release kinetics of drugs from micelles in the tumor environment.

A great advantage for acid-responsive degradation is a broad choice of acid-labile linkages, such as acetals/ketals, imines, hydrazones and oximes, which show various cleavage kinetics under acidic conditions. Some linkages are rapidly cleaved under very mild conditions, even at physiological pH, while other linkages are very stable under acidic environments (pH = 4.5-5.5). Their cleavage kinetics have been known to be further tuned through the design of chemical structures and neighboring groups associated with these linkages. For example, ketals and imines are known to rapidly degrade under physiological pH (pH = 7.4), thus their positioning in the hydrophobic core of micelles could slow down their hydrolysis in the blood stream while leading to burst release in the acidic environment of endosomes or lysosomes. On the other hand, due to their mediocre rate of hydrolysis, benzylic acetals and hydrazones are more suitable for the interface of polymeric micelles for the purpose of PEG shedding in the slightly acidic environment of tumor tissue. The more hydrolytically stable functional groups, such as acetaldehyde acetals and oximes are more suited when sustained drug release of cargo is needed. It should be noted that unlike the hydrolytic properties of acid-cleavable functional groups in small molecules, the degradation behavior of acid-cleavable functionalities in macromolecules is intricately regulated by various factors, including molecular weight, DP, hydrophobic content, crystallinity of the polymer as well as the particle size and the location of the cleavable linkage in the nanoassemblies. For example, drastically conflicting results have been reported in the literature for drug release performance of block copolymers containing acetaldehyde acetal compared to its hydrolysis kinetic in small molecules.[89, 90, 177] This also necessitates improving consistency in experimental conditions (temperature, buffer concentration, volume of release media, *etc.*) for drug release investigations of acid-cleavable block copolymers among different research groups.

Once the target site is reached, the drug-loaded nanoassemblies should have tunable and programmable release of drugs for better biodistribution and greater efficacy of the drug molecules. Upon acid-cleavable degradation, degraded products containing cytotoxic chemical moieties, such as aldehyde and hydrazine are generated. Careful design of acid-degradable block copolymers and meticulous dosage injection are required to minimize bioaccumulation of these substances in the body. Furthermore, tumors are highly heterogeneous environments. Consequently, the pH conditions are not universally consistent to various cancer cell lines, which could make acidic-degradable nanocarriers ineffective to certain tumors. Understanding the

acidity of each tumor tissue should be a prerequisite when acid-degradable block copolymer nanoassemblies are designed.

Chapter 3: Imidazole-mediated dual location disassembly of acid-degradable intracellular drug delivery block copolymer nanoassemblies

3.1 Introduction

The development of well-defined block copolymer-based nanoassemblies which are degradable in response to biological stimuli (or endogenous triggers) has been extensively explored as promising candidates for polymer-based drug delivery systems. At optimal sizes, these nanoassemblies can minimize renal clearance and side effects associated with small molecular weight anticancer drugs in conventional chemotherapy.[79-82] Moreover, they are prone to be accumulated in tumor tissues through the EPR effect, improving biodistribution of small drug molecules.[7] In particular, acidic pH-responsive degradable nanoassemblies show potential in targeted drug delivery due to the difference in pH between tumor tissues (pH = 6.5-6.9) and cancerous endosomes/lysosomes (pH = 4.2-5.3) from normal tissues and blood (pH = 7.4).[74] These acid-degradable nanoassemblies can enter into tumor tissues and cancer cells *via* extravasation and endocytosis, where the acidic environments of these tissues can degrade the nanoassemblies, thus leading to the enhanced and controlled release of the encapsulated drug molecules.

To explore the acidic pH-triggered disassembly, several approaches for the synthesis of acid-degradable block copolymer nanoassemblies have been developed. Most approaches involve the integration of acid-cleavable linkages, such as acetal/ketal, imine, and boronic ester groups, in nanoassemblies. These linkages are incorporated in the hydrophobic cores for core-degradable nanoassemblies or at the interfaces between hydrophilic coronas and cores for shell-sheddable nanoassemblies.[31, 35, 48, 96] In an acidic environment, these nanoassemblies disintegrate through unique degradation mechanisms depending on the position of acid-labile linkages in their parent block copolymers. Shell-sheddable nanoassemblies utilize the corona detachment upon the cleavage of acid-labile linkage at the block junction,[2, 98, 158, 160, 161, 164, 172, 173, 175, 223, 242-244] while core-degradable micelles undergo a change in the hydrophobic/hydrophilic balance upon the cleavage of the pendant acid-labile linkage in the hydrophobic block.[122-128, 130, 131, 245] Despite these advances, single location systems have several limitations: sluggish degradation for core-degradable nanoassemblies, undesired aggregation of degraded products for shell-sheddable

nanoassemblies, and difficulty in controlled and on-demand drug release.[24] Developing the synthesis of acid-degradable nanoassemblies bearing acid-labile linkages in dual locations, both in cores and at interfaces, will be crucial for showing the accelerated degradation and drug release through synergistic degradation mechanisms (i.e., change in the hydrophobic/hydrophilic balance and corona detachment) at two locations.

Another challenge in designing acid-cleavable nanoassemblies is achieving rapid disassembly in acidic pH values (4.2-6.9) while remaining structurally stable in physiological pH. Successfully achieving this balance will improve the biodistribution and on-demand release of drug molecules in targeted sites, which will minimize the premature release of drugs and circumvent the undesired occurrence of large aggregates in the blood. One approach to achieve this is to incorporate acid-ionizable groups into the structure of the acid-cleavable micelle cores. Tertiary dialkylamino groups such as dimethylaminoethyl,[185] diethylaminoethyl,[187] and diisopropylaminoethyl [186] groups have been explored as acid-ionizable groups. In acidic pH lower than their pKa values, these groups can be protonated, which increases the polarity of the hydrophobic cores. As a result, more protons have access to acid-labile linkages, leading to the enhanced hydrolysis of pendant orthoester and trimethoxyphenylacetal groups in the hydrophobic cores. However, these groups retain relatively rapid acid-catalyzed hydrolysis and the dialkylamino groups could hamper the ability of the cores to encapsulate hydrophobic drug molecules due to their increased hydrophilicity induced by their weak protonation at pH = 7.4. Studies have also shown the slow hydrolysis of acetaldehyde acetal groups in acidic environments at pH = 5.3 and even at pH = 4.[90, 132, 246] Moreover, the imidazole ring has its pKa = 6.7 higher than endo/lysosomal pH ranges.[247, 248] The aromaticity of the ring could enhance the loading capacity and efficiency of aromatic drug molecules such as Dox.[249, 250]

In this work, we explored a dual location acid-responsive degradation platform by synthesizing well-defined acid-cleavable block copolymers with an acetaldehyde acetal linkage positioned both in the hydrophobic block and at the hydrophilic/hydrophobic block junction (Figure 3.1). Biocompatible PEG was used as the hydrophilic block. These copolymers self-assembled in an aqueous solution to form spherical nanoassemblies with acetal linkages in dual locations (cores and interfaces). In acidic pH, these nanoassemblies degraded through dual mechanisms, which consists of the detachment of the PEG corona upon the cleavage of acetal linkages at the interfaces and the disruption of the hydrophobic/hydrophilic balance upon the

cleavage of pendant acetal linkages in hydrophobic cores. Their acid-catalyzed degradation was systematically examined in both homogeneous and heterogeneous media to obtain insight into dual location acid degradation and the effect of nanoassembly concentration. Furthermore, the effect of pendant imidazole groups incorporated in micelle cores on aqueous micellization, acid-responsive degradation, loading, and acid-responsive release of Dox was investigated. Finally, these copolymers were evaluated as effective intracellular drug delivery nanocarriers for *in vitro* toxicity and cellular uptake with HeLa cancer cell lines.

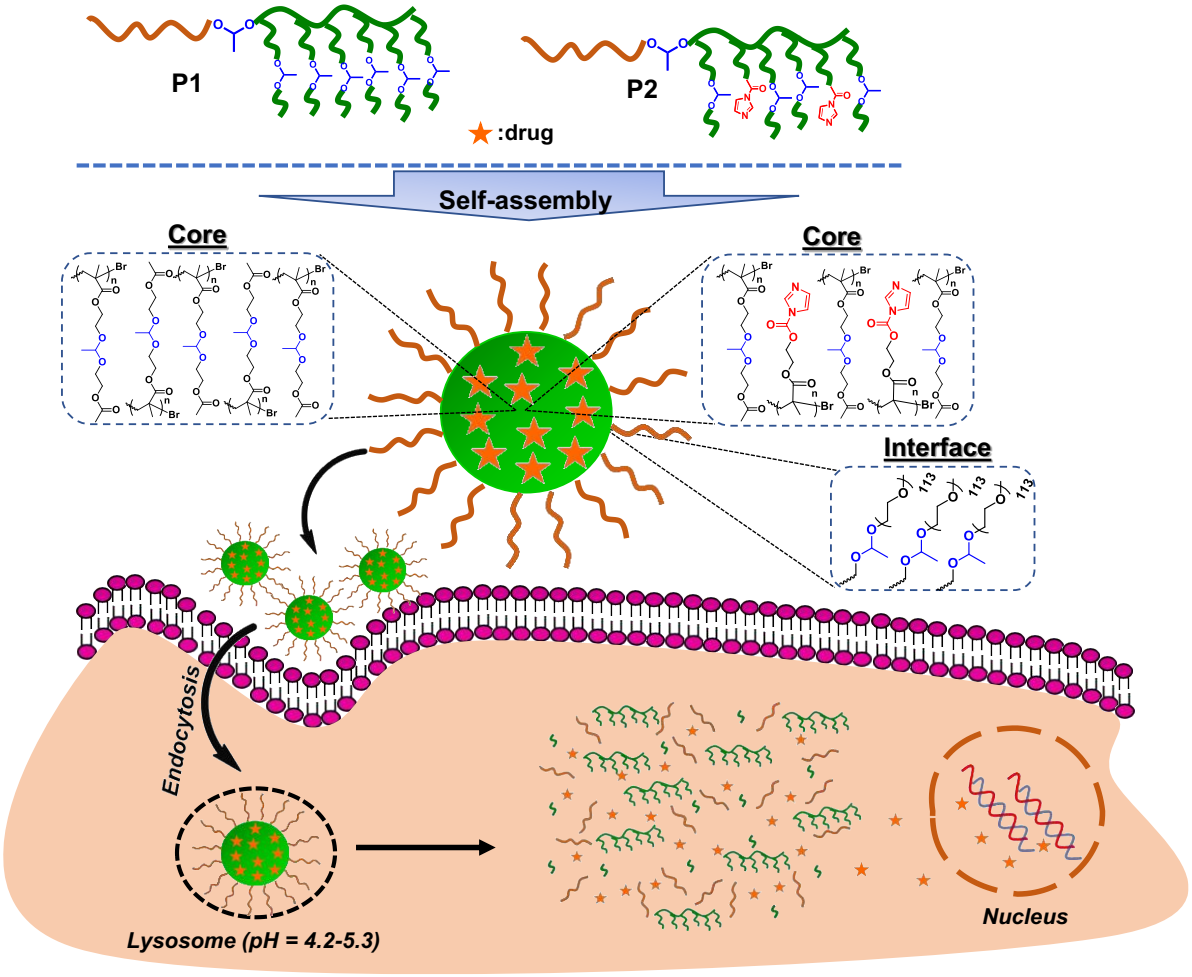

Figure 3.1 Schematic illustration of intracellular drug delivery of Dox-loaded acid-cleavable nanoassemblies with acetal linkages located at interfaces and in micelles cores.

3.2 Experimental

3.2.1 Instrumentation. ^{1}H-NMR spectra were recorded using a 500 MHz Varian spectrometer. The deuterated chloroform ($CDCl_3$) singlet at 7.26 ppm and deuterated dimethyl sulfoxide (DMSO-d_6) quintet at 2.5 ppm were selected as the reference standard. For the synthesis of (co)polymers, monomer conversion was determined by proton nuclear magnetic resonance spectroscopy (^{1}H-NMR) analysis. Spectral features are tabulated in the following order: chemical shift (ppm); multiplicity (s - singlet, d - doublet, t – triplet, m - complex multiple); number of protons; position of protons. Molecular weight and molecular weight distribution were determined by gel permeation chromatography (GPC). An Agilent GPC was equipped with a 1260 Infinity Isocratic Pump and a RI detector. Two Agilent PLgel mixed-C and mixed-D columns were used with dimethylformamide (DMF) containing 0.1 mol % LiBr at 50 °C at a flow rate of 1.0 mL/min. Linear poly(methyl methacrylate) standards from Fluka were used for calibration. Aliquots of the polymer samples were dissolved in DMF/LiBr. The clear solutions were filtered using a 0.40 mm polytetrafluoroethylene (PTFE) filter to remove any DMF-insoluble species. A drop of anisole was added as a flow rate marker. The size of micelles in hydrodynamic diameter by volume was measured by dynamic light scattering (DLS) at a fixed scattering angle of 175° at 25 °C with a Malvern Instruments Nano S ZEN1600 equipped with a 633 nm He-Ne gas laser. Fluorescence spectra on a Varian Cary Eclipse fluorescence spectrometer and ultraviolet/visible (UV/vis) spectra on an Agilent Cary 60 UV/vis spectrometer were recorded using a 1 cm wide quartz cuvette.

Transmission Electron Microscopy (TEM) images were obtained using a Thermo Scientific Talos F200X G2 S/TEM. To prepare specimens, aqueous P1-NPs or P2-NPs dispersions were dropped onto copper TEM grids (400 mesh, carbon coated), blotted and allowed to air dry at room temperature. Size determinations were carried out using ImageJ using 60 nanoparticles.

3.2.2 Materials. Most reagents including triethylamine (Et_3N, 99.5%), carbonyl diimidazole (CDI, ≥ 90%), 2-hydroxyethyl methacrylate (HEMA, ≥ 99%), acetyl chloride (≥ 98%), ethylene glycol vinyl ether (≥ 97%), pyridinium p-toluenesulfonate (PPTS, 98%), Nile Red (NR), doxorubicin (Dox, -$NH_3^+Cl^-$ form, >98%), Tris(2-pyridylmethyl)amine (TPMA, 98%), tin(II) 2-ethylhexanoate (Sn(II)$(EH)_2$, 95%), and deuterium chloride solution (DCl, 35 wt% in D_2O) were purchased from Sigma-Aldrich and used as received. Poly(ethylene glycol) monomethyl ether

(PEG, MW = 5000 g/mol, EO# = 113) was dried by azeotropic distillation with toluene to remove residual moisture. An acetal-labeled bromine-functionalized PEG (PEG-AC-Br) was synthesized according to our previous publications.[224]

3.2.3 Synthesis of ACMA. In the first step to synthesize acetyl vinyl ether (ACVE), acetyl chloride (9.7 g, 123 mmol) was added dropwise to a solution containing vinyl ether ethylene glycol (9.1 g, 103 mmol) and Et_3N (12.5 g, 123 mmol) dissolved in anhydrous dichloromethane (DCM, 200 mL) in an ice-bath for 20 min. The resulting mixture was stirred at room temperature overnight. After the removal of formed by-products (Et_3N-HBr adducts) by vacuum filtration, additional DCM (150 mL) was added. The mixture was washed with brine and distilled water (150 mL) six times and then dried over sodium sulfate. After removal of the solvent by rotary evaporation, the product was dried in vacuum oven overnight. Light-yellow residue with yield = 12.2 g (91%); R_f = 0.55 on silica (7.5/2.5 v/v hexane/ethyl acetate).

In the second step to synthesize acetyl methacrylate (ACMA), HEMA (4.4 g, 33.8 mmol) was added dropwise to a clear solution of ACVE (4.4 g, 33.8 mmol) and PPTS (0.84 g, 3.38 mmol) dissolved in anhydrous DCM (60 mL) in an ice-bath for 20 min. The reaction mixture was stirred vigorously overnight at room temperature and then quenched by the addition of Et_3N (0.5 mL). After being washed with phosphate buffered saline (PBS, pH 7.4, 200 mL) three times, the product was purified by silica gel column chromatography using hexane/ethyl acetate (2/1 v/v). The product was collected as the second of the total two bands off a silica gel column and then dried for 24 hours. Yellow oil with yield = 3.3 g (38%); R_f = 0.42 on silica (7.5/2.5 v/v hexane/ethyl acetate).

3.2.4 Synthesis of carbonyl imidazole methacrylate (CIMA). HEMA (6 g, 46.1 mmol) was added dropwise to a clear solution containing CDI (9.9 g, 61.3 mmol) and anhydrous DCM (120 mL) in an ice bath for 20 min. The reaction mixture was stirred vigorously for 18 hrs at room temperature, and then washed with distilled water (100 mL) three times, and then dried over sodium sulfate. After removal of the solvent by rotary evaporator, the product was dried by vacuum oven for 12 hours. Colorless oil with yield= 10.3 g (99.2%); R_f = 0.42 on silica (7.5/2.5 v/v hexane/ethyl acetate).

3.2.5 Synthesis of P1 and P2 block copolymers by ATRP. To synthesize P1, PEG-AC-Br (0.25 g, 0.047 mmol), ACMA (0.74 g, 2.84 mmol), TPMA (0.5 g, 7.1 μmol), [Cu(II)TPMA-

Br]Br (0.5 g, 2.4 μmol), and anisole (2.5 g) were mixed in a 25 mL Schlenk flask and deoxygenated by nitrogen purging for 1 h in an oil bath heated to 40 °C. Following purging in nitrogen, a pre-purged solution of $Sn(II)(EH)_2$ (8 mg, 19.0 μmol) in anisole was injected into the Schlenk flask to initiate polymerization. Polymerization was stopped by cooling down the solution to room temperature in an ice bath and exposing it to air. For purification, the as-synthesized polymer was dissolved in acetone passed through a basic alumina column to remove residual copper species. After the removal of the solvent by rotary evaporation at room temperature, the product was isolated by precipitation from hexane and dried in a vacuum oven at room temperature for 15 hrs.

For the synthesis of P2, a similar procedure was used except for the use of PEG-AC-Br (0.14 g, 0.026 mmol), ACMA (0.35 g, 1.34 mmol), CIMA (0.05 mg, 0.23 mmol), TPMA (1.15 mg, 3.96 μmol), [Cu(II)TPMA-Br]Br (6.8 mg, 1.31 μmol), anisole (0.9 g), and $Sn(II)(EH)_2$ (4.3 mg, 10.5 μmol).

3.2.6 Determination of CMC using a NR probe. A stock solution of NR in tetrahydrofuran (THF) at 1 mg/mL and stock solutions of P1 or P2 in THF at 1 mg/mL and 0.1 μg/ml were prepared. Water (10 mL) was then added dropwise into mixtures consisting of the same amount of the stock solution of NR (0.5 mL, 0.5 mg NR) and various amounts of the stock solution of P1 and P2. The resulting dispersions were stirred for 24 hrs to remove THF, and then were subjected to filtration using 0.45 μm polyethersulfone (PES) filter to remove excess NR. A series of NR-loaded micelles at various concentrations of P1 or P2 ranging from 10^{-6} to 0.1 mg/mL were formed. From their fluorescence spectra recorded with λex= 480 nm, the fluorescence intensity at maximum λem = 620 nm was recorded.

3.2.7 Aqueous micellization by nanoprecipitation method. PBS (pH = 7.4, 10 mL) was added dropwise to an organic solution of copolymer dissolved in THF (2 mL) using a syringe pump equipped with a plastic syringe (20 mL volume, 20 mm diameter) at an addition rate of 0.2 mL/min. The resulting dispersion was dialyzed against PBS solution (1 L) twice for 24 hrs, yielding aqueous micellar dispersion at 1 mg/mL concentration.

3.2.8 Investigation of acidic pH-responsive degradation. The aliquots of P1 or P2 (0.02 g) were dissolved in DMF (3 mL), mixed with 20 μL of HCl, and stirred for 24 hrs and GPC

analysis was followed. For ^{1}H-NMR analysis of P1, its aliquot (0.01 g) was dissolved in DMSO (1 mL) and mixed with DCl (10 μL).

An aqueous dispersion of P1-based nanoassemblies was formed in PBS (pH = 7.4) as described above. They were mixed with acetate buffer (pH = 5.3) to bring the final concentration of polymer in the dispersion to 1.7 and 0.06 mg/mL. After 72 hrs stirring at room temperature, the residues were dried and then analyzed by GPC.

3.2.9 Preparation of aqueous Dox-loaded micelle dispersions (Dox-NPs). An organic solution consisting of Dox (2 mg), Et_3N (5 μL), and P1 or P2 (20 mg) in DMF (1.6 mL) was mixed with PBS at pH = 7.4 (10 mL) under magnetic stirring. The resulting mixture was placed in a dialysis tubing (molecular weight cut off (MWCO) = 12000 g/mol) for dialysis over PBS (1 L) for 24 hrs. The formed dispersion was passed through 0.45 μm PES filter, yielding aqueous Dox-loaded micelle dispersion. To determine the loading capacity of Dox using UV/vis spectroscopy, an aliquot of aqueous Dox-loaded micelle dispersion (1 mL) was mixed with DMF (5 mL) to form a clear solution. After being passed through 0.25 μm PTFE filter, its UV/vis spectrum was recorded. The loading capacity was determined by the weight ratio of loaded Dox to P1 or P2.

3.2.10 Acidic pH-responsive Dox release from aqueous Dox-NPs. Aliquots of Dox-NPs (1.4 mg/mL, 2 mL) were transferred into dialysis tubing (MWCO = 12,000 g/mol) and immersed in outer buffer solutions (40 mL and 150 mL) prepared under various conditions: aqueous PBS at pH = 7.4 and aqueous acetate buffer solution at pH = 5.3. Aliquots of the outer buffer solutions (3.5 mL) were taken, and their fluorescence spectra were recorded at λ_{ex} = 470 nm. The equal volume of fresh buffer was added to keep the same volume of outer buffer.

3.2.11 *In vitro* cytotoxicity and cellular uptake. In a 96-well plate, HeLa cells (6000 cells/well) were seeded and incubated at 37 °C in Dulbecco's Modified Eagle Medium (DMEM) (100 μL) containing 10 vol% fetal bovine serum (FBS) and 1 vol% penicillin-streptomycin solution. Viability of HeLa cells by Alamar Blue assay and cellular uptake by fluorescence microscopy were measured as described in our previous publication.[244]

3.3 Results and discussion

3.3.1 Synthesis of P1 and P2 block copolymers. Our experiment began with the synthesis of a methacrylate monomer bearing a pendant acetaldehyde acetal linkage (ACMA), as depicted in Figure A1. Our careful analyses by ^{1}H-NMR (Figure A1), ^{13}C-NMR (Figure A2 and A3), and mass spectroscopy (m/z experimental for $(ACMA+Na)^{+}$= 283.11474) confirmed the successful synthesis of ACMA at 38% yield. After synthesis and characterization, ATRP[251, 252] was examined to synthesize well-controlled acid-degradable diblock copolymers with acetal linkages positioned in dual locations at the block junction and in the hydrophobic block. As illustrated in Figure 3.2, a PEG bearing bromine and an acetal linkage (PEG-AC-Br) (AC: acetaldehyde acetal) was used as a macroinitiator for ATRP of ACMA to synthesize P1 (without imidazole pendants) and a mixture of ACMA with CIMA for P2 (with imidazole pendants). Activators ReGenerated by Electron Transfer (ARGET) process for ATRP was employed with TPMA/Cu(II)Br_2 active catalyst complex and $Sn(EH)_2$ as the reducing agent to convert Cu(II) to Cu(I) and to initiate polymerization at 40 °C. The initial mole ratio of $[monomer(s)]_o/[PEG\text{-}AC\text{-}Br]_o$ was set to be 60/1 as the DP at complete monomer conversion. Polymerizations were stopped when conversions reached greater than 80%. After purification, which was achieved by passing the crude product through a basic aluminum oxide column to remove residual Cu species, followed by precipitation in hexanes to remove unreacted monomers, the copolymers were analyzed for their chemical structures with ^{1}H-NMR and their molecular weight by GPC. Table A1 summarizes the characteristics and properties of P1 and P2.

P1 is a PEG-based diblock copolymer with a PACMA homopolymer block, thus it is abbreviated as PEG-AC-PACMA. Its ^{1}H-NMR in Figure 3.3a shows the presence of acetal moieties at 1.3 ppm (c) and 4.8 ppm (b) as well as ethylene oxide moieties (EO and a) at 3.5-3.7 ppm. Using the integral ratio of these peaks with the DP = 113 for the PEG block, the DP of the PACMA block was determined to be 57. This value is slightly larger than the theoretically estimated DP = 49 determined by ^{1}H-NMR spectroscopy at 82% monomer conversion. GPC analysis confirms that P1 had the molecular weight as the number average molecular weight (M_n) = 28 kg/mol and $Đ$ = 1.13 (Figure A4). Its GPC trace clearly evolved to the high molecular weight region with negligible PEG-AC-Br macroinitiator residue.

P2 is a PEG-based diblock copolymer with P(CIMA-co-ACMA) random copolymer block, thus it is abbreviated as PEG-AC-P(CIMA-co-ACMA). A 15 mol% CIMA (i.e., pendant imidazole groups) of total methacrylates in the feed was chosen based on the reported result.[187] ^{1}H-NMR in Figure 3.3b shows the presence of imidazole rings at 7.1-8.3 ppm (j, k, l), along with the presence of pendant acetal linkages and EO moieties. In a similar way, ^{1}H-NMR analysis allows the determination of the DP of CIMA units to be 11 and ACMA units to be 51, corresponding to 15.7 mol% of pendant imidazole groups. The synthesized P2 had M_n = 28.6 kg/mol with $Đ$ = 1.21 by GPC analysis.

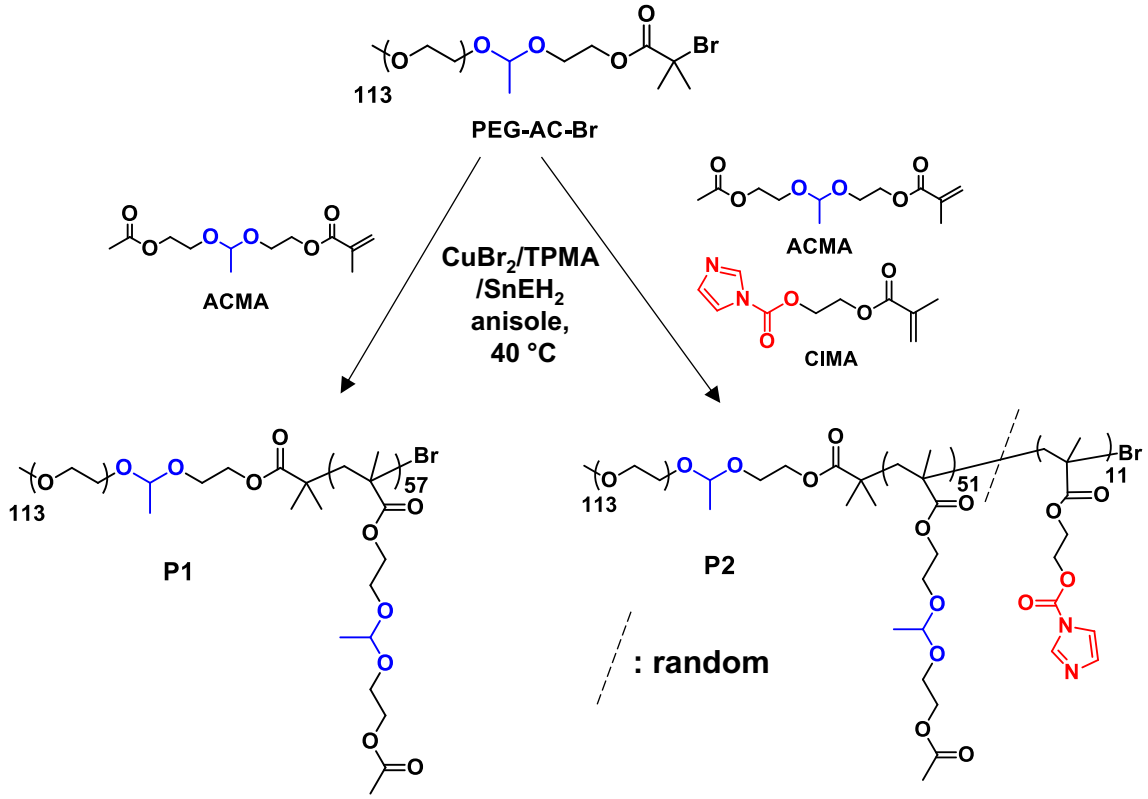

Figure 3.2 Synthesis of P1 and P2 by ATRP.

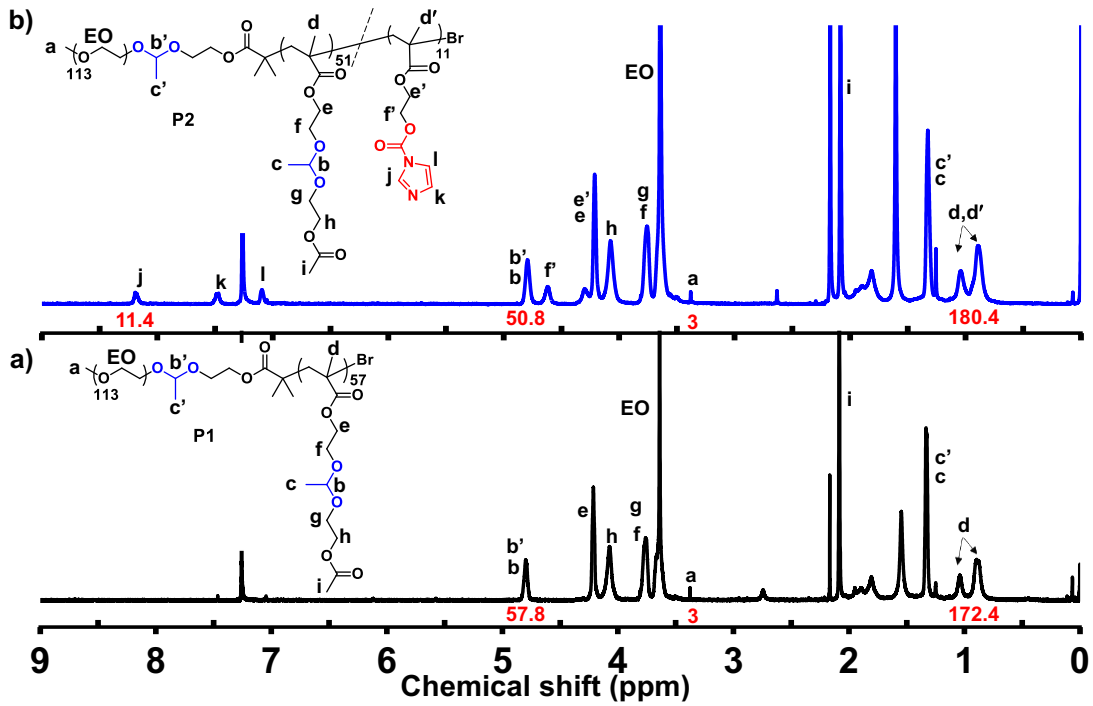

Figure 3.3 ^{1}H-NMR spectra in $CDCl_3$ for P1 (a) and P2 (b).

3.3.2 Aqueous micellization and colloidal stability. The synthesized P1 and P2 were first characterized for their aqueous micellization. Their CMC was determined using the fluorescence spectroscopy technique with a NR probe as described in our previous publications. A fluorescence intensity plot at 620 nm was constructed with increasing concentrations of P1 (Figure A5) and P2 (Figure A6). Using the extrapolation of two linear regressions in the lower and higher concentration regions, the CMC values were determined to be 16 µg/mL for P1, which is greater than the CMC value of P2 (13 µg/mL). In the view of the core hydrophobicity, the CMC is expected to be greater for P2 than P1, since the P2 core could be more hydrophilic due to the presence of pendant imidazole groups. The plausible reason for the lower CMC value of P2 is the presence of aromatic imidazole pendants that increase π-π interactions with NR molecules, as suggested in the other literatures.[247, 248]

At concentrations above the CMC, amphiphilic P1 and P2 copolymers self-assembled to form nanoassemblies (or micelle aggregates) in aqueous solution. Dialysis method was used to form nanoassemblies in PBS solution (pH = 7.4) at 1 mg/mL. DLS analysis confirmed that P1-micelles had a hydrodynamic diameter of 40 nm with a negligible population of large aggregates (<1%), while P2-micelles had a multimodal distribution, and their major population had a diameter of 62 nm (Figure A7). Note that the P2 micelles became turbid and unstable after 3

days, which could be attributed to a possible cleavage of imidazole groups even in the phosphate buffer solution.

3.3.3 Acid-catalyzed degradation of P1. P1 copolymer labeled with an acetal linkage at the block junction and pendant acetals in the hydrophobic block (no pendant imidazole groups) was first examined. Upon the cleavage of the acetal linkages in acidic pH, P1 degrades to PEG-OH, PHEMA-OH, acetyl ethylene glycol and acetaldehyde (Figure 3.4a). To get an insight into the acid-catalyzed degradation, we conducted the experiment in an organic solution where P1 chains are dissolved in macromolecular levels. For GPC analysis, an aliquot of P1 was incubated in acidic DMF at room temperature for 24 hrs. As shown in Figure 3.4b, the GPC diagram became bimodal and shifted to the lower molecular weight region, with a significant decrease in molecular weight from M_n = 28 to 14 kg/mol. A shoulder in the low molecular weight region appeared to overlap with the PEG-AC-Br precursor. Furthermore, P1 was incubated with DCl in DMSO-d_6 ([DCl] = 0.32 M) for ^{1}H-NMR analysis. As seen in Figure 3.4c, a peak at 9.6 ppm corresponding to acetaldehyde (highlighted with light orange as a degraded product) newly appeared, while the peak at 1.3 ppm (highlighted with grey) that was assigned to the methyl group of the acetal moieties decreased. Using the integral ratios, >88% of acetal linkages is cleaved in the given acidic condition.

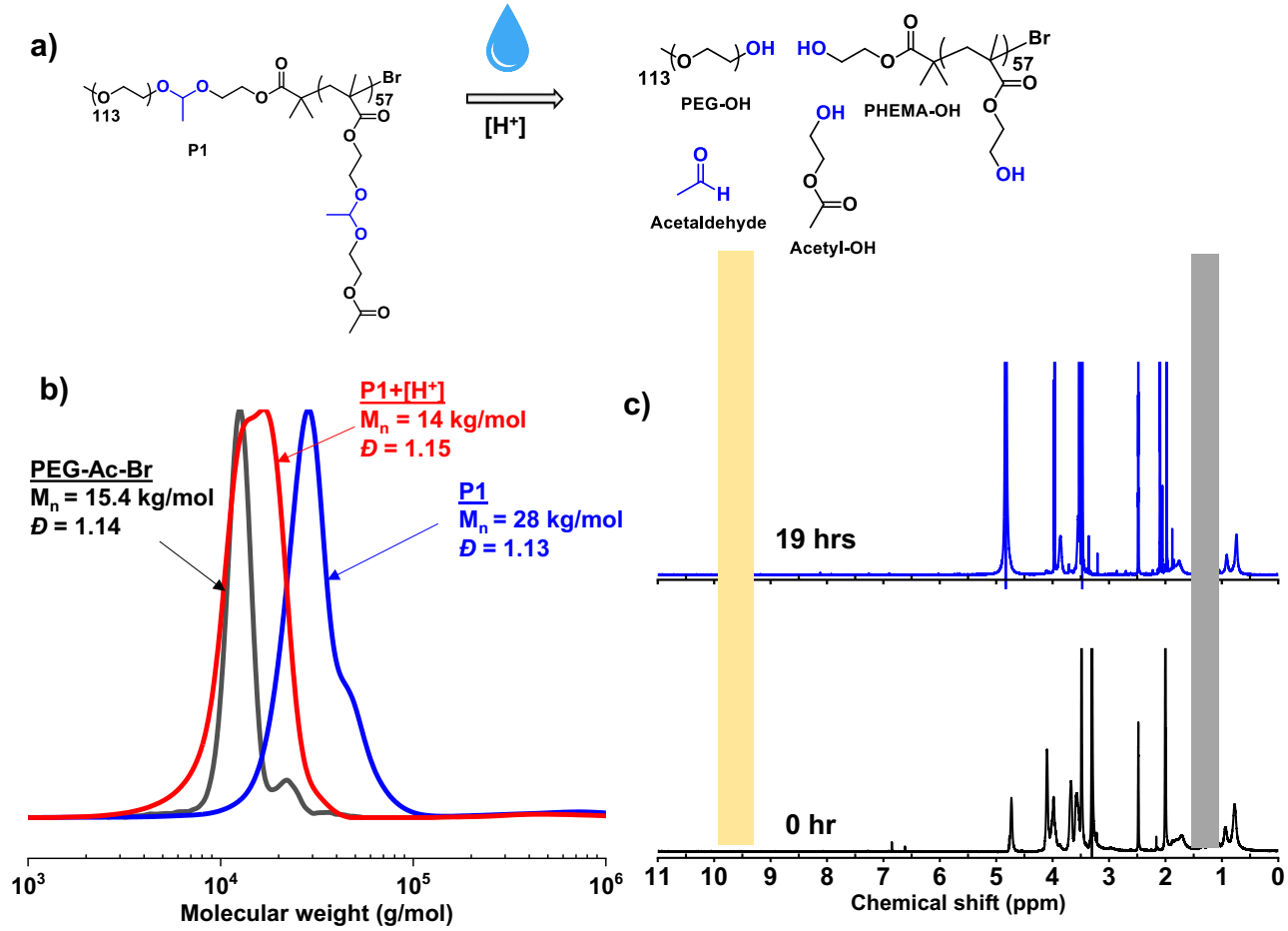

Figure 3.4 For P1, schematic illustration of acidic-responsive degradation (a), GPC diagrams before and after treatment with HCl (20 μL) in DMF, compared with that of the PEG-AC-Br macroinitiator (b), and ^{1}H-NMR spectra before and 19 hrs after treatment with DCl (10 μL) in DMSO-d_6 (c).

Given this preliminary result in a homogeneous solution, we investigated the acid-catalyzed degradation of P1 in aqueous micelles forms. We investigated the effect of the concentration of P1 in a given volume of aqueous solution on the acid-catalyzed degradation of P1 upon the cleavage of acetal linkages. In a given acidic pH (i.e., given proton concentration), the mole ratio of the proton to acetal linkage becomes greater at a lower concentration of P1. Such a higher mole ratio could lead to more rapid hydrolysis of acetal linkages. To test our hypothesis, an aliquot of P1 was dissolved in aqueous acetate buffer solution at pH = 5.3 whose concentrations were adjusted to 1.7 and 0.06 mg/mL. The mole equivalent ratio of proton/acetal is calculated to be 21.5 at 0.06 mg/mL, which is much greater than 0.75 at 1.7 mg/mL. After 72 hrs incubation, their degradation was monitored by GPC. As shown in Figure 3.5a, the GPC diagram of P1 remained unchanged at 1.7 mg/mL (higher P1 concentration), suggesting no significant cleavage

of acetal linkages in both acidic conditions. At 0.06 mg/mL (28 times lower than 1.7 mg/mL), its molecular weight distribution became bimodal and shifted to the lower molecular weight region with the appearance of a shoulder corresponding to the PEG precursors. The change in molecular weight distribution can be attributed to the cleavage of acetal linkages both in hydrophobic cores and at core/corona interfaces. These results demonstrate the importance of polymer concentration (e.g. mole equivalent ratio of proton/acetal) in acid-catalyzed hydrolysis of acetal and subsequent polymer degradation. However, the quantitative analysis of the cleavage of acetal linkages at block junction and in pendant chains was not straightforward.

3.3.4 Acid-catalyzed degradation and crosslinking of P2-based nanoassemblies. Given our results of the P1 micelles, the degradation of P2 (having 15.7 mol% pendant imidazole groups) in the micellar form at 1.7 mg/mL (higher concentration) was examined in aqueous acetate buffer solutions at pH = 5.3. As seen in Figure 3.5b, when P2 micelles were incubated at pH = 5.3 for 72 hrs, its molecular weight distribution became multimodal with the appearance of two peaks: the peak equivalent to the PEG species in lower molecular weight region as well as the multiple shoulders in the higher molecular weight region. Compared with P1 showing no change in its molecular weight distribution at 1.7 mg/mL (see Figure 3.5a), this result suggests that the incorporation of imidazole pendants promotes the hydrolysis of acetal linkages not only in the core but also at the interfaces. The cleavage of acetal groups at the interfaces sheds the PEG coronas from the hydrophobic cores, loosening polymer chains in the cores and generating hydrophilic pores. This process could facilitate the access of hydronium ions to acetal linkages in the cores, which can further accelerate the cleavage of acetal groups. GPC analysis for P2 at a lower concentration (0.06 mg/mL) was not straightforward because of the more rapid and intensive degradation, followed by crosslinking to form larger-sized branched and gel-like species.

Another interesting aspect to acidic degradation of P2 micelles is the occurrence of crosslinking in micelle cores in an acidic condition. The GPC diagrams in Figure 3.5b show multiple shoulders in the higher molecular weight region (>10^5 g/mol), which could be highly branched or gel-like species. As proposed in Figure 3.5c, such high molecular weight species could be formed through the reaction of reactive imidazole with pendant hydroxyl groups generated through the cleavage of acetal groups in acidic pHs, leading to the occurrence of crosslinking in degraded micelle cores. In an aqueous environment, the nanoassemblies could be

disintegrated (or destabilized) upon the cleavage of acetal linkages and protonation of pendant imidazole groups as well as the occurrence of core crosslinking. This combined process could result in unexpected aggregation.

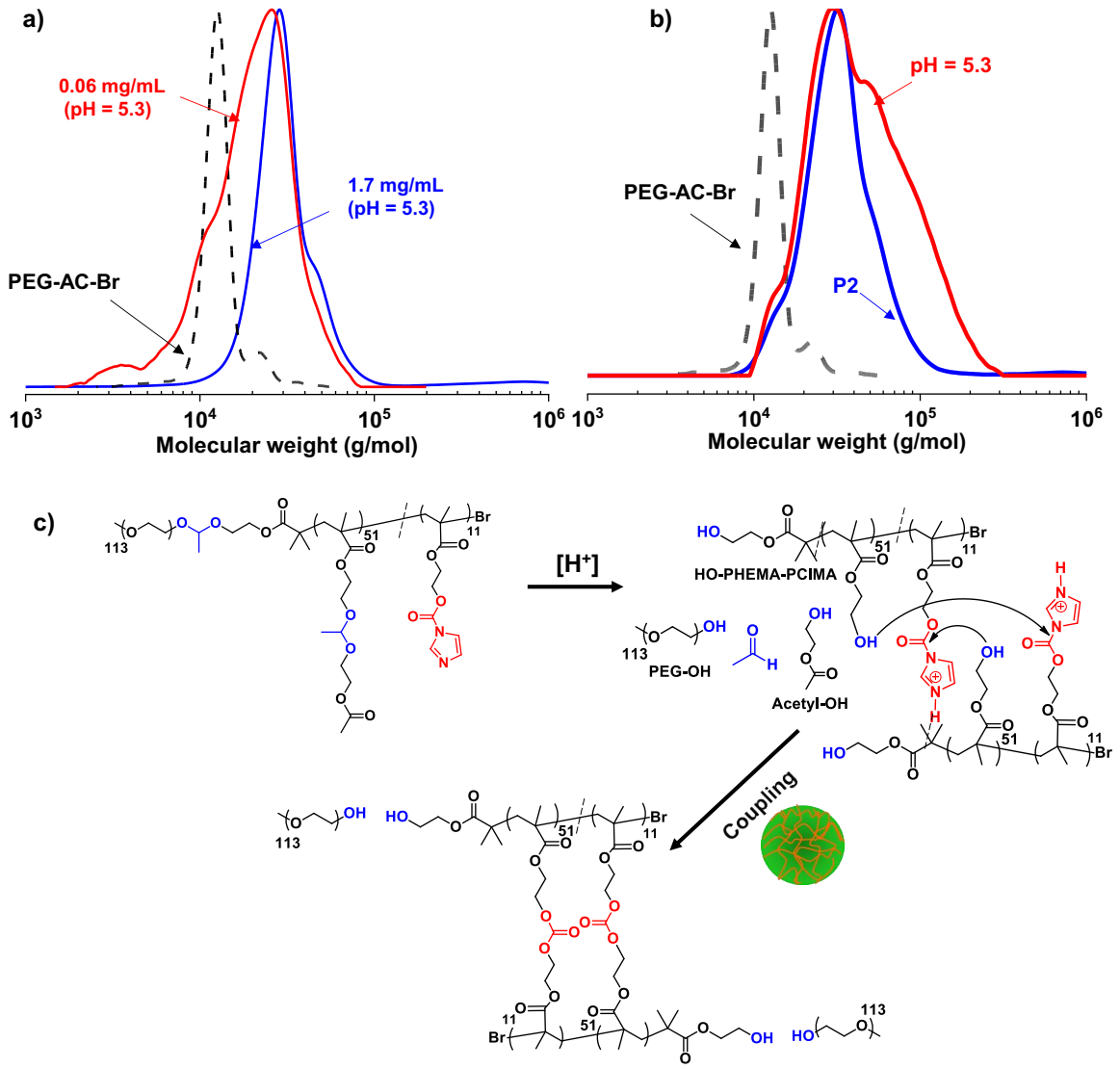

Figure 3.5 Acid-catalyzed degradation of P1 and P2 nanoassemblies in aqueous acetate buffer solution at pH = 5.3. GPC diagrams of P1 before and after 72 hrs incubation at 1.7 and 0.06 mg/mL, compared with PEG-AC-Br precursor (a); GPC diagrams of P2 nanoassemblies at 1.7 mg/mL before and after 72 hr incubation, compared with PEG-AC-Br precursor (b); and schematic illustration of crosslinking for P2 micelles during acid-catalyzed degradation (c).

3.3.5 Encapsulation of Drug molecules. Dox (a clinically-used anticancer drug) was used for encapsulation using a dialysis method. An organic solution of Dox was treated with Et_3N in DMF to form neutral forms of Dox and then mixed with PBS (pH = 7.4) *via* stirring. The

resulting mixture was subjected to intensive dialysis over PBS to remove free (not encapsulated) Dox, yielding Dox-loaded micelles (Dox-NPs) at 1.4 mg/mL. After filtration to remove unexpectedly-formed aggregates, the formed Dox-NPs were characterized for their sizes and morphologies (Figure 3.6a and 3.6b). DLS analysis confirms the diameter by volume to be 45.3 nm (PDI = 0.25) for P1-Dox-NPs and 61 nm (PDI = 0.18) for P2-Dox-NPs. Note that the latter is larger by 20 nm, which could be due to the presence of imidazole in the cores. TEM analysis suggests that the dried Dox-NPs appeared to be spherical. Unfortunately, our efforts to determine their mean diameters were not conclusive due to the poor quality of the images. To determine the loading capacity of Dox, their UV/Vis spectra were recorded in a mixture of DMF/water = 5/1 (v/v) (Figure A8). Using the Beer-Lambert equation with absorbance and the pre-determined extinction coefficient of Dox (12,400 M^{-1} cm^{-1}) at 620 nm,[46] the loading capacity of Dox was determined to be 1.1% for P1 and 4% for P2. The greater loading capacity of P2 could be attributed to π-π interaction and hydrogen bonding of the Dox molecules and the imidazole rings.[247, 253]

3.3.6 Acid-responsive Dox release. Aliquots of P1 Dox-NPs in dialysis tubing were placed in an outer buffer solution at pH = 5.3 (mimic to endo/lysosomal pH) and pH = 7.4 at 70 μg/mL of Dox-NPs. Dox molecules released from Dox-NPs could be diffused out of a dialysis tubing to the outer buffer solutions. Under sink condition, fluorescence spectroscopy was used to determine the cumulative %Dox release using a pre-determined Dox calibration curve at λ_{max}= 593 nm reported in our previous publication.[223] As seen in Figure 3.6c, Dox was slowly released, reaching 13% after 190 hrs at pH = 7.4 (no acid), which is mainly attributed to natural leak. At pH = 5.3, %Dox release is faster, compared at pH = 7.4; however, it gradually increased, reaching 45% in 190 hrs. Such a slow release could be the result of the slow hydrolysis of acetaldehyde acetal linkages at the given concentration. This result appears to be similar to those reported for other types of copolymer micelles labeled with acetaldehyde acetal linkages.[92, 231, 254] However, rapid Dox release with acetaldehyde acetal is also reported; >70% Dox release in 60 hrs in pH = 5 from micelles based on a triblock copolymer of PCL and PEG having acetaldehyde acetal linkage at the block junctions.[159] Such discrepancy in drug release for the acetaldehyde acetal-bearing copolymer micelles could be attributed to the difference in experimental conditions such as concentration of the copolymers.[114, 177] To investigate the effect of concentration of Dox-NPs on its release profile, the Dox release experiment was conducted at a

lower concentration, 20 μg/mL. As seen in Figure 3.6d, at pH = 7.4, %Dox reached 25%, which is larger than the %Dox release (13%) in 70 μg/mL polymeric concentration. As expected, rapid Dox release was observed at acidic pH = 5.3, with an accelerated drug release within 10 hrs (up to 60% release) and a gradual release in 72 hrs (> 95% release).

P2 was also evaluated for the Dox release under similar conditions. P2 had %Dox release similar to P1 in 70 μg/mL (Figure 3.6c). Interestingly, its %Dox release was slower than P1 in 20 μg/mL (lower concentration) (Figure 3.6d). Given the faster degradation of P2 compared to P1 in the acidic environment, there could be various opposing effects that contribute to the delayed drug release of P2. In addition to the degradation of P2-Dox-NPs upon the cleavage of acetal linkages both in the cores and at the core/corona interfaces, the protonation of pendant imidazole groups could result in a rapid shift from hydrophobicity to hydrophilicity, leading to rapid Dox release. Furthermore, the protonation of amino groups of Dox molecules could induce enhanced Dox release from protonated imidazole-containing P2 nanoassemblies. However, the occurrence of core-crosslinking could impede drug release since the formed networks introduce steric barriers that can slow down the diffusion of Dox molecules. Additionally, there could be a possibility that Dox molecules react with pendant imidazole groups, which results in the covalent conjugation of Dox to the copolymers. Overall, our release profiles of encapsulated Dox at acidic pH were distinct from those at pH = 7.4 for both P1 and P2-Dox NPs.

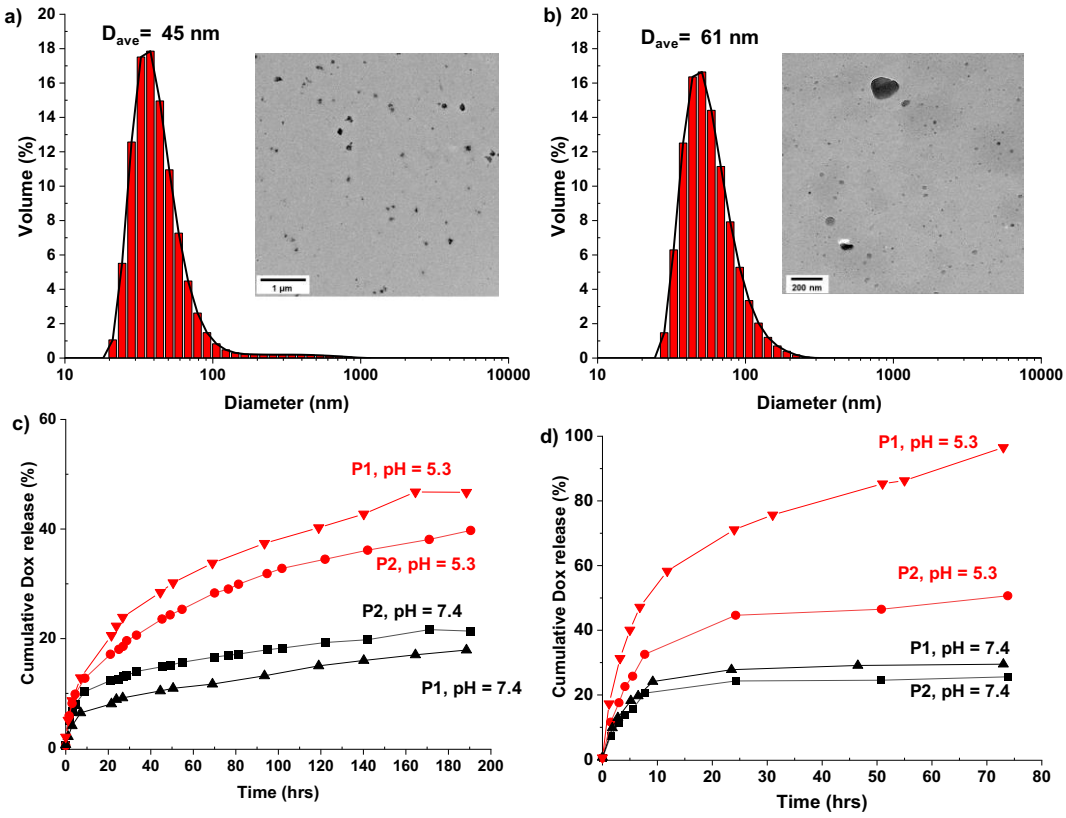

Figure 3.6 DLS diagram and TEM image of Dox-NPs of P1 (a) and P2 (b) and %Dox release at pH = 7.4 and 5.4 in 70 μg/mL (c) and 20 μg/mL (d) for Dox-NPs of P1 and P2.

3.3.7 *In vitro* anti-tumor activity and intracellular trafficking of Dox-NPs. Given our promising results of acid-responsive degradation and enhanced Dox release kinetics, the P1 and P2 nanoassemblies were further investigated to see their feasibility for effective intracellular drug delivery targeting tumors. It is important that the empty nanocarriers are non-toxic to cells, while Dox-NPs should retain anti-tumoral activity. Figure 3.7a shows that the viability of HeLa cells determined by Alamar Blue Assay was greater than 80% in the presence of empty P1 and P2 micelles, suggesting they are not toxic to the cells up to a concentration of 500 μg/mL. Promisingly, the viability of HeLa cells decreased when the concentration of both Dox NPs increased (Figure 3.7b). Note that free Dox appeared to be more potent, compared to P1 and P2 Dox-NPs, possibly due to its easier penetration into the cells. In our experiment, IC_{50} was determined to be 0.28 μg/mL for free Dox, which is lower than 1.1 μg/mL for P1-Dox-NPs, and 1.2 μg/mL for P2-Dox-NPs.

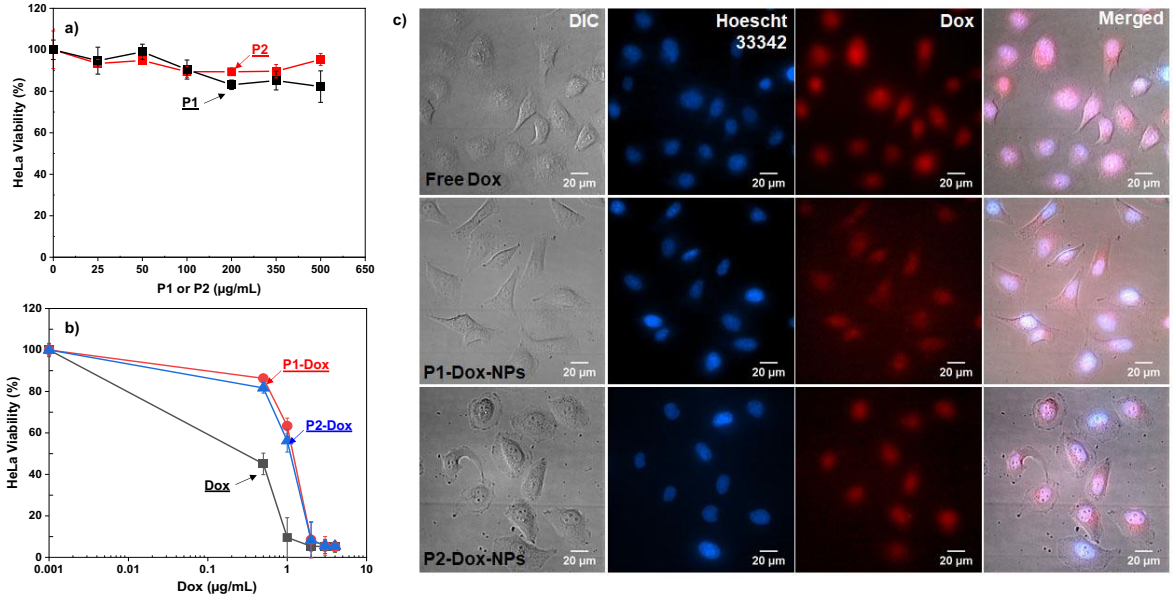

Figure 3.7 For P1 and P2 copolymers, viability of HeLa cells incubated with empty micelles (a) and Dox-NPs (b), compared with free Dox for 48 hrs, determined by Alamar Blue Assay; time-lapse fluorescence microscopy images of HeLa cells incubated with Dox-NPs (encapsulated Dox = 2.5 μg/mL), compared with free Dox (2.5 μg/mL) for 4 hrs (c). Scale bar = 20 μm.

Cellular uptake of Dox-NPs was investigated using fluorescence microscopy. Figure 3.7c shows the fluorescence images of HeLa cells after 4 hrs of incubation with P1-Dox-NPs and P2-Dox-NPS, along with free Dox. The nuclei were stained with Hoechst 33342 is shown in blue and Dox fluorescence is shown in red. Although free Dox had greater cellular uptake, both P1 and P2 Dox-NPs show strong Dox signals in the nuclei, suggesting that they were taken by cells through endocytosis. The presence of pendant imidazole at pH = 7.4 (close to its pKa = 6.7) could facilitate the endocytosis of P2-Dox-NPs. However, their larger size over P1-Dox-NPs could induce delayed endocytosis. Due to the competing effects, the two nanoparticles have similar the cellular entry. Overall, empty P1 and P2 NPs and their Dox-NPs exhibit no significant difference in cytotoxicity and cellular uptake.

3.4 Conclusion

We synthesized dual location acid-responsive degradable block copolymers labeled with acetaldehyde acetal linkages at the block junction and as pendant chains in the hydrophobic block with and without pendant imidazole groups by ATRP in the presence of an acid-cleavable bromine macroinitiator. Due to their amphiphilicity, these block copolymers self-assembled to form spherical nanoassemblies where acetal linkages are positioned in dual locations, both at the

interfaces and in micelle cores. Their degradation was driven by acid-catalyzed hydrolysis of acetal linkages and could be promoted with acetal linkages positioned in dual locations. Additionally, their kinetics for acid-catalyzed degradation and release of encapsulated Dox molecules were significantly influenced by block copolymer concentration and pH. An integration of imidazole pendants rendered micelle cores to be hydrophilic and sensitive to environments while improving the loading capacity of Dox, an aromatic drug, through π-π interactions. It enhanced the hydrolysis of acetal linkages located both in the micelle cores and at the interfaces; however, it induced crosslinking in micelle cores, which impeded Dox release. Such competing processes can affect acid-catalyzed Dox release kinetics. Promisingly, dual location acid-degradable nanoassemblies with and without pendant imidazole groups show biocompatibility, anti-cancer activity, and cellular uptake with HeLa cancer cells.

Chapter 4: Dual location dual acidic pH/reduction-responsive degradable block copolymers prepared *via* ATRP

4.1 Introduction

In recent years stimuli-responsive (or smart) copolymers and particularly block copolymers have emerged as promising building blocks of choice in the construction of advanced nanomaterials for the plethora of applications in nanoscience, nanotechnology, and pharmaceutic science.[65, 255-260] Upon being triggered by external stimuli, these stimuli-responsive copolymers undergo either a physical or a chemical transition, depending on the nature of stimuli-responsive moieties (or groups) within the structures. In comparison with a physical transition leading to a change in volume or phase in response to physical stimuli (mostly, temperature and pH),[261-263] chemical transition involves the incorporation of cleavable (or labile) covalent bonds into the design of block copolymers. So-called stimuli-responsive degradable copolymers degrade to their appropriate products upon the cleavage of labile linkages when chemical or biological stimuli present.[26, 28, 64] As a consequence, SRD polymers, particularly those with amphiphilic properties (called SRD-exhibiting ABPs) and their self-assembled nanoassemblies have been specifically studied for on-demand drug delivery.[27, 68, 264] Acidic pH, light, reductive, oxidative, and enzymatic reactions are typical stimuli of great interest and promises that can cleave the corresponding labile linkages. In particular, acidic pH has received increasing attention owing to the slightly acidic pH of the tumor microenvironment (pH = 6.5-6.9) as well as endosomes and lysosomes (pH = 4.5-6.5) as compared to normal tissues (pH = 7.4).[74] Acetal, ketal, orthoester, hydrazone, imine, and β-thiopropionate are typical acidic pH-labile linkages.[31] In addition to acidic pH, the reductive reaction has been extensively explored with unique disulfide linkage as a promising reduction-responsive degradable linkage.[40, 69, 193] In biological environments, cellular GSH presents at millimolar concentrations (≈10 mM) in the intracellular compartment, compared with that (<10 μM) in the extracellular compartment, and further, elevated concentration (3-4 times) in tumor tissues and cancer cells.[38]

Given numerous strategies to synthesize novel SRD block copolymers labeled with a single type of cleavable linkages exhibiting single stimulus-response,[66, 67, 265] an increasing attention has been drawn on stimuli-responsive block copolymers that can be triggered by two or more stimuli.[102-104] Such dual or multi-stimuli-responsiveness displays analogous features to natural

macromolecules within the body, whose behavior is governed by cumulative effects of stimuli, rather than a single factor. Various strategies that have enabled the synthesis of dual- and multi-stimuli-responsive block copolymers have been reviewed.[29, 105, 106] Most strategies have utilized a combination of chemical, biological, and physical stimuli. Despite these advances, the development of SRD-block copolymers having only stimuli-responsive cleavable (degradable) linkages is more promising because of the propensity to complete and controlled disassembly or chemical degradation of nanoassemblies.[230, 231, 266, 267] Furthermore, dual and multiple stimuli-responsive degradable block copolymers which can be triggered by two endogenous acidic pH and reduction are in high demand.[268]

A few examples of dual acidic pH/reduction-responsive degradable (or cleavable) block copolymers have been demonstrated, where acidic pH-cleavable linkages are positioned in the side chains of hydrophobic blocks[210, 269] or as crosslinks,[199, 200, 207, 208] thus single location. Other block copolymers were also synthesized with acidic pH-labile acetal or benzoic imine linkage positioned at the junction of hydrophilic and hydrophobic blocks. However, they were brush-type block copolymers[213-216] and liner PCL-based triblock copolymers[217] with a single disulfide linkage positioned in the center of the main chains. To the best of our knowledge, no reports describe a dual acidic pH/reduction-responsive degradable block copolymer comprising a ketal group at the block junction and disulfide pendants in the hydrophobic blocks. The copolymer self-assembles to nanoassemblies with multiple disulfide linkages in the cores and ketal linkage at the core/corona interfaces, thus attaining dual location dual acidic pH/disulfide-responsive degradation. Such a strategy can offer versatility in that multi-stimuli responses to each stimulus can independently and precisely regulate the release of encapsulated biomolecules at dual or multiple locations.[270] Compared with acetals and other acid-labile linkages, the ketal group has very rapid hydrolysis kinetics in the acidic environment, particularly acidic pH, thus leading to rapid hydrolysis rate and unique degradation pattern.[90] However, its degradation can be varied with substituents as well as their hydrophobic-hydrophilic environments in the copolymers where they are situated.[89, 91, 184]

In this work, we have investigated a new strategy utilizing ATRP to synthesize a dual location dual acidic pH/reduction-responsive degradable block copolymer (DLDSRD). The diblock copolymer is composed of a hydrophilic PEG block covalently conjugated through a ketal linkage with a hydrophobic polymethacrylate block having pendant disulfide linkages

(PHMssEt), thus PEG-ketal-PHMssEt block copolymer. The strategy requires the synthesis of a novel PEG-based bromine macroinitiator labeled with a ketal linkage (PEG-ketal-Br) for the ATRP of HMssEt. A robust route with multiple steps utilizing the carbamate chemistry, which was stable to hydrolytic conditions and protection/deprotection chemistry, allowed for the synthesis of the macroinitiator. Other routes were also investigated to understand the unexpected side reactions associated with the high sensitivity of ketal linkage. A series of ATRP of HMssEt in the presence of the synthesized PEG-ketal-Br as well as the instability of ketal group under ATRP conditions was systematically investigated. Furthermore, the synthesized block copolymer after purification was characterized for aqueous micellization through self-assembly and dual acidic pH/reduction-responsive cleavage of ketal and disulfide linkages.

4.2 Experimental

4.2.1 Instrumentation. The same instrumentation and method were used as described in chapter 3.

4.2.2 Materials. Most reagents including triethylamine (Et_3N), bromoisobutyryl bromide (Br-iBuBr), and tin(II) 2-ethylhexanoate ($SnEH_2$, 95%) used in our synthesis were purchased from Sigma Aldrich Canada and used as received, except for disuccinimidyl carbonate (DSC) from Toronto Research Chemicals and 1-ethyl-3-(3-dimethylaminopropyl)carbodiimide-HCl salt (EDC) from Matrix Innovation. Poly(ethylene glycol) monomethyl ether (PEG, MW= 5000 g/mol, EO# = 113) was dried by azeotropic distillation with toluene to remove residual moistures. Solvents include ethyl acetate (EA), hexane (HE), dichloromethane (DCM), tetrahydrofuran (THF), and methanol (MeOH). Tris(2-pyridylmethyl)amine (TPMA),[271] a methacrylate having a pendant disulfide linkage (HMssEt),[272] and PEG-functionalized bromide (PEG-Br)[273] were synthesized as described elsewhere.

4.2.3. Synthesis of PEG-ketal-Br initiator. The detailed procedures for the synthesis of PEG-ketal-Br are described here. Other attempts to synthesize the initiator are detailed in Appendix B.

4.2.3.1 AC1: Ethyl trifluoroacetate (50.2 g, 354 mmol) was added dropwise to a solution consisting of ethanolamine (18.0 g, 295 mmol) and Et_3N (44.7 g, 442 mmol) dissolved in MeOH (300 mL) in an ice bath at 0 °C for 20 min and then the mixture was stirred at room temperature for 12 hrs. After the removal of solvents by rotary evaporation, the residues were dissolved in

saturated brine (100 mL), extracted from EA (200 mL) four times, and dried over sodium sulfate. After the solvent was evaporated, the product was purified by silica gel column chromatography with EA as an eluent. The product, a white solid, was collected as the first of a total of two bands from a silica gel column, yield 35.5 g (76.5%). R_f = 0.5 on silica (EA as an eluent). ^{1}H-NMR ($CDCl_3$, ppm): 6.85 (s, 1H, $F_3CC(O)\underline{NH}C$-), 3.80 (t, 2H, $F_3CC(O)NH\underline{CH_2}CH_2OH$), 3.54 (t, 2H, $F_3CC(O)NHCH_2\underline{CH_2}OH$), 2.05 (s, 1H, $F_3CC(O)NHCH2CH2\underline{OH}$). ^{13}C-NMR (DMSO, ppm): 158.0, 116.03, 59.45, 42.10. Mass calculated for ($C_4O_2NF_3H_6Na^+$): 180.02428. Found: 180.02451.

4.2.3.2 AC2: AC1 (12.2 g, 77.6 mmol) dissolved in anhydrous THF (300 mL) was mixed with PPTS (1.2 g, 4.6 mmol) under vigorous stirring for 1 hr. After the addition of molecular sieves (5 Å, 1.6 mm pellet, pre-dried at 100 °C for 72 hrs, 150 g), the resulting mixture was kept at 0 °C for 30 min under magnetic stirring. Followed by the addition of a solution of 2-methoxypropene (1.4 g, 19.4 mmol) dissolved in cold anhydrous THF (15 mL), the mixture was stirred overnight at room temperature, and then quenched by the addition of Et_3N (6.2 mL). Molecular sieves by filtration and solvents by rotary evaporation were removed, and then residues were dissolved in PBS (pH 7.4, 150 mL), and then extracted from EA (200 mL) three times. After the solvent was evaporated, the product was purified by silica gel column chromatography (1/1 v/v EA/HE). The product, a white solid, was collected as the second of the total three bands off a silica gel column, yielding 3.3 g (48.2%). R_f = 0.67 on silica (1/1 v/v EA/HE). ^{1}H-NMR ($CDCl_3$, ppm): 6.8 (s, 2H, $CF_3C(O)\underline{NH}CH_2CH_2OC(CH_3)_2O$-), 3.5 (s, 8H, $F_3CC(O)NH\underline{CH_2}\underline{CH_2}OC(CH_3)_2O$-), 1.37 (s, 6H, $-CH_2OC(\underline{CH_3})_2OCH_2$-). ^{13}C-NMR ($CDCl_3$, ppm): 158.0, 116.03, 101.0, 59.45, 39.92, 22.5. Mass calculated for ($C_{11}O_4F_6N_2H_{16}Na^+$): 377.09065. Found: 377.09190

4.2.3.3 AC3: AC2 (2.8 g, 7.9 mmol) was dissolved in 6 M aqueous sodium hydroxide (NaOH) solution (60 mL) and stirred for 4.5 hrs at room temperature. The product was extracted from DCM (150 mL) and dried over sodium sulfate. The solvent was evaporated by rotary evaporation to yield an amber-colored oil (1.2 g, 89.7%). ^{1}H-NMR ($CDCl_3$, ppm): 3.4 (t, 4H, $NH_2CH_2\underline{CH_2}OC(CH_3)_2O$-), 2.8 (t, 4H, $NH_2\underline{CH_2}CH_2OC(CH_3)_2O$-), 1.37 (s, 6H, $-CH_2OC(\underline{CH_3})_2OCH_2$-). ^{13}C-NMR ($CDCl_3$, ppm): 100.50, 63.23, 42.2, 25.12. Mass calculated for ($C_7N_2O_2H_{18}Na^+$): 185.12605. Found: 185.12578

4.2.3.4 AC4: Ethyl trifluoroacetate (0.87 g, 6.2 mmol) was dropwise added to a clear solution containing AC3 (1.0 g, 6.2 mmol), Et_3N (0.74 g, 7.4 mmol), and MeOH (15 mL) in an ice bath for 20 min. The reaction mixture was stirred overnight at room temperature, and then solvents were evaporated. The residues were dissolved in PBS (pH 7.4, 50 mL) and extracted from DCM (100 mL) three times. After the evaporation of the solvent, the product was purified by silica gel column chromatography deactivated with Et_3N using DCM/MeOH (9/1 v/v). The product, a yellow oil, was collected as the second of the total three bands off a silica gel column, yielding 0.35 g (22.4%). $R_f = 0.54$ on silica (8/2 v/v DCM/MeOH; ninhydrin was used for visualization). ^{1}H-NMR ($CDCl_3$, ppm): 3.68 (t, 2H, -$CF_3C(O)NH\underline{CH_2}CH_2OC(CH_3)_2O\underline{-}$), 3.54 (m, 4H, -$\underline{CH_2}OC(CH_3)_2O\underline{CH_2}$-), 2.8 (t, 2H, -$OC(CH_3)_2OC\underline{H_2}C\underline{H_2}NH_2$), 1.37 (s, 6H, -$CH_2OC(\underline{CH_3})_2OCH_2$-). ^{13}C-NMR ($CDCl_3$, ppm): 157.5, 116.0, 99.9, 61.65, 58.05, 40.95, 40.45, 24.74. Mass calculated for ($C_9N_2O_3F_3H_{17}Na^+$): 281.10830. Found: 281.10770

4.2.3.5 PEG-DSC: A solution containing PEG (5.0 g, 1.0 mmol), Et_3N (0.30 g, 3.0 mmol), and DSC (0.77 g, 3.0 mmol) dissolved in anhydrous DCM (220 mL) was purged with nitrogen for 20 min and then stirred for 28 hrs at room temperature. The product, a white solid, was precipitated from anhydrous diethyl ether (600 mL), isolated by vacuum filtration, and dried in a vacuum oven at room temperature for 12 hrs, yielding 5.0 g (97%). ^{1}H-NMR ($CDCl_3$, ppm): 4.45 (t, 2H, $\underline{CH_2}OC(O)$-), 3.45-3.80 (m, -$\underline{CH_2CH_2}O$- of PEG main chain), 3.37 (s, 3H, $\underline{CH_3}O$-), 2.83 (s, 4H, -$(O)C\underline{CH_2CH_2}C(O)$-).

4.2.3.6 AC5: A solution containing the purified, dried PEG-DSC (1.5 g, 0.29 mmol) and Et_3N (0.06 g, 0.61 mmol) in chloroform (110 mL) was mixed with a solution of AC4 (0.17 g, 0.67 mmol) in chloroform (5 mL) in an ice bath. The mixture was stirred for 22 hrs at room temperature. The product, a white solid, was precipitated from anhydrous diethyl ether (500 mL), isolated by vacuum filtration, and dried in a vacuum oven at room temperature for 12 hrs, yielding 1.4 g (93.2%). ^{1}H-NMR ($CDCl_3$, ppm): 4.21 (t, 2H, $\underline{CH_2}OC(O)$-), 3.45-3.80 (m, -$\underline{CH_2CH_2}O$- of PEG main chain), 3.37 (s, 3H, $\underline{CH_3}O$-), 1.36 (s, 6H, -$CH_2OC(\underline{CH_3})_2OCH_2$-).

4.2.3.7 AC6: A solution of AC5 (1.4 g, 0.26 mmol) dissolved in MeOH (30 mL) was mixed with a solution of potassium carbonate (0.25 g, 1.85 mmol) in water (6 mL). The mixture was stirred overnight at room temperature and concentrated by rotary evaporation. The residues were dissolved in water (50 mL) and extracted from DCM (250 mL) three times. The product, a white

solid, was precipitated from anhydrous diethyl ether (500 mL), isolated by vacuum filtration, and dried in a vacuum oven at room temperature for 12 hrs, yielding 1.23 g (91.7%).[1]H-NMR ($CDCl_3$, ppm): 4.21 (t, 2H, $\underline{CH_2}OC(O)$-), 3.45-3.80 (m, -$\underline{CH_2CH_2}O$- of PEG main chain), 3.37 (s, 3H, $\underline{CH_3}O$-), 2.85 (t, 2H,-$OCH_2\underline{CH_2}NH_2$), 1.36 (s, 6H, -$CH_2OC(\underline{CH_3})_2OCH_2$-).

4.2.3.8 PEG-ketal-Br (AC7): Br-iBuBr (0.13 g, 0.59 mmol) was added to a solution containing AC6 (1.23 g, 0.24 mmol) and Et_3N (0.35 g, 3.56 mmol) dissolved anhydrous THF (100 mL) in an ice bath. The mixture was stirred for 90 mins. The formed solids (Et_3N-HBr adducts) were removed by vacuum filtration and the solvent was evaporated. The residues were dissolved in DCM (300 mL) and the solution was washed with water two times, and then dried over sodium sulfate. The product, a white solid, was precipitated from anhydrous diethyl ether (500 mL), isolated by vacuum filtration, and dried in a vacuum oven at room temperature for 12 hrs, yielding 1.1 g (87.9%). [1]H-NMR ($CDCl_3$, ppm): 4.21 (t, 2H, $\underline{CH_2}OC(O)$-), 3.45-3.80 (m, -$\underline{CH_2CH_2}O$- of PEG main chain), 3.37 (s, 3H, $\underline{CH_3}O$-), 1.95 (s, 6H, -$NHC(O)C(\underline{CH_3})_2Br$),) 1.36 (s, 6H, -$CH_2OC(\underline{CH_3})_2OCH_2$-).

4.2.4 Synthesis of DLDSRD block copolymers by ATRP. To synthesize DLDSRD-1 as an example, PEG-ketal-Br (0.24 g, 45.7 μmol), HMssEt (0.8 g, 2.28 mmol), [Cu(II)TPMABr]Br (1.17 mg, 2.27 μmol), TPMA (1.99 mg, 6.8 μmol), and anisole (3.5 g) were mixed in a 15 mL Schlenk flask. The mixture was deoxygenated by purging under nitrogen for 1 hr and then placed in an oil bath at 40 °C. A nitrogen pre-purged solution of Sn(II)(EH)2 (7.41 mg, 18.3 μmol) dissolved in anisole (0.5 g) was injected into the Schlenk flask to initiate polymerization. Polymerization was stopped after 2.3 hrs by cooling the reaction mixture in an ice bath and exposing it to air. For kinetic studies, aliquots of the samples were taken periodically to follow monomer conversion using [1]H-NMR analysis. Polymerization was stopped by cooling and exposing the reaction mixture to air.

Similar procedure was applied except for the use of PEG-ketal-Br (0.13 g, 25.6 μmol), HMssEt (0.45 g, 1.28 mmol), [Cu(II)TPMABr]Br (0.66 mg, 1.28 μmol), TPMA (1.12 mg, 3.85 μmol), and anisole (3.0 g) for DLDSRD-2, and PEG-ketal-Br (0.18 g, 33.7 μmol), HMssEt (0.3 g, 0.85 mmol), [Cu(II)TPMABr]Br (0.88 mg, 1.71 μmol), TPMA (1.49 mg, 5.13 μmol), and anisole (3.0 g) for DLDSRD-3.

For purification, the as-prepared polymer solution was diluted with acetone and passed through a basic alumina column to remove residual copper species. The solvent was removed under rotary evaporation at room temperature, and the polymer was isolated by precipitation from hexane, then dried under vacuum at room temperature for 15 hrs.

4.2.5 ATRP to synthesize PEG-b-PHMssEt block copolymer (control). PEG-Br (0.10 g, 19.4 μmol), HMssEt (0.34 g, 0.97 mmol), [Cu(II)TPMABr]Br (0.5 mg, 0.97 μmol), TPMA (0.85 mg, 2.92 μmol), and anisole (3.4 g) were mixed in a 15 mL Schlenk flask. The mixture was deoxygenated by purging under nitrogen for 1 hr and then placed in an oil bath at 40 °C. A nitrogen pre-purged solution of Sn(II)(EH)2 (3.15 mg, 7.77 μmol) dissolved in anisole (0.5 g) was injected into the Schlenk flask to initiate polymerization. Polymerization was stopped after 2 hrs by cooling the reaction mixture in an ice bath and exposing it to air.

4.2.6 ^{1}H-NMR investigation of ketal cleavage under ATRP condition. PEG-ketal-Br (30 mg, 5.6 μmol) dissolved in DMSO-d_6 (1 mL) was mixed with $CuBr_2$ (2 mg, 8.95μmol). ^{1}H-NMR spectra of the resulting mixture were recorded over time.

4.2.7 Dual stimuli-responsive cleavage of DLDSRDs. Selected with DLDSRD-1, for acidic pH response, its aliquot (1 mg) dissolved in $CDCl_3$ was mixed with a drop of HCl. After 45 min, the mixture was analyzed by ^{1}H-NMR. For dual responses, its aliquot (10 mg) dissolved in DMF (10 mL) was mixed with DTT (4 mg, 1.2 moles equivalent to pendant disulfides) and a drop of HCl (0.63 mmol) under stirring at room temperature for 1 day. An aliquot was taken to analyze molecular weight distribution using GPC.

4.2.8 Aqueous micellization using dialysis method. Water (10 mL) was added drop-wise to an organic solution of DLDSRD-1 (15 mg) in THF (2 mL) using a syringe pump equipped with a plastic syringe (20 mL volume, 20 mm diameter) at an addition rate of 0.2 mL/min. The resulting dispersion was placed in a dialysis tubing with MWCO = 3500 g/mol and dialyzed against water (1 L) for 24 hrs. Outer water was changed twice to yield aqueous micellar aggregates at 1.5 mg/mL.

4.3 Results and discussion

4.3.1 Synthesis of PEG-ketal-Br ATRP initiator. Our approach to synthesize PEG-ketal-Br initiator began with the synthesis of a diamine precursor labeled with a ketal linkage (AC3) as described in the previous publications.[274] As illustrated in Scheme 4.1, the first step was the protection of amine group in ethanolamine with ethyl trifluoroacetate in the presence of Et_3N (a base) in MeOH to synthesize AC1 at 76% yield. The second step was the reaction of AC1 with 2-methoxypropene in the presence of pyridinium *p*-toluenesulfonate (PPTS) in THF, yielding AC2 at 48% yield. The use of molecular sieves with 5 Å pore size is essential to remove the formed MeOH. Both AC1 and AC2 were purified by column chromatography and their structures were confirmed by ^{1}H-NMR and ^{13}C-NMR analysis (Figure 4.1a, Figure B1 and B2), along with high resolution mass spectroscopy to determine their absolute molecular weights. The next step was the deprotection of trifluoroacetamide groups in AC2 in the presence of a 6 M aqueous NaOH solution. ^{1}H- and ^{13}C-NMR (Figure B3), as well as further COSY NMR analysis (Figure B4) confirm the synthesis of AC3 at 89% yield.

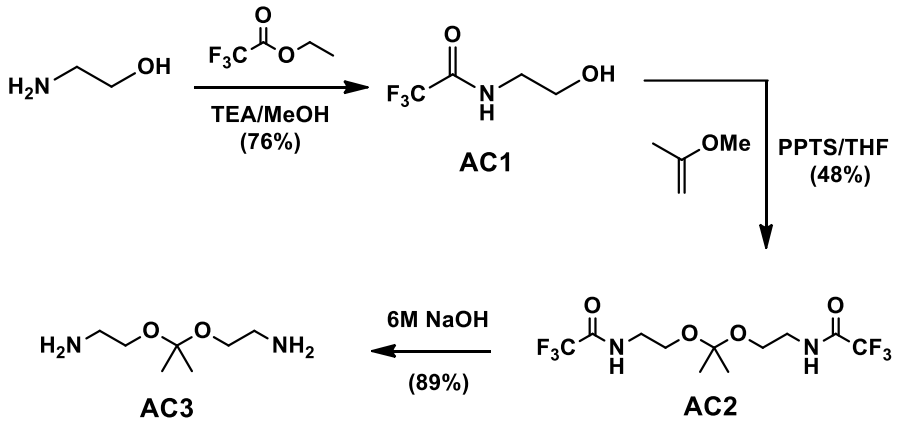

Scheme 4.1 Synthetic route to AC3.

Given the successful synthesis of AC3, Scheme 4.2 illustrates our successful route (I) to the synthesis of PEG-ketal-Br functionalized with a ketal linkage and a bromo group (AC7). This synthetic route centers on the use of carbamate linkage between PEG and AC4, which is stable under alkaline deprotection processes. A few reports describe the utilization of stable carbamate linkages for the synthesis of polymer-drug conjugates and hydrogels.[161, 275, 276] The first step was the protection of one amine group in AC3 with ethyl trifluoroacetate (an electron-withdrawing group) in a basic condition. Column chromatography was required to isolate AC4 from the corresponding dimer at 22% yield. The chemical structure of the purified AC4 was confirmed by

^{1}H-NMR (Figure 4.1b) and ^{13}C-NMR (Figure B5) as well as further COSY NMR analysis (Figure B6).

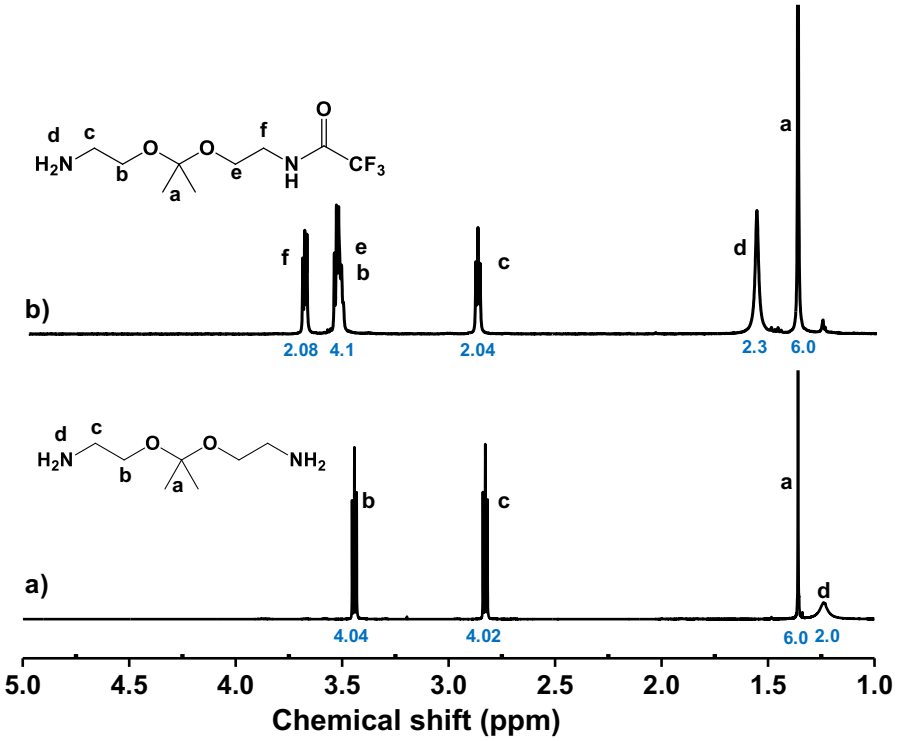

Figure 4.1 ^{1}H-NMR spectra of AC3 (a) and AC4 (b) in $CDCl_3$. Note that the values under each spectrum are integrals.

In a separate set, the hydroxyl group of PEG was activated with DSC in the presence of Et_3N. After purification from diethyl ether, the structure of the formed PEG-DSC is confirmed by ^{1}H-NMR analysis (Figure 4.2a). The second step was the conjugation of PEG-DSC with AC4 through the formation of a carbamate bond to synthesize AC5. The third step was the treatment of AC5 with K_2CO_3 in a mixture of MeOH and water. This step allows for the cleavage of trifluoroacetamide group to generate the corresponding amino group, thus yielding AC6. Both AC5 and AC6 were purified by precipitation from diethyl ether and the purified products were characterized by ^{1}H-NMR analysis (Figure 4.2b and 4.2c). For example, with AC6, the typical peaks include the peak (b) corresponding methylene group adjacent to ester bond, the peak (f) to two methyl groups in the ketal linkage, and the peak (h) to methylene group adjacent to the amine group. Their integral ratio was close to 2/6/2, which is equivalent to that of their proton numbers. Further, the complete deprotection of the trifluoroacetamide protecting group is confirmed with ^{19}F-NMR spectroscopy (Figure B7). The final step was the coupling reaction of

the purified AC6 with Br-iBuBr to synthesize AC7. HBr (a strong acid) is released as a result of the coupling reaction. Thus, the use of excess Et_3N (15 moles equivalent to AC6) to facilitate the formation of HBr-Et_3N salts as well as the reaction time of <3 hrs at room temperature were adopted, in order to minimize the unexpected cleavage of ketal linkages during coupling reaction. ^{1}H-NMR spectrum in Figure 4.2d shows the peak (j) corresponding to two methyl groups in bromo moieties. The quantitative mole ratio of the peaks a/f/j = 3/6/6, suggesting the successful synthesis of PEG-ketal-Br.

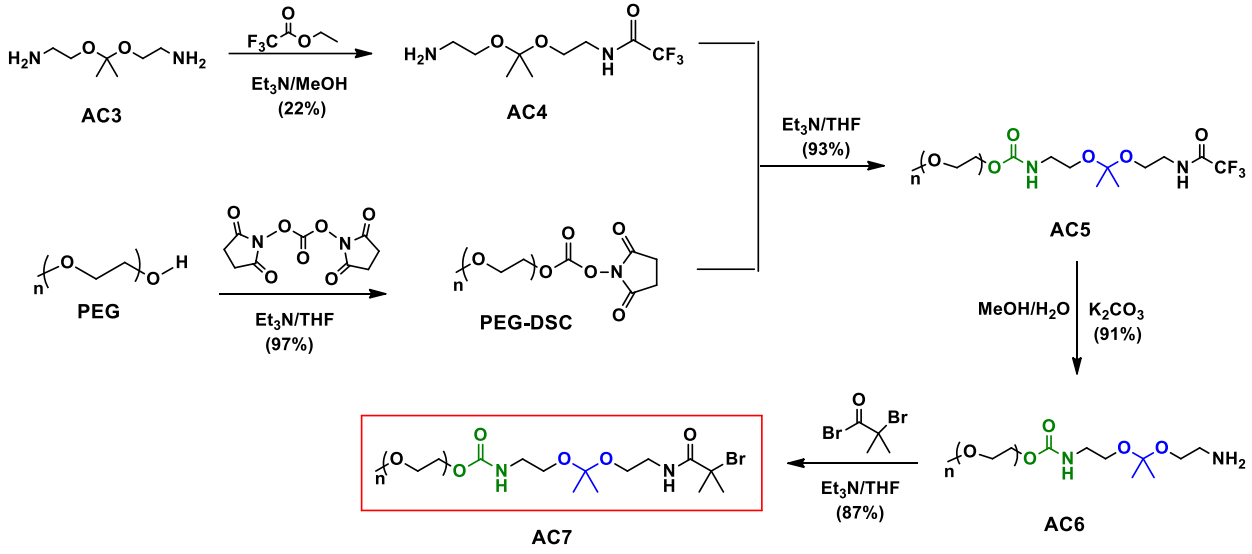

Scheme 4.2 Synthetic route (I) to PEG-ketal-Br initiator, starting with AC3.

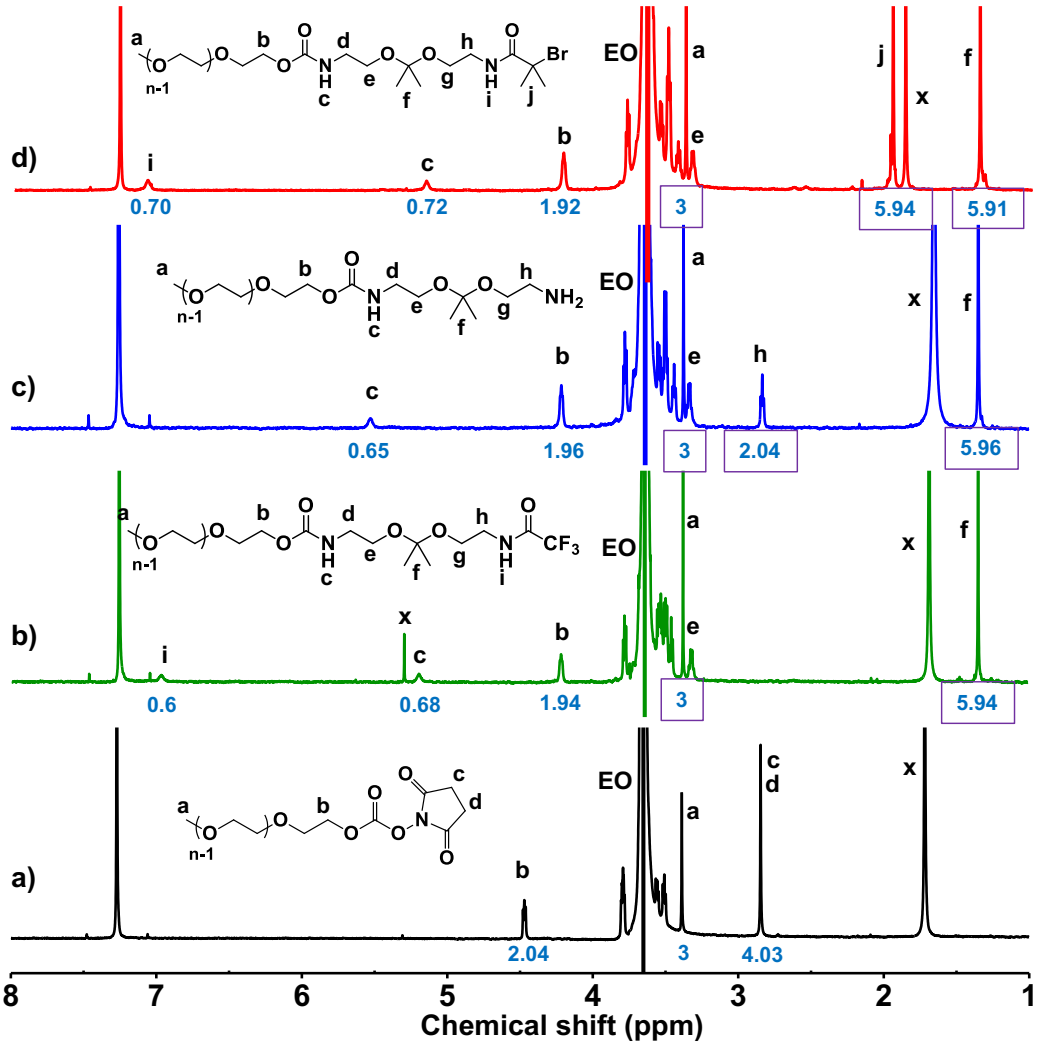

Figure 4.2 ^{1}H-NMR spectra of PEG-DSC (a), AC5 (b), AC6 (c), and AC7 (d, PEG-ketal-Br) in $CDCl_3$. Note that the values under each spectrum are integrals. x denotes impurities including water.

Given the robust route (I) that allows for the successful synthesis of PEG-ketal-Br, two other routes (II and III), which were not straightforward and successful, were also explored in an attempt to synthesize PEG-ketal-Br. As illustrated in Scheme B1, route (II) is similar to the above route (I) but differs with the use of ester bond between PEG and AC4 (Scheme B1). The route (III) in Scheme B2 centers on the synthesis of AC12 functionalized with both amine and bromo groups, which could yield a PEG-ketal-Br by its direct coupling with a COOH-functionalized PEG (PEG-COOH). The detailed procedures and results including NMR spectra (Figures B8-B13) are described in supporting information.

4.3.2 Synthesis of PEG-ketal-PHMssEt and kinetic investigation. Given our successful synthesis and characterization of PEG-ketal-Br initiator, ATRP, a successful CRP technique, was examined to synthesize PEG-ketal-PHMssEt (DLDSRD) block copolymers. ARGET process for ATRP[251, 277] was employed since this process requires the use of a minimal amount of Cu species (<50 ppm). As illustrated in Figure 4.3, the polymerization was mediated with Cu(II)/TPMA complexes in the presence of the PEG-ketal-Br initiator. $Sn(II)EH_2$ was used as a reducing agent to convert Cu(II) species to active Cu(I) species. Under the conditions for typical ARGET ATRP including $[PEG\text{-}ketal\text{-}Br]_0/[Cu(II)Br_2]_0/[TPMA]_0/[Sn(II)EH_2]_0$ = 1/0.05/0.15/0.4 in anisole at 40 °C, the initial mole ratio of $[HMssEt]_0/[PEG\text{-}ketal\text{-}Br]_0$ as the targeting DP at he complete monomer conversion was varied with 50/1 and 25/1. Polymerization was stopped and ^{1}H-NMR analysis was used to determine conversion.

After purification by filtration through a basic alumina column to remove residual metal species and the following precipitation from hexane to remove unreactive monomers, the copolymers were characterized for their structures and molecular weights. For an example with DLDSRD-1, its ^{1}H-NMR spectrum in Figure 4.3 shows the typical peaks at 3.7 ppm corresponding to methylene protons in PEG block and 0.8-1.2 ppm equivalent to methyl protons on backbones in PHMssEt block. Their integral ratio was analyzed to determine the DP of PHMssEt to be 164 at conversion = 0.66. GPC analysis in Figure 4.4 (red line for DLDSRD-1) indicates the molecular weight as the number average molecular weight (M_n) = 87.4 kg/mol with molecular weight distribution as Đ = 1.18. Note that a small peak observed in the high molecular weight region could be attributed to high molecular species formed by undesired side reactions during ATRP. Similar protocols were used to analyze other DLDSRD copolymers and their characteristics and results are summarized in Table 4.1.

Table 4.1 Characteristics and properties of DLDSRD block copolymers synthesized by ARGET ATRP of HMssEt in the presence of PEG-ketal-Br.[a)]

DLDSRD	$[HMssEt]_0/[I]_0$	HMssEt/anisole (wt/wt)	Time (hrs)	Conv[b)]	DP[b)] PHMssEt	M_n[c)] (kg/mol)	Đ[c)]
1	50	0.23	2.3	0.66	164	87.4	1.18
2	50	0.10	6.4	0.58	159	51.4	1.07
3	25	0.15	2.0	0.54	110	55.6	1.11

a) Conditions for ATRP: $[PEG\text{-}ketal\text{-}Br]_0/[Cu(II)Br_2]_0/[TPMA]_0/[Sn(II)EH_2]_0$ = 1/0.05/0.15/0.4 in anisole at 40 °C; b) Determined by ^{1}H-NMR; c) Determined by GPC with PMMA standards.

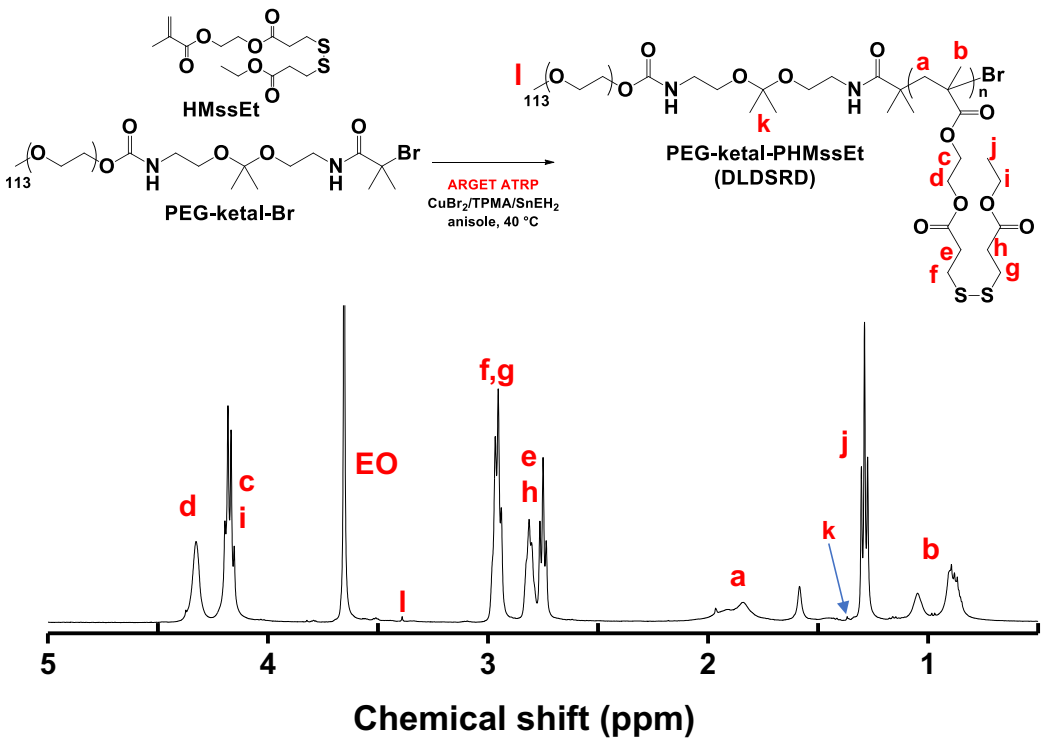

Figure 4.3 Scheme to synthesis DLDSRD block copolymers by ARGET ATRP and ^{1}H-NMR spectrum of DLDSRD-1 in $CDCl_3$ as an example.

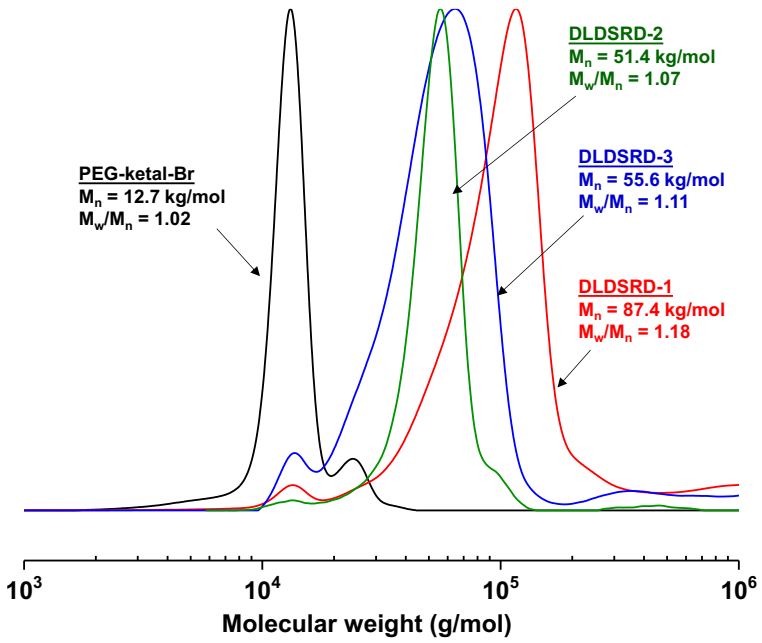

Figure 4.4 GPC diagrams of DLDSRD block copolymers, compared with PEG-ketal-Br initiator.

Kinetics of ATRP of HMssEt in the presence of PEG-ketal-Br was investigated by analysing samples taken periodically (not purified). Figure 4.5 shows that $\ln([M]_0/[M])$ linearly increased with time, suggesting that the polymerization is first-order. This result indicates the constant concentration of active centers during polymerization, up to 60% conversion. The polymerization was well-controlled. As expected, polymerization slowed down when the wt ratio of HMssEt/anisole decreased (more anisole) from 0.23 (DLDSRD-1) to 0.10 (DLDSRD-2) at 40 °C.

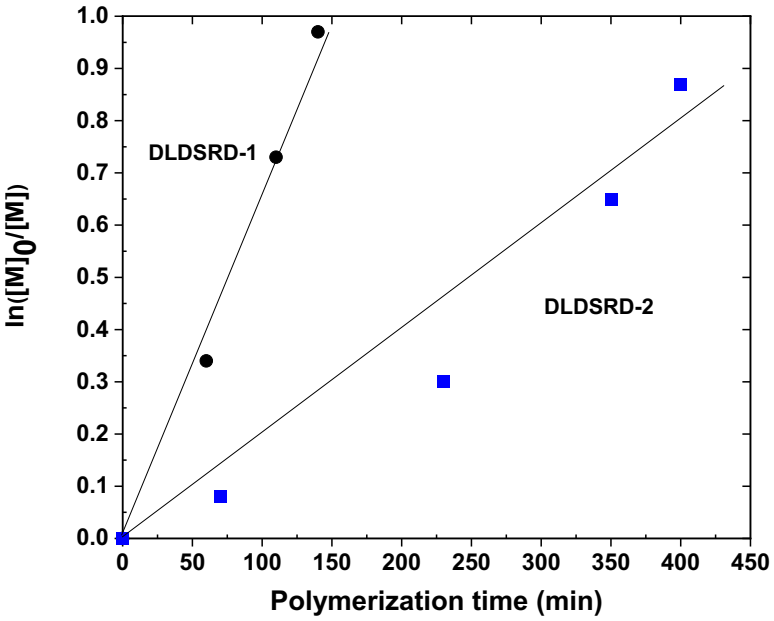

Figure 4.5 First-order kinetic plot over polymerization time for ARGET ATRP of HMssEt in the presence of PEG-ketal-Br in anisole at 40 °C.

4.3.3 Stability of ketal linkages during ATRP. Our careful analysis suggests that all three copolymers after purification presented in Table 4.1 had the DPs of PHMssEt blocks much greater than those calculated based on conversion and targeting DPs. For example with the purified DLDSRD-3, the DP of PHMssEt block was 110 determined by ^{1}H-NMR analysis, while it can be estimated to be 14, based on conversion (0.54) and targeting DP = 25. The plausible reason for such large discrepancy of the DPs of DLDSRD block copolymers was investigated.

The samples taken during ATRP to investigate its kinetics were analyzed for the DPs of PHMssEt block. Note that those samples were not purified by our standard protocol (filtration with basic Al_2O_3 column and then precipitation from hexane). Our ^{1}H-NMR analysis indicates that the determined DPs of the samples were very close to DPs theoretically calculated with

targeting DP over conversion (Figure 4.6). This result appeared to be quite different from the DPs (110-164) of the purified DLDSRD copolymers. We then carefully examined the purification steps of the copolymers.

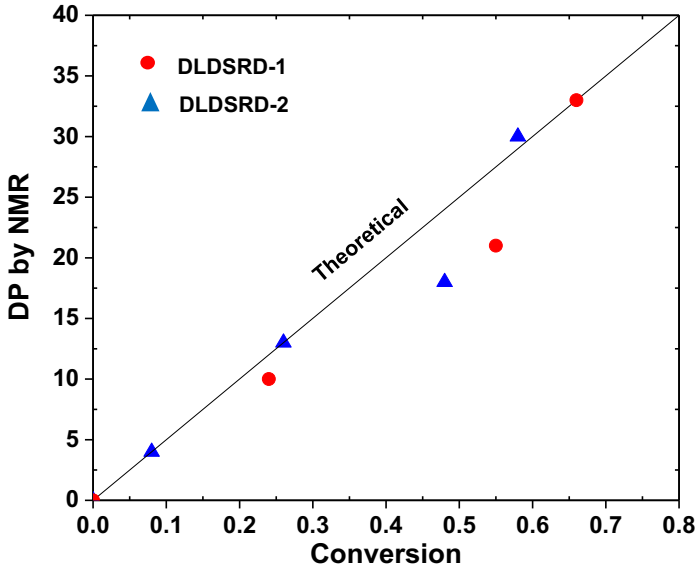

Figure 4.6 DP determined by ^{1}H-NMR analysis for the samples taken during ATRP over conversion. The theoretical DP values are calculated with the targeting DP = 50 over conversions.

The first step of our standard purification protocol is the filtration of copolymer solution through a basic alumina column to remove Cu species. As compared in Figure B14, the GPC diagram of the copolymer before filtration exhibits the presence of an important amount of PEG homopolymers, which could not be covalently attached to PHMssEt blocks. After filtration, the peak equivalent to PEG homopolymer significantly reduced (or disappeared). These results suggest that the ketal linkages labeled in PEG-ketal-Br or PEG-ketal-PHMssEt could be cleaved during ATRP.

Followed by filtration, the second step is the precipitation of copolymers from hexane (a poor solvent). After precipitates were isolated by vacuum filtration, the supernatant was analyzed by ^{1}H-NMR and GPC techniques after the removal of solvents. The results shown in Figure B15 indicate that the residue dissolved in hexane is PHMssEt homopolymer. Interestingly, the homopolymer had a high molecular weight with broad molecular weight distribution.

For comparison, a control experiment was conducted with PEG-Br (a similar structure, but with no ketal linkage) for ARGET ATRP of HMssEt under similar conditions with PEG-ketal-

Br: $[HMssEt]_0/[PEG\text{-}Br]_0/[Cu(II)Br_2]_0/[TPMA]_0/[Sn(II)EH_2]_0 = 50/1/0.05/0.15/0.4$ in anisole at 40 °C. At the conversion of HMssEt = 0.48, the purified PEG-b-PHMssEt was characterized with the DP of PHMssEt block = 25 by ^{1}H-NMR (Figure B16), which is close to the DP = 24 theoretically estimated with the targeting DP = 50. This result not only confirms the reproducibility of our previous publication,[272] but also confirms the possibility of the cleavage of the ketal linkages labeled in PEG-ketal-Br or PEG-ketal-PHMssEt under ATRP conditions.

Given the above results, a cleavage of ketal linkages was examined for PEG-ketal-Br in the presence of $CuBr_2$ in DMSO-d_6 using ^{1}H-NMR spectroscopy. Their concentrations were designed to be similar to those used for ARGET ATRP above. As seen in Figure 4.7, the integral of the peak at 1.3 ppm corresponding to two ketal methyl groups decreased, while the integral of the peak at 2.1 ppm to acetone released as a result of the cleavage of ketal linkages increased. From the integrals, the extent of ketal cleavage was quantitatively estimated. It reached >70% within 4 hrs. Note that no cleavage was found in the absence of $CuBr_2$. These results suggest that the ketal linkages in PEG-ketal-Br and PEG-ketal-PHMssEt could be cleaved under ATRP conditions.

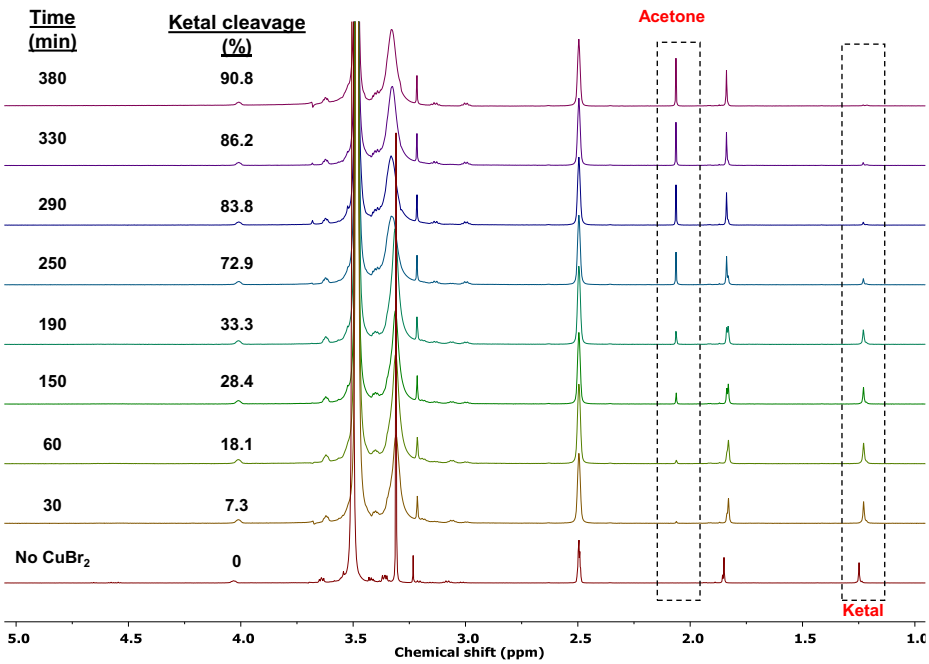

Figure 4.7 Evolution of ^{1}H-NMR spectra and extent of ketal cleavage for a mixtrue of PEG-ketal-Br in the presence of $CuBr_2$ in DMSO-d_6 over time at room temperature.

4.3.4 Aqueous micellization and preliminary investigation of dual stimuli response of DLDSRDs. Given the above results, some portion of ketal linkages at block junctions of DLDSRDs was cleaved during ATRP. Nevertheless, both PEG and PHMssEt homopolymers generated from the unexpected cleavage during ATRP could be removed by the established purification process with precipitation and filtration. Consequently, the purified DLDSRD copolymers consist of hydrophilic PEG and hydrophobic PHMssEt blocks.

Due to the amphiphilic nature, the DLDSRD copolymer formed colloidally stable micellar aggregates with the diameter = 198 nm by aqueous micellization through self-assembly in an aqueous solution (Figure B17). Furthermore, the purified DLDSRD contains both a ketal linkage at the block junction as well as disulfide pendants in the hydrophobic PHMssEt block. The labile linkages can be cleaved in response to acidic pH and reduction individually or dually (Figure 4.8a). The feasibility of dual stimuli-responsive degradation of DLDSRD copolymers was examined in organic solution by GPC and ^{1}H-NMR techniques. Note that the kinetics of dual stimuli-responsive degradation of copolymers in organic solution could be different from their nanoassemblies in water. The response of ketal linkage to acidic pH was first examined as an aliquot of DLDSRD-1 was dissolved in $CDCl_3$ and treated with a trace amount of HCl. ^{1}H-NMR spectrum in Figure 4.8b shows the new peak at 2.18 ppm corresponding to acetone released as a consequence of the cleavage of block junction ketal linkages, suggesting the cleavage of ketal linkage in an acidic condition. A similar result was observed for the PEG-ketal-Br initiator being treated with HCl (Figure B18). Then, the response to dual acidic pH and reduction was examined as DLDSRD-1 was mixed with an excess DTT (1.2 equivalents to pendant disulfide linkages) and HCl (0.63 mmol). As shown in Figure 4.8c, the GPC trace was shifted to the molecular weight region as a result of the cleavage of both one ketal linkage and 164 disulfide pendants.

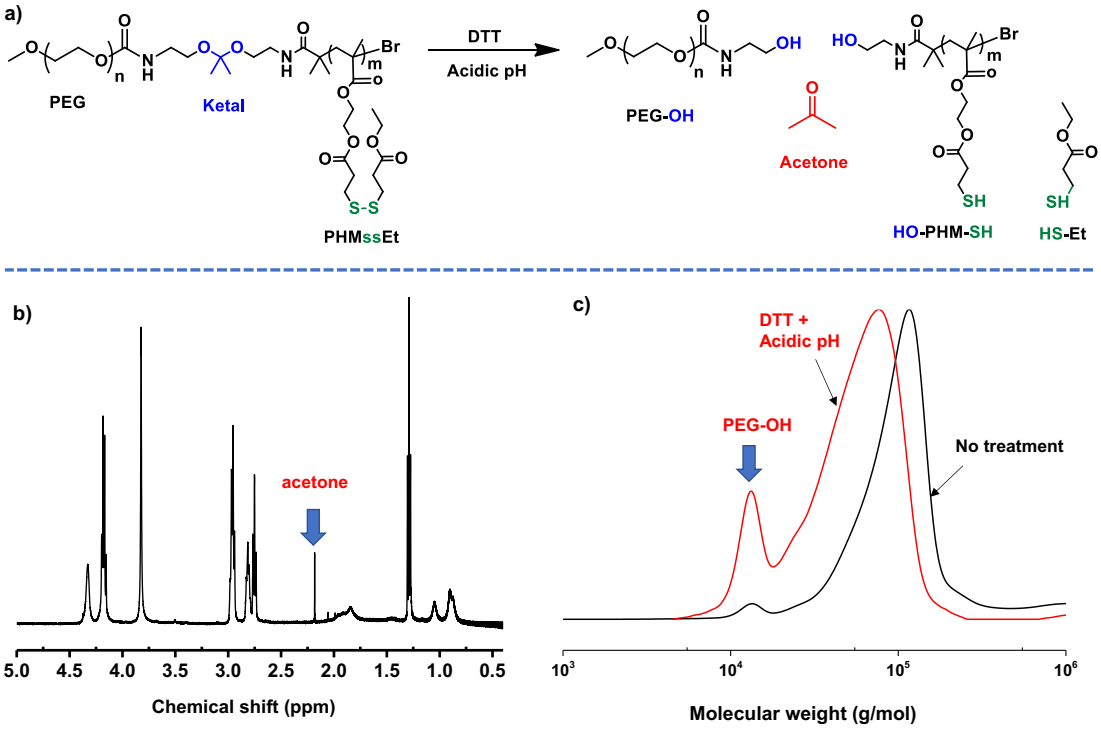

Figure 4.8 Schematic illustration of dual-stimuli acidic pH and reduction-responsive cleavage of a ketal linkage and disulfide pendants of DLDSRD (a), ^{1}H-NMR spectrum of DLDSRD-1 treated with a trace amount of HCl (b), and GPC diagrams of DLDSRD-1 in the absence and presence of excess DTT (1.2 equivalent to pendant disulfides) and HCl (0.63 mmol) in DMF (c).

4.4 Conclusion

A new strategy utilizing ATRP was investigated to synthesize PEG-ketal-PHMssEt DLDSRDs consisting of a hydrophilic PEG block covalently conjugated through a ketal linkage with a hydrophobic polymethacrylate block having pendant disulfide linkages. The synthesis of a PEG-ketal-Br macroinitiator was not straightforward because of the unexpected side reactions associated with the high sensitivity of ketal linkage to environments. The carbamate group was found to be stable to a basic hydrolysis condition, compared to ester and carbonate groups. Carbamate chemistry and required protection/deprotection chemistries allowed for the development of a robust route with multiple steps to the synthesis of PEG-ketal-Br macroinitiator. Under ATRP conditions, the ketal linkages in the macroinitiators and polymeric species were unstable and likely cleaved. This ketal instability could result in the synthesis of PEG-ketal-PHMssEt with 3-4 times higher DP of PHMssEt block, compared to theoretically-estimated ones (thus, DP of PHMssEt = 100~150). Promisingly, the purified DLDSRDs enabled self-assembly to form nanoassemblies with ketal at core/corona interfaces and multiple disulfide

linkages in hydrophobic cores. Furthermore, ^{1}H-NMR and GPC results confirm the dual acidic pH/reduction-responsive cleavage of ketal and disulfide linkages in dual locations.

Chapter 5: Tumor-targeting intracellular drug delivery based on dual acid/reduction-degradable nanoassemblies with ketal interface and disulfide core locations

5.1 Introduction

In the past decades, self-assembled nanoaggregates (or micelles) from ABPs have received considerable attention as an effective drug delivery carrier,[10, 278, 279] owing to their ability to increase the solubility of hydrophobic drugs by encapsulating them in their hydrophobic reservoir and passively target the tumor via EPR effect.[77-82] Nevertheless, the poor release profile of drugs from the micelles has hampered their practical application and clinical success. The introduction of cleavable chemical linkages which are prone to degrade in the tumor environment (e.g reductive environment of cytosol or acidic pH of endosome and lysosome) has recently witnessed significant growth.[26, 28, 67] However, most of the reported polymers contain the acid and GSH cleavable linkages at only one location in the micelles.[67] These systems provide restricted control over drug release performance of micellar carriers and are unable to fully degrade and synergistically release the drugs in the intracellular environment due to the heterogenous presence of GSH and acidic pH in different intracellular organelles.[52, 68] In addition, the degradation of single location GSH or acidic degradable nanoassemblies can only lead to limited destabilization of nanoassemblies due to minimal change in hydrophobic-hydrophilic balance or agglomeration of hydrophobic cores.[22, 127, 245] Such drawbacks may not only produce sluggish drug release but could present difficulty in elimination of degraded products out of biological systems.

Researchers have recently begun to realize the potential advantages of dual location GSH/acid degradable block copolymer to address the poor drug release performance of single location systems. Several reports describe the synthesis of PCL-based grafted copolymers bearing pendant acetal junction and single disulfide linkages on the hydrophobic backbone[213-215] and a PEG-based polypeptide bearing dimethylmaleic anhydride junction and thiol pendant.[220] These copolymers self-assembled to form dual acid/reduction-degradable nanoassemblies/nanogels with acid-labile interfaces and disulfide cores. The biggest drawbacks of these systems are their incomplete disassembly due to the presence of a single disulfide in the

hydrophobic backbone or difficulty in control of disulfide-crosslink formation through uncontrolled oxidation of pendant thiols.

In chapter 4, we explored the synthesis of a novel block copolymer having a ketal linkage at block junction and multiple disulfide pendants in the hydrophobic block. Our initial attempt with ATRP technique was not straightforward because of the instability of ketal linkages at interfaces under ATRP conditions. Herein, we report our further investigation to RAFT polymerization as a robust means to the successful synthesis of a ketal-linked diblock copolymer composed of hydrophilic PEG block connected through a ketal linkage with a hydrophobic methacrylate having pendant disulfide linkages (HMssEt), thus forming PEG-ketal-PHMssEt (P5). Our approach centers on the synthesis of a new PEG-based RAFT agent labeled with a ketal linkage, thus PEG-ketal-RAFT (P4). As illustrated in Figure 5.1, the formed P5 self-assembled to form dual acid/reduction-degradable nanoassemblies with ketal linkages at interfaces and disulfide pendants in micellar cores. Given dual acid/reduction responses at dual core and interface locations, they exhibit synergistic and excellent release of encapsulated anticancer drugs, compared with their single response counterparts. These dual location dual acid/reduction-degradable nanoassemblies were further evaluated *in vitro* cell viability and cellular uptake to demonstrate their versatility for effective tumor-targeting intracellular drug delivery.

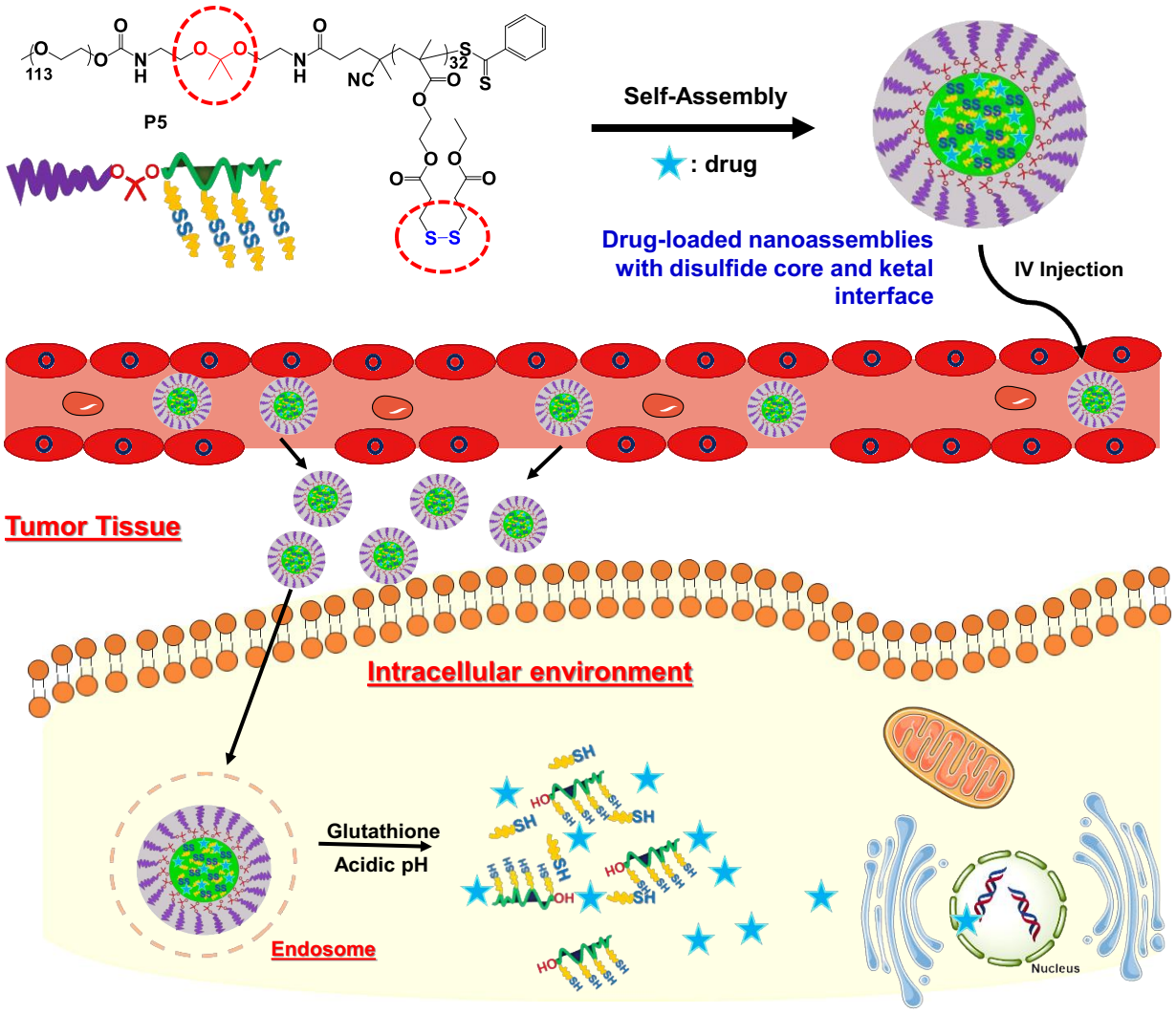

Figure 5.1 Illustration of tumor-targeting intracellular drug delivery of Dox-loaded dual acid/reduction-degradable nanoassemblies with ketal linkages at interfaces and disulfide pendants in micellar cores self-assembled from a well-controlled ketal-linked diblock copolymer composed of hydrophilic PEG block connected through a ketal linkage with a hydrophobic methacrylate having pendant disulfide linkages (PEG-ketal-PHMssEt, P5) synthesized by RAFT polymerization.

5.2 Experimental

5.2.1 Instrumentation. The same instrumentation and method were used as chapter 3 except that TEM images were obtained using a Philips Tecnai 12 TEM, operated at 80kV and equipped with a thermionic LaB6 filament. An AMT V601 DVC camera with point-to-point resolution and line resolution of 0.34 nm and 0.20 nm respectively were used to capture images in 2048 by 2048 pixels. To prepare specimens, aqueous Dox-loaded NP dispersion was dropped onto copper TEM grids (400 mesh, carbon-coated), blotted, and allowed to air dry at room temperature.

Subsequently, uranyl acetate (1%) was applied on the TEM grids and then dried again at room temperature.

5.2.2 Materials. 4-(Dimethylamino)pyridine (DMAP, 99 %), 4-cyano-4-(phenylcarbonothioylthio)pentanoic acid (CPTP, 97%), Nile Red (NR), glutathione (GSH), doxorubicin (Dox, -$NH_3^+Cl^-$ forms, >98%), and 1,4-dithreithiol (DTT) from Sigma Aldrich, and 1-ethyl-3-(3-dimethylaminopropyl)carbodiimide-HCl salt (EDC) from Matrix Innovation, and 2,2′-azodi(2-methylbutyronitrile) (AMBN) from Wako chemicals were purchased and used as received. A methacrylate having pendant a disulfide linkage (HMssEt) was synthesized according to the previous publication.[272]

5.2.3 Synthesis of a PEG-labeled macro-RAFT agent (P4). Precursors P1-P3 shown in Figure 5.1a were synthesized as described in chapter 4. To synthesize P4, a solution of EDC (0.12 g, 0.63 mmol) dissolved in DCM (15 mL) was dropwise added to a solution of P3 (1.17 g, 0.23 mmol), DMAP (11.0 mg, 0.09 mmol), and CPTP (0.12 g, 0.45 mmol) in DCM (80 mL) in an ice bath. After being stirred for 19 hrs at room temperature, the reaction mixture was washed with deionized water (30 mL) three times and precipitated from cold diethyl ether. The product was collected by filtration and dried in a vacuum oven at room temperature for 12 hrs: pink residues, 1.1 g (92%).

5.2.4 Synthesis of P5 block copolymers by RAFT. As an example, to synthesize P5-A, P4 (0.15 g, 29.1 μmol), HMssEt (0.5 g, 1.48 mmol), AMBN (1.7 mg, 8.7 μmol), and anisole (0.9 g) were mixed in a 15 mL Schlenk flask. The mixture was deoxygenated by purging under nitrogen for 1 hr and then placed in an oil bath at 73 °C to initiate polymerization. Aliquots of the samples were taken periodically to follow monomer conversion using ^{1}H-NMR and molecular weight and molecular weight distribution by GPC. After 2.5 hr, the polymerization was stopped by cooling the reaction mixture in an ice bath and exposing it to air. For purification, the as-prepared polymer solution was diluted with acetone and precipitated from hexane, then dried under vacuum at room temperature for 15 hrs.

5.2.5 Determination of CMC using a NR probe. A stock solution of NR in tetrahydrofuran (THF) at 1 mg/mL and stock solutions of P5 in THF at 1 mg/mL and 0.1 μg/ml were prepared. Water (10 mL) was then added dropwise into mixtures consisting of the same amount of the

stock solution of NR (0.5 mL, 0.5 mg NR) and various amounts of the stock solution of P5. The resulting dispersions were stirred for 40 hrs to remove THF, and then were subjected to filtration using a 0.45 μm PES filter to remove excess NR. A series of NR-loaded micelles at various concentrations of P5 ranging from 10^{-6} to 0.1 mg/mL were formed. From their fluorescence spectra recorded with λ_{ex}= 480 nm, the fluorescence intensity at maximum λ_{em} = 620 nm was recorded.

5.2.6 Aqueous micellization by dialysis method. PBS (pH = 7.4, 10 mL) was added dropwise to an organic solution of P5 dissolved in THF (2 mL) using a syringe pump equipped with a plastic syringe (20 mL volume, 20 mm diameter) at an addition rate of 0.2 mL/min. the resulting dispersion was dialyzed against PBS solution (1 L) twice for 24 h, yielding aqueous micellar dispersion at 0.9 mg/mL concentration.

5.2.7 Investigation of dual acid/reduction-responsive degradation. For P5 block copolymer, a solution of P5 (5 mg) dissolved in DMF (1 mL) was mixed with acetate buffer (pH = 5.3, 2 mL) for acidic pH response, DTT (7.7 mg, 5 moles equivalents to pendant disulfides) for reduction response, and a combination of DTT (7.7 mg, 5 moles equivalents to pendant disulfides) with acetate buffer (pH = 5.3, 2 mL) for dual acidic pH/reduction responses. GPC was used to follow any changes in molecular weight and its distribution. ^{1}H-NMR analysis was conducted for a solution of P5 (1 mg) dissolved in DMSO-d_6 mixed with a drop of DCl.

For aqueous micelles of P4 (1 mg/mL), their aliquot (1 mL) was mixed with 10 mM aqueous stock solution of GSH (3 mL) in PBS (pH = 7.4) for GSH response. Separately, their aliquots (1 mL) were mixed with aqueous acetate buffer solution at pH = 5.4 (3 mL) for acidic pH response, and aqueous acetate buffer solution containing GSH (10 mM) at pH = 5.4 (3 mL) for dual acidic pH/GSH responses. DLS was used to follow any changes in sizes and size distributions of the micelles.

5.2.8 Preparation of aqueous Dox-loaded micellar dispersions (Dox-NPs). An organic solution consisting of Dox (2 mg), Et_3N (5 μL), and P5 (20 mg) dissolved in DMF (1.6 mL) was mixed with PBS at pH = 7.4 (10 mL) under magnetic stirring. The resulting mixture was placed in a dialysis tubing (MWCO = 12000 g/mol) for dialysis over PBS (1 L) for 24 hrs. The formed

dispersion was passed through a 0.45 μm PES filter, yielding aqueous Dox-loaded micellar dispersion at 1.6 mg/mL.

To determine the loading level of Dox using UV/vis spectroscopy, an aliquot of aqueous Dox-loaded micellar dispersion (1 mL) was mixed with DMF (5 mL) to form a clear solution. After being passed through a 0.25 μm PTFE filter, its UV/vis spectrum was recorded. The loading level was determined by the weight ratio of loaded Dox to P5.

5.2.9 Dual acid/reduction-responsive Dox release from aqueous Dox-loaded micelles. Aliquots of Dox-loaded micellar dispersion (1.6 mg/mL, 2 mL) were transferred into dialysis tubing (MWCO = 12,000 g/mol) and immersed in outer buffer solutions (40 mL) prepared under various conditions: aqueous PBS at pH = 7.4 and aqueous acetate buffer solution at pH = 5.3 with and without 10 mM GSH. Aliquots of the outer buffer solutions (3.5 mL) were taken and their fluorescence spectra were recorded at λ_{ex} = 470 nm. The equal volume of fresh buffer was added to keep the same volume of outer buffer.

For quantitative analysis, aqueous Dox solutions (10 mL) were prepared as Dox (46 μg) being dissolved in PBS at pH = 7.4, Dox (50 μg) in acetate buffer solution at pH = 5.3, and Dox (47 μg) in aqueous PBS at pH = 7.4 with 10 mM GSH. The resultant solutions were diluted to prepare a series of solutions at various concentrations of Dox. Their fluorescence spectra were recorded at λ_{ex} = 470 nm to construct the calibration curves.

5.2.10 Cell culture. HeLa cervical cancer cells were cultured in DMEM (Dulbecco's modified Eagle's medium) containing 10% fetal bovine serum (FBS) and 1% antibiotics (50 units/mL penicillin and 50 units/mL streptomycin) at 37 °C in a humidified atmosphere containing 5% CO_2.

5.2.11 Flow cytometry. HeLa cells were plated at densities of 5×10^5 cells/well in 6-well dishes and kept at 37 °C. After 24 h, cells were treated with Dox-NPs (encapsulated Dox = 2.5 μg/mL) for 4 hrs. The cells were then washed with PBS three times and treated with trypsin. The cells were suspended in DMEM (500 μL) for flow cytometry measurements using a FACSCanto II flow cytometer (BD Biosciences) and FACSDiva software (BD Biosciences).

5.2.12 Live cell imaging by epifluorescence microscopy. HeLa cells were plated at densities of 1×10^5 cells/well in a glass-bottomed plate (MatTek Corporation) and incubated in media (2 mL) at 37 °C for 18 hrs. The cells were stained with Hoechst 33342 dye for 15 min. Then, the cells were washed with PBS three times to remove the excess dye. Phenol red-free DMEM medium (0.5 mL) was added to the cells for imaging. The appropriate amount of free Dox or Dox-micelles was added to attain a final Dox concentration of 2.5 μg/mL and incubated for 4 hrs. Images were captured by a Nikon TI-E microscope equipped with LED Heliophors with a Photometrics Evolve EMCCD camera. Dox and Hoescht33342 were excited at 405 nm and at 555 nm, respectively.

5.2.13 Cell viability using 3-(4,5-dimethylthiazol-2-yl)-2,5-diphenyl-2H-tetrazolium bromide (MTT) assay. HeLa cells were plated at 5 x 10^5 cells per well into a 96-well plate and incubated for 24 h in DMEM (100 μL) containing 10 % FBS and 1 % antibiotics. Then, they were incubated with various concentrations of empty (Dox-free), free Dox, and Dox-NPs for 48 hrs. Blank controls without nanoparticles (cells only) were run simultaneously as control. Cell viability was measured using the CellTiter 96 Non-Radioactive Cell Proliferation Assay kit (MTT, Promega) according to the manufacturer's protocol. Briefly, 3-(4,5-dimethylthiazol-2-yl)-2,5-diphenyltetrazolium bromide (MTT) solution (15 μL) was added to each well. After 4 hrs of incubation, the medium containing unreacted MTT was carefully removed. DMSO (100 μL) was added to each well to dissolve the formed formazan purple crystals, and then the absorbance at λ = 570 nm was recorded using a Powerwave HT Microplate Reader (Bio-Tek). Cell viability was calculated as the percent ratio of absorbance of mixtures with micelles to control (cells only without NPs).

5.2.14 Cell viability using Live Dead Cell Assay. HeLa cells were plated at 1 x 10^4 cells per well into a 96-well plate and incubated at 37 °C in DMEM (100 μL) containing 10% FBS and 1% antibiotics for 24 hrs. Cells were then treated with Dox-NPs to have the concentrations of Dox at 0.5, 1, and 2 μg/mL in DMEM containing either sodium bicarbonate (1.5 g/L, pH 7.4) for the control and both 10 mM GSH-OEt and 15 mM HEPES buffer (pH = 6.8) for dual acid/reduction stimuli. Blank samples without Dox-NPs were run simultaneously as controls. Cell viability was measured using the Live Dead Cell Assay Kit (Invitrogen) according to the manufacturer's protocol. After 48 hr incubation at 37 °C, the cells were treated with DMEM

(phenol red-free) containing Calcein-AM (1 μM) and ethidium homodimer (5 μM) for 30 min. Images were obtained with an inverted fluorescent microscope (Nikon Eclipse TiE inverted epifluorescence microscope) and the number of live cells were counted using ImageJ software. Cell viability was calculated by the percent ratio of the number of live cells incubated with Dox-NPs to control (without Dox-NPs).

5.3 Results and discussion

5.3.1 Synthesis of P5. Figure 5.2a illustrates our approach employing the RAFT polymerization technique to the synthesis of well-controlled P5. The approach involves the synthesis of a PEG-based macro-RAFT agent that is labeled with both a ketal linkage and a dithioester group (P4). The detailed synthesis of the PEG-based precursor labeled with a terminal amine group (PEG-ketal-NH_2, P3) is reported. Briefly, a DSC-activated PEG (P1) was converted to P2, followed by the deprotection of trifluoroacetate group in an alkaline condition, yielding P3. Each step was carefully characterized with ^{1}H-NMR analysis. The resultant P3 reacted with CPTP in the presence of DMAP as a base catalyst through a facile EDC coupling reaction. ^{1}H-NMR of P4 in Figure 5.2b shows the presence of two methyl groups of ketal moieties at 1.3 ppm (d), ethylene oxide moieties at 3.2-3.7 (EO and a), and phenyl groups of dithioester moieties at 7.3-7.9 ppm (i). Using the integral ratio of the peaks, the conjugation efficiency of the RAFT agent was determined to be >95%.

After successful synthesis and characterization, the P4 was used as a macro-RAFT agent for RAFT polymerization of HMssEt initiated with AMBN (an azo-type initiator) in anisole at 73 °C. The initial mole ratio of $[HMssEt]_o/[P4]_o$ was varied at 50/1, 65/1, and 100/1 to demonstrate that our RAFT-based approach is robust in the synthesis of a series of well-controlled P5 block copolymers with different DPs of PHMssEt block (named P5-A, P5-B and P5-C). With $[HMssEt]_o/[P4]_o$ = 50/1 as an example, the kinetics of RAFT polymerization were studied. Samples taken during the polymerization were analyzed for monomer conversion by ^{1}H-NMR and molecular weight by GPC. As shown in Figure C1, the RAFT polymerization of HMssEt in the presence of P4 was well-controlled: first-order kinetics after an induction period for 25 min, linear increase in molecular weight over conversion, and narrow molecular weight distribution (Đ <1.15).

Then, the formed P5-A was purified by precipitation from hexane to remove unreacted HMssEt monomers at 72% monomer conversion. ^{1}H-NMR of the purified P5-A in Figure 5.2b shows the peak at 1.3 ppm (d) corresponding to two methyl protons in ketal moieties as well as peaks corresponding to PHMssEt block, along with PEG block. Using the integral ratio of the peaks (EO and k) with the DP of PEG block = 113, the DP of PHMssEt block was determined to be 32. This quantity is very close to the theoretically estimated one (DP = 36) at 76% monomer conversion. GPC analysis in Figure C2 indicates that GPC trace of P5-A evolved to a high molecular weight region with increasing molecular weight as number average molecular weight (M_n) to 24.6 kg/mol (close to the theoretically estimated M_n = 18.5 kg/mol) and narrow dispersity as Đ = 1.15. A small shoulder that appeared in the low molecular weight region is attributed to a negligible trace of non-functionalized PEG species. The results obtained from NMR and GPC analysis clearly suggest that the ketal linkages at the block junctions are stable under the RAFT condition. In a similar way, other P5-B and P5-C copolymers were synthesized and characterized and the results are summarized in Table 5.1.

Table 5.1. Characteristics and properties of P5 block copolymers synthesized by RAFT polymerization of HMssEt in the presence of P4 macro-RAFT agent.[a)]

P5	$[HMssEt]_0/[P4]_0$	Time (hrs)	Conv[b)]	DP		M_n[d)]	Đ [d)]
				Theo[c)]	NMR		
A	50	2.4	0.72	36	32	24.6	1.15
B	65	3.8	0.63	41	35	25	1.16
C	100	6.7	0.66	66	59	29.3	1.21

a) Conditions for RAFT polymerization: $[P4]_o/[AMBN]_o$ = 1/0.3 in anisole at 73 °C, HMssEt/anisole = 0.6 wt/wt; b) ^{1}H-NMR; c) DP (theoretical) = $[HMssEt]_o/[P4]_o$×conversion; d) GPC with PMMA standards.

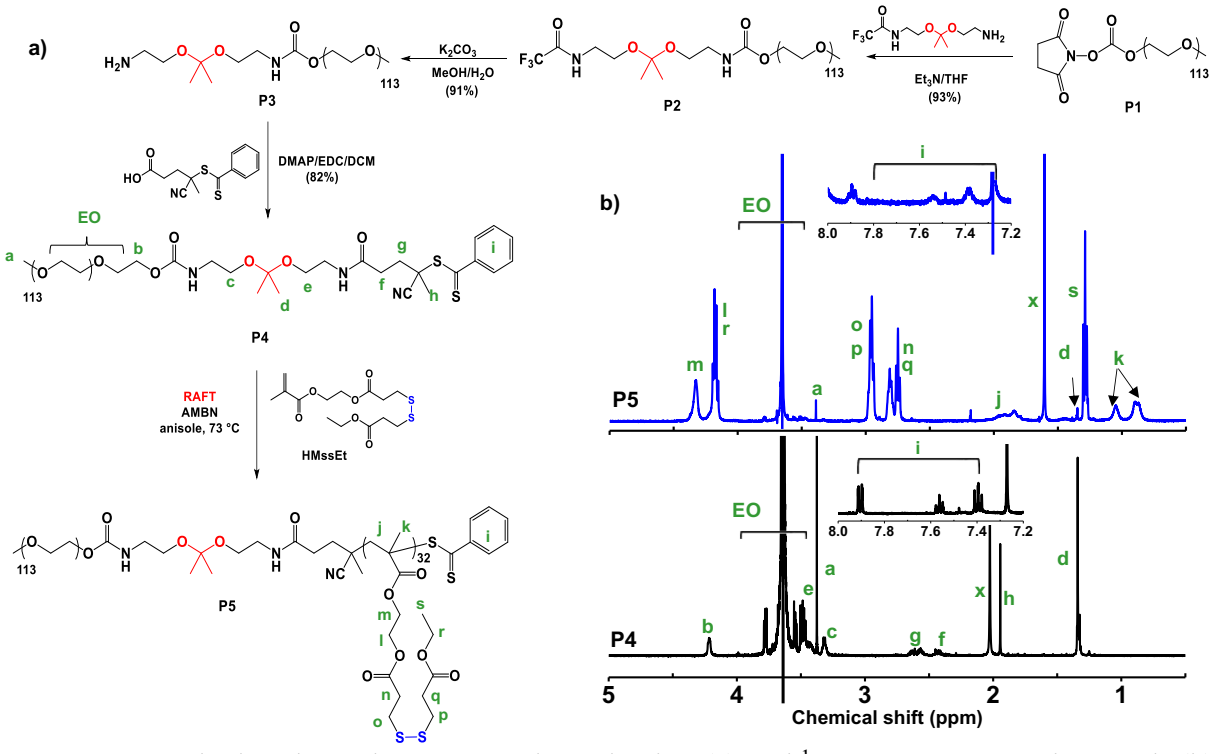

Figure 5.2 Synthetic scheme by RAFT polymerization (a) and ^{1}H-NMR spectrum in $CDCl_3$ (b) for dual acidic pH/reduction-responsive P5-A as an example, compared with P4, its macro-RAFT agent. Conditions for RAFT polymerization: $[HMssEt]_o/[P4]_o/[AMBN]_o$ = 50/1/0.3 in anisole at 73 °C, HMssEt/anisole = 0.6 wt/wt.

5.3.2 Aqueous micellization and colloidal stability. Note that the P5-A (denoted as P5 hereafter) was examined for further characterizations and evaluations. The CMC of P5 was determined using fluorescence spectroscopy with a NR probe. This method utilizes the low fluorescence of NR in an aqueous environment because of its low solubility in water. However, the NR fluorescence intensifies when NR stays in a hydrophobic environment. Figure 5.3a (inset) shows the overlaid fluorescence spectra of NR over an increasing concentration of P5. At its lower concentration, the NR fluorescence intensity kept low because of the existence of most NR molecules in an aqueous solution. Upon increasing the concentration of P5, the intensity increased, indicating the encapsulation of NR in micellar cores. As shown in Figure 5.3a, two linear regressions of maximum fluorescence intensity allow for the determination of CMC to be 8.2 μg/mL, which is in a typical range of CMC for ABPs.

Due to the amphiphilic nature, the P5 self-assembled in the aqueous solution to form micellar aggregates at concentrations above CMC. For example, a dialysis method was examined with

THF to form aqueous micellar aggregates at 0.9 mg/mL. DLS analysis indicates the diameter = 84.5 nm, along with the negligible presence of large aggregates (<1%) (Figure C3).

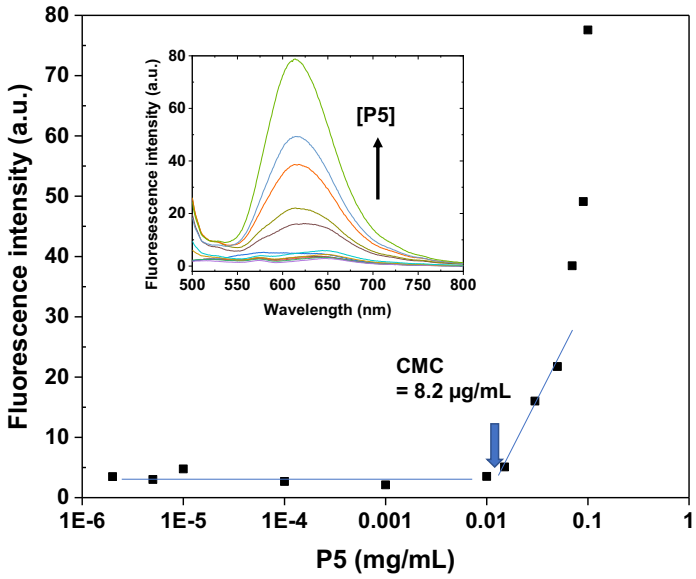

Figure 5.3 Overlaid fluorescence spectra (inset) and fluorescence intensity at maximum wavelength for aqueous mixtures consisting of NR with various amounts of P5 to determine CMC.

5.3.3 Investigation of dual acidic pH/reduction-responsive degradation. Figure 5.4a shows the anticipated responses of P5 diblock copolymer to single and dual acidic pH/reduction stimuli. Such dual degradation was first investigated in DMF using a GPC technique to follow changes in molecular weights and distributions of the P5 (Figure 5.4b). When being incubated at acidic pH, the ketal linkages at PEG/PHMssEt block junctions could be cleaved to yield PEG-OH and OH-PHMssEt as degraded products. The GPC trace of the degraded product was shifted to the lower molecular weight region, with the decrease in molecular weight from 24.6 to 15.9 kg/mol. It became bimodal, with a shoulder overlapped with the GPC trace of P4 PEG-based macro-RAFT agent. To further examine acidic pH-responsive cleavage of the ketal linkages using ^{1}H-NMR spectroscopy, an aliquot of the P5 was incubated with DCl in a NMR tube. Figure C4 shows the appearance of the new peak at 2.1 ppm presenting acetone as well as the disappearance of the peak at 1.3 ppm corresponding to two methyl groups in ketal moieties, as a consequence of the cleavage of ketal linkage in P5 at acidic pH. In the presence of excess DTT (5 equivalent to disulfides), the P5 could degrade to PEG-ketal-PHMSH upon cleavage pendant disulfides to the thiols in PHMssEt blocks. Similar to acid response, the GPC trace of the

degraded product was shifted to the lower molecular weight region, with the decrease in molecular weight from 24.6 to 19.6 kg/mol. An interesting observation was the presence of a small peak which is overlapped with the peak for the P4 (PEG-macro-RAFT agent). This result could suggest the possibility of partial cleavage of ketal linkages in the presence of DTT. Next, when being treated with both stimuli, both ketal junction and disulfide pendants could be cleaved, generating PEG-OH and HO-PHMSH as the major degraded products. The GPC trace shows two peaks: a peak appeared in low molecular weight region corresponds to PEG-OH and the other peak corresponds to HO-PHMSH.

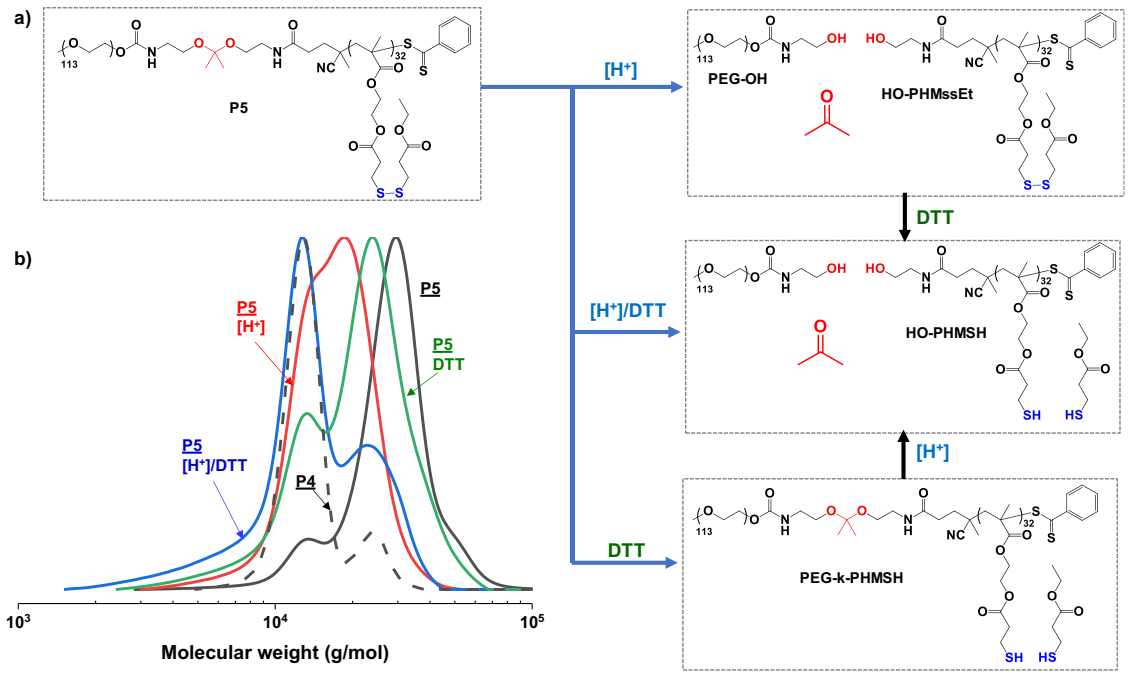

Figure 5.4 Schematic illustration of dual acidic pH/reduction-responsive degradation (a) and GPC traces of P5 before and after treatment with single and dual stimuli in DMF, compared with that of P4 macro-RAFT agent (b).

Given our comprehensive investigation in DMF (a homogeneous solution), we then investigated dual acidic pH/reduction-responsive degradation for aqueous micelles (a heterogeneous system). Figure 5.5a shows the schematic illustration of micelle degradation as a consequence of the cleavage of the ketal linkages at core/corona interfaces and the cleavage of disulfide pendants in micellar cores. Figure 5.5b shows the typical DLS diagrams of micelles incubated at acidic pH = 5.4 as well as physiological pH = 7.4 with and without 10 mM GSH for 6 hrs. Note that pH = 7.4 without GSH was included as a control with no stimuli. Their diameter changes were monitored with z-average diameter (by light scattering intensity) over incubation

time (Figure 5.5c). When the micelles were exposed to acidic pH, the size distribution became multimodal with the occurrence of large aggregation. Such change in size distribution could be indicated by an abrupt increase in their z-average diameter within 12 hrs. To get more insight into the acidic pH-responsive degradation of P5 micelles, the degraded products were further analyzed after the separation of precipitates from the supernatant (water). ^{1}H-NMR spectra in Figure C5 show that the precipitates mainly include HO-PHMssEt homopolymer and the residues in supernatant contain mostly PEG-OH homopolymer. Their GPC analysis shown in Figure C6 appears to be in full agreement with the NMR analysis. Consequently, the results from all NMR and GPC confirm the detachment of PEG coronas from PHMssEt micellar cores upon the cleavage of ketal linkages, causing destabilization of micelles to large aggregates. In the presence of 10 mM GSH, the size distribution became bimodal with the important population of large aggregates. This could be due to the destabilization of the micelles through polarity change of PHMssEt chains to the more hydrophilic PHMSH chains in micelle cores upon the cleavage of pendant disulfide groups. The z-average diameter gradually increased over incubation time for 20 hrs. The destabilization could be attributed to a change in hydrophobic/hydrophilic balance upon the cleavage of pendant disulfides to corresponding hydrophilic thiols. When being incubated with 10 mM GSH at pH = 5.4 (with dual stimuli), the z-average diameter increased more rapidly up to 8 hrs, compared with a single stimulus; however, upon further incubation, it decreased gradually over incubation time. After 24 hrs, the DLS diagram shows a significant population of small species with diameter < 1 nm. Different from single stimuli, this result is very promising because the degraded products in dual stimuli could exist at the molecular level as being soluble in the aqueous environment.

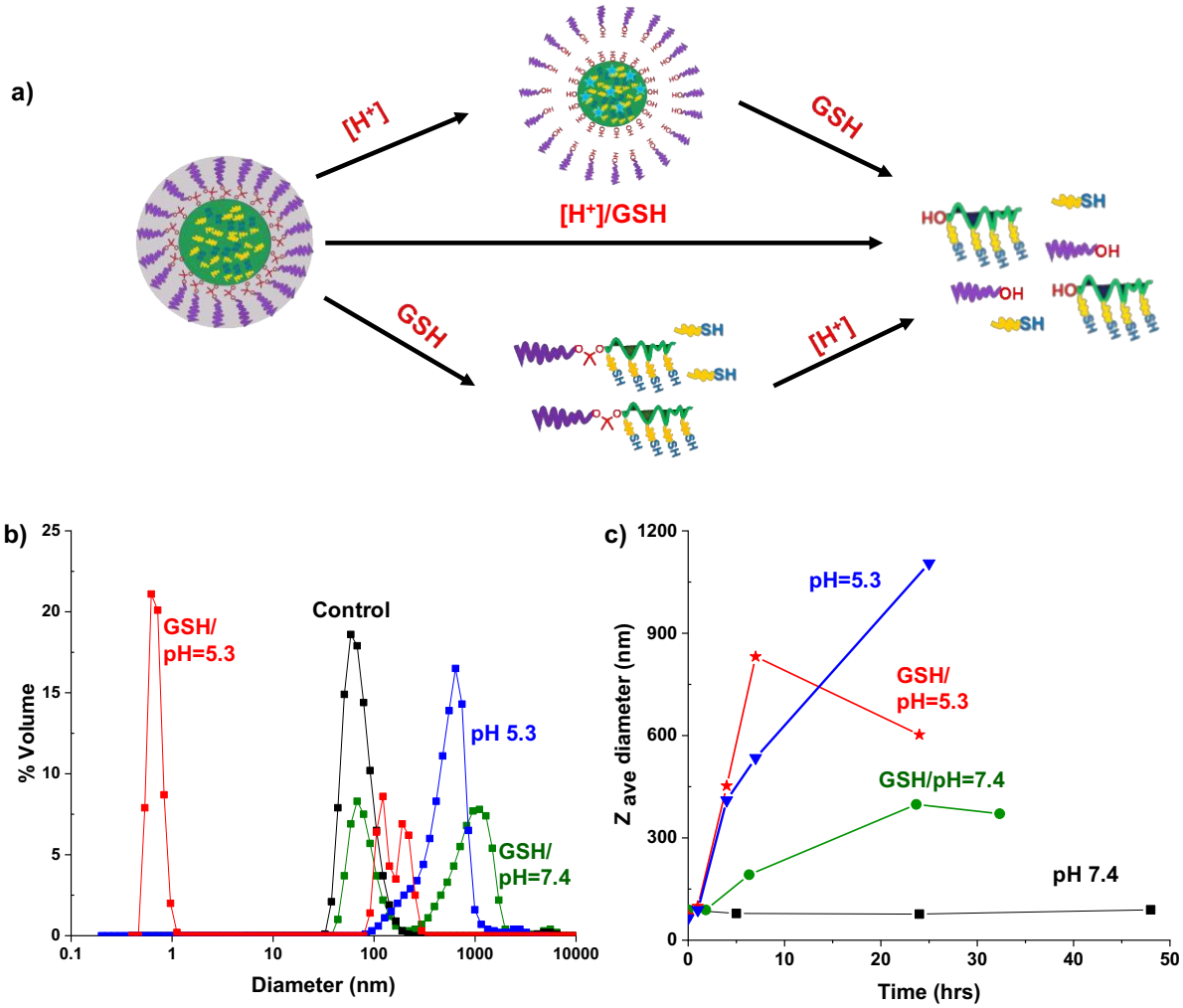

Figure 5.5 Schematic illustration of dual acidic pH/reduction-responsive degradation (a), typical examples of DLS diagrams after 6 hrs (b), and evolution of z-average diameter of micelles over time (c) incubated at acidic pH = 5.4 and physiological pH = 7.4 with and without 10 mM GSH.

5.3.4 Preparation of Dox-loaded micelles. Dox was selected as a clinically used anticancer drug. To encapsulate Dox in micelles, an organic solution of Dox treated with Et_3N in DMF was mixed with PBS (pH = 7.4) under stirring. The resulting mixture was subjected to intensive dialysis over PBS to remove free (not encapsulated) Dox and Et_3N, yielding Dox-loaded micelles (Dox-NPs) at 1.6 mg/mL. After filtration to remove unexpectedly formed aggregates, the UV/Vis spectrum of the dispersion was recorded (Figure C7). Using the pre-determined extinction coefficient of Dox (12,400 $M^{-1}cm^{-1}$) in DMF/water = 5/1 (v/v),[46] the loading level of Dox was determined to be 2.5 wt%. Next, the size and morphology of Dox-NPs were characterized using DLS and TEM techniques. The average diameter was determined to be 116.4 ± 4.0 nm for the micelles in dispersed form by DLS (Figure 5.6a). TEM analysis indicates

spherical micelles with diameter = 79 ± 30 nm in the dried state (Figure 5.6b). Note that the size by TEM is smaller than that by DLS one, which is attributed to the dehydrated state of micelles on TEM grids.

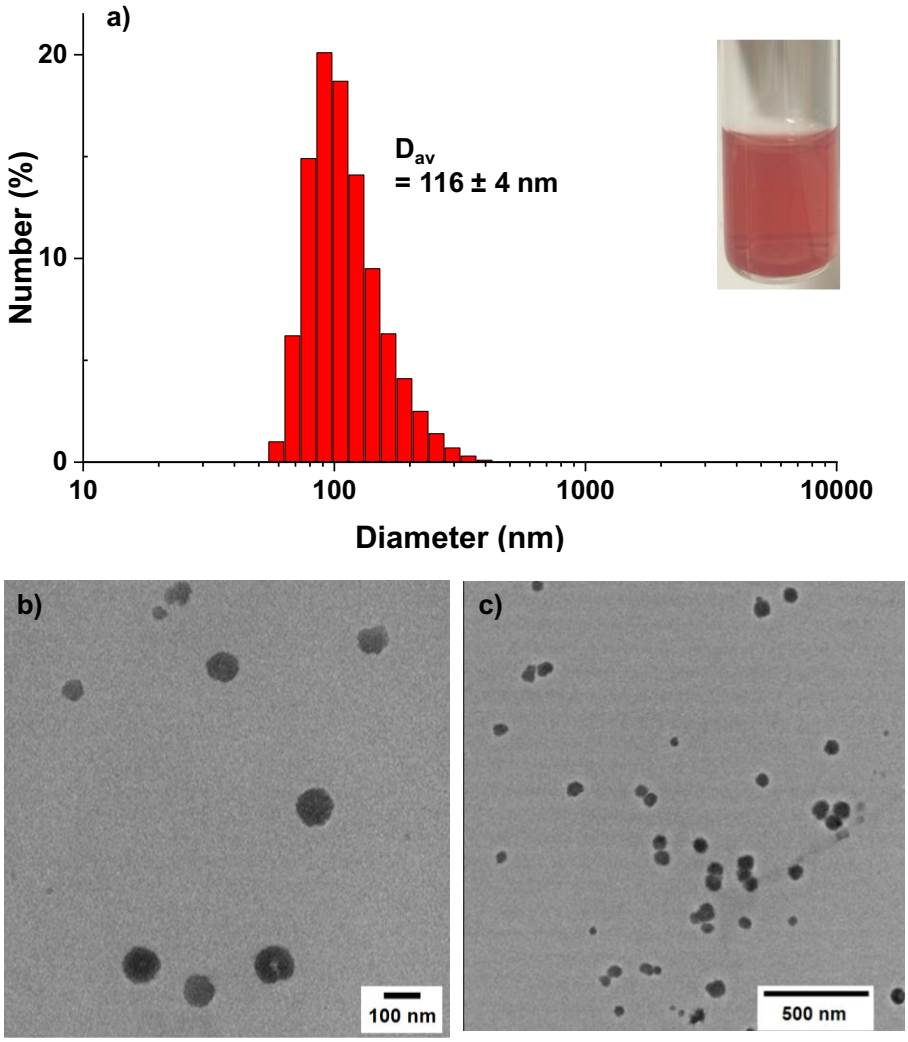

Figure 5.6 DLS diagram and digital image (inset) (a) and TEM images at high (b) and low (c) magnifications of Dox-NPs. For TEM analysis, >80 micelles were selected randomly to manually calculate the average diameter.

5.3.5 Dual location dual acidic pH/reduction-responsive release of encapsulated Dox. *In vitro* release of Dox from Dox-NPs was examined as to follow the fluorescence intensity of Dox using fluorescence spectroscopy. For the method, aliquots of Dox-NPs were placed in a dialysis tubing (MWCO = 12 kDa) and placed in an outer buffer solution under different conditions. Upon stimuli-responsive degradation of the micelles, Dox could be released from micelles and diffused out of dialysis bag into an outer buffer. Aliquots (3 mL) of outer buffer were removed at

given times to record their fluorescence spectra upon excitation at λ_{ex} = 470 nm. To maintain a sink condition, the same volume of fresh outer buffer was added to keep the same total volume of outer buffer solution. The fluorescence intensity at λ_{max}= 593 nm was used to determine the cumulative %Dox release. For the quantitative analysis, the correlation curves of fluorescence intensity at λ_{max}= 593 nm over various concentration of free Dox was constructed at pH = 7.4 and 5.4 with and without 10 mM GSH. Their slopes estimated from linear regression were similar (Figure C8), suggesting that Dox fluorescence could not be affected under these conditions.

Figure 5.7 shows the %Dox release over incubation time in the presence of dual pH = 5.4/10 mM GSH, compared with a single stimulus (pH = 5.4 or 10 mM GSH) as well as a control with no stimuli. Separately, %Dox release at pH = 7.4 was examined in triplicate as an example to analyze the standard deviation of our %Dox release (Figure C9). In the absence of stimuli (i.e. pH = 7.4), the release of Dox was slow as %Dox release reached a plateau to be ≈25% after 24 hrs. In the presence of a single stimulus (i.e. acidic pH = 5.4 and 10 mL GSH), the Dox release was enhanced to some degree. For example, %Dox release reached ≈50% when Dox-NPs were incubated at pH = 5.4. Such enhanced Dox release could be attributed to acid-responsive PEG shedding upon the cleavage of ketal linkages at block junctions. Interestingly, %Dox release also reached ≈50% in the presence of 10 mM GSH, which could be due to GSH-responsive core degradation because of the cleavage of disulfide pendants. Furthermore, Dox release was synergistically accelerated when Dox-NPs were incubated with 10 mM GSH at pH = 5.4 buffer solution. %Dox release reached >80% within 48 hrs. Such rapid Dox release could be attributed to the degradation of Dox-NPs through both PEG detachment and core polarity change upon the cleavage of both ketal junction and disulfide pendants located both at interfaces and in cores. These results show the faster release kinetics with GSH in acidic pH, compared with not only single stimuli but also neutral pH, suggesting the clear benefits for dual location dual acid/reduction degradation systems.

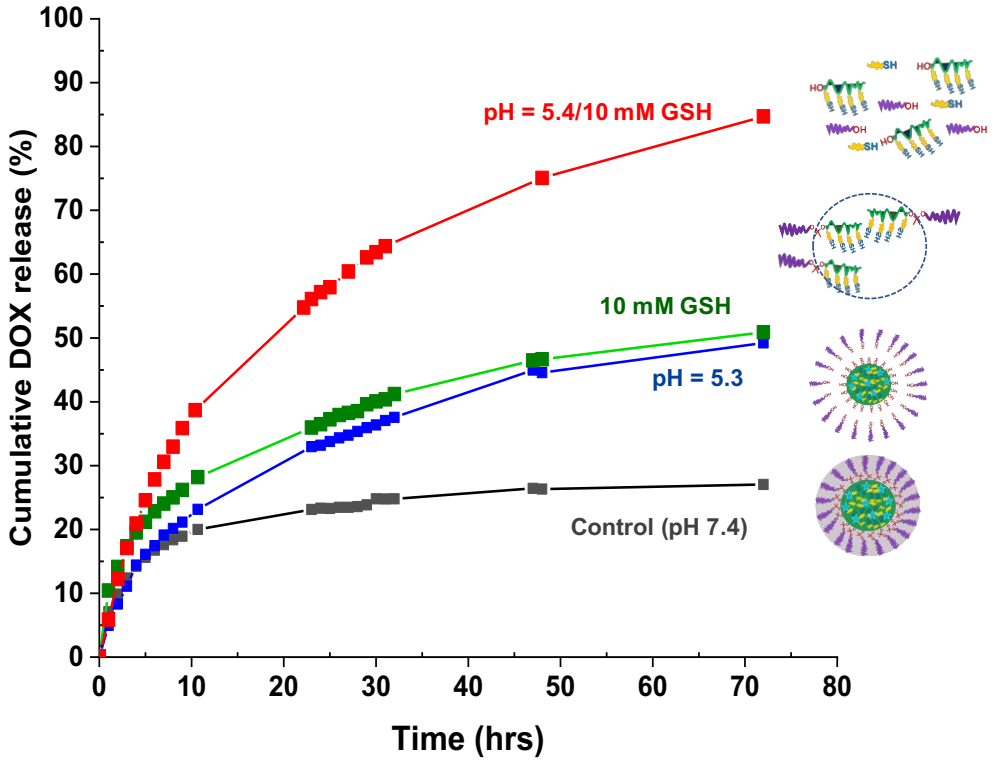

Figure 5.7 %Dox release from Dox-NPs being incubated at pH = 5.4 and 7.4 with and without 10 mM GSH.

5.3.6 Intracellular trafficking and anti-tumor activity of Dox-NPs. Cellular uptake of Dox-NPs was first investigated using flow cytometry and fluorescence microscopy. Figure 5.8 shows flow cytometry histograms of free Dox and Dox-NPs. Fluorescence intensity of Dox-NPs was much greater, compared with HeLa cells only as a control; however, the fluorescence intensity of free Dox was much greater. This could be due to the differences in internalization mechanism where Dox easily diffuses into the cells through the passive diffusion mechanism. Figure 5.9 shows fluorescence images of HeLa cells after 4 hr incubation with free Dox and Dox-NPs. The nuclei were stained with Hoechst 33342 shown in blue, and Dox fluorescence shown in red. For Dox-NPs, strong Dox signal in the perinuclear region while the weak signal in the nuclei was observed, suggesting cellular uptake of Dox-NPs. On the other hand, free Dox accumulated only in nuclei.

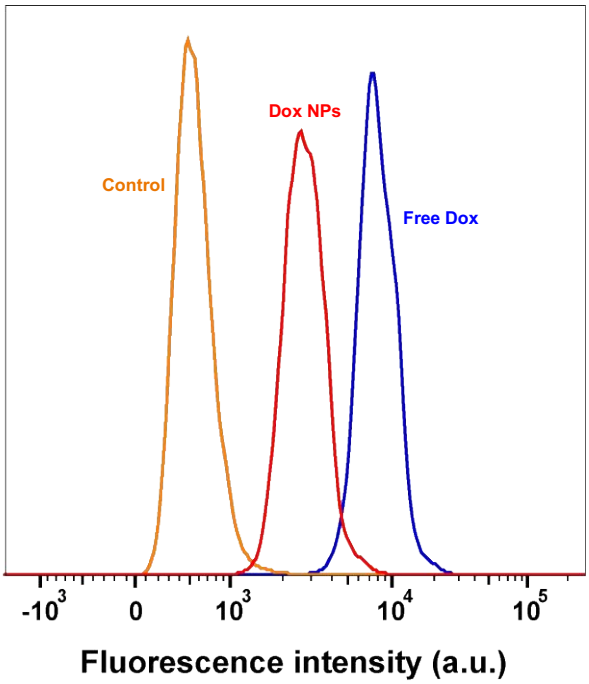

Figure 5.8 Flow cytometric histograms of HeLa cells incubated with Dox-NPs (encapsulated Dox = 2.5 μg/mL), compared with free Dox (2.5 μg/mL), for 4 hrs.

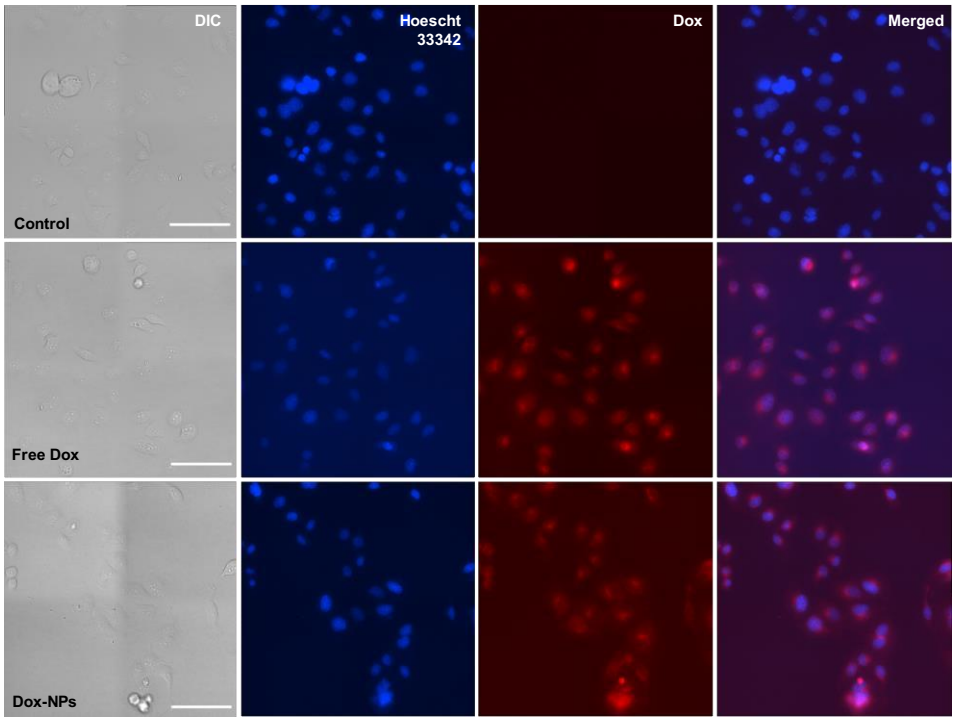

Figure 5.9 Time-lapse fluorescence microscopy images of HeLa cells incubated with Dox-NPs (encapsulated Dox = 2.5 μg/mL), compared with free Dox (2.5 μg/mL), for 4 hrs. Scale bar = 100 μm.

Next, antitumor activity of Dox-NPs was evaluated on HeLa cervical cancer cells. First, a MTT assay was used to examine the cytotoxicity of P5 empty micelles. As seen in Figure 5.10a, the viability of HeLa cells was >80% in the presence of empty micelles up to 300 μg/mL, suggesting that they are not toxic to HeLa cells. When being incubated with Dox-NPs in cell media at pH = 7.4, their viability decreased (Figure 5.10b). Given that empty micelles were biocompatible, this result suggests that the inhibition of HeLa cell proliferation is presumably due to the release of Dox from Dox-NPs. Note that the viability of HeLa cells was lower for free Dox at similar concentrations, compared with Dox-NPs.

Further to see the significance of dual acid/reduction responses at dual core/interface to cell toxicity, we have designed an experiment where HeLa cells were incubated with Dox-NPs (i.e. Dox) in the presence of 10 mM GSH (as GSH-OEt) at pH = 6.8 for 48 hrs. The mild pH condition should be examined since cell viability is significantly low at pH = 5.4. Live/Dead Cell Assay was employed to determine the HeLa viability as the percent ratio of live cells with Dox-NPs to control (no Dox-NPs) through image analysis (see Figure C10 and C11). Figure 5.10c shows the fluorescence microscopy images of live cells incubated with the various amounts of Dox-NPs (as encapsulated Dox) in dual acidic pH = 6.8/GSH condition, compared with the control at pH = 7.4 (no stimuli). For both cases, the density of live cells decreased with an increasing amount of Dox-NPs. As seen in Figure 5.10d, the HeLa viability decreased accordingly. At first glance, the viability was somewhat lower with both acid/GSH, compared to the control with no stimuli at pH = 7.4. IC_{50} value was as low as 0.5 μg/mL with both acid/GSH, which is significantly lower than that (1.04 μg/mL) for the control (pH = 7.4). However, the density of live cells is relatively quite low even without Dox-NPs when HeLa cells are incubated with 10 mL GSH-OEt at pH = 6.8 (see Figure 5.10c of dual). This result suggests the potential cytotoxicity of the combined GSH-OEt/pH = 6.8 stimuli. Although further evaluation should be followed, our preliminary result suggests the versatility of our dual location dual-responsive Dox-NPs toward effective drug delivery.

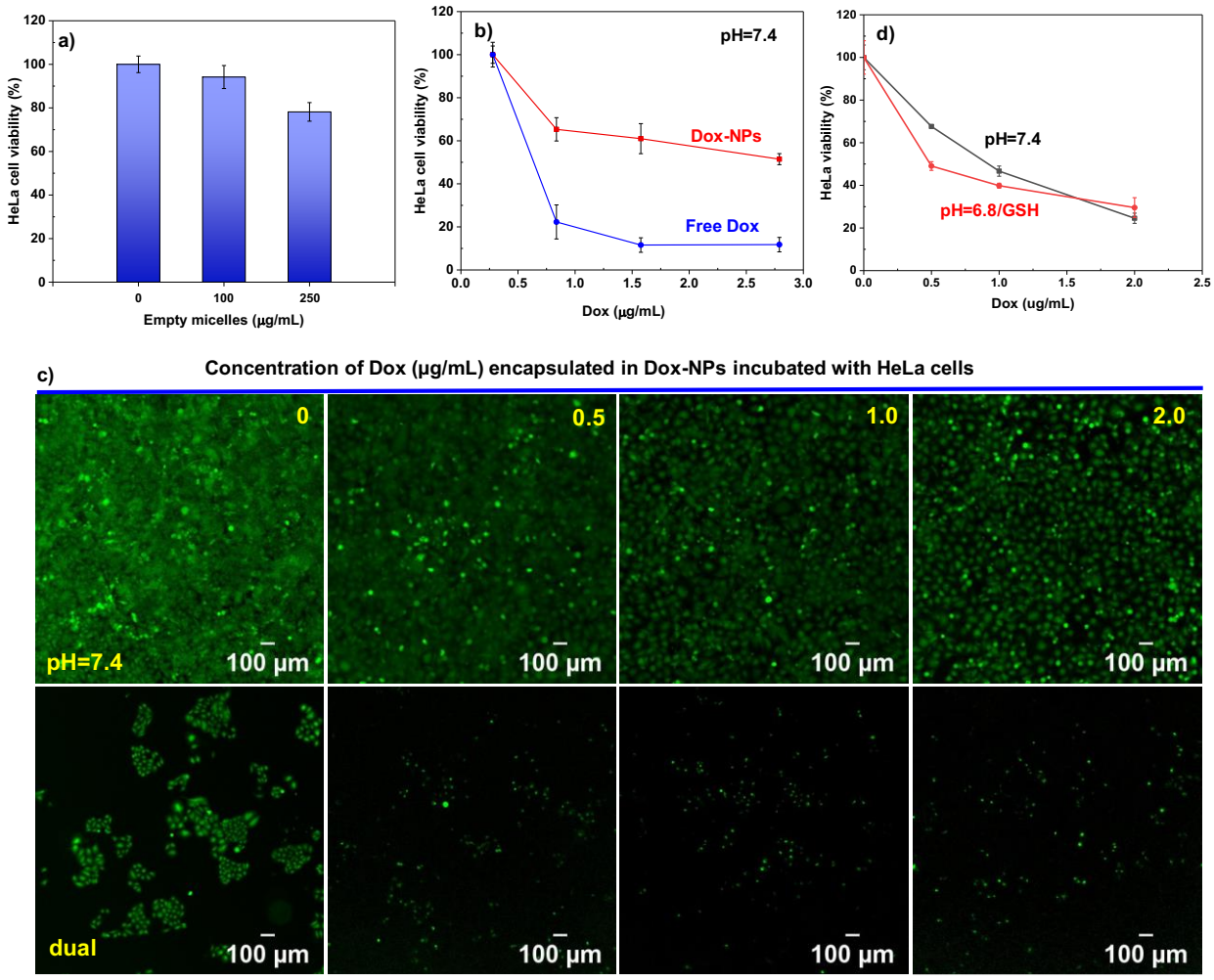

Figure 5.10 Viability of HeLa cells incubated with empty micelles (a) and Dox-NPs and free Dox at physiological pH = 7.4 (b), determined by MTT assay; fluorescence microscopy images of live cells (c) and their viability (d) incubated with and without the various amounts of Dox-NPs (as encapsulated Dox) in the presence of dual acidic pH = 6.8/GSH-OEt, compared with the control at pH = 7.4, determined by Live/Dead Cell Assay.

5.4 Conclusion

A new approach utilizing RAFT polymerization technique enabled the synthesis of a well-defined diblock copolymer composed of hydrophilic PEG and the hydrophobic PHMssEt blocks, with a ketal linkage at the block junction and disulfide pendants in hydrophobic block. Kinetic investigation with ^{1}H-NMR and GPC techniques confirms the control over RAFT polymerization of HMssEt in the presence of a PEG-based macro-RAFT agent and the stability of ketal linkages at the block junctions under the RAFT condition. The block copolymer retained amphiphilicity, thus forming Dox-loaded nanoassemblies with diameter = 188 nm at a concentration above its CMC to be 8.2 μg/mL determined by fluorescence spectroscopy with a

NR probe. The formed Dox-loaded micelles responded to reduction, acidic pH, and their combination at different locations (micellar cores and core/corona interfaces). Dual location dual responses significantly enhanced the release profile of encapsulated Dox as dual response at dual core and interface exhibits synergistic and accelerated Dox release, compared to single reduction at the core and acidic pH at the interface. Furthermore, they had great anti-tumor activity upon cellular uptake to inhibit the proliferation of cancer cells due to the effective and rapid release of Dox. Consequently, these results suggest the versatility of dual location systems for advanced drug delivery and cancer therapy.

Chapter 6: Facile strategies to synthesize dual location dual acidic pH/reduction-responsive degradable block copolymers bearing acetal/disulfide block junctions and disulfide pendants

6.1 Introduction

Block copolymers consist of two or more covalently linked blocks, each characterized with different properties such as polarity. A particular interest is an ABP designed with hydrophilic (or water-soluble) and hydrophobic blocks. Because of the amphiphilicity, well-defined ABPs are capable of self-assembly to form nanoassemblies and nanostructured materials in aqueous solution and film. Further to the amphiphilic nature, an introduction of additional functionalities into the design of ABPs and ABP-based nanoassemblies provide the versatility and multifunctionality toward various applications in pharmaceutical and materials science.[280-285] Particularly, stimuli-responsive degradation (SRD) utilizes unique dynamic covalent chemistry with labile linkages that can be cleaved in response to external stimuli (or triggers).[27, 286] Acidic pH, light, and ultrasound as well as reductive, oxidative, and enzymatic reactions are typical stimuli that have been extensively explored. The stimuli-responsive cleavage of the dynamic linkages causes the degradation of ABPs and nanoassemblies and changes their physical, chemical, and spectroscopic properties.[28, 32, 66, 287-289] These unique properties of SRD have prompted SRD-exhibiting ABPs and SRD-polymers to be useful as effective building blocks in the construction of multifunctional nanoassemblies not only as drug delivery nanocarriers[26, 65, 69, 290, 291] but also biosensors, smart films, and surfaces.[257, 265, 292-294]

Numerous strategies have been proposed for the development of SRD-exhibiting ABPs and their nanoassemblies, based on the number and location of stimuli-responsive cleavable linkages. Early strategies involve the incorporation of single-type cleavable linkages in one position of ABPs, namely as in the backbone, in pendant chain of hydrophobic blocks, or at the junction of hydrophobic and hydrophilic blocks. This, so-called single location strategies, create nanoassemblies with cleavable linkages either in the core of the micelles or at core/corona interface[67, 71] The incorporation of multiple distinct stimulus-responsive linkages has been further explored for the synthesis of dual or multi-stimuli-responsive degradable systems that can be triggered by two or more stimuli.[102-104] Similar to single stimulus-responsive systems, dual or multiple linkages are positioned predominantly in hydrophobic blocks, thus in micellar cores. A few reports describe sheddable ABPs with dual cleavable linkages positioned at block junctions,

including acetal/o-nitrobenzyl (acid/light),[231] disulfide/o-nitrobenzyl (reduction/light),[266, 295] and disulfide/thioketal (reduction/oxidation).[296] However, these shell-sheddable systems have been synthesized by coupling reaction of two homopolymers bearing either or both the cleavable linkages. Therefore, the method has limited practical application due to low coupling efficiency and difficulty in the purification of homopolymers from targeted ABPs.[297]

Recent advances include the development of a new strategy that allows for the synthesis of robust ABPs and their nanoassemblies with single disulfide or combined linkages positioned at dual or multiple locations (core, interlayer, and core/corona interface).[68, 298, 299] This strategy, referred as dual location-dual stimuli responsive degradation (DL-DSRD), can offer the versatility in that dual or multi-stimuli responses to each stimulus can independently and precisely regulate the release of encapsulated biomolecules at dual or multiple locations, as both micellar core and core/corona interface. Given the promising features, several novel DL-DSRD-exhibiting ABPs have been synthesized, particularly for endogenous and exogenous responses to dual stimuli including acidic pH/reduction,[210] reduction/acidic pH,[213, 217, 222] and light/reduction[270] at dual locations (micellar core/interface). Despite these advances, the systems present the position of a single-type disulfide or acid-labile linkage at the block junction, and thus at the core/corona interface of nanoassemblies.

ATRP and RAFT polymerization have been viewed as the most successful CRP techniques.[251, 300] They enable the synthesis of well-defined block copolymers including SRD-exhibiting ABPs with pre-determined molecular weight and narrow molecular weight distribution.[64, 301] In addition to the utilization of a single CRP technique, the combination of two distinct CRP techniques is a highly appealing approach to synthesize the arrays of multifunctional ABPs.[302-304] Furthermore, the interplay of ATRP and RAFT polymerization in the presence of RAFT mediators such as dithioesters, dithiocarbamates, and trithiocarbonates allows for the synthesis of orthogonal polymers.[305-308] As such, the rational selection of the synthetic pathways can allow for the control over morphology, architecture, orthogonality, and functionality of the resultant ABPs.

Herein, we report the synthesis of new DL-DSRD-exhibiting ABPs having dual acidic pH-labile acetal (AC) linkage and reductively cleavable disulfide (SS) bond at the hydrophilic/hydrophobic block junction as well as pendant disulfide bonds in the hydrophobic

block. The block copolymers consist of a hydrophilic poly(oligo(ethylene oxide) monomethyl ether methacrylate) (POEOMA) block and a hydrophobic polymethacrylate block having multiple disulfide pendants (PHMssEt). Through self-assembly, the formed nanoassemblies present dual acidic pH/reduction responses at interfaces and single reduction response in micellar cores, thus attaining dual stimuli responsive degradation (DSRD) at dual locations. Our synthetic pathways center on the use of a new hetero-functional bromine initiator labeled with both acetal and disulfide groups (A2). Employing a novel macroinitiator approach, three strategies utilizing a combination of ATRP and RAFT polymerization by their sequential or concurrent (or interplay) mechanism were established. Dual acidic pH/reduction-responsive degradation was investigated to understand not only site-specific responses but also the architectures and orthogonality of the formed block copolymers as diblock or triblock copolymers.

6.2 Experimental

6.2.1 Instrumentation. Fourier transform infrared spectroscopy (FT-IR) was recorded on a Nicolet iS5 spectrometer (Thermo Scientific). Other instrumentation and method were the same as in chapter 3.

6.2.2 Materials. Most reagents including triethylamine (Et_3N, 99.5%), bromoisobutyryl bromide (Br-iBuBr, 98%), pyridinium p-toluenesulphonate (PPTS, 98%), 4-cyano-4-(phenylcarbonothioylthio)pentanoic acid (CPTP), 1,4-dithiothreitol (DTT), and deuterium chloride (DCl) were purchased from Sigma Aldrich, except for 1-ethyl-3-(3-dimethylaminopropyl)carbodiimide-HCl salt (EDC) from Matrix Innovation and 2,2′-azodi(2-methylbutyronitrile) (AMBN) from Wako chemicals. Solvents include ethyl acetate (EA), hexane (HE), dichloromethane (DCM), tetrahydrofuran (THF), chloroform ($CHCl_3$), methanol (MeOH), and diethyl ether (Et_2O). All chemicals and solvents were used as received. Oligo(ethylene glycol) monomethyl ether methacrylate (OEOMA) with MW= 300 g/mol purchased from Sigma Aldrich was purified by passing through a column filled with basic aluminum oxide to remove inhibitor. Tris(2-pyridylmethyl)amine (TPMA)[271] and a methacrylate having a pendant disulfide linkage (HMssEt)[272] were synthesized as described elsewhere.

6.2.3 Synthesis of vinyl ether-Br (A1). Br-iBuBr (17.2 g, 74.9 mmol) was added dropwise to a solution containing vinyl ether ethylene glycol (6 g, 68.0 mmol) and Et_3N (8.2 g, 81.7 mmol) dissolved in DCM (60 mL) in an ice bath for 20 min. The resulting mixture was stirred at room

temperature for 5 hrs. After the removal of formed by-products (Et_3N-HBr adducts) by vacuum filtration, additional DCM (150 mL) was added. The mixture was washed with brine (150 mL) five times, and then dried over sodium sulfate. The evaporation of solvent yielded the product, a dark yellow residue (14.5 g, 90%); $R_f = 0.93$ on silica (6/4 v/v HE/EA).

6.2.4 Synthesis of Br-AC-SS-OH (A2). A1 (9.2 g, 38.9 mmol) was added dropwise to a clear solution containing 2-hydroxyethyl disulfide (6 g, 38.9 mmol), PPTS (0.97 g, 3.89 mmol), and anhydrous DCM (150 mL) in an ice bath for 20 min. The reaction mixture was stirred vigorously for 6.5 hrs at room temperature, and then quenched by the addition of Et_3N (1 mL). After being washed with PBS (pH 7.4, 100 mL) three times, the product was purified by silica gel column chromatography using HE/EA (6/4 v/v). The product, yellow oil, was collected as the second of the total two bands off a silica gel column, yielding 6.4 g (42%); $R_f = 0.33$ on silica (6/4 v/v HE/EA).

6.2.5 General procedure for ATRP. Initiator, monomer (either OEOMA or HMssEt), [Cu(II)TPMABr]Br complex, TPMA, and anisole were mixed in a 25 mL Schlenk flask. The mixture was deoxygenated by purging under nitrogen for 1 hr and then placed in an oil bath pre-heated at 40 °C. A nitrogen pre-purged solution of $Sn(II)(EH)_2$ dissolved in anisole (0.5 g) was injected to initiate polymerization. Polymerization was stopped by cooling the reaction mixture in an ice bath and exposing it to air.

Synthesis: A2 (260 mg, 0.66 mmol), OEOMA (4.0 g, 13.3 mmol), [Cu(II)TPMABr]Br (1.71 mg, 33.3 μmol), TPMA (29.0 mg, 0.10 mmol), $Sn(II)(EH)_2$ (0.10 g, 0.26 mmol), and anisole (17.4 g) for P1-20; A2 (60 mg, 0.16 mmol), OEOMA (2.5 g, 8.0 mmol), [Cu(II)TPMABr]Br (4.3 mg, 8.0 μmol), TPMA (7.3 mg, 25.0 μmol), $Sn(II)(EH)_2$ (270 mg, 0.067 mmol), and anisole (11.0 g) for P1-50; A2 (30 mg, 83.3 μmol), OEOMA (2.5 g, 8.33 mmol), [Cu(II)TPMABr]Br (2.1 mg, 4.17 μmol), TPMA (3.6 mg, 12.5 μmol), $Sn(II)(EH)_2$ (13 mg, 33.0 μmol), and anisole (11.0 g) for P1-100; P5 (0.12 g, 24.5 μmol), HMssEt (0.3 g, 0.85 mmol), [Cu(II)TPMABr]Br (0.62 mg, 1.22 μmol), TPMA (1.1 mg, 3.67 μmol), $Sn(II)(EH)_2$ (4.0 mg, 9.79 μmol), and anisole (1.7 g) for P6; P8 (0.22 g, 28.6 μmol), HMssEt (0.4 g, 1.14 mmol), [Cu(II)TPMABr]Br (0.73 mg, 1.43 μmol), TPMA (1.24 mg, 4.28 μmol), $Sn(II)(EH)_2$ (4.63 mg, 11.4 μmol), and anisole (2.2 g) for P9.

For purification, the as-prepared polymer solution was diluted with acetone and passed through a basic alumina column to remove residual copper species. The solvent was removed under rotary evaporation at room temperature. The polymer was isolated by precipitation from HE, and dried in a vacuum oven at room temperature for 15 hrs.

For kinetic studies, aliquots of the samples were taken periodically to follow monomer conversion by ^{1}H-NMR and molecular weight by GPC.

6.2.6 General procedure for RAFT polymerization. A RAFT agent, monomer (either OEOMA or HMssEt), AMBN, and anisole were mixed in a 15 mL Schlenk flask. The mixture was deoxygenated by purging with nitrogen for 1 hr and then placed in an oil bath pre-heated at 70 °C to initiate polymerization. Polymerization was stopped by cooling the reaction mixture in an ice bath.

Synthesis: P2 (0.27 g, 45.7 μmol), HMssEt (0.8 g, 2.28 mmol), AMBN (2.6 mg, 13.7 μmol), and anisole (1.3 g) for P3; and CPTP (0.14 g, 0.53 mmol), OEOMA (4.0 g, 13.3 mmol), AMBN (30.8 mg, 0.16 mmol), and anisole (6.7 g) for P7.

For purification, the as-prepared polymer solutions were precipitated from HE. The precipitates were dried in a vacuum oven at room temperature for 15 hrs.

For kinetic studies, aliquots of the samples were taken periodically to follow monomer conversion by ^{1}H-NMR and molecular weight by GPC.

6.2.7 Synthesis of P2. A solution of EDC (52 mg, 0.27 mmol) dissolved in anhydrous DCM (15 mL) was added dropwise to a solution containing the purified P1-20 (0.8 g, 0.13 mmol), Et_3N (54 mg, 0.53 mmol), CPTP (69 mg, 0.24 mmol), and anhydrous DCM (80 mL) in an ice bath. After being stirred for 24 hrs at room temperature, the resulting mixture was washed with PBS solution (pH = 7.4, 100 mL) twice, and dried over sodium sulfate. The product was precipitated from cold HE/Et_2O (6/1 v/v) twice, and dried in a vacuum oven at room temperature for 12 hrs, yielding a pink residue (0.7 g, 91%).

6.2.8 Synthesis of P4. A mixture containing the purified P1-20 (1.2 g, 0.24 mmol) and NaN_3 (0.4 g, 6.2 mmol) in DMF (15 mL) was immersed in an oil-bath pre-heated to 60 °C under magnetic stirring for 1 day. After the evaporation of the solvent, the residue was dissolved in chloroform (300 mL). The resulting solution was washed with PBS (pH = 7.4, 200 mL) twice,

and then dried over sodium sulfate. After the evaporation of the solvent, the product was purified by precipitation from HE and dried in a vacuum oven at room temperature for 12 hrs, yielding a light green residue (1.1 g, 90%).

6.2.9 Synthesis of P5. Br-iBuBr (44.0 mg, 0.19 mmol) was added dropwise to a solution containing P4 (0.25 g, 54.6 μmol), Et_3N (66.3 mg, 0.65 mmol), and anhydrous THF (30 mL) in an ice bath. The reaction mixture was stirred for 4 hrs, and then filtered to remove the formed Et_3N-HBr adducts. After the evaporation of solvent, the residue was re-suspended in DCM (300 mL), washed with PBS (pH = 7.4, 150 mL) twice, and then dried over sodium sulfate. After the evaporation of the solvent, the product was purified by precipitation from HE and dried in a vacuum oven at room temperature for 12 hrs, yielding a light green residue (0.2 g, 87%).

6.2.10 Synthesis of P8. A solution of EDC (61.5 mg, 0.32 mmol) dissolved in anhydrous DCM (5 mL) was added dropwise to a solution of P7 (0.6 g, 0.08 mmol), Et_3N (40.5 mg, 0.40 mmol), and A2 (0.15 g, 0.4 mmol) dissolved in anhydrous DCM (7 mL) in an ice bath. The reaction mixture was stirred for 24 hrs at room temperature, washed with PBS (pH = 7.4, 200 mL) twice, and dried over sodium sulfate. The product was precipitated from cold HE and dried in a vacuum oven at room temperature for 12 hrs, yielding a pink residue (0.6 g, 93%).

6.2.11 Acidic pH-responsive degradation. A solution of polymer (10 mg) dissolved in DMF (3 mL) was mixed with HCl (20 μL, 0.24 mmol) for 72 hrs. The degraded mixture was characterized using GPC to follow any change in molecular weight and its distribution. For ^{1}H-NMR analysis, a solution of polymer (50.6 mg) dissolved in DMSO-d_6 (1.5 mL) was mixed with DCl (0.19 mmol) for 24 hrs.

6.2.12 Reduction-responsive degradation. A solution of polymer (10 mg) dissolved in DMF (2.5 mL) was mixed with DTT (5 mole equivalent to disulfide linkages in the polymer) for 24 hrs. The degraded mixture was characterized using GPC to follow any change in molecular weight and its distribution.

6.3 Results and discussion

6.3.1 Synthesis of Br-AC-SS-OH initiator (A2). Three different strategies that have been explored in this work focus on the synthesis of a novel A2 initiator functionalized with an acetal, a disulfide, a hydroxyl, and a bromine group. Scheme 6.1 depicts its synthetic approach with two steps. The first step was the esterification of ethylene glycol vinyl ether with Br-iBuBr in the presence of Et_3N (a base) as described in the literature.[309] This step enabled the synthesis of A1 at 90% yield. The second step was the coupling reaction of the purified A1 with 2-hydroxyethyl disulfide in the presence of PPTS. A 1/1 mole equivalent ratio of A1 to 2-hydroxyethyl disulfide was designed to minimize the formation of a dibromide side product and facilitate the isolation of A2 from unreacted 2-hydroxyethyl disulfide. The product (A2) was purified by column chromatography at 42% yield. The structures of A1 and A2 were confirmed by NMR analysis: ^1H (Figure 6.1), ^{13}C (Figure D1 and D2), and COSY (Figure D3) NMR spectra.

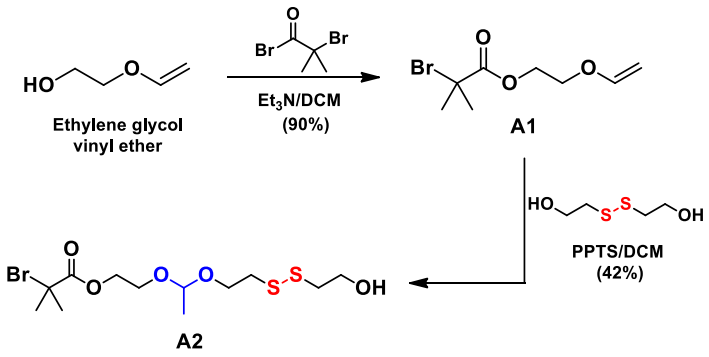

Scheme 6.1 Synthetic route to Br-AC-SS-OH (A2).

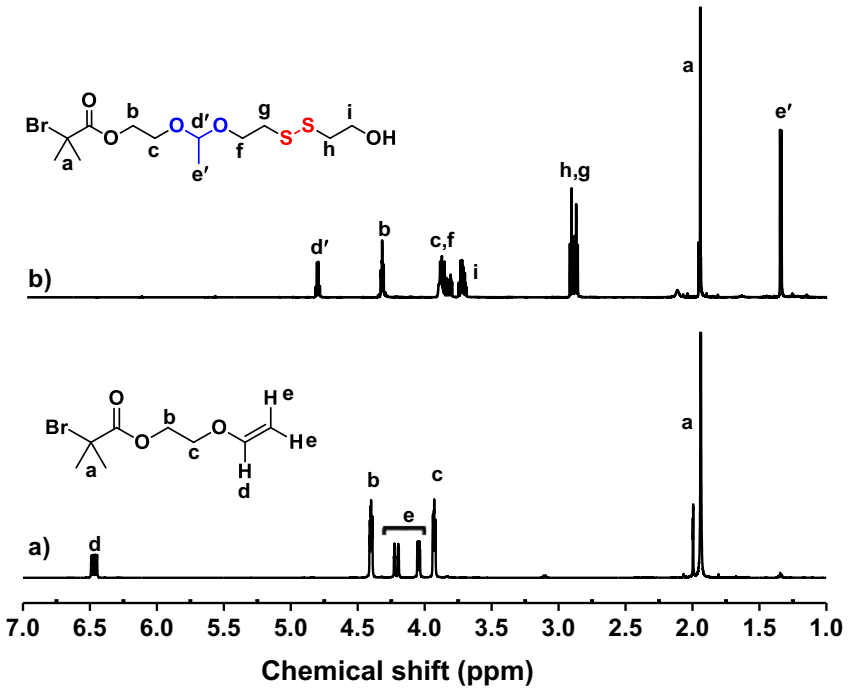

Figure 6.1 ^{1}H-NMR spectra of A1 (a) and A2 (b) in $CDCl_3$.

6.3.2 Strategies to synthesize diblock copolymers. Given the successful synthesis and characterization of A2 as an ATRP initiator, two strategies were explored to synthesize well-controlled diblock copolymers that consist of POEOMA and PHMssEt blocks. As illustrated in Scheme 6.2, two strategies differ with the utilization of both ATRP and RAFT polymerization techniques for the strategy I and only ATRP for strategy II. To achieve this, the strategies require employing facile coupling reactions to convert P1 precursor to either macro-RAFT agent or ATRP macroinitiator.

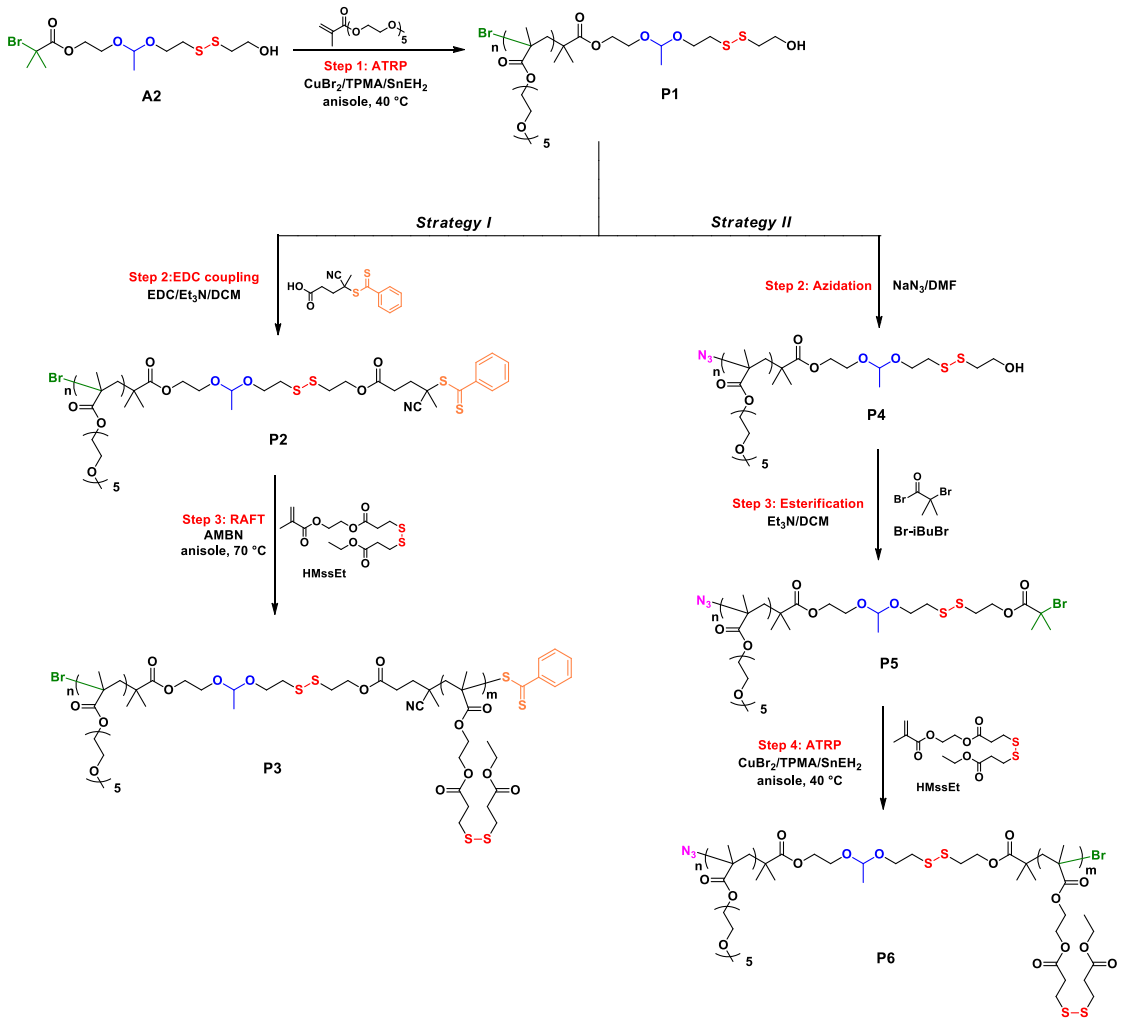

Scheme 6.2 Strategies I and II to synthesize well-defined diblock copolymers composed of POEOMA and PHMssEt blocks.

6.3.2.1 Synthesis of P1 and investigation of ATRP kinetics. The first step for both strategies I and II is the ATRP of OEOMA in the presence of an A2 initiator to synthesize a well-controlled POEOMA-AC-SS-OH (P1) homopolymer. The initial mole ratio of $[OEOMA]_o/[A2]_o$ can be defined as the DP of POEOMA when monomer conversion is complete. Here, the ratio was varied with 20/1, 50/1, and 100/1 (P1-20, P1-50 and P1-100, respectively) under similar conditions for ATRP. To investigate their kinetics, aliquots were taken periodically during polymerization to determine monomer conversion by ^{1}H-NMR and molecular weight and its distribution by GPC. As seen in Figure 6.2a, all three polymerizations were first order, indicating a constant concentration of active centers during the polymerizations. Polymerization was faster in the order of the $[OEOMA]_o/[A2]_o$ = 20/1>50/1>100/1, which is

consistent with the increasing order of A2 initiator concentration. Note that the rate of ATRP is proportional to the concentration of the ATRP initiator. Molecular weight increased monotonically with conversion, and dispersity remained low, Đ <1.2 up to 65% monomer conversion (Figure 6.2b). GPC traces evolved to a high molecular weight region over time (Figure D4). However, the molecular weights of P1 homopolymers determined by GPC, calibrated with PMMA standards, appeared to deviate from theoretically-calculated ones over conversions. Such difference is due to the different hydrodynamic volume of POEOMA, compared with PMMA standards. Overall, these results with first-order kinetics, linear increase of molecular weight, and narrow dispersity over conversion suggest that the ATRP of OEOMA in the presence of A2 is well-controlled, enabling the synthesis of well-defined P1 polymers with various DPs and narrow molecular weight distributions.

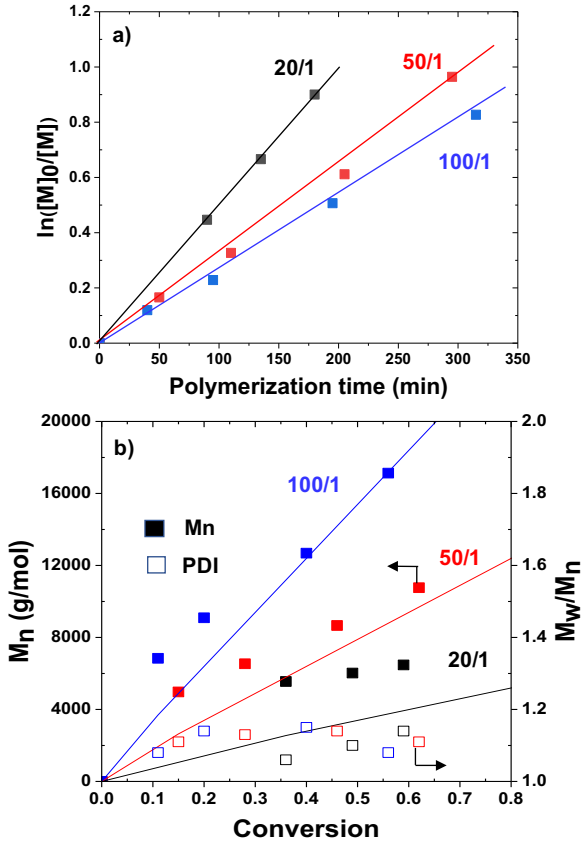

Figure 6.2 First-order kinetic plot over time (a) and evolution of molecular weight and molecular weight distribution over conversion (b) for ATRP of OEOMA in the presence of A2 initiator, with various initial mole ratios of $[OEOMA]_o/[A2]_o$ = 20/1, 50/1, and 100/1. The straight lines in (b) are theoretically calculated M_n values at conversion. Conditions for ATRP: $[A2]_o/[Cu(II)Br_2]_o/[TPMA]_o/[Sn(II)EH_2]_o$ = 1/0.05/0.15/0.4 in anisole at 40 °C, OEOMA/anisole = 0.23 wt/wt.

The formed polymers were purified by passing through a basic aluminum oxide column to remove Cu and tin species, followed by precipitation from HE to remove unreacted OEOMA monomers. As seen in Figure 6.3a, ^{1}H-NMR spectrum of the purified P1-20, as an example, shows the peaks at 4.8 ppm (e) corresponding to a methine proton of acetal group, 2.9 ppm (f and g) corresponding to four methylene protons adjacent to disulfide linkage, and 0.8-1.1 ppm (a) corresponding to the backbone methyl protons. Their integral ratios [(a/3)/(f +g/4)] were used to determine the DP of POEOMA block for P1-20 to be 14. GPC analysis indicates the purified P1-20 had the M_n = 6.7 kg/mol and Đ = 1.14 (Figure D5). The other two P1 polymers (P1-50 and P1-100) were also characterized in similar ways and the results are summarized in Table 6.1. Note that the DPs of POEOMA blocks determined by ^{1}H-NMR analysis are close to the theoretically-calculated values.

Table 6.1. Characteristics and properties of P1 homopolymers synthesized by ATRP of OEOMA in the presence of A2.[a)]

P1	$[OEOMA]_o/[A2]_o$	Time (hrs)	Conv[b)]	DP		M_n[d)] (kg/mol)	Đ [d)]
				Theo[c)]	NMR		
P1-20	20	3	0.59	12	14	6.7	1.14
P1-50	50	4.9	0.62	31	32	11	1.11
P1-100	100	5.2	0.56	56	61	17.3	1.08

a) Conditions for ATRP: $[A2]_o/[Cu(II)Br_2]_o/[TPMA]_o/[Sn(II)EH_2]_o$ = 1/0.05/0.15/0.4 in anisole at 40 °C, OEOMA/anisole = 0.23 wt/wt; b) Determined by ^{1}H-NMR; c) DP (theoretical) = $[OEOMA]_o/[A2]_o$ ×conversion; d) Determined by GPC with PMMA standards.

6.3.2.2 Strategy I (ATRP-RAFT). Given the synthesis of well-defined P1-20 by ATRP, the next step for the strategy I is the EDC-mediated coupling reaction of the terminal hydroxyl (OH) group of P1-20 with the carboxylic acid of CPTP (a RAFT agent) in presence of Et_3N as a catalyst, to synthesize P2, a POEOMA-based macro-RAFT agent. The product was precipitated from a mixture of HE/Et_2O (6/1 v/v) to remove excess CPTP from P2. ^{1}H-NMR in Figure 6.3b shows the appearance of the new peaks at 7.3-7.9 ppm (h) corresponding to aromatic protons in CPTP moieties. Combined with a change in color from white to pink, the ^{1}H-NMR analysis suggests the successful conjugation of CPTP to P1. Then, the purified P2 was used as a macro-agent for RAFT polymerization of HMssEt, initiated with AMBN (an azo-type initiator) to synthesize POEOMA-AC-SS-PHMssEt (P3) block copolymer. With the initial mole ratio of $[HMssEt]_o/[P2\ initiator]_o$ = 50/1 in anisole at 70 °C, the polymerization was stopped at 79% monomer conversion. After being purified by precipitation from hexane, the product was

analyzed by ^{1}H-NMR and GPC. ^{1}H-NMR of P3 in Figure 6.3c shows the presence of pendant methylene groups adjacent to disulfide linkages at 1.3 ppm (p) and pendant OEO moieties at 3.4-3.7 ppm (EO). Using the integral ratio of the peak (c) and the peak (p), with the DP of POEOMA block = 14, the DP of PHMssEt block was determined to be 48. GPC analysis indicates that GPC traces evolved to high molecular weight region, with M_n = 14.0 kg/mol and Đ = 1.24 (Figure D5). The characteristics and properties of the P3 block copolymer are summarized in Table 6.2.

The RAFT polymerization kinetics of HMssEt in the presence of P2-macro-RAFT agent was studied. As seen in Figure 6.4, the polymerization was well-controlled. Polymerization was first-order after an induction period of 30 min, which is due to the slow establishment of RAFT equilibrium. Molecular weight evolved to high molecular region over conversion, and dispersity remained low (Đ < 1.2) during polymerization. Furthermore, the possible activation of bromine end groups of the P2 macro-RAFT agent under RAFT polymerization condition at 70 °C could not be significant.[304, 306]

These results suggest that the strategy I composed of three steps in the order of 1) ATRP, 2) carbodiimide-coupling reaction, and 3) RAFT polymerization enables the synthesis of well-controlled block copolymers consisting of a POEOMA block covalently linked to a PHMssEt block through a spacer functionalized with dual acetal and disulfide linkages, thus POEOMA-AC-SS-PHMssEt diblock copolymer.

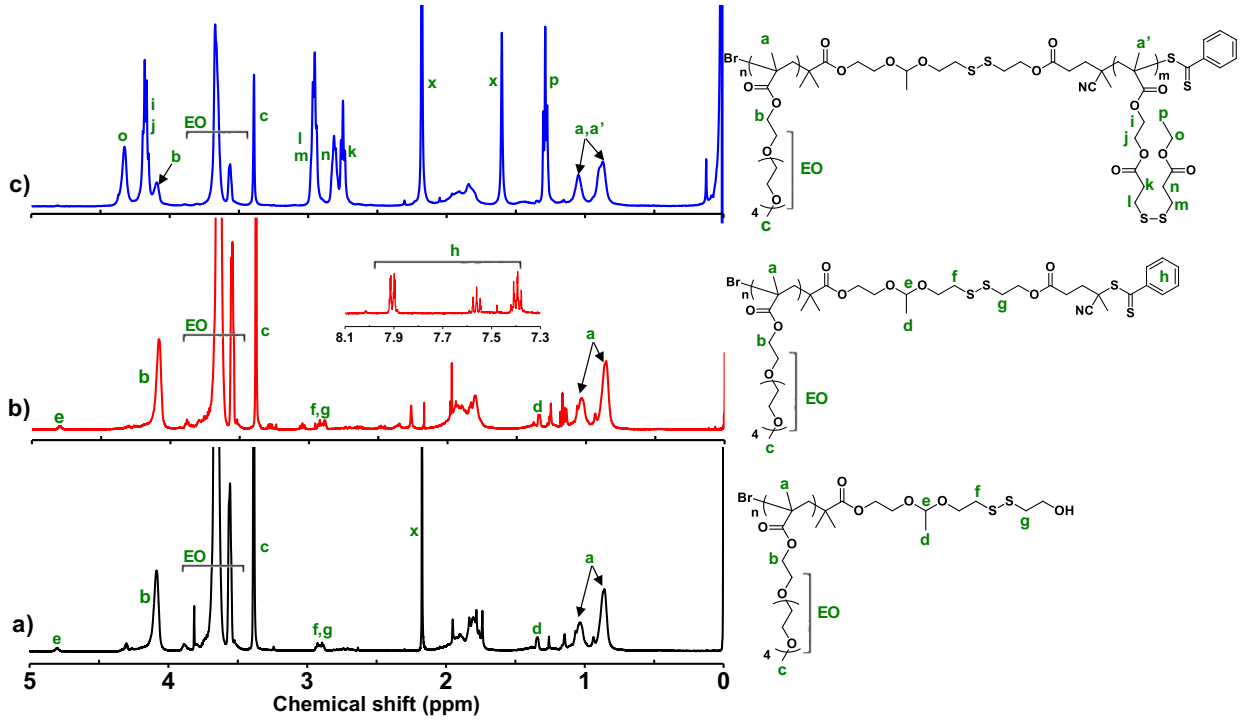

Figure 6.3 ^{1}H-NMR spectra of P1 (a), P2 (b), and P3 (c) in $CDCl_3$. Note that x denotes impurities including water and acetone.

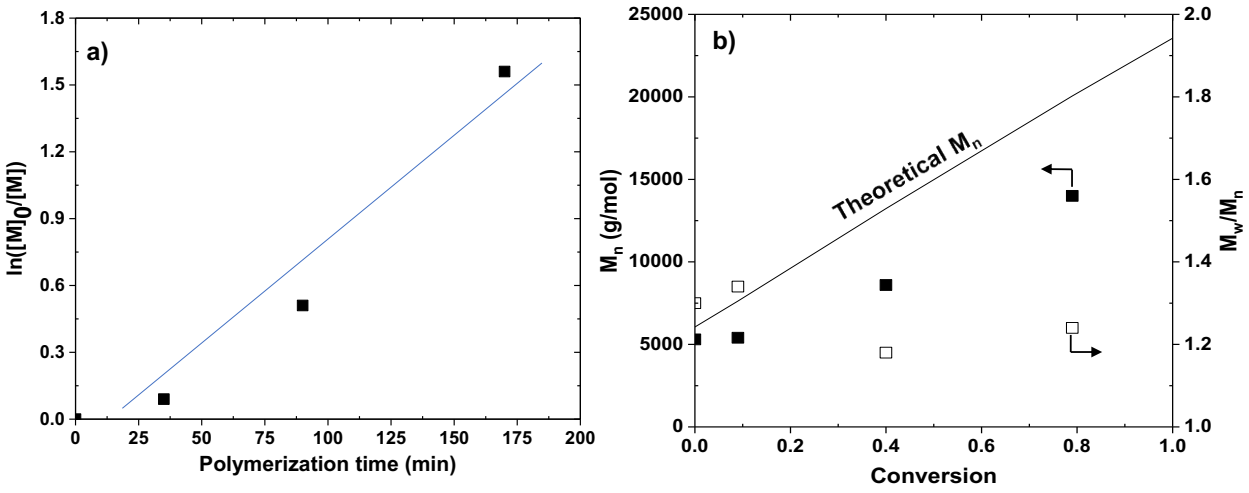

Figure 6.4 First-order kinetic plot over time (a) and evolution of molecular weight and molecular weight distribution over conversion (b) for RAFT polymerization of HMssEt, initiated with AMBN in the presence of P2 macro-RAFT agent. Conditions for RAFT polymerization: $[HMssEt]_o/[P2]_o/[AMBN]_o$ = 50/1/0.3 in anisole at 70 °C, HMssEt/anisole = 0.6 wt/wt.

Table 6.2 Characteristics and properties of block copolymers.

ABP	Precursor	$[HMssEt]_o/[P]_o$	Time (hrs)	Conv[c]	DP		M_n [e] (kg/mol)	Đ [e]
					Theo[d]	NMR		
P3[a]	P2	50	2.8	0.79	40	48	14	1.24
P6[b]	P5	35	2.1	0.85	30	30	19.1	1.25
P9[b]	P8	40	2.2	0.65	26	30	10.5	1.16

a) Conditions for RAFT polymerization: $[P2]_o/[AMBN]_o$ = 1/0.3 in anisole at 70 °C, HMssEt/anisole= 0.6 wt/wt; b) Conditions for ATRP: $[P5 \text{ or } P8]_o/[Cu(II)Br_2]_o/[TPMA]_o/[Sn(II)EH_2]_o$ = 1/0.05/0.15/0.4 in anisole at 40 °C, HMssEt/anisole = 0.18 wt/wt; c) Determined by ^{1}H-NMR; d) DP (theoretical) = $[HMssEt]_o/[precursor]_o \times$conversion; e) Determined by GPC with PMMA standards.

6.3.2.3 Strategy II (ATRP-ATRP). Given the synthesis of well-defined P1-20 by ATRP, the second step for strategy II is the azidation to convert the terminal bromine group of P1 to the corresponding azido group. Adopted from literature,[310] the azidation used excess sodium azide (25 moles equivalent to Br groups of P1) in DMF at 60 °C, yielding an azido-terminated P4 homopolymer. Attempt to quantify the azidation with the end group analysis by ^{1}H-NMR was not straightforward due to the bulkiness of POEOMA (Figure D6). GPC analysis shows no significant change in molecular weight after azidation (Figure D7). However, FT-IR could be used to follow the azidation as the FT-IR spectrum of P4 shows the presence of terminal azido groups at 2117 cm^{-1} (Figure 6.5). Then, the third step was a base-catalyzed coupling reaction of the terminal OH group of P4 with Br-iBuBr, yielding a bromine-terminated P5 macroinitiator for ATRP. To prevent the possible cleavage of the acetal group by HBr (a strong acid) formed during the reaction, a large excess of Et_3N (12 mole equivalent to polymer) was used. ^{1}H-NMR analysis indicates >95% coupling efficiency (Figure D8a).

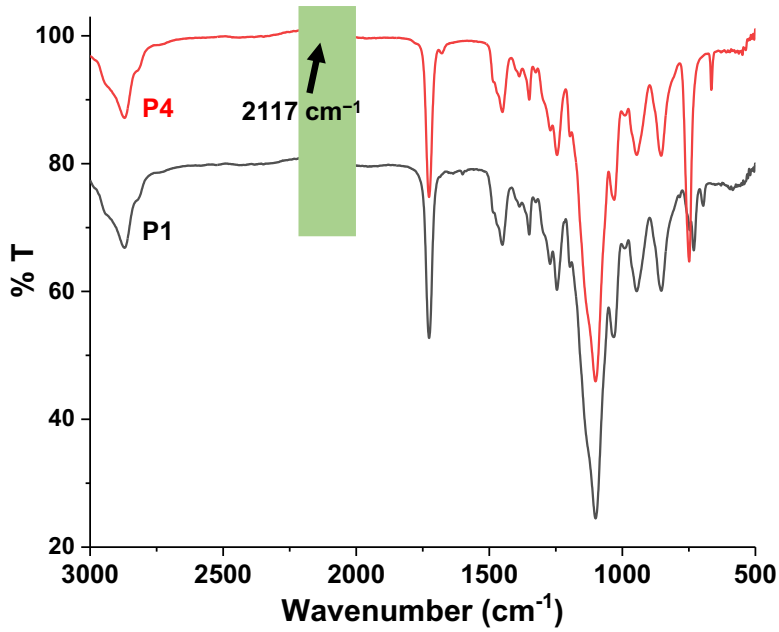

Figure 6.5 FT-IR spectrum of P4, compared with P1. The spectrum of P1 is shifted for better visualization.

In the last step, the purified P5 was used as a macroinitiator for ATRP of HMssEt, mediated with $CuBr_2$/TPMA complex, under the conditions: $[HMssEt]_o/[P5]_o$ $/[Cu(II)Br_2]_o/[TPMA]_o/[Sn(II)EH_2]_o$ = 35/1/0.05/0.15/0.4 in anisole at 40 °C. The polymerization of HMssEt in the presence of P4 was well-controlled with first-order kinetics, linear increase in molecular weight, and narrow molecular weight distribution (Figure D9). After being purified at monomer conversion= 85%, the purified P6 copolymer was characterized (see Table 6.2). ^{1}H-NMR in Figure D8b shows the presence of pendant disulfide linkages at 2.9 ppm (l and m) and pendant OEO moieties at 3.4-3.7 ppm (EO). Using their integral ratio with the DP of POEOMA block = 14, the DP of PHMssEt block was determined to be 30. GPC analysis shows that the molecular weight distribution of the copolymer clearly evolved to high molecular weight region with no evidence of a significant amount of residual P5 ATRP macroinitiator. The copolymer had the M_n = 19.1 kg/mol and Đ = 1.25 (Figure D7).

These results suggest that the strategy II is composed of four steps in the order of 1) ATRP, 2) azidation, 3) base-catalyzed-coupling, and 4) ATRP enables the formation of well-controlled block copolymers of POEOMA-AC-SS-PHMssEt diblock copolymer.

6.3.3 Strategy III exploring concurrent ATRP/RAFT to synthesize triblock copolymer.

As illustrated in Scheme 6.3, strategy III began with RAFT polymerization of OEOMA initiated with AMBN in anisole at 70 °C. The polymerization was mediated with CPTP as being designed with the $[OEOMA]_o/[CPTP]_o = 25/1$. As seen in Figure D10, the RAFT polymerization of OEOMA is well-controlled; the polymerization was first-order with an induction period of 40 min and GPC traces evolved to high molecular weight region over conversion. After purification at monomer conversion = 71%, the formed POEOMA homopolymer bearing terminal RAFT moieties and COOH group (P7) was analyzed. ^{1}H-NMR in Figure 6.6a shows the presence of aromatic groups at 7.3-7.9 ppm (g) and pendant OEO groups at 4.2 ppm (b) and 3.4-3.7 ppm (EO). Using their integral ratio, the DP of the POEOMA block was determined to be 24, which is 6 units greater than the theoretically-calculated DP (DP=18). GPC analysis indicates the M_n = 5.1 kg/mol with Đ = 1.21 (Figure D11).

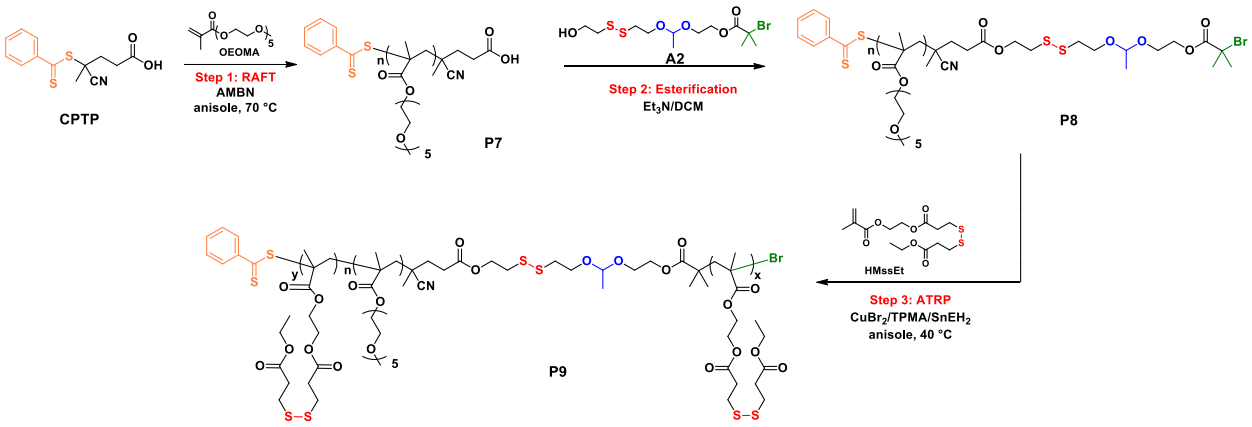

Scheme 6.3 Synthetic approach III to synthesize triblock copolymer consisting of POEOMA and PHMssEt blocks.

The second step was the carbodiimide-mediated coupling reaction of the carboxylic acid group of P7 with excess A2 (5 moles equivalent to COOH groups in P7) in presence of Et_3N. The formed product was purified by precipitation from HE. ^{1}H-NMR spectrum in Figure 6.6b shows the appearance of new peaks corresponding to protons in A2 species (d, e, f, g, h). Their integral ratio to aromatic protons in RAFT species confirms a quantitative coupling efficiency (>98%), suggesting the successful synthesis of a POEOMA bearing a terminal bromine group (P8). The third step was the ATRP of HMssEt in the presence of a P8 macroinitiator. Under the conditions of $[HMssEt]_o/[P8\text{-}Br]_o/[Cu(II)Br_2]_o/[TPMA]_o/[Sn(II)EH_2]_o = 40/1/0.05/0.15/0.4$ in

anisole at 40 °C, monomer conversion increased over time; however, the polymerization rate slowed down after 1 hr (Figure D12). This is presumably due to the loss of the terminal bromine groups or Cu(I) active centers. After being purified at 65% monomer conversion, the ^{1}H-NMR spectrum in Figure 6.6c shows the presence of pendant OEO units at 3.4-3.7 ppm and 4.2 ppm, and pendant disulfide species at 2.9 ppm. Their integral ratio with the DP of POEOMA = 24 allows for the determination of the DP of PHMssEt block to be 30, which is in good agreement with the theoretically-calculated value (DP = 26). GPC analysis indicates that the resulting block copolymer had an M_n = 10.5 kg/mol with Đ = 1.16 (Figure D11).

The P8 is functionalized with both phenyl dithioester and bromine groups at the chain ends. Under ATRP conditions, the dithioester group acts as an alkyl pseudo-halide for the ATRP mechanism.[305] Consequently, the P8 macro-RAFT agent could facilitate the polymerization of HMssEt to form PHMssEt blocks through concurrent ATRP/RAFT mechanism, thus yielding $PHMssEt_x$-AC-SS-$POEOMA_{24}$-b-$PHMssEt_y$ triblock copolymer (where x+y = 30). The formation of the triblock copolymer is further supported with our stimuli-responsive degradation study in the next section.

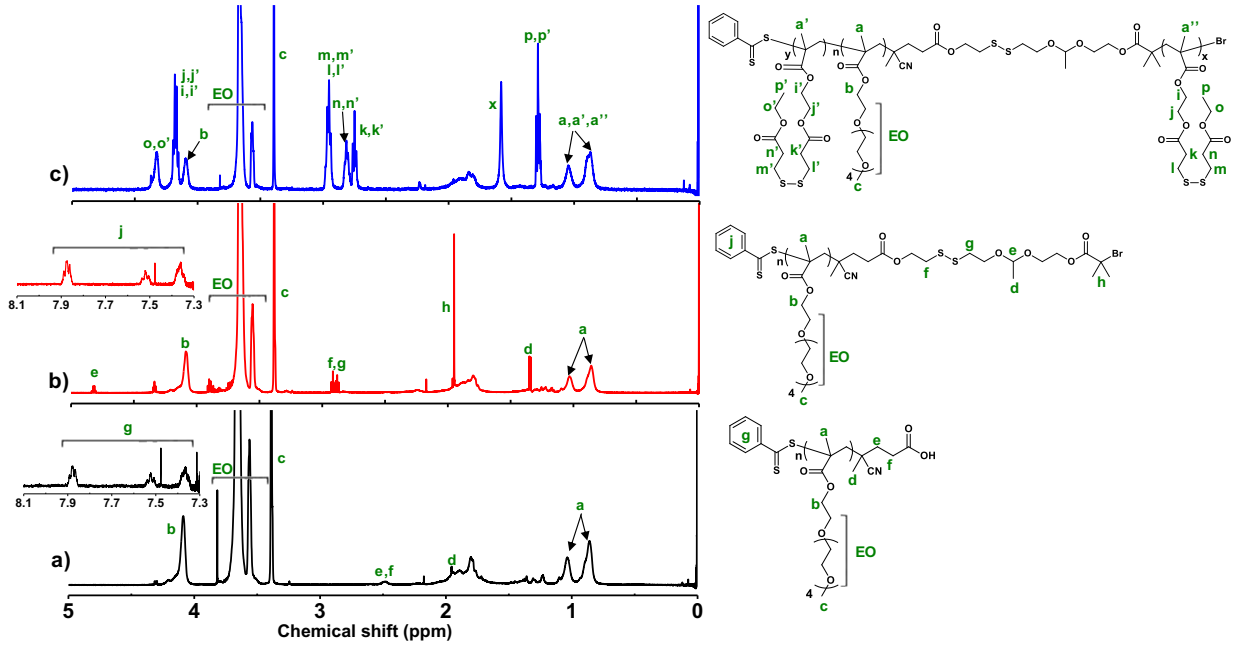

Figure 6.6 ^{1}H-NMR spectra of P7 (a), P8 (b), and P9 (c) in $CDCl_3$.

6.3.4 Stimuli-responsive degradation and structural investigation of block copolymers.

The formed block copolymers contain both acetal and disulfide linkages at the block junction as well as pendant disulfide linkages in the PHMssEt block. These labile linkages can be cleaved in the presence of a reducing agent (to disulfide) or acidic pH (to acetal). Here, reduction- and acidic pH-responsive degradation of the three copolymers (P3, P6, and P9) were examined in organic solution. Their aliquots dissolved in an organic solvent (either DMF or chloroform) were treated with either hydrogen chloride (HCl) for 72 hrs or DTT as a typical reducing agent (5 moles equivalent to disulfide linkages in the copolymers) for 24 hrs. The degradation of P3 copolymer synthesized through the strategy I was first investigated and Figure 6.7a shows the degraded products of P3 in response to acidic pH and reduction.

P3 diblock copolymer was first examined. Figure 6.7b compares the GPC traces of P3 before and after treatment with stimuli (DTT or HCl), compared with P1 precursor (POEOMA-AC–SS-OH homopolymer). Upon the cleavage of a junction acetal linkage with acid treatment, the possible degraded products include POEOMA-OH, acetaldehyde, and OH-SS-PHMssEt. The GPC trace of degraded products shows two peaks with a decrease in the M_n from 14.0 kg/mol (Đ = 1.24) to 9.9 kg/mol (Đ = 1.19). The peak in the lower molecular weight region overlapped with the GPC trace of P1 POEOMA precursor, suggesting the presence of POEOMA-OH species. To analyze the nature of the other peak shown in the higher molecular weight region, the degraded products were precipitated from MeOH. ^{1}H-NMR analysis indicates that the precipitate is mainly PHMssEt homopolymer (Figure D13) and its GPC trace overlapped with the peak in the high molecular weight region (Figure D14). These results confirm the presence of HO-SS-PHMssEt species. In addition to GPC analysis, ^{1}H-NMR analysis of degraded products shows the presence of acetaldehyde at 9.6 ppm (corresponding to aldehyde proton) as a consequence of the cleavage of the junction acetal linkage of P3 copolymer (Figure D15). Upon the cleavage of disulfide linkages with DTT, the degraded products include POEOMA-AC-SH, HS-PHMSH, and Et-SH. The GPC trace of the degraded products shows two peaks with a decreasing M_n from 14.0 kg/mol to 9.2 kg/mol (Đ = 1.19). Similarly, the peaks correspond to POEOMA and PHMSH species. These results confirm that P3 is a diblock copolymer consisting of POEOMA and PHMssEt blocks as the strategy I is designed to synthesize the diblock copolymer. During the RAFT polymerization in the presence of P2 (containing both bromine and RAFT groups), the bromine group in P2 did not appear to be activated toward ATRP.

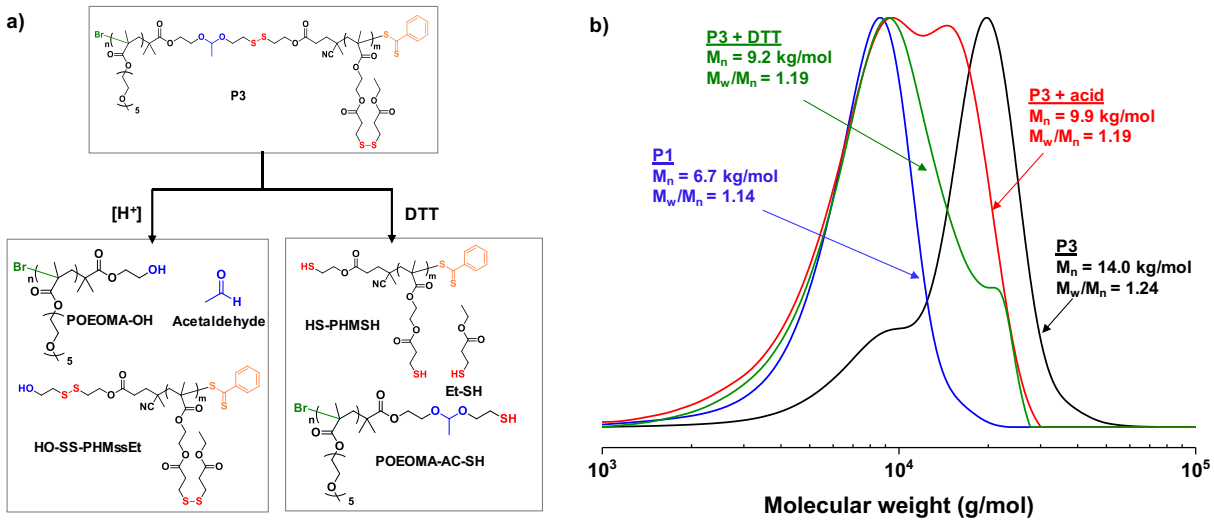

Figure 6.7 Schematic illustration of degradation (a) and GPC traces (b) of P3 before and after treatment with acid and DTT, compared with P1 precursor (POEOMA homopolymer) (b).

Figure D16 compares the GPC traces of P6 copolymer synthesized through strategy II before and after acid treatment. Similar to P3, the majority of the GPC trace of degraded products overlapped with the GPC trace of P1 POEOMA homopolymer, suggesting the generation of POEOMA-OH species as a result of the cleavage of the junction acetal linkage. Their molecular weight decreased from the M_n = 19.1 kg/mol to 8.4 kg/mol. Similar to P3, these results suggest that P6 synthesized through strategy II is the diblock copolymer consisting of POEOMA and PHMssEt blocks. This means that the conversion of bromine to azido group could be very quantitative; otherwise, triblock copolymer could be formed as a result of the chain extension of HMssEt at both end chains of POEOMA (P6).

Next, the P9 triblock copolymer synthesized through strategy III was examined. Figure 6.8a shows the possible degraded products in response to acidic pH or DTT. Figure 6.8b compares the GPC traces of P9 before and after treatment with acid. The molecular weight of the degraded products decreased from M_n =10.5 kg/mol to 9.2 kg/mol; however, unlike P3 and P6, their GPC trace did not overlap with that of its P7 POEOMA precursor. Considering that the copolymer contains 41 wt% of OEOMA units (DP = 24 for OEOMA units and 30 for HMssEt units), the GPC analysis suggests no presence of POEOMA homopolymer block in the P9 copolymer. When the P9 was incubated with DTT, similar results from GPC analysis were observed for reduction-responsive degraded products: decrease in molecular weight and no overlap with P7 precursor. Combined with the reported results that dithioester species can be activated under

ATRP conditions for styrene and methacrylate monomers,[305] our dual stimuli-responsive degradation results support that strategy III enables the synthesis of a triblock copolymer consisting of POEOMA and PHMssEt blocks.

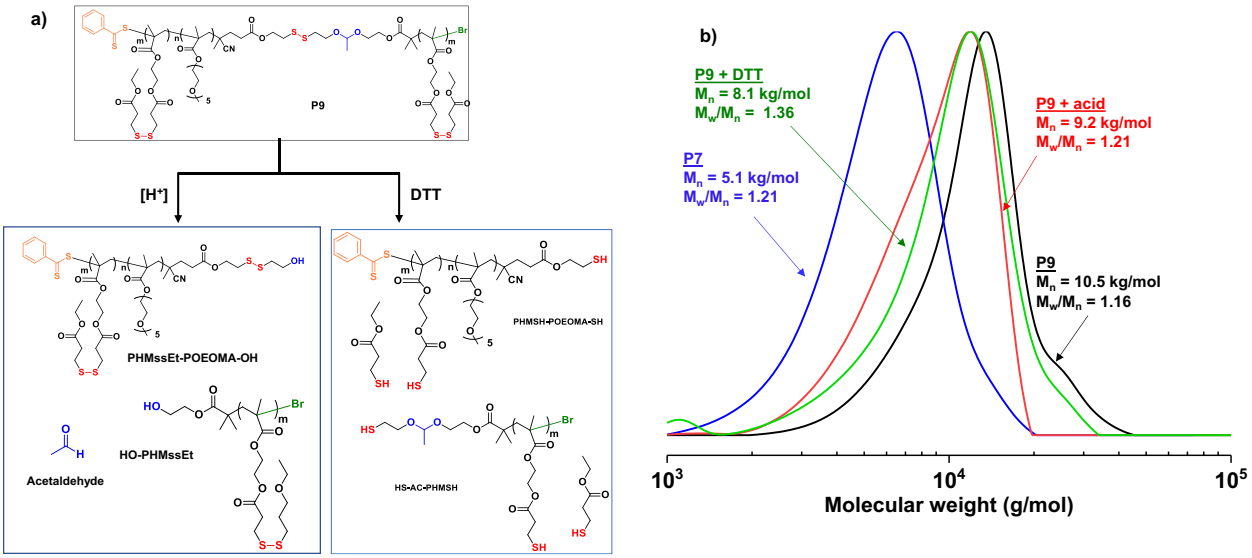

Figure 6.8 Schematic illustration of degradation (a) and GPC traces (b) of P9 before and after treatment with acid and DTT, compared with P7 precursor.

6.4 Conclusion

Well-defined ABPs featured with dual acetal/disulfide linkage junction at hydrophilic POEOMA and hydrophobic PHMssEt blocks were synthesized. Three strategies exploring the combination of ATRP and RAFT polymerization techniques in sequential or concurrent mechanisms were established with a dual acidic pH/reduction-responsive initiator having terminal hydroxyl and bromine groups. Two strategies I and II employing sequential ATRP-RAFT and ATRP-ATRP mechanism resulted in the synthesis of diblock copolymers of POEOMA-AC-SS-PHMssEt (P3 and P6), allowing for the similar control over chain lengths of both blocks, with different chain end groups. Another strategy III utilizing RAFT polymerization followed by ATRP in the presence of a dithioester-labeled macro-ATRP initiator resulted in the synthesis of a triblock copolymer of PHMssEt-AC-SS-POEOMA-b-PHMssEt (P9) through a concurrent mechanism of ATRP and RAFT polymerization. Further investigation into dual stimuli-responsive degradation provided additional confirmation to the structural analysis of the synthesis of diblock and triblock copolymers.

Chapter 7: Conclusion and future works

7.1 Conclusion

My PhD research brings out new strategies to develop acid and GSH cleavable ABPs and characterize their properties, which pave the way for future studies on acid-cleavable ABPs. In this dissertation, I report new synthetic strategies using RDRP and facile coupling reactions to prepare ABPs with acid-degradable linkages at dual locations (e.g. at the block junction and/or pendant chain of the hydrophobic block). Moreover, I demonstrated synthetic strategies to incorporate disulfide bonds, as a GSH-degradable linkage, into the structure of dual location acid-degradable block copolymers. The successful acidic or dual acid/GSH-responsive degradation, disassembly, and drug release from the block copolymers and their nanoassemblies were confirmed by several analytical methods, such as GPC, NMR, DLS, UV-VIS, and fluorescence spectroscopy. The studies revealed that the cleavage of acid-labile and GSH-cleavable linkages results in disassembly of nanoassemblies due to the synergistic shedding of hydrophilic corona as well as the loss of the hydrophobic/hydrophilic balance of micelles core. Moreover, accelerated drug release and anti-tumor activity were observed in drug-loaded nanoassemblies of the ABPs reported in this thesis. The importance of this dissertation lies in the introduction and characterization of the first examples of acid-degradable block copolymers with two degradable linkages.

In chapter 3, an acid-cleavable ABPs labeled with acetaldehyde acetal groups in hydrophobic pendant chain and at the interfaces of hydrophilic-hydrophobic block were synthesized by ATRP using an acetal labeled PEG-macroinitiator and methacrylate monomers. The fabricated nanoassemblies from these ABPs exhibited synergistic acid response at dual locations and rapid drug release. Our systematic analysis demonstrated that their acid-catalyzed degradation and disassembly are further enhanced with decreasing copolymer concentration (e.g. increasing proton/acetal mole ratio). Moreover, the incorporation of acid-ionizable imidazole pendants in the hydrophobic cores improved the encapsulation of Dox (anti-cancer drug) through π-π stacking interactions. The imidazole also enhanced acid-catalyzed hydrolysis of acetal linkages located in the core and at the interface; however, the presence of imidazole pendants induced the occurrence of core-crosslinking that compensated acetal hydrolysis and drug release.

In chapter 4, we explored ATRP to synthesize a dual location dual acidic pH/GSH-responsive degradable block copolymer (PEG-ketal-PHMssEt) labeled with an acidic pH-labile ketal linkage at the block junction and pendant disulfide groups in the hydrophobic block. A robust route with multiple steps utilizing carbamate chemistry to endow stability during protection/deprotection steps enabled the synthesis of a novel PEG-based ATRP macroinitiator labeled with a ketal linkage (PEG-ketal-Br macroinitiator). Conducting ATRP allowed for the synthesis of a series of dual location dual stimuli-responsive diblock copolymers consisting of a hydrophilic PEG block covalently conjugated through a ketal linkage with a hydrophobic polymethacrylate block having multiple disulfide pendants. Analysis showed an unexpectedly high DP of the hydrophobic polymethacrylate block that could be attributed to the instability and degradation of ketal linkages under ATRP conditions.

In chapter 5, a robust synthetic method with RAFT polymerization was used to synthesize the dual acid/GSH degradable block copolymer that was introduced in chapter 4. The synthesis of a new PEG-based macro-RAFT agent labeled with a ketal linkage (PEG-ketal-RAFT) and their subsequent polymerization with HMssEt was demonstrated. The ABPs fabricated Dox-loaded nanoassemblies using the nanoprecipitation method. The degradation of the block copolymers induced by acidic cleavage of the ketal linkages at interfaces and the reductive cleavage of pendant disulfides in the core led to the disassembly and accelerated drug release. Furthermore, *in vitro* cell culture experiments including cell viability and cellular uptake demonstrated the versatility of dual location dual acidic pH/GSH-responsive degradation platform in the development of tumor-targeting intracellular drug delivery vehicles for cancer chemotherapy.

In chapter 6, we investigated new strategies utilizing ATRP and RAFT polymerizations to synthesize new designs of dual acid/GSH cleavable block copolymers that consist of pendant oligo(ethylene glycol) and disulfide groups. Both blocks are covalently connected with an acetal linkage and disulfide bond at the junction, thus forming dual location acidic pH and GSH degradable nanoassemblies. The presence of degradable linkages at the junction of block copolymer enabled the characterization of block copolymer for their final architecture and orthogonality control during polymerization. These results revealed that the bromine terminus remains inactive during RAFT polymerization and the resulting polymer is diblock copolymer. However, the dithioester groups are activated during ATRP and likely produce triblock

copolymers. Finally, the approach with ATRP and post-polymerization azidation allowed for the synthesis of diblock copolymers.

7.2 Future works

Although several systems of dual location acid and GSH cleavable ABPs have been developed and well-characterized in this dissertation, there still exist some challenges that necessitate future research. The future direction for this dissertation should be viewed from three perspectives: 7.2.1) SRD micelles drug delivery 7.2.2) dual location acid-cleavable nanoassemblies 7.2.3) structural designs.

7.2.1 SRD micelles drug delivery

Successful clinical translation of many nanoparticle formulations has demonstrated the promise of nanoparticles for cancer treatment; however, there are still many roadblocks to overcome for accelerating the clinical translations of nanoparticles. There are excellent review articles that cover the challenges and promises of SRD nanoparticles[12, 311] but here we name a few of the most important hurdles and future directions in this field of research. 1) The literature is replete with numerous complex examples and structural designs of ABP nanoassemblies; nevertheless, only 1 formulation of ABP nanoassemblies have been approved by regulatory organizations worldwide which happened to have a very simple structural design with a short synthetic procedure.[11-13] The challenges of scaling up the complex formulations will be a significant barrier to the clinical applicability of nanomedicine, which requires the researcher's consideration before embarking on synthesizing new nanoparticle formulations. 2) Despite tremendous works on the synthesis and characterization of SRD-exhibiting ABP-based nanoassemblies, the *in vivo* investigation is still insufficient. Many studies have demonstrated the advantage of ABP-based nanoparticles for improved *in vivo* biodistribution and anti-tumor efficacy compared to free drugs. However, the *in vivo* efficacy comparison with control block copolymers (lacking the SRD linkages) is still in infancy and only a few studies have explored this concept[175, 312] The successful demonstration of the effectiveness of SRD linkages in the block copolymer requires close collaboration among cancer cell biologists, polymer chemists, pharmaceutical scientists, nanotechnology scientists, and scientists in other disciplines. 3) There has been an ongoing controversy about the extent of tumor accumulation of nanomedicines via

the EPR effect. EPR has especially been variable in different patients due to the heterogeneity and complexity of the tumor environment.[20, 77, 313] New approaches to improve the accessibility of nanoparticles to the cancer cells in the tumor by controlling the intratumoral environment, improving vascular translocation and tumor penetration should be advantageous.

7.2.2 Dual location acid-cleavable nanoassemblies

Drug delivery designs of nanoassemblies must be improved to not only improve their drug release at the tumor site but also facilitate their cellular uptake, tumor penetration, and organelle targeting. Promisingly, dual location degradable nanoparticles can provide a platform for developing a block copolymer which can produce two series of response in different sites in the tumor. For example, a new structure of block copolymer can be designed with benzylic acetal (sensitive to pH = 6.6-7.2 in the tumor tissues) at the junction and pendant disulfide bonds (sensitive to 10 mM GSH in cancer cells) in the hydrophobic core (Figure 7.1). The sequential degradation of these nanoassemblies at the tumor can potentially facilitate their cellular uptake by circumventing the poor cellular uptake of PEG nanocarriers (known as the PEG dilemma) followed by improved drug release at the cytosolic environment. This system may be further tailored to exhibit rapid particle size change by shedding the corona immediately at the tumor tissue or endosome/lysosome to improve tumor penetration or nuclear targeting of the nanoparticles, respectively.

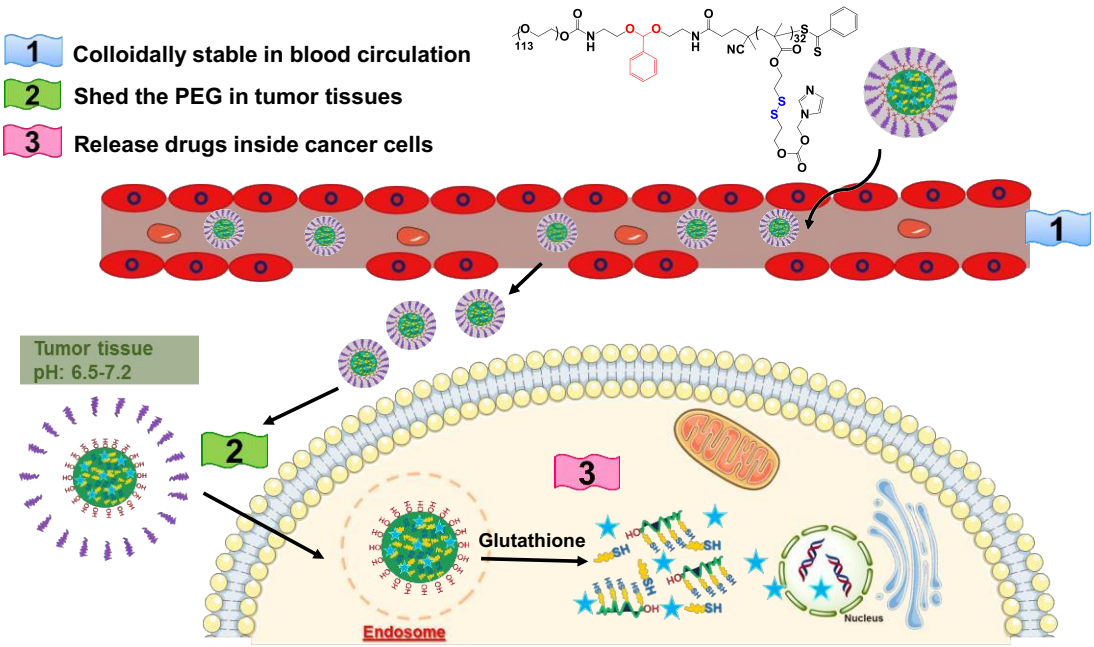

Figure 7.1 Schematic illustration of a new design of dual location acid and GSH cleavable nanoassemblies with benzylic acetal linkages at interfaces and disulfide bonds in micellar cores with potential ability to sequentially degrade in tumor tissues and intracellular environments.

Another important area that needs special attention to realize the full potential of dual location acid-cleavable nanoassemblies is to compare their degradation rate, drug release as well as their *in vitro* and *in vivo* biological activities with control block copolymers that contain no degradable linkages or degradable linkages in a single location. For instance, a comparison of dual location acid-cleavable block copolymers with a block copolymer that is designed with acid-cleavable linkages in the pendant chain may elucidate the significance of acid degradation at the junction. This, however, requires careful design of the control block copolymers with analogous molecular weight, dispersity, particle size, and so on to enable a conclusive inference.

It is very important to understand the fate and toxicity of degraded products of dual location acid-cleavable nanoassemblies. The detachment of hydrophilic corona of nanoassemblies could lead to aggregation in the tumor microenvironment, which could consequently prevent the access of stimuli to the core linkages and pose a barrier to fast drug release and elimination of nanoparticles from the tumor. Although the full understanding of this phenomenon could be very challenging, the fluorescence labeling of each block and monitoring their behavior in the 3-D tumor spheroid models or animal models using fluorescence microscopy techniques or *in vivo*

fluorescence imaging techniques can provide valuable information about the fate of degraded block copolymers in the tumor.

Finally, new techniques in the synthesis of SRD block copolymers can be used to eliminate tedious multi-step synthesis of dual locations acid-cleavable nanoassemblies. Importantly, radical ring opening polymerization (rROP)[314] can be used to synthesize block copolymers with degradable linkages at the junction and pendant chain by subsequent introduction of degradable cyclic monomers and the degradable pendant monomers. This can not only eliminate the need for the development of a new junction-degradable macroinitiator or macro-RAFT agent, but it can also allow for simultaneous labeling of the junction of block copolymers with multiple degradable linkages in one polymerization reaction.

7.2.3 Structural designs

For chapter 3 where the dual location dual acid-cleavable ABP was introduced, acetaldehyde acetal linkage exhibited slow hydrolysis kinetics even in acidic pH (pH = 5.3). Although the drug release was rapid within the same time, such a rapid release could be partially attributed to the protonation of amines in Dox. Investigation of the release with drugs with non-ionizable species such as paclitaxel and CPT would provide a clearer picture of drug release from these nanoassemblies. In addition, to benefit from the full potential of dual location acid-cleavable nanoparticles, it is hypothesized that new acid-cleavable linkages with a more rapid rate of hydrolysis, such as benzylic acetals could produce faster drug release. Since the ACMA linkage in the P1 and P2 ABPs were found to contain small hydrophobic characteristics, it is envisaged that changing an acetaldehyde acetal linkage to a benzylic acetal should improve drug loading by introducing π-π interactions. Another challenge in this work was the reactivity of CDI moieties which led to crosslinking and slow release of Dox from P2 nanoassemblies. Imidazole without carbonate bond would prevent crosslinking, while it can still yield imidazole-promoted hydrolysis in the tumor.

For chapter 4 where dual acid/GSH cleavable ABP was synthesized by ATRP, a new and facile approach to synthesize the ketal labeled macroinitiator or macro-RAFT agent can be examined by adaptation from new procedure in the literature.[315] As illustrated in Scheme 7.1, the proposed route is anticipated to reduce the synthetic steps to four. Moreover, advances in RDRP in the last 5 years have led to the development of new ATRP techniques, such as iron-catalyzed

ATRP,[316] photo-ATRP,[317] and metal-free ATRP[318, 319] which can eliminate the need for the use of copper and allow for more facile synthesis of ketal-based polymers by ATRP.

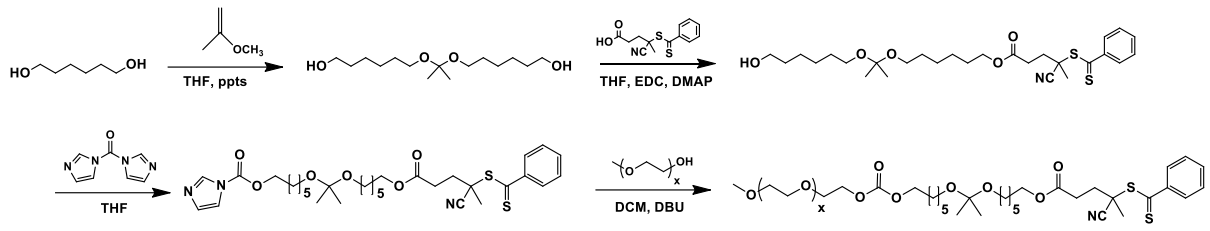

Scheme 7.1 Proposed reaction scheme to optimize the synthesis of ketal-labeled ATRP macroinitiator.

For chapter 5 where dual acid/GSH-cleavable ABPs were evaluated for drug delivery, the instability of ketal caused *in vivo* failure of the formed nanoassemblies. It is worthwhile to seek the development of acid-cleavable linkages that show sufficient stability in the physiological pH while degrading rapidly in the tumor tissues. Another challenge in this area is that our knowledge about the true concentration and the co-occurrence of GSH and acidic pH in the cytosolic environment is inadequate especially in the 2D *in vitro* cells experiment, mainly due to the heterogeneity of cancer cells and the existence of 2D cells outside of their natural environment. Meanwhile, the *in vivo* redox environment of cancer cells is very complex which is governed not only by GSH but by various other redox processes such as oxygen/superoxide (O2/O2•−) system, nicotinamide adenine dinucleotide phosphate (NADP+/NADPH) system, and numerous enzymes such as thioredoxin reductase, NADH-oxidase, etc.[40] *In vitro* release and anti-cancer activity studies provided preliminary results about the promise of our dual acid/GSH degradable nanoassemblies but can never guarantee successful anti-tumor activity in animal studies. In line with this, our result from the MTT assay shows free Dox is more potent compared to Dox-NPs. Although this observation is not unprecedented among other stimuli responsive ABP micelles, future experiments should be performed to investigate the underlying reason for this observation by measuring *in vitro* concentration of GSH and pH of HeLa cells.

For chapter 6 where new design of acid/GSH-cleavable ABP with two cleavable linkages at the junction was developed, the initial design was aimed to incorporate two degradable linkages with similar degradation rate to achieve accelerated corona shedding in the tumor environment. However, our results found that acetaldehyde acetal exhibits a slower degradation profile compared to disulfide in response to biologically relevant levels of acidity (pH = 5.3) and GSH

(10 mM). This undermines our purpose to achieve promoted degradation of junction in the cancer cells. The plausible solution would be to incorporate an acid-cleavable linkage with a faster hydrolysis rate.

Another challenge in our presented synthetic strategies is that both route #1 and route #2 require post-polymerization addition of a precursor, whether it is the RAFT agent or sodium azide and bromoisobutyrl bromide. Due to great steric barriers, some polymers still remain unfunctionalized even when a large excess of the small molecule reagents are used. This consequently results in some homopolymers contamination in the final batch of block copolymers, which can even be observed as a small shoulder in the GPC traces. We have tried to address this problem in our most recent work by synthesizing a new iniferter which is labeled with both Br and dithioester (Figure 7.2). Nevertheless, even this approach has the limitation of only forming triblock copolymers due to the occurrence of the concurrent ATRP and RAFT polymerization. A possible solution to a diblock copolymer without post-polymerization modification would be to synthesize a new iniferter with Br and trithiocarbonate RAFT agent, rather than dithioester, because the trithiocarbonate moieties are found to stay inactive during ATRP polymerization condition.[173]

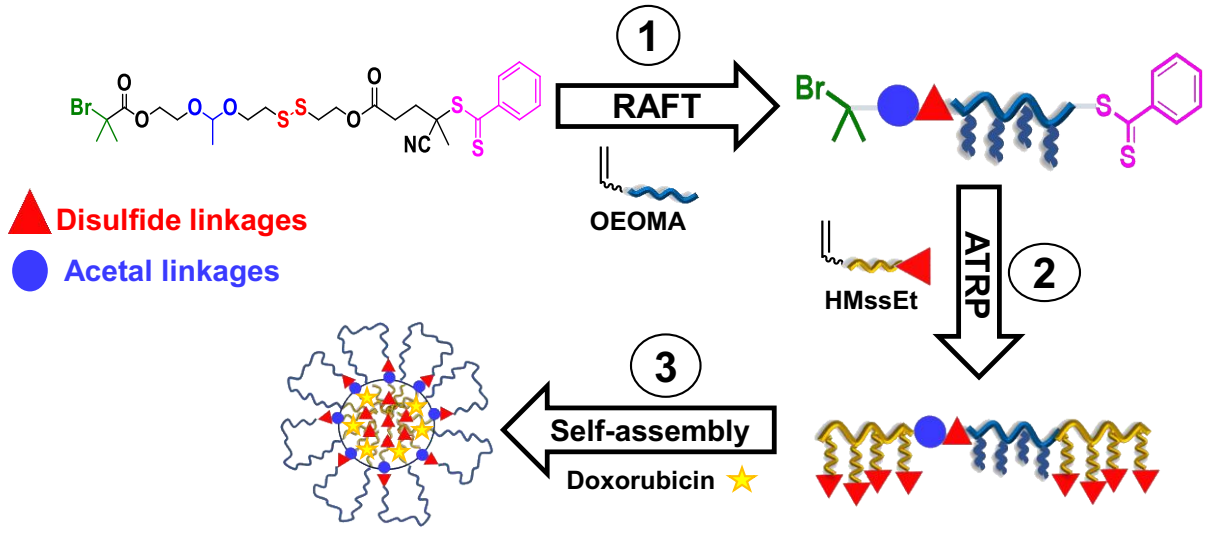

Figure 7.2 Schematic illustration of a new approach to synthesize a triblock copolymer with acetal and disulfide junctions without post-polymerization modification.

Finally, the concurrent RAFT and ATRP were observed in the strategy III. The question remains that whether the triblock copolymers formed from this synthetic route have an

approximately identical numbers of repeating units on each side. It is well-known that RAFT polymerization has an induction period and a different initiation rate than ATRP.[56] This increases the possibility of the formation of asymmetric triblock copolymer. The understanding of the exact composition of the ABPs, their DP and identity of the end group of each block requires careful purification of each block after degradation.

References

1. Provisional data on causes of death, January to April 2019 and January to April 2020, https://www150.statcan.gc.ca/n1/daily-quotidien/200703/dq200703b-eng.htm, (accessed 28 May 2021).
2. Q. Jin, Y. Deng, X. Chen and J. Ji, *ACS Nano*, 2019, **13**, 954-977.
3. F. Saraci, V. Quezada-Novoa, P. R. Donnarumma and A. J. Howarth, *Chem. Soc. Rev.*, 2020, **49**, 7949-7977.
4. M. Elsabahy, G. S. Heo, S.-M. Lim, G. Sun and K. L. Wooley, *Chem. Rev.*, 2015, **115**, 10967-11011.
5. M. W. Tibbitt, J. E. Dahlman and R. Langer, *J. Am. Chem. Soc.*, 2016, **138**, 704-717.
6. Y. Matsumura and H. Maeda, *Cancer Res.*, 1986, **46**, 6387-6392.
7. H. Maeda, J. Wu, T. Sawa, Y. Matsumura and K. Hori, *J. Controlled Release*, 2000, **65**, 271-284.
8. S. Behzadi, V. Serpooshan, W. Tao, M. A. Hamaly, M. Y. Alkawareek, E. C. Dreaden, D. Brown, A. M. Alkilany, O. C. Farokhzad and M. Mahmoudi, *Chem. Soc. Rev.*, 2017, **46**, 4218-4244.
9. Z. Ahmad, A. Shah, M. Siddiq and H.-B. Kraatz, *RSC Adv.*, 2014, **4**, 17028-17038.
10. C. Allen, D. Maysinger and A. Eisenberg, *Colloids Surf., B*, 1999, **16**, 3-27.
11. H. Cabral and K. Kataoka, *J. Controlled Release*, 2014, **190**, 465-476.
12. L. Houdaihed, J. C. Evans and C. Allen, *Mol. Pharmaceutics*, 2017, **14**, 2503-2517.
13. H. He, L. Liu, E. E. Morin, M. Liu and A. Schwendeman, *Acc. Chem. Res.*, 2019, **52**, 2445-2461.
14. I. W. Wyman and G. Liu, *Polymer*, 2013, **54**, 1950-1978.
15. X.-Y. Tu, M.-Z. Liu and H. Wei, *J. Polym. Sci., Part A Polym. Chem.*, 2016, **54**, 1447-1458.
16. K. Khanna, S. Varshney and A. Kakkar, *Polym. Chem.*, 2010, **1**, 1171-1185.
17. K. Knop, R. Hoogenboom, D. Fischer and U. S. Schubert, *Angew. Chem., Int. Ed.*, 2010, **49**, 6288-6308.
18. D. Hwang, D. Ramsey Jacob and V. Kabanov Alexander, *Adv Drug Deliv Rev*, 2020, **156**, 80-118.
19. C. Englert, J. C. Brendel, T. C. Majdanski, T. Yildirim, S. Schubert, M. Gottschaldt, N. Windhab and U. S. Schubert, *Prog. Polym. Sci.*, 2018, **87**, 107-164.
20. H. Cabral, K. Miyata, K. Osada and K. Kataoka, *Chem. Rev.*, 2018, **118**, 6844-6892.
21. A. Blanazs, S. P. Armes and A. J. Ryan, *Macromol. Rapid Commun.*, 2009, **30**, 267-277.
22. Y. Huang, A. Moini Jazani, E. P. Howell, J. K. Oh and M. G. Moffitt, *ACS Appl. Mater. Interfaces*, 2020, **12**, 177-190.
23. K. E. B. Doncom, L. D. Blackman, D. B. Wright, M. I. Gibson and R. K. O'Reilly, *Chem. Soc. Rev.*, 2017, **46**, 4119-4134.
24. N. Kamaly, B. Yameen, J. Wu and O. C. Farokhzad, *Chem. Rev.*, 2016, **116**, 2602-2663.
25. S. Fredenberg, M. Wahlgren, M. Reslow and A. Axelsson, *Int. J. Pharm.*, 2011, **415**, 34-52.

26. H. Wei, R.-X. Zhuo and X.-Z. Zhang, *Prog. Polym. Sci.*, 2013, **38**, 503-535.
27. C. J. F. Rijcken, O. Soga, W. E. Hennink and C. F. van Nostrum, *J. Controlled Release*, 2007, **120**, 131-148.
28. A. W. Jackson and D. A. Fulton, *Polym. Chem.*, 2013, **4**, 31-45.
29. S. Guragain, B. P. Bastakoti, V. Malgras, K. Nakashima and Y. Yamauchi, *Chem. Eur. J.*, 2015, **21**, 13164-13174.
30. Q. Hu, P. S. Katti and Z. Gu, *Nanoscale*, 2014, **6**, 12273-12286.
31. S. Binauld and M. H. Stenzel, *Chem. Commun.*, 2013, **49**, 2082-2102.
32. Y. Ding, Y. Kang and X. Zhang, *Chem. Commun.*, 2015, **51**, 996-1003.
33. F. D. Jochum and P. Theato, *Chem. Soc. Rev.*, 2013, **42**, 7468-7483.
34. T. Manouras and M. Vamvakaki, *Polym. Chem.*, 2017, **8**, 74-96.
35. G. Kocak, C. Tuncer and V. Butun, *Polym. Chem.*, 2017, **8**, 144-176.
36. J. K. Oh, *Polym. Chem.*, 2019, **10**, 1554-1568.
37. B. Deng, P. Ma and Y. Xie, *Nanoscale*, 2015, **7**, 12773-12795.
38. G. Saito, J. A. Swanson and K.-D. Lee, *Adv. Drug Deliv. Rev.*, 2003, **55**, 199-215.
39. M. Huo, J. Yuan, L. Tao and Y. Wei, *Polym. Chem.*, 2014, **5**, 1519-1528.
40. J. F. Quinn, M. R. Whittaker and T. P. Davis, *Polym. Chem.*, 2017, **8**, 97-126.
41. S. Y. An, S. H. Hong, C. Tang and J. K. Oh, *Polym. Chem.*, 2016, **7**, 4751-4760.
42. N. R. Ko, J. Cheong, A. Noronha, C. J. Wilds and J. K. Oh, *Colloids Surf., B*, 2015, **126**, 178-187.
43. B. Khorsand, G. Lapointe, C. Brett and J. K. Oh, *Biomacromolecules*, 2013, **14**, 2103-2111.
44. D. Biswas, S. Y. An, Y. Li, X. Wang and J. K. Oh, *Mol. Pharmaceutics*, 2017, **14**, 2518-2528.
45. A. Nelson-Mendez, S. Aleksanian, M. Oh, H.-S. Lim and J. K. Oh, *Soft Matter*, 2011, **7**, 7441-7452.
46. N. Chan, S. Y. An and J. K. Oh, *Polym. Chem.*, 2014, **5**, 1637-1649.
47. N. Chan, B. Khorsand, S. Aleksanian and J. K. Oh, *Chem. Commun.*, 2013, **49**, 7534-7536.
48. A. M. Jazani and J. K. Oh, *Polym. Chem.*, 2020, **11**, 2934-2954.
49. Z. Xu, S. Liu, Y. Kang and M. Wang, *ACS Biomater. Sci. Eng.*, 2015, **1**, 585-592.
50. L. Billiet, D. Fournier and F. Du Prez, *Polymer*, 2009, **50**, 3877-3886.
51. B. Andrade-Gagnon, M. Belanger-Bouliga, P. Trang Nguyen, D. Nguyen Thi Hong, S. Bourgault and A. Nazemi, *Nanomaterials*, 2021, **11**.
52. K. K. Bawa, A. M. Jazani, C. Shetty and J. K. Oh, *Macromol. Rapid Commun.*, 2018, **39**, 1800477.
53. K. K. Bawa, A. M. Jazani, Z. Ye and J. K. Oh, *Polymer*, 2020, **194**, 122391.
54. K. Matyjaszewski, *Macromolecules*, 2012, **45**, 4015-4039.
55. C. Boyer, V. Bulmus, T. P. Davis, V. Ladmiral, J. Liu and S. Perrier, *Chem. Rev.*, 2009, **109**, 5402-5436.

56. G. Moad, *Polym. Chem.*, 2017, **8**, 177-219.

57. C. J. Hawker, A. W. Bosman and E. Harth, *Chem. Rev.*, 2001, **101**, 3661-3688.

58. Y. Huang, A. M. Jazani, E. P. Howell, L. A. Reynolds, J. K. Oh and M. G. Moffitt, *ACS Biomater. Sci. Eng.*, 2020, **6**, 5069-5083.

59. C. E. Hoyle and C. N. Bowman, *Angew. Chem., Int. Ed.*, 2010, **49**, 1540-1573.

60. B. Le Droumaguet and K. Velonia, *Macromol. Rapid Commun.*, 2008, **29**, 1073-1089.

61. B. Pelaz, C. Alexiou, R. A. Alvarez-Puebla, F. Alves, A. M. Andrews, S. Ashraf, L. P. Balogh, L. Ballerini, A. Bestetti, C. Brendel, S. Bosi, M. Carril, W. C. W. Chan, C. Chen, X. Chen, X. Chen, Z. Cheng, D. Cui, J. Du, C. Dullin, A. Escudero, N. Feliu, M. Gao, M. George, Y. Gogotsi, A. Gruenweller, Z. Gu, N. J. Halas, N. Hampp, R. K. Hartmann, M. C. Hersam, P. Hunziker, J. Jian, X. Jiang, P. Jungebluth, P. Kadhiresan, K. Kataoka, A. Khademhosseini, J. Kopecek, N. A. Kotov, H. F. Krug, D. S. Lee, C.-M. Lehr, K. W. Leong, X.-J. Liang, M. Ling Lim, L. M. Liz-Marzan, X. Ma, P. Macchiarini, H. Meng, H. Moehwald, P. Mulvaney, A. E. Nel, S. Nie, P. Nordlander, T. Okano, J. Oliveira, T. H. Park, R. M. Penner, M. Prato, V. Puntes, V. M. Rotello, A. Samarakoon, R. E. Schaak, Y. Shen, S. Sjoeqvist, A. G. Skirtach, M. G. Soliman, M. M. Stevens, H.-W. Sung, B. Z. Tang, R. Tietze, B. N. Udugama, J. S. VanEpps, T. Weil, P. S. Weiss, I. Willner, Y. Wu, L. Yang, Z. Yue, Q. Zhang, Q. Zhang, X.-E. Zhang, Y. Zhao, X. Zhou and W. J. Parak, *ACS Nano*, 2017, **11**, 2313-2381.

62. A. Kakkar, G. Traverso, O. C. Farokhzad, R. Weissleder and R. Langer, *Nat. Rev. Chem.*, 2017, **1**, 0063.

63. C. Alvarez-Lorenzo and A. Concheiro, *Chem. Commun.*, 2014, **50**, 7743-7765.

64. V. Delplace and J. Nicolas, *Nat. Chem.*, 2015, **7**, 771-784.

65. S. Mura, J. Nicolas and P. Couvreur, *Nat. Mater.*, 2013, **12**, 991-1003.

66. Y. Wang, H. Xu and X. Zhang, *Adv. Mater.*, 2009, **21**, 2849-2864.

67. Q. Zhang, N. R. Ko and J. K. Oh, *Chem. Commun.*, 2012, **48**, 7542-7552.

68. K. K. Bawa and J. K. Oh, *Mol. Pharmaceutics*, 2017, **14**, 2460-2474.

69. C. Deng, Y. Jiang, R. Cheng, F. Meng and Z. Zhong, *Nano Today*, 2012, **7**, 467-480.

70. R. Cheng, F. Feng, F. Meng, C. Deng, J. Feijen and Z. Zhong, *J. Controlled Release*, 2011, **152**, 2-12.

71. M. Segal, R. Avinery, M. Buzhor, R. Shaharabani, A. J. Harnoy, E. Tirosh, R. Beck and R. J. Amir, *J. Am. Chem. Soc.*, 2017, **139**, 803-810.

72. Z. Deng, J. Hu and S. Liu, *Macromol. Rapid Commun.*, 2017, **38**, 1600685.

73. W. Zhang, X. Hu, Q. Shen and D. Xing, *Nat. Commun.*, 2019, **10**, 1-14.

74. I. F. Tannock and D. Rotin, *Cancer Res*, 1989, **49**, 4373-4384.

75. Y. Kato, S. Ozawa, C. Miyamoto, Y. Maehata, A. Suzuki, T. Maeda and Y. Baba, *Cancer Cell Int.*, 2013, **13**, 89.

76. J. R. Griffiths, *Br. J. Cancer*, 1991, **64**, 425-427.

77. S. Taurin, H. Nehoff and K. Greish, *J. Controlled Release*, 2012, **164**, 265-275.

78. L. Zhang, Y. Li and J. C. Yu, *J. Mater. Chem. B*, 2014, **2**, 452-470.

79. J. W. Nichols and Y. H. Bae, *Nano Today*, 2012, **7**, 606-618.

80. Y. H. Bae and K. Park, *J. Controlled Release*, 2011, **153**, 198-205.

81. O. C. Farokhzad and R. Langer, *ACS Nano*, 2009, **3**, 16-20.

82. A. Prokop and J. M. Davidson, *J. Pharm. Sci.*, 2008, **97**, 3518-3590.

83. H. Cabral, Y. Matsumoto, K. Mizuno, Q. Chen, M. Murakami, M. Kimura, Y. Terada, M. R. Kano, K. Miyazono, M. Uesaka, N. Nishiyama and K. Kataoka, *Nat Nanotechnol*, 2011, **6**, 815-823.

84. J. Wang, W. Mao, L. L. Lock, J. Tang, M. Sui, W. Sun, H. Cui, D. Xu and Y. Shen, *ACS Nano*, 2015, **9**, 7195-7206.

85. S. Bazban-Shotorbani, M. M. Hasani-Sadrabadi, A. Karkhaneh, V. Serpooshan, K. I. Jacob, A. Moshaverinia and M. Mahmoudi, *J. Controlled Release*, 2017, **253**, 46-63.

86. E. Schopf, J. Sankaranarayanan, M. Chan, R. Mattrey and A. Almutairi, *Mol. Pharmaceutics*, 2012, **9**, 1911-1918.

87. F. Seidi, R. Jenjob and D. Crespy, *Chem. Rev.*, 2018, **118**, 3965-4036.

88. J.-L. Dong, L.-S.-H. Yu and J.-W. Xie, *ACS Omega*, 2018, **3**, 4974-4985.

89. B. Liu and S. Thayumanavan, *J. Am. Chem. Soc.*, 2017, **139**, 2306-2317.

90. R. Jain, S. M. Standley and J. M. J. Frechet, *Macromolecules*, 2007, **40**, 452-457.

91. S. E. Paramonov, E. M. Bachelder, T. T. Beaudette, S. M. Standley, C. C. Lee, J. Dashe and J. M. J. Frechet, *Bioconjugate Chem.*, 2008, **19**, 911-919.

92. B. Louage, M. J. van Steenbergen, L. Nuhn, M. D. P. Risseeuw, I. Karalic, J. Winne, S. Van Calenbergh, W. E. Hennink and B. G. De Geest, *ACS Macro Lett.*, 2017, **6**, 272-276.

93. A. P. Griset, J. Walpole, R. Liu, A. Gaffey, Y. L. Colson and M. W. Grinstaff, *J. Am. Chem. Soc.*, 2009, **131**, 2469-2471.

94. J. Kalia and R. T. Raines, *Angew. Chem., Int. Ed.*, 2008, **47**, 7523-7526.

95. J. Collins, Z. Xiao and L. A. Connal, *J. Polym. Sci., Part A Polym. Chem.*, 2017, **55**, 3826-3831.

96. X. Qu and Z. Yang, *Chem. - Asian J.*, 2016, **11**, 2633-2641.

97. S. Samanta, C. C. De Silva, P. Leophairatana and J. T. Koberstein, *J. Mater. Chem. B*, 2018, **6**, 666-674.

98. L. Kong, F. Campbell and A. Kros, *Nanoscale Horizons*, 2019, **4**, 378-387.

99. L.-J. Zhang, B.-T. Dong, F.-S. Du and Z.-C. Li, *Macromolecules* 2012, **45**, 8580-8587.

100. Z. Cui, B. H. Lee and B. L. Vernon, *Biomacromolecules*, 2007, **8**, 1280-1286.

101. Q. Zhang, Z. Hou, B. Louage, D. Zhou, N. Vanparijs, B. G. De Geest and R. Hoogenboom, *Angew. Chem., Int. Ed.*, 2015, **54**, 10879-10883.

102. R. Cheng, F. Meng, C. Deng, H.-A. Klok and Z. Zhong, *Biomaterials*, 2013, **34**, 3647-3657.

103. P. Schattling, F. D. Jochum and P. Theato, *Polym. Chem.*, 2014, **5**, 25-36.

104. G. Pasparakis and M. Vamvakaki, *Polym. Chem.*, 2011, **2**, 1234-1248.

105. J. Zhuang, M. R. Gordon, J. Ventura, L. Li and S. Thayumanavan, *Chem. Soc. Rev.*, 2013, **42**, 7421-7435.

106. Z.-Q. Cao and G.-J. Wang, *Chem. Rec.*, 2016, **16**, 1398-1435.

107. S. Samanta, D. R. Bogdanowicz, H. H. Lu and J. T. Koberstein, *Macromolecules*, 2016, **49**, 1858-1864.

108. A. Moreno, G. Lligadas, J. C. Ronda, M. Galia and V. Cadiz, *Polym. Chem.*, 2019, **10**, 5215-5227.

109. G. R. Escalona, J. Sanchis and M. J. Vicent, *Macromol. Biosci.*, 2018, **18**, 1700302.

110. M. J. L. Tschan, N. S. Ieong, R. Todd, J. Everson and A. P. Dove, *Angew. Chem., Int. Ed.*, 2017, **56**, 16664-16668.

111. Y. Jin, L. Song, Y. Su, L. Zhu, Y. Pang, F. Qiu, G. Tong, D. Yan, B. Zhu and X. Zhu, *Biomacromolecules*, 2011, **12**, 3460-3468.

112. K. Dan and S. Ghosh, *Angew. Chem., Int. Ed.*, 2013, **52**, 7300-7305.

113. J. Chen, J. Ding, Y. Zhang, C. Xiao, X. Zhuang and X. Chen, *Polym. Chem.*, 2015, **6**, 397-405.

114. D. Huang, F. Yang, X. Wang, H. Shen, Y. You and D. Wu, *Polym. Chem.*, 2016, **7**, 6154-6158.

115. S. Fu, G. Yang, J. Wang, X. Wang, X. Cheng, Q. Zha and R. Tang, *Eur. Polym. J.*, 2017, **95**, 275-288.

116. M. Ding, N. Song, X. He, J. Li, L. Zhou, H. Tan, Q. Fu and Q. Gu, *ACS Nano*, 2013, **7**, 1918-1928.

117. L. Zhou, D. Liang, X. He, J. Li, H. Tan, J. Li, Q. Fu and Q. Gu, *Biomaterials*, 2012, **33**, 2734-2745.

118. R. A. Shenoi, J. K. Narayanannair, J. L. Hamilton, B. F. L. Lai, S. Horte, R. K. Kainthan, J. P. Varghese, K. G. Rajeev, M. Manoharan and J. N. Kizhakkedathu, *J. Am. Chem. Soc.*, 2012, **134**, 14945-14957.

119. C. Tonhauser, C. Schuell, C. Dingels and H. Frey, *ACS Macro Lett.*, 2012, **1**, 1094-1097.

120. I. Lee, M. Park, Y. Kim, O. Hwang, G. Khang and D. Lee, *Int. J. Pharm.*, 2013, **448**, 259-266.

121. F. Huang, R. Cheng, F. Meng, C. Deng and Z. Zhong, *Biomacromolecules*, 2015, **16**, 2228-2236.

122. X. Huang, F. Du, J. Cheng, Y. Dong, D. Liang, S. Ji, S.-S. Lin and Z. Li, *Macromolecules* 2009, **42**, 783-790.

123. Z.-Y. Qiao, R. Ji, X.-N. Huang, F.-S. Du, R. Zhang, D.-H. Liang and Z.-C. Li, *Biomacromolecules*, 2013, **14**, 1555-1563.

124. R. Tang, W. Ji and C. Wang, *Macromol. Biosci.*, 2010, **10**, 192-201.

125. R. Tang, W. Ji, D. Panus, R. N. Palumbo and C. Wang, *J. Controlled Release*, 2011, **151**, 18-27.

126. H. Cao, C. Chen, D. Xie, X. Chen, P. Wang, Y. Wang, H. Song and W. Wang, *Polym. Chem.*, 2018, **9**, 169-177.

127. S. Jiang, Y. Yao, Y. Nie, J. Yang and J. Yang, *J. Colloid Interface Sci.*, 2011, **364**, 264-271.

128. J. Zhao, J. Liu, S. Han, H. Deng, L. Deng, J. Liu, A. Meng, A. Dong and J. Zhang, *Polym. Chem.*, 2014, **5**, 1852-1856.

129. P. Pramanik, D. Halder, S. S. Jana and S. Ghosh, *Macromol. Rapid Commun.*, 2016, **37**, 1499-1506.

130. S. Van Herck, L. Van Hoecke, B. Louage, L. Lybaert, R. De Coen, S. Kasmi, A. P. Esser-Kahn, S. A. David, L. Nuhn, B. Schepens, X. Saelens and B. G. De Geest, *Bioconjugate Chem.*, 2018, **29**, 748-760.

131. W. Chen, F. Meng, F. Li, S.-J. Ji and Z. Zhong, *Biomacromolecules*, 2009, **10**, 1727-1735.

132. J. Song, E. Hwang, Y. Lee, L. Palanikumar, S.-H. Choi, J.-H. Ryu and B.-S. Kim, *Polym. Chem.*, 2019, **10**, 582-592.

133. E. Hwang, K. Kim, C. G. Lee, T.-H. Kwon, S.-H. Lee, S. K. Min and B.-S. Kim, *Macromolecules* 2019, **52**, 5884-5893.

134. V. T. T. Thuy, C. W. Lim, J. H. Park, C.-H. Ahn and D. Kim, *J. Mater. Chem. B*, 2015, **3**, 2978-2985.

135. F. Li, J. He, M. Zhang and P. Ni, *Polym. Chem.*, 2015, **6**, 5009-5014.

136. N. Liu, B. Li, C. Gong, Y. Liu, Y. Wang and G. Wu, *Colloids Surf., B*, 2015, **136**, 562-569.

137. J.-Z. Du, X.-J. Du, C.-Q. Mao and J. Wang, *J. Am. Chem. Soc.*, 2011, **133**, 17560-17563.

138. Y. Yu, C.-K. Chen, W.-C. Law, H. Sun, P. N. Prasad and C. Cheng, *Polym. Chem.*, 2015, **6**, 953-961.

139. B. Ma, W. Zhuang, Y. Wang, R. Luo and Y. Wang, *Acta Biomaterialia*, 2018, **70**, 186-196.

140. J. Mao, Y. Li, T. Wu, C. Yuan, B. Zeng, Y. Xu and L. Dai, *ACS Appl. Mater. Interfaces*, 2016, **8**, 17109-17117.

141. Y. Gu, Y. Zhong, F. Meng, R. Cheng, C. Deng and Z. Zhong, *Biomacromolecules*, 2013, **14**, 2772-2780.

142. Q. Zhou, Y. Hou, L. Zhang, J. Wang, Y. Qiao, S. Guo, L. Fan, T. Yang, L. Zhu and H. Wu, *Theranostics*, 2017, **7**, 1806-1819.

143. Y. Zhou, Y. Dong, G. Huang, Y. Wang, X. Huang, F. Zhang, D. A. Boothman, J. Gao and W. Liang, *J. Mater. Chem. B*, 2016, **4**, 7429-7440.

144. Z. Zhang, X. Chen, L. Chen, S. Yu, Y. Cao, C. He and X. Chen, *ACS Appl. Mater. Interfaces*, 2013, **5**, 10760-10766.

145. E. M. Bachelder, T. T. Beaudette, K. E. Broaders, J. Dashe and J. M. J. Frechet, *J. Am. Chem. Soc.*, 2008, **130**, 10494-10495.

146. H. Qiao, X. Chen, E. Chen, J. Zhang, D. Huang, D. Yang, Y. Ding, H. Qian, J. Feijen and W. Chen, *Biomater. Sci.*, 2019, **7**, 2749-2758.

147. H. Deng, J. Liu, X. Zhao, Y. Zhang, J. Liu, S. Xu, L. Deng, A. Dong and J. Zhang, *Biomacromolecules*, 2014, **15**, 4281-4292.

148. X. Wang, L. Wang, S. Yang, M. M. Zhang, Q. Xiong, H. Zhao and L. Liu, *Macromolecules* 2014, **47**, 1999-2009.

149. Y. Azuma, T. Terashima and M. Sawamoto, *Macromolecules*, 2017, **50**, 587-596.

150. A. W. Jackson and D. A. Fulton, *Chem. Commun.*, 2011, **47**, 6807-6809.

151. A. W. Jackson and D. A. Fulton, *Chem. Commun.*, 2010, **46**, 6051-6053.

152. A. W. Jackson, C. Stakes and D. A. Fulton, *Polym. Chem.*, 2011, **2**, 2500-2511.

153. J. Hu, J. He, D. Cao, M. Zhang and P. Ni, *Polym. Chem.*, 2015, **6**, 3205-3216.

154. H. T. T. Duong, C. P. Marquis, M. Whittaker, T. P. Davis and C. Boyer, *Macromolecules* 2011, **44**, 8008-8019.

155. L. Nuhn, S. Van Herck, A. Best, K. Deswarte, M. Kokkinopoulou, I. Lieberwirth, K. Koynov, B. N. Lambrecht and B. G. De Geest, *Angew. Chem., Int. Ed.*, 2018, **57**, 10760-10764.

156. X. Xu, J. D. Flores and C. L. McCormick, *Macromolecules*, 2011, **44**, 1327-1334.

157. S.-J. Lee, K.-H. Min, H.-J. Lee, A.-N. Koo, H.-P. Rim, B.-J. Jeon, S.-Y. Jeong, J.-S. Heo and S.-C. Lee, *Biomacromolecules*, 2011, **12**, 1224-1233.

158. K. Satoh, J. E. Poelma, L. M. Campos, B. Stahl and C. J. Hawker, *Polym. Chem.*, 2012, **3**, 1890-1898.

159. H. Wang, J. He, M. Zhang, Y. Tao, F. Li, K. C. Tam and P. Ni, *J. Mater. Chem. B*, 2013, **1**, 6596-6607.

160. J. Hu, J. He, M. Zhang and P. Ni, *Polym. Chem.*, 2015, **6**, 1553-1566.

161. H. Wang, J. He, D. Cao, M. Zhang, F. Li, K. C. Tam and P. Ni, *Polym. Chem.*, 2015, **6**, 4809-4818.

162. W.-X. Wu, N. Wang, B.-Y. Liu, Q.-F. Deng and X.-Q. Yu, *Soft Matter*, 2014, **10**, 1199-1213.

163. S. Zhang, J. Xu, H. Chen, Z. Song, Y. Wu, X. Dai and J. Kong, *Macromol. Biosci.*, 2017, **17**, 1600258.

164. Y. Hao, J. He, S. Li, J. Liu, M. Zhang and P. Ni, *J. Mater. Chem. B*, 2014, **2**, 4237-4249.

165. S. S. Patil and P. P. Wadgaonkar, *J. Polym. Sci., Part A Polym. Chem.*, 2017, **55**, 1383-1396.

166. J. Sun, S. Fransen, X. Yu and D. Kuckling, *Polym. Chem.*, 2018, **9**, 3287-3296.

167. D. Babikova, R. Kalinova, D. Momekova, I. Ugrinova, G. Momekov and I. Dimitrov, *ACS Biomater. Sci. Eng.*, 2019, **5**, 2271-2283.

168. H. Rongbin, X. Lei, L. Ying, D. Xiangping, C. Xuan, L. Lanfang, Y. Cuiyun, T. Guotao and C. Yanming, *J Pharm Pharmacol*, 2016, **68**, 751-761.

169. Z. Yang, N. Sun, R. Cheng, C. Zhao, Z. Liu, X. Li, J. Liu and Z. Tian, *Biomaterials*, 2017, **147**, 53-67.

170. F. Zhu, Q. Yang, Y. Zhuang, Y. Zhang, Z. Shao, B. Gong and Y.-M. Shen, *Polymer*, 2014, **55**, 2977-2985.

171. C.-Y. Sun, S. Shen, C.-F. Xu, H.-J. Li, Y. Liu, Z.-T. Cao, X.-Z. Yang, J.-X. Xia and J. Wang, *J. Am. Chem. Soc.*, 2015, **137**, 15217-15224.

172. X. Huang, S. I. Sevimli and V. Bulmus, *Eur. Polym. J.*, 2013, **49**, 2895-2905.

173. X. Sui, Z. Zhang, S. Guan, Y. Xu, C. Li, Y. Lv, A. Chen, L. Yang and L. Gao, *Polym. Chem.*, 2015, **6**, 2777-2782.

174. S. Lin, F. Du, Y. Wang, S. Ji, D. Liang, L. Yu and Z. Li, *Biomacromolecules*, 2008, **9**, 109-115.

175. C.-Y. Sun, Y. Liu, J.-Z. Du, Z.-T. Cao, C.-F. Xu and J. Wang, *Angew. Chem., Int. Ed.*, 2016, **55**, 1010-1014.

176. L. Xiao, L. Huang, F. Moingeon, M. Gauthier and G. Yang, *Biomacromolecules*, 2017, **18**, 2711-2722.

177. S. Liu, R. J. Ono, C. Yang, S. Gao, J. Y. Ming Tan, J. L. Hedrick and Y. Y. Yang, *ACS Appl. Mater. Interfaces*, 2018, **10**, 19355-19364.

178. S. Petrova, E. Jager, R. Konefal, A. Jager, C. G. Venturini, J. Spevacek, E. Pavlova and P. Stepanek, *Polym. Chem.*, 2014, **5**, 3884-3893.

179. M. Worm, B. Kang, C. Dingels, F. R. Wurm and H. Frey, *Macromol. Rapid Commun.*, 2016, **37**, 775-780.

180. J. Fan, F. Zeng, S. Wu and X. Wang, *Biomacromolecules*, 2012, **13**, 4126-4137.

181. D. Wang, Y. Su, C. Jin, B. Zhu, Y. Pang, L. Zhu, J. Liu, C. Tu, D. Yan and X. Zhu, *Biomacromolecules*, 2011, **12**, 1370-1379.

182. R. Ji, J. Cheng, T. Yang, C.-C. Song, L. Li, F.-S. Du and Z.-C. Li, *Biomacromolecules*, 2014, **15**, 3531-3539.

183. K. Nishida, A. Tamura and N. Yui, *Polym. Chem.*, 2015, **6**, 4040-4047.

184. J. Sankaranarayanan, E. A. Mahmoud, G. Kim, J. M. Morachis and A. Almutairi, *ACS Nano*, 2010, **4**, 5930-5936.

185. H. Deng, X. Zhao, J. Liu, J. Zhang, L. Deng, J. Liu and A. Dong, *Nanoscale*, 2016, **8**, 1437-1450.

186. M. Tang, Z. Yang, Z. Feng, J. Zhou, J. Liu, J. Liu, W. Wang, J. Zhao, A. Dong and L. Deng, *Polym. Chem.*, 2015, **6**, 6671-6679.

187. C.-C. Song, C.-C. Su, J. Cheng, F.-S. Du, D.-H. Liang and Z.-C. Li, *Macromolecules*, 2013, **46**, 1093-1100.

188. J. Olejniczak, V. A. Nguyen Huu, J. Lux, M. Grossman, S. He and A. Almutairi, *Chem. Commun.*, 2015, **51**, 16980-16983.

189. P. Wei, S. Goetz, S. Schubert, J. C. Brendel and U. S. Schubert, *Polym. Chem.*, 2018, **9**, 2634-2642.

190. K. A. Miller, E. G. Morado, S. R. Samanta, B. A. Walker, A. Z. Nelson, S. Sen, D. T. Tran, D. J. Whitaker, R. H. Ewoldt, P. V. Braun and S. C. Zimmerman, *J. Am. Chem. Soc.*, 2019, **141**, 2838-2842.

191. A. Russo, W. DeGraff, N. Friedman and J. B. Mitchell, *Cancer Res.*, 1986, **46**, 2845-2848.

192. P. Kuppusamy, H. Li, G. Ilangovan, A. J. Cardounel, J. L. Zweier, K. Yamada, M. C. Krishna and J. B. Mitchell, *Cancer Res.*, 2002, **62**, 307-312.

193. M. H. Lee, Z. Yang, C. W. Lim, Y. H. Lee, D. Sun, C. Kang and J. S. Kim, *Chem. Rev.* , 2013, **113**, 5071-5109.

194. F. Meng, W. E. Hennink and Z. Zhong, *Biomaterials*, 2009, **30**, 2180-2198.

195. N. Ma, Y. Li, H. Xu, Z. Wang and X. Zhang, *J. Am. Chem. Soc.*, 2010, **132**, 442-443.

196. Y. S. Birhan, B. Z. Hailemeskel, T. W. Mekonnen, E. Y. Hanurry, H. F. Darge, A. T. Andrgie, H.-Y. Chou, J.-Y. Lai, G.-H. Hsiue and H.-C. Tsai, *Int. J. Pharm.*, 2019, **567**, 118486.

197. J.-W. Xu, X. Ge, L.-H. Lv, F. Xu and Y.-L. Luo, *Macromol. Rapid Commun.*, 2018, **39**, 1800628.

198. S. A. Salma, M. P. Patil, D. W. Kim, C. M. Q. Le, B.-H. Ahn, G.-D. Kim and K. T. Lim, *Polym. Chem.*, 2018, **9**, 4813-4823.

199. A. W. Jackson and D. A. Fulton, *Macromolecules* 2012, **45**, 2699-2708.

200. X.-Q. Yi, Q. Zhang, D. Zhao, J.-Q. Xu, Z.-L. Zhong, R.-X. Zhuo and F. Li, *Polym. Chem.*, 2016, **7**, 1719-1729.

201. C. Wei, J. Guo and C. Wang, *Macromol. Rapid Commun.*, 2011, **32**, 451-455.

202. T. C. Lai, H. Cho and G. S. Kwon, *Polym. Chem.*, 2014, **5**, 1650-1661.

203. L. Wang, B. Tian, J. Zhang, K. Li, Y. Liang, Y. Sun, Y. Ding and J. Han, *Int. J. Pharm.*, 2016, **501**, 221-235.

204. J. Li and P. Liu, *Macromol. Rapid Commun.*, 2018, **39**, 1800381.

205. W. Yuan, J. Wang, L. Li, H. Zou, H. Yuan and J. Ren, *Macromol. Rapid Commun.*, 2014, **35**, 1776-1781.

206. Y. Zhang, J. He, D. Cao, M. Zhang and P. Ni, *Polym. Chem.*, 2014, **5**, 5124-5138.

207. X. Hu, H. Li, S. Luo, T. Liu, Y. Jiang and S. Liu, *Polym. Chem.*, 2013, **4**, 695-706.

208. D. Xiong, N. Yao, H. Gu, J. Wang and L. Zhang, *Polymer*, 2017, **114**, 161-172.

209. H. Chen, Y. Ma, H. Lan, Y. Zhao, D. Zhi, S. Cui, J. Du, Z. Zhang, Y. Zhen and S. Zhang, *J. Mater. Chem. B*, 2018, **6**, 7530-7542.

210. W. Chen, P. Zhong, F. Meng, R. Cheng, C. Deng, J. Feijen and Z. Zhong, *Journal of Controlled Release*, 2013, **169**, 171-179.

211. Y. Wang, L. Zhang, X. Zhang, X. Wei, Z. Tang and S. Zhou, *ACS Appl. Mater. Interfaces*, 2016, **8**, 5833-5846.

212. A. Klaikherd, C. Nagamani and S. Thayumanavan, *J. Am. Chem. Soc.*, 2009, **131**, 4830-4838.

213. A. Zhu, K. Miao, Y. Deng, H. Ke, H. He, T. Yang, M. Guo, Y. Li, Z. Guo, Y. Wang, X. Yang, Y. Zhao and H. Chen, *ACS Nano*, 2015, **9**, 7874-7885.

214. H. Liu, C. Li, D. Tang, X. An, Y. Guo and Y. Zhao, *J. Mater. Chem. B*, 2015, **3**, 3959-3971.

215. K. Miao, W. Shao, H. Liu and Y. Zhao, *Polym. Chem.*, 2014, **5**, 1191-1201.

216. W. Shao, K. Miao, H. Liu, C. Ye, J. Du and Y. Zhao, *Polym. Chem.*, 2013, **4**, 3398-3410.

217. N. Song, M. Ding, Z. Pan, J. Li, L. Zhou, H. Tan and Q. Fu, *Biomacromolecules*, 2013, **14**, 4407-4419.

218. M. Ding, J. Li, X. He, N. Song, H. Tan, Y. Zhang, L. Zhou, Q. Gu, H. Deng and Q. Fu, *Adv. Mater.*, 2012, **24**, 3639-3645.

219. Y. Cao, J. Zhao, Y. Zhang, J. Liu, J. Liu, A. Dong and L. Deng, *RSC Adv.*, 2015, **5**, 28060-28069.

220. Y. Ding, C. Du, J. Qian, L. Zhou, Y. Su, R. Zhang and C.-M. Dong, *Polym. Chem.*, 2018, **9**, 3488-3498.

221. Z. Su, Y. Xu, Y. Wang, W. Shi, S. Han and X. Shuai, *Biomater. Sci.*, 2019, **7**, 3821-3831.

222. A. M. Jazani and J. K. Oh, *Macromolecules* 2017, **50**, 9427-9436.

223. A. M. Jazani, N. Arezi, C. Shetty, S. H. Hong, H. Li, X. Wang and J. K. Oh, *Polym. Chem.*, 2019, **10**, 2840-2853.

224. K. Maruya-Li, C. Shetty, A. Moini Jazani, N. Arezi and J. K. Oh, *ACS Omega*, 2020, **5**, 3734-3742.

225. A. M. Jazani, N. Arezi, K. Maruya-Li, S. Jung and J. K. Oh, *ACS Omega*, 2018, **3**, 8980-8991.

226. F. Jia, Y. Wang, H. Wang, Q. Jin, T. Cai, Y. Chen and J. Ji, *Polym. Chem.*, 2015, **6**, 2069-2075.

227. Y.-B. Long, W.-X. Gu, C. Pang, J. Ma and H. Gao, *J. Mater. Chem. B*, 2016, **4**, 1480-1488.

228. L. Meng, W. Huang, D. Wang, X. Huang, X. Zhu and D. Yan, *Biomacromolecules*, 2013, **14**, 2601-2610.

229. G. Pasparakis, T. Manouras, M. Vamvakaki and P. Argitis, *Nat. Commun.*, 2014, **5**, 4623/4621-4623/4629.

230. Q. Jin, T. Cai, H. Han, H. Wang, Y. Wang and J. Ji, *Macromol. Rapid Commun.*, 2014, **35**, 1372-1378.

231. N. Kalva, N. Parekh and A. V. Ambade, *Polym. Chem.*, 2015, **6**, 6826-6835.

232. P. S. Pramod, R. Shah and M. Jayakannan, *Nanoscale*, 2015, **7**, 6636-6652.

233. Z. Duan, H. Cai, H. Zhang, K. Chen, N. Li, Z. Xu, Q. Gong and K. Luo, *ACS Appl. Mater. Interfaces*, 2018, **10**, 35770-35783.

234. Y. Ou, K. Chen, H. Cai, H. Zhang, Q. Gong, J. Wang, W. Chen and K. Luo, *Biomater. Sci.*, 2018, **6**, 1177-1188.

235. X. Wei, Q. Luo, L. Sun, X. Li, H. Zhu, P. Guan, M. Wu, K. Luo and Q. Gong, *ACS Appl. Mater. Interfaces*, 2016, **8**, 11765-11778.

236. N. Rohani, L. Hao, M. S. Alexis, B. A. Joughin, K. Krismer, M. N. Moufarrej, A. R. Soltis, D. A. Lauffenburger, M. B. Yaffe, C. B. Burge, S. N. Bhatia and F. B. Gertler, *Cancer Res.*, 2019, **79**, 1952-1966.

237. C. Li, H. Li, Q. Wang, M. Zhou, M. Li, T. Gong, Z. Zhang and X. Sun, *J. Controlled Release*, 2017, **246**, 133-141.

238. N. Dararatana, F. Seidi, J. Hamel and D. Crespy, *Polym. Chem.*, 2020, **11**, 1752-1762.

239. H. Matsukizono and T. Endo, *J. Am. Chem. Soc.*, 2018, **140**, 884-887.

240. N. Boehnke, C. Cam, E. Bat, T. Segura and H. D. Maynard, *Biomacromolecules*, 2015, **16**, 2101-2108.

241. J. Rao and A. Khan, *Polym. Chem.*, 2013, **4**, 2691-2695.

242. T. Terashima, S. Nishioka, Y. Koda, M. Takenaka and M. Sawamoto, *J. Am. Chem. Soc.*, 2014, **136**, 10254-10257.

243. W. X. Wu, N. Wang, B. Y. Liu, Q. F. Deng and X. Q. Yu, *Soft Matter*, 2014, **10**, 1199-1213.

244. C. Shetty, A. Noronha, A. Pontarelli, C. J. Wilds and J. K. Oh, *Mol. Pharmaceutics*, 2020, **17**, 3979-3989.

245. X. Hu and J. K. Oh, *Macromol. Rapid Commun.*, 2020, **41**, 2000394.

246. E. Hwang, K. Kim, C. G. Lee, T.-H. Kwon, S.-H. Lee, S. K. Min and B.-S. Kim, *Macromolecules*, 2019, **52**, 5884-5893.

247. Y. Shi, R. van der Meel, B. Theek, E. Oude Blenke, E. H. E. Pieters, M. H. A. M. Fens, J. Ehling, R. M. Schiffelers, G. Storm, C. F. van Nostrum, T. Lammers and W. E. Hennink, *ACS Nano*, 2015, **9**, 3740-3752.

248. Y. Shi, M. J. van Steenbergen, E. A. Teunissen, L. Novo, S. Gradmann, M. Baldus, C. F. van Nostrum and W. E. Hennink, *Biomacromolecules*, 2013, **14**, 1826-1837.

249. E. B. Anderson and T. E. Long, *Polymer*, 2010, **51**, 2447-2454.

250. Y. Shi, T. Lammers, G. Storm and W. E. Hennink, *Macromol. Biosci.*, 2017, **17**, 1600160.

251. K. Matyjaszewski and J. Xia, *Chem. Rev.*, 2001, **101**, 2921-2990.

252. M. Kamigaito, T. Ando and M. Sawamoto, *Chem. Rev.* , 2001, **101**, 3689-3745.

253. C. J. Rijcken, C. J. Snel, R. M. Schiffelers, C. F. van Nostrum and W. E. Hennink, *Biomaterials*, 2007, **28**, 5581-5593.

254. L. Zheng, X. Zhang, Y. Wang, F. Liu, J. Peng, X. Zhao, H. Yang, L. Ma, B. Wang, C. Chang and H. Wei, *Biomacromolecules*, 2018, **19**, 3874-3882.

255. M. Motornov, Y. Roiter, I. Tokarev and S. Minko, *Prog. Polym. Sci.*, 2010, **35**, 174-211.

256. E. Cabane, X. Zhang, K. Langowska, C. G. Palivan and W. Meier, *Biointerphases*, 2012, **7**, 9.

257. M. Wei, Y. Gao, X. Li and M. J. Serpe, *Polym. Chem.*, 2017, **8**, 127-143.

258. D. Roy, J. N. Cambre and B. S. Sumerlin, *Prog. Polym. Sci.*, 2010, **35**, 278-301.

259. G. K. Such, Y. Yan, A. P. R. Johnston, S. T. Gunawan and F. Caruso, *Adv. Mater.*, 2015, **27**, 2278-2297.

260. Y. Lu, W. Sun and Z. Gu, *J. Controlled Release*, 2014, **194**, 1-19.

261. N. Rapoport, *Prog. Polym. Sci.*, 2007, **32**, 962-990.

262. C. Alexander and K. M. Shakesheff, *Adv. Mater.*, 2006, **18**, 3321-3328.

263. H. Meng and G. Li, *J. Mater. Chem. A*, 2013, **1**, 7838.

264. K. Loomis, K. McNeeley and R. V. Bellamkonda, *Soft Matt.*, 2011, **7**, 839-856.

265. C. Li and S. Liu, *Chem. Commun.* , 2012, **48**, 3262-3278.

266. J. Xuan, D. Han, H. Xia and Y. Zhao, *Langmuir*, 2014, **30**, 410-417.

267. X. Wu, L. Zhou, Y. Su and C.-M. Dong, *Polym. Chem.*, 2015, **6**, 6857-6869.

268. R. Li and Y. Xie, *J. Controlled Release*, 2017, **251**, 49-67.

269. X. Liu, D. Hu, Z. Jiang, J. Zhuang, Y. Xu, X. Guo and S. Thayumanavan, *Macromolecules*, 2016, **49**, 6186-6192.

270. T. Sun, P. Li and J. K. Oh, *Macromol. Rapid Commun.*, 2015, **36**, 1742-1748.

271. G. J. P. Britovsek, J. England and A. J. P. White, *Inorg. Chem.*, 2005, **44**, 8125-8134.

272. Q. Zhang, S. Aleksanian, S. M. Noh and J. K. Oh, *Polym. Chem.*, 2013, **4**, 351-359.

273. D. Biswas, P. Li, D. Liu and J. K. Oh, *RSC Adv.*, 2015, **5**, 107938-107948.

274. Z.-K. Wang, L.-H. Wang, J.-T. Sun, L.-F. Han and C.-Y. Hong, *Polym. Chem.*, 2013, **4**, 1694-1699.

275. N. Cengiz, H. Kabadayioglu and R. Sanyal, *J. Polym. Sci., Part A Polym. Chem.*, 2010, **48**, 4737-4746.

276. D. Aydin, M. Arslan, A. Sanyal and R. Sanyal, *Bioconjugate Chem.*, 2017, **28**, 1443-1451.

277. W. Jakubowski and K. Matyjaszewski, *Macromolecules*, 2005, **38**, 4139-4146.

278. A. S. Mikhail and C. Allen, *J. Controlled Release*, 2009, **138**, 214-223.

279. X.-B. Xiong, A. Falamarzian, S. M. Garg and A. Lavasanifar, *J. Controlled Release*, 2011, **155**, 248-261.

280. M. A. Hillmyer, *Adv. Polym. Sci.*, 2005, **190**, 137-181.

281. H. Cui, Z. Chen, S. Zhong, K. L. Wooley and D. J. Pochan, *Science*, 2007, **317**, 647-650.

282. L. Zhang, K. Yu and A. Eisenberg, *Science*, 1996, **272**, 1777-1779.

283. S. Sugihara, A. Blanazs, S. P. Armes, A. J. Ryan and A. L. Lewis, *J. Am. Chem. Soc.*, 2011, **133**, 15707-15713.

284. J. Hu, G. Liu and G. Nijkang, *J. Am. Chem. Soc.*, 2008, **130**, 3236-3237.

285. X. Wang, G. Guerin, H. Wang, Y. Wang, I. Manners and M. A. Winnik, *Science*, 2007, **317**, 644-647.

286. K. Loomis, K. McNeeley and R. V. Bellamkonda, *Soft Matter*, 2011, **7**, 839-856.

287. S. Binauld and M. H. Stenzel, *Chem. Commun.*, 2013, **49**, 2082-2102.

288. Y. Zhao, *Macromolecules* 2012, **45**, 3647-3657.

289. B. L. Allen, J. D. Johnson and J. P. Walker, *ACS Nano*, 2011, **5**, 5263-5272.

290. C. Alvarez-Lorenzo and A. Concheiro, *Chem. Commun.*, 2014, **50**, 7743-7765.

291. Z. Ge and S. Liu, *Chem. Soc. Rev.*, 2013, **42**, 7289-7325.

292. M. H. Lee, Z. Yang, C. W. Lim, Y. H. Lee, D. Sun, C. Kang and J. S. Kim, *Chem. Rev.*, 2013, **113**, 5071-5109.

293. H. Zhao, E. S. Sterner, E. B. Coughlin and P. Theato, *Macromolecules* 2012, **45**, 1723-1736.

294. J. Hu and S. Liu, *Macromolecules* 2010, **43**, 8315-8330.

295. J.-Y. Fang, Y.-K. Lin, S.-W. Wang, Y.-C. Yu and R.-S. Lee, *RSC Adv.*, 2016, **6**, 107669-107682.

296. C. He, Q. Yang, L. Tan, B. Liu, Z. Zhu, B. Gong, Y.-M. Shen and Z. Shao, *Eur. Polym. J.*, 2016, **85**, 38-52.

297. B. Khorsand Sourkohi, A. Cunningham, Q. Zhang and J. K. Oh, *Biomacromolecules*, 2011, **12**, 3819-3825.

298. N. Chan, B. Khorsand, S. Aleksanian and J. K. Oh, *Chem. Commun.*, 2013, **49**, 7534-7536.

299. N. R. Ko and J. K. Oh, *Biomacromolecules*, 2014, **15**, 3180-3189.

300. K. Matyjaszewski and T. P. Davis, eds., *Handbook of Radical Polymerization*, John Wiley & Sons Inc., 2002.

301. M. D. Rikkou and C. S. Patrickios, *Prog. Polym. Sci.*, 2011, **36**, 1079-1097.

302. S. Pearson, C. St Thomas, R. Guerrero-Santos and F. D'Agosto, *Polym. Chem.*, 2017, **8**, 4916-4946.

303. Y.-Y. Tong, Y.-Q. Dong, F.-S. Du and Z.-C. Li, *Macromolecules* 2008, **41**, 7339-7346.

304. H. Wei, J. G. Schellinger, D. S. H. Chu and S. H. Pun, *J. Am. Chem. Soc.*, 2012, **134**, 16554-16557.

305. Y. Kwak, R. Nicolay and K. Matyjaszewski, *Macromolecules* 2008, **41**, 6602-6604.

306. R. Nicolay, Y. Kwak and K. Matyjaszewski, *Macromolecules*, 2008, **41**, 4585-4596.

307. R. Nicolay and Y. Kwak, *Isr. J. Chem.*, 2012, **52**, 288-305.

308. A. M. Elsen, R. Nicolay and K. Matyjaszewski, *Macromolecules* 2011, **44**, 1752-1754.

309. Y.-Y. Yang, H. Hu, X. Wang, F. Yang, H. Shen, F.-J. Xu and D.-C. Wu, *ACS Appl. Mater. Interfaces*, 2015, **7**, 12238-12248.

310. Z. Cao, H. Wu, J. Dong and G. Wang, *Macromolecules*, 2014, **47**, 8777-8783.

311. S. Eetezadi, S. N. Ekdawi and C. Allen, *Adv. Drug Deliv. Rev.*, 2015, **91**, 7-22.

312. X. Chuan, Q. Song, J. Lin, X. Chen, H. Zhang, W. Dai, B. He, X. Wang and Q. Zhang, *Mol. Pharmaceutics*, 2014, **11**, 3656-3670.

313. S. Sindhwani, A. M. Syed, J. Ngai, B. R. Kingston, L. Maiorino, J. Rothschild, P. MacMillan, Y. Zhang, N. U. Rajesh, T. Hoang, J. L. Y. Wu, S. Wilhelm, A. Zilman, S. Gadde, A. Sulaiman, B. Ouyang, Z. Lin, L. Wang, M. Egeblad and W. C. W. Chan, *Nat. Mater.*, 2020, **19**, 566-575.

314. A. Tardy, J. Nicolas, D. Gigmes, C. Lefay and Y. Guillaneuf, *Chem. Rev.*, 2017, **117**, 1319-1406.

315. Q. Li, S. Ma, P. Li, B. Wang, H. Feng, N. Lu, S. Wang, Y. Liu, X. Xu and J. Zhu, *Macromolecules*, 2021, **54**, 1742-1753.

316. S. Dadashi-Silab and K. Matyjaszewski, *Molecules*, 2020, **25**, 1648.

317. S. Dadashi-Silab, S. Doran and Y. Yagci, *Chem. Rev.*, 2016, **116**, 10212-10275.

318. E. H. Discekici, A. Anastasaki, J. Read de Alaniz and C. J. Hawker, *Macromolecules*, 2018, **51**, 7421-7434.

319. Q. Ma, J. Song, X. Zhang, Y. Jiang, L. Ji and S. Liao, *Nat. Commun.*, 2021, **12**, 429.

Appendix A

Supporting information and figures for chapter 3

Figure A1. Synthesis (a) and ^{1}H-NMR spectra in $CDCl_3$ of ACVE (b) ACMA (c).

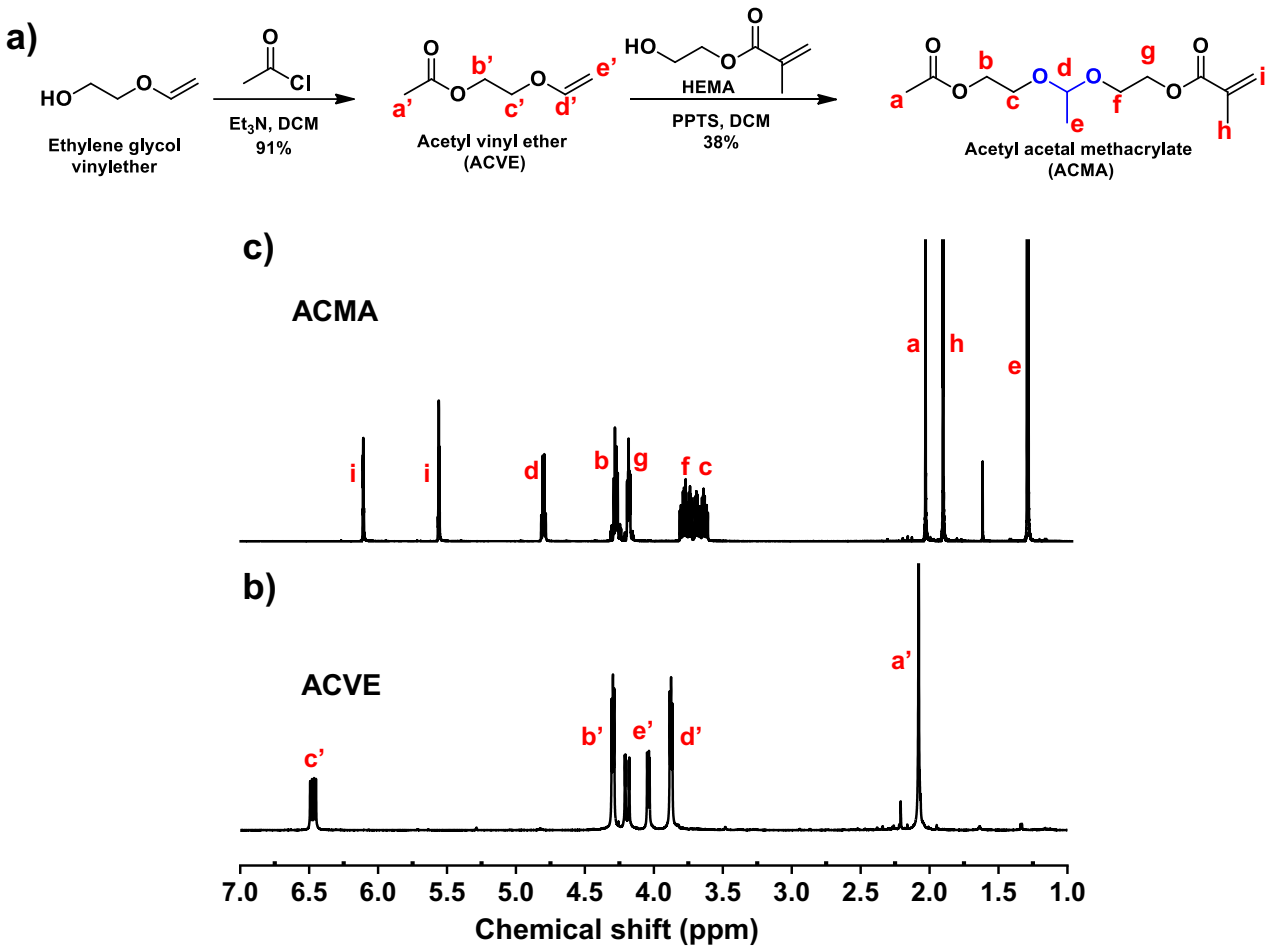

Figure A2. ^{13}C-NMR spectrum of ACVE in $CDCl_3$.

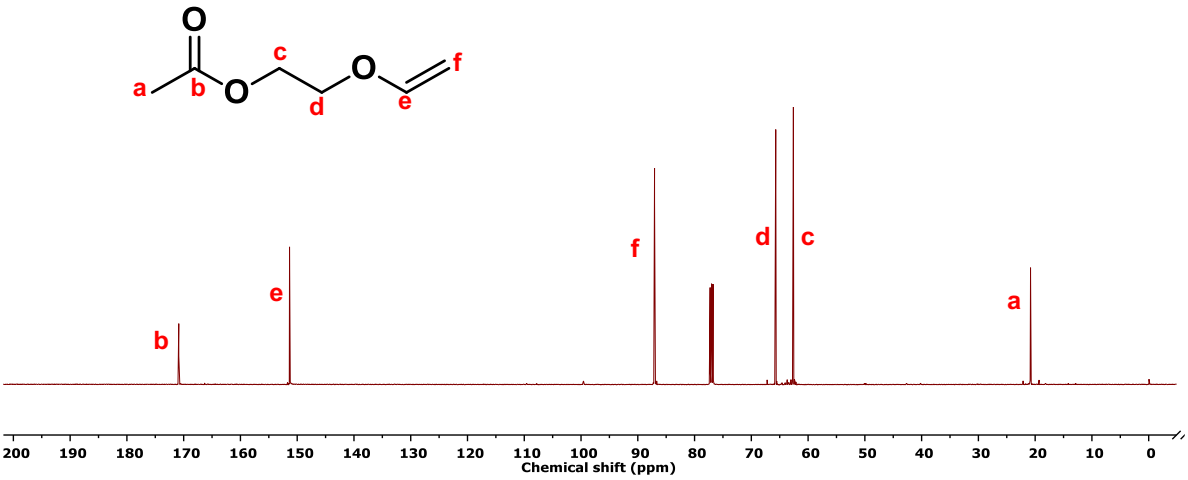

Figure A3. ^{13}C-NMR spectrum of ACMA in $CDCl_3$.

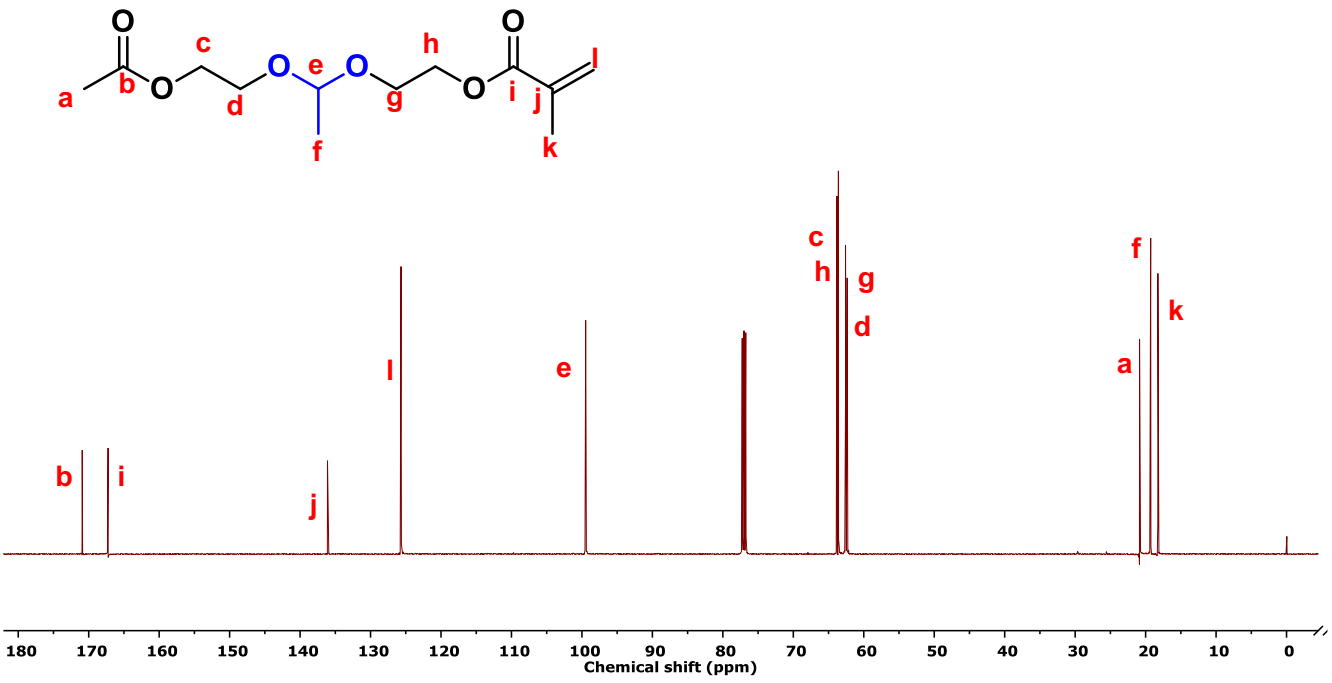

Figure A4. GPC traces of P1 and P2, compared with PEG-AC-Br macroinitiator.

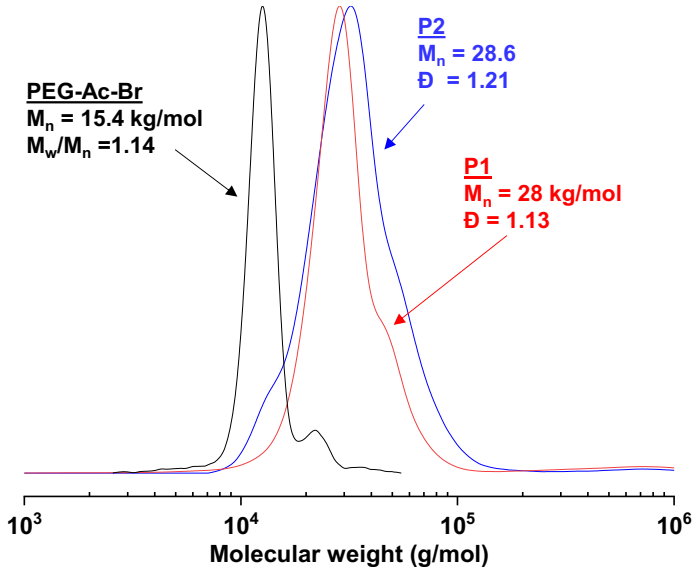

Figure A5. Overlaid fluorescence spectra (a) and fluorescence intensity at maximum wavelength (b) for aqueous mixtures consisting of NR with various amounts of P1 to determine CMC.

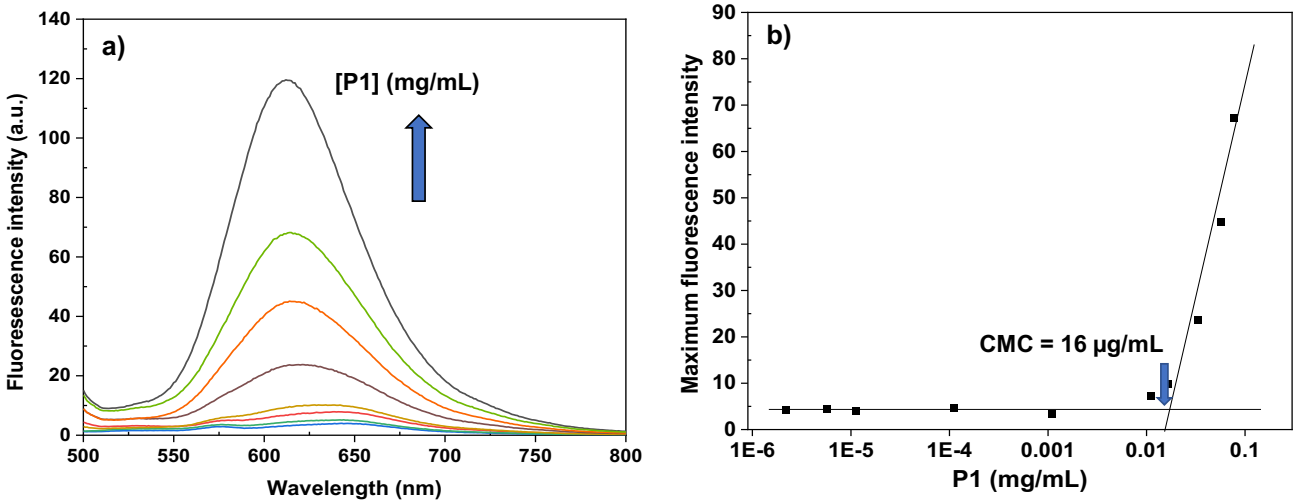

Figure A6. Overlaid fluorescence spectra (a) and fluorescence intensity at maximum wavelength (b) for aqueous mixtures consisting of NR with various amounts of P2 to determine CMC.

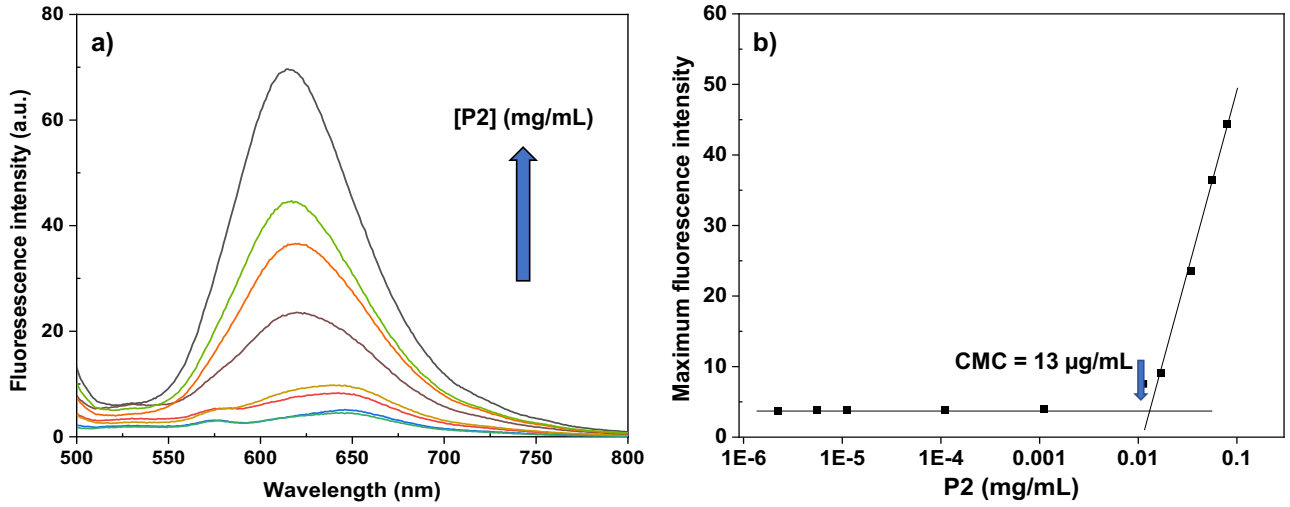

Figure A7. DLS diagrams of P1 and P2 nanoparticles at pH = 7.4.

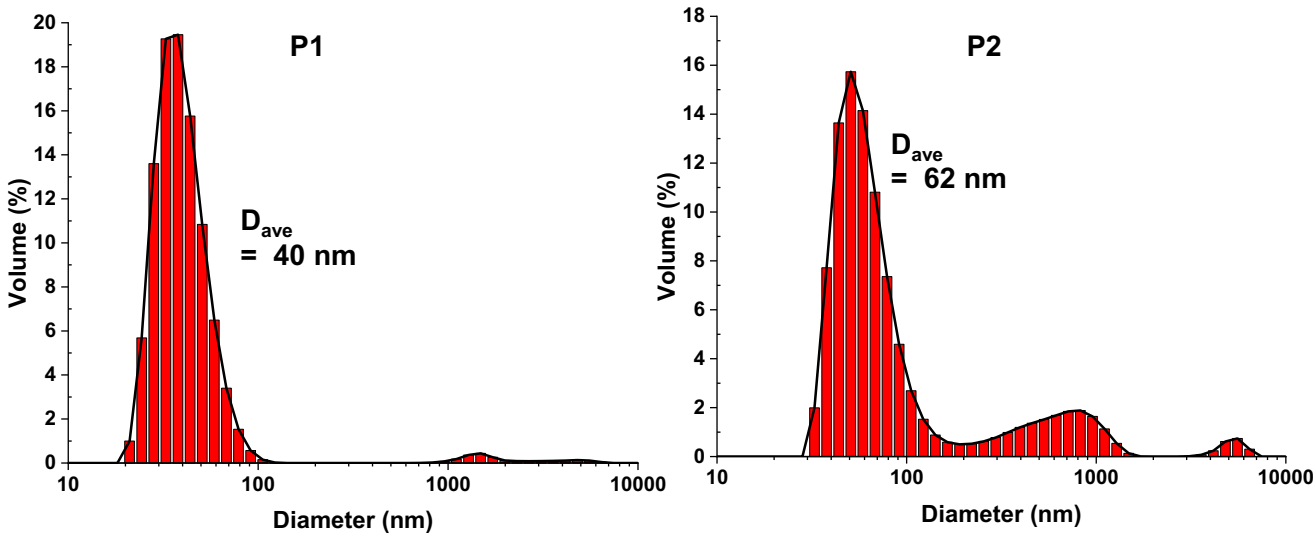

Figure A8. Digital image of Dox-NPs (inset) and UV/Vis spectrum of a mixture of aqueous P1-Dox-NPs (a) and P2-Dox-NPs (b) (1 mL) with DMF (5 mL).

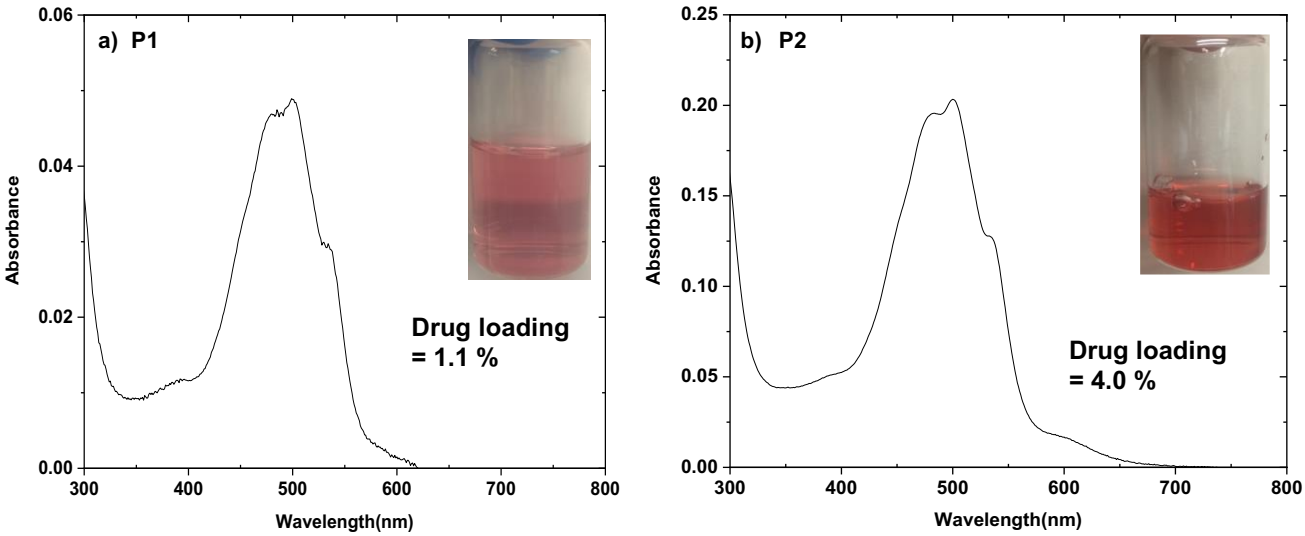

Table A1. Characteristics and properties of P1 and P2 diblock copolymers synthesized by ARGET ATRP of a mixture of ACMA with CIMA in the presence of PEG-AC-Br macroinitiator.[a)]

Polymer	$[ACMA]_0/[CIMA]_0/[PEG\text{-}AC\text{-}Br]_0$	Time (hrs)	Conv[b)]	DP[c)]		M_n[d)] (kg/mol)	Đ[d)]
				ACMA	CIMA		
P1	60/0/1	3.2	0.82	57	0	28	1.13
P2	50/10/1	1.9	0.83	51	11	28.6	1.21

a) Conditions for ATRP: $[PEG\text{-}AC\text{-}Br]_o/[Cu(II)Br]/[TPMA]_o$ = 1/0.3/0.05/0.15 in anisole at 73 °C, ACMA/anisole = 0.3 wt/wt for P1 and (ACMA+CIMA)/anisole = 0.4 wt/wt for P2; b, c) ^{1}H-NMR; and d) GPC with PMMA standards.

Appendix B

Supporting information and figures for chapter 4

I) Synthesis of PEG-ketal-Br

Figure B1. ^{1}H-NMR spectrum in $CDCl_3$ and ^{13}C-NMR spectrum in DMSO-d_6 of AC1.

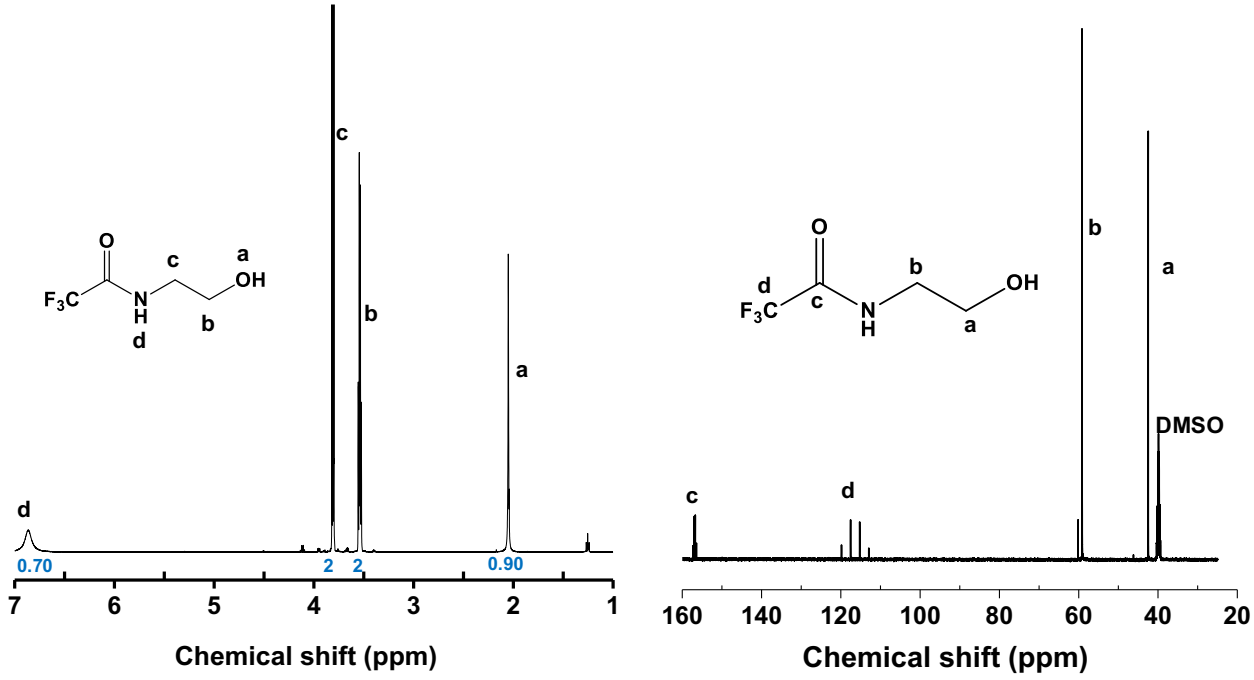

Figure B2. ^{1}H-NMR and ^{13}C-NMR spectra of AC2 in $CDCl_3$.

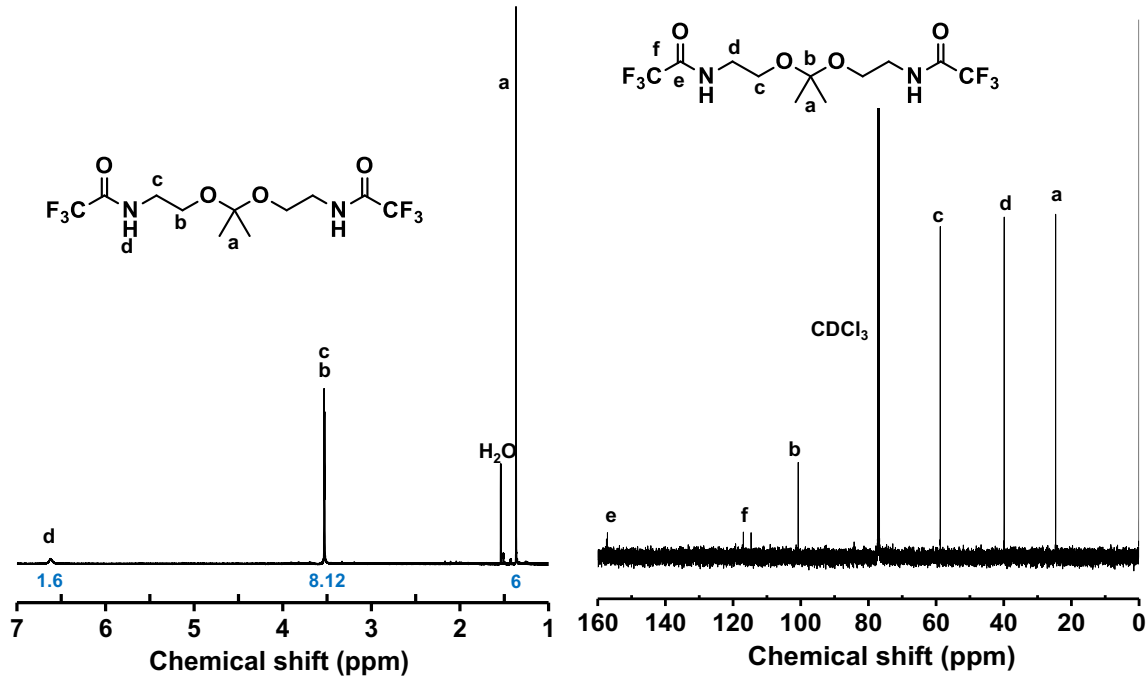

Figure B3. ^{1}H-NMR and ^{13}C-NMR spectra of AC3 in $CDCl_3$.

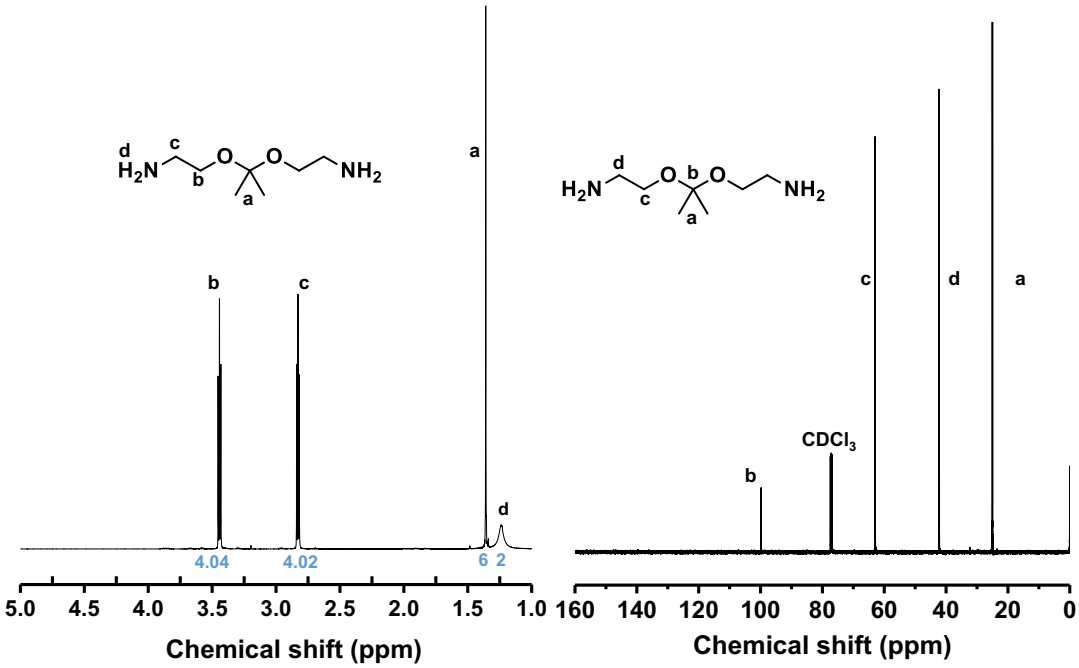

Figure B4. COSY NMR spectrum of AC3 in $CDCl_3$.

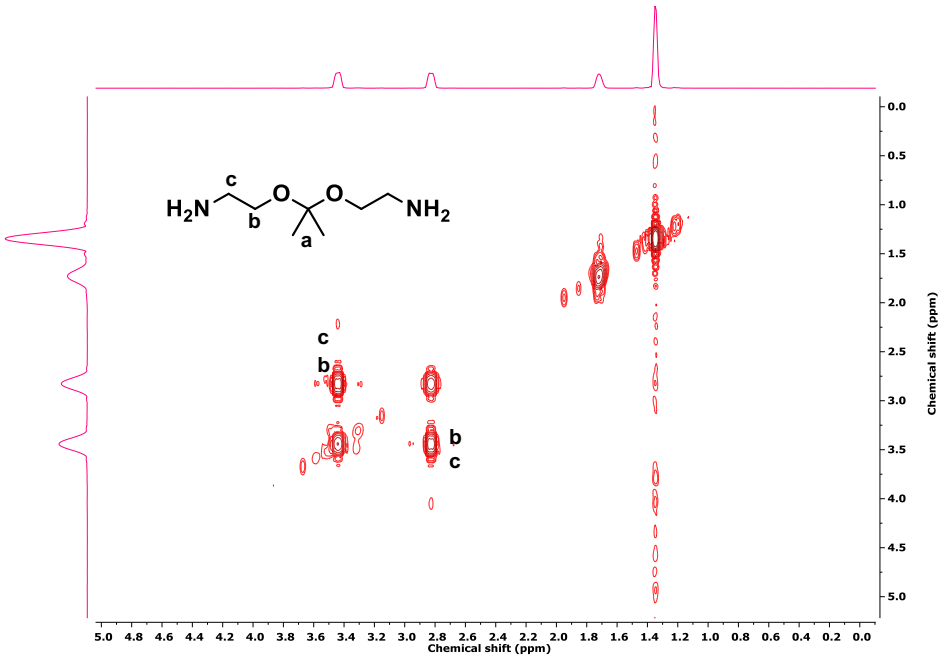

Figure B5. ^{13}C-NMR spectrum of AC4 in $CDCl_3$. X denotes impurities including methanol.

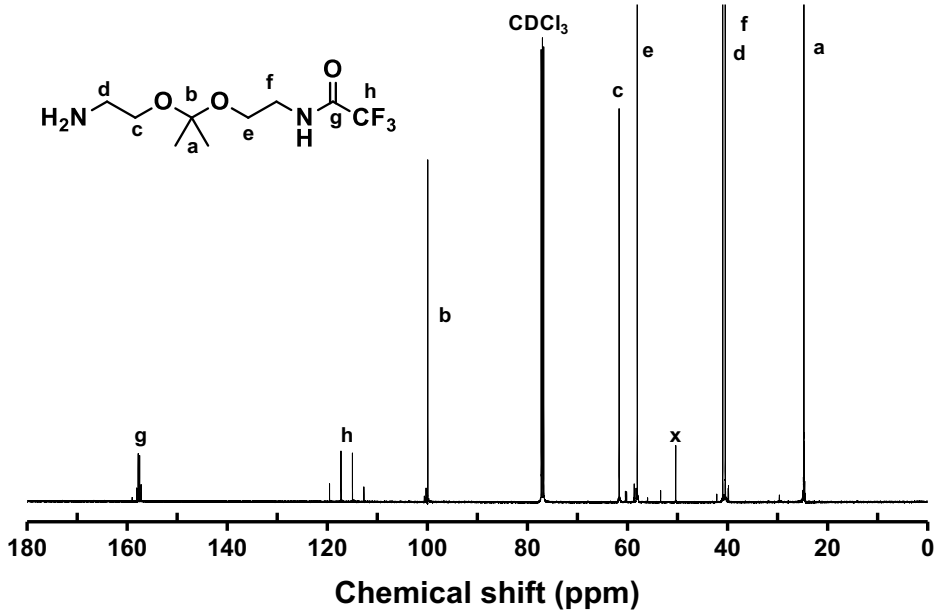

Figure B6. COSY NMR spectrum of AC4 in $CDCl_3$.

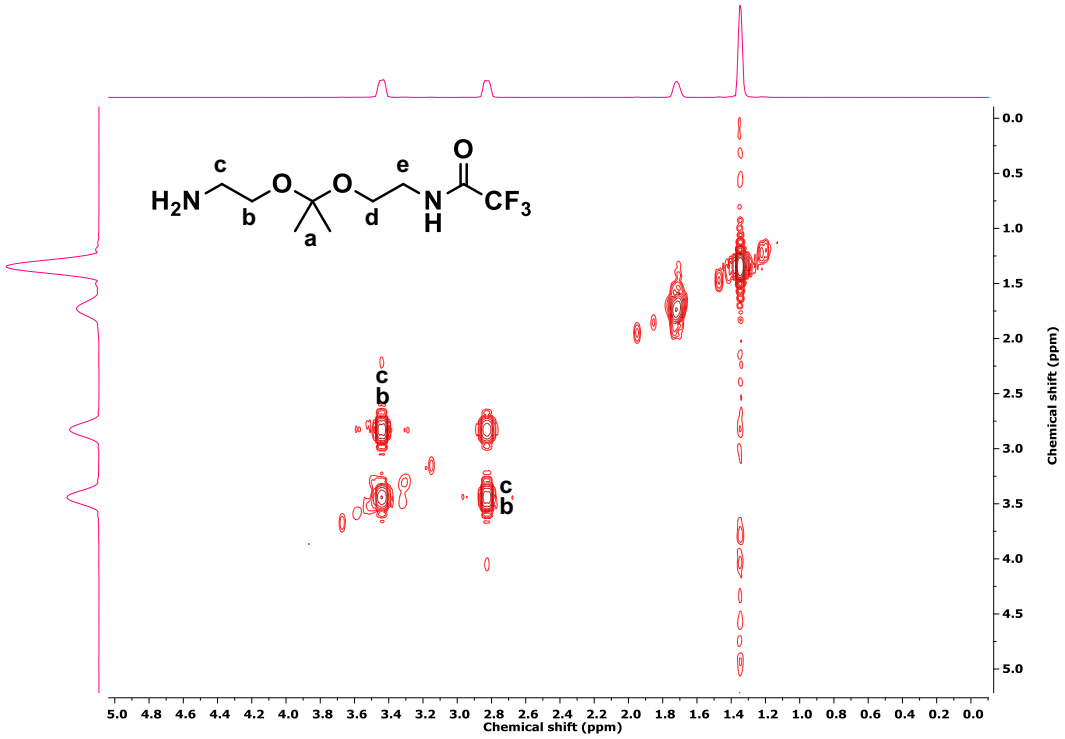

Figure B7. ^{19}F-NMR spectrum of AC5 and AC6 in $CDCl_3$.

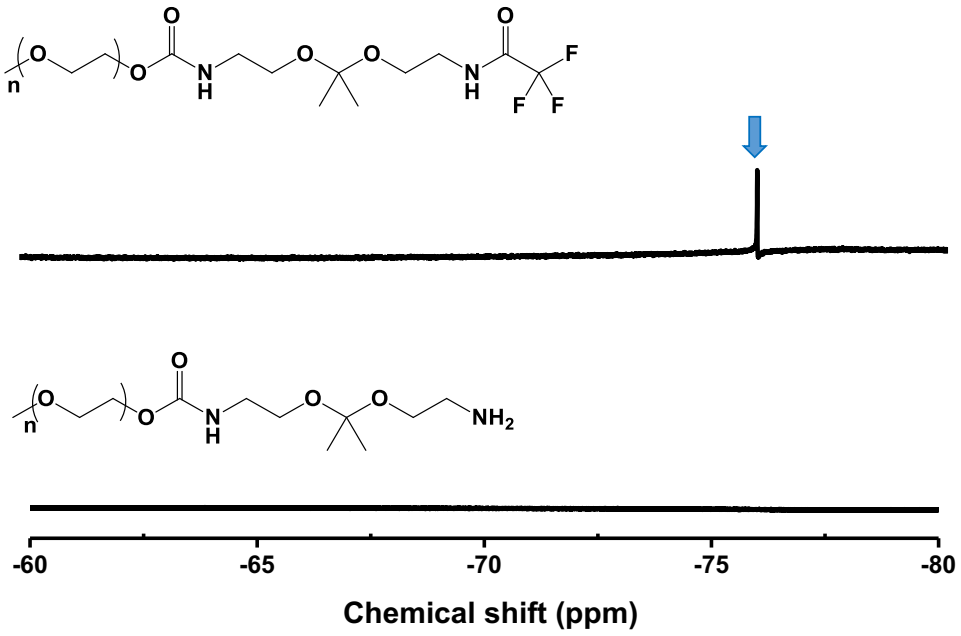

II) Attempts to synthesis of PEG-ketal-Br (unsuccessful synthesis)

Synthetic procedure

PEG-COOH: A solution containing PEG (25.0 g, 5 mmol) and DMAP (0.61 g, 5 mmol) dissolved in dry THF (200 mL) was mixed with succinic anhydride (2.5 g, 25.0 mmol) at room temperature for 22 hrs. After the removal of solvents by rotary evaporation, the residues were dissolved in chloroform (300 mL). The solution was washed with saturated brine solution (250 mL) three times and dried over anhydrous sodium sulfate. After the organic solution was concentrated, the product was precipitated from cold hexane, isolated by vacuum filtration, and dried in a vacuum oven at room temperature for 24 hrs. Yield: 18.1 g (71.1%). ^{1}H-NMR ($CDCl_3$, ppm): 4.21 (t, 2H, -$\underline{CH_2}$OC(O)-), 3.45-3.80 (m, -$\underline{CH_2CH_2}$O- of PEG main chain), 3.37 (s, 3H, $\underline{CH_3}$O-), 2.65 (m, 4H, -$\underline{CH_2CH_2}$C(O)OH).

PEG-NHS: A solution of EDC (1.6 g, 8.53 mmol) dissolved in chloroform (30 mL) was dropwise added to a solution of PEG-COOH (13.6 g, 2.66 mmol), DMAP (0.049 g, 0.40 mmol), and n-hydroxysuccinimide (NHS) (0.92 g, 7.99 mmol) in chloroform (200 mL) in an ice bath. The mixture was stirred for 18 hrs at room temperature, and then washed with a brine solution (100 mL) three times. The organic solution was dried over sodium sulfate and the product was precipitated from cold hexane. The resulting white solids were collected by filtration and dried in a vacuum oven at room temperature for 12 hrs, yielding 10.5 g (75.9%). ^{1}H-NMR ($CDCl_3$, ppm): 4.21 (t, 2H, $\underline{CH_2}$OC(O)-), 3.45-3.80 (m, -$\underline{CH_2CH_2}$O- of PEG main chain), 3.37 (s, 3H, $\underline{CH_3}$O-), 2.97 (t, 2H, -$CH_2\underline{CH_2}$C(O)ONC(O)-), 2.84 (s, 4H, -OC$\underline{CH_2CH_2}$CO-), 2.79 (t, 2H, -$\underline{CH_2}CH_2$C(O)ONC(O)-).

AC8: A solution consisting of the purified, dried PEG-NHS (3.41 g, 0.65 mmol) and Et_3N (0.17 g, 1.70 mmol) in chloroform (65 mL) was mixed with a solution of AC4 (0.50 g, 1.96 mmol) in chloroform (5 mL) in an ice bath at room temperature for 22 hrs. Chloroform (200 mL) was added, and the mixture was washed with PBS solution (pH 7.4, 200 mL) two times and dried over sodium sulfate. The organic solution was concentrated by rotary evaporation and the product was precipitated from cold hexane. The resulting white solids were collected by filtration and dried in a vacuum oven at room temperature for 12 hrs. Yield: 2.9 g (86.2%).^{1}H NMR ($CDCl_3$, ppm): 4.21 (t, 2H, $\underline{CH_2}$OC(O)-), 3.45-3.80 (m, -$\underline{CH_2CH_2}$O- of PEG main chain), 3.37 (s, 3H, $\underline{CH_3}$O-), 2.70 (t, 2H, -$CH_2\underline{CH_2}$C(O)NH-), 2.50 (t, 2H, -$\underline{CH_2}CH_2$C(O)NH-), 1.36 (s, 6H, -$CH_2OC(\underline{CH_3})_2OCH_2$-).

AC8→AC9: Typically, a solution of potassium carbonate (7.5 mg) in water (5 mL) mixed with a solution of AC8 (130 mg) in MeOH (15 mL) at room temperature for 12 hrs. After the solvent was evaporated, the residues were dissolved in water, extracted from DCM two times, and then analyzed by ^{1}H-NMR spectroscopy.

AC3 → AC11/AC12: Br-iBuBr (0.35 g, 1.52 mmol) was added via syringe to a solution containing AC3 (0.98 g, 6.04 mmol) and Et_3N (0.92 g, 9.0 mmol) dissolved in anhydrous THF (120 mL). The resulting mixture was stirred for 14 hrs at room temperature and the white solids (Et_3N-HBr adducts) formed during the reaction were removed by vacuum filtration. The filtrates were then concentrated by rotary evaporation and purified by silica gel column chromatography

(9.5/0.5 v/v DCM/MeOH). The product (AC11), a white solid, was collected as the first of a total of four bands. ^{1}H-NMR ($CDCl_3$, ppm): 7.05 (s, 2H, -$CH_2CH_2\underline{NH}C(O)C(CH_3)_2Br$), 3.53 (t, 4H, -$OC(CH_3)_2OCH_2\underline{CH_2}NHC(O)C(CH_3)_2Br$), 3.45 (q, 4H, -$\underline{CH_2}OC(CH_3)_2O\underline{CH_2}$-), 1.95 (s, 12H, -$CH_2CH_2NHC(O)C(\underline{CH_3})_2Br$), 1.37 (s, 6H, -$CH_2OC(\underline{CH_3})_2OCH_2$-). Mass calculated for ($C_{15}O_4N_2Br_2H_{28}Na^+$): 429.06256. Found: 429.06073

AC13: Br-iBuBr (0.50 g, 2.2 mmol) was added to a clear solution containing AC5 (0.23 g, 0.73 mmol), Et_3N (1.12 g, 11.1 mmol), and anhydrous THF (5 mL) in an ice bath under magnetic stirring. 10 w/v% aqueous potassium carbonate solution (30 mL) was added, and the reaction mixture was stirred for additional 40 min. The product was extracted from EA (40 mL) two times and solvent was evaporated to yield a yellow oil (0.2 g, 71%) ^{1}H-NMR ($CDCl_3$, ppm): 3.4-3.6 (t, 8H, $CF_3C(O)NH\underline{CH_2CH_2}O\ C(CH_3)_2O\underline{CH_2CH_2}NHC(O)C(CH_3)_2$ Br), 1.95 (s, 6H, -$OC(CH_3)_2OCH_2CH_2NHC(O)C(\underline{CH_3})_2Br$), 1.37 (s, 6H, -$CH_2OC(\underline{CH_3})_2OCH_2$). ^{13}C-NMR ($CDCl_3$, ppm): 172.10, 157.0, 116.0, 100.50, 63.1, 58.75, 59.35, 40.25, 39.80, 32.5, 24.70. Mass calculated for ($C_{13}H_{22}BrF_3N_2O_4$): 429.06256. Found: 429.06073

AC13 → AC12: AC13 (0.15 g, 0.36 mmol) was mixed with 6M aqueous NaOH solution (10 mL) under stirring for 2.5 hr at room temperature. The residues were extracted from DCM (40 mL) four times and analyzed by ^{1}H-NMR spectroscopy.

Ethylene diamine and Br-iBuBr reaction: Br-iBuBr (0.57 g, 2.4 mmol) was added to a solution of ethylenediamine (0.59 g, 10 mmol) dissolved in THF (35 mL) in an ice-bath and stirred for 5 hours. The white formed solids were removed by vacuum filtration, and then the solvent was removed by rotary evaporation. The residues were dissolved in DCM and washed with water two times.

Route (II)

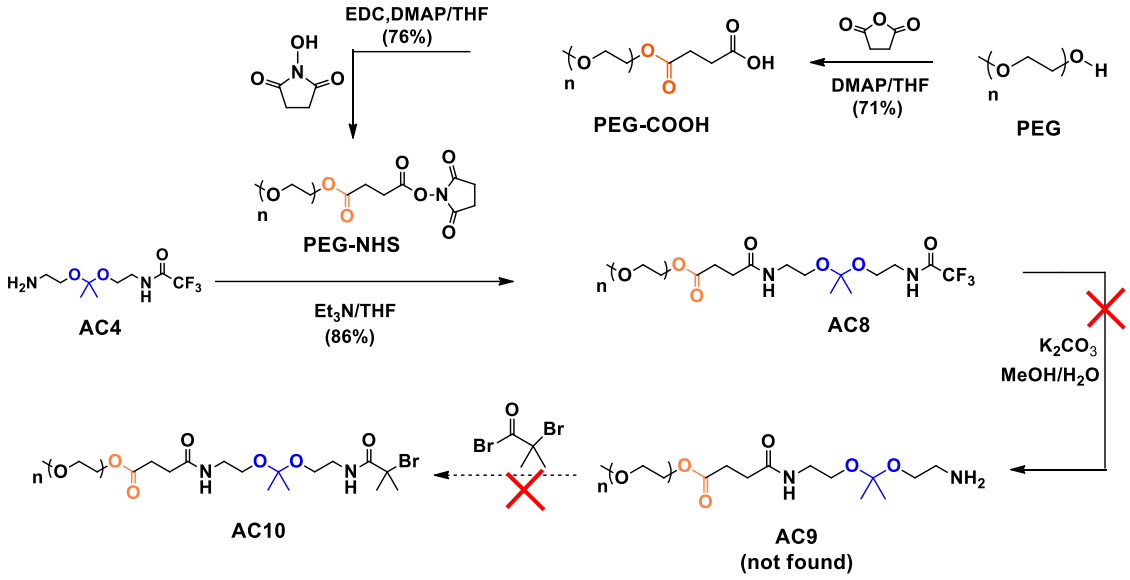

Scheme B1. Illustration of our synthetic route (II) (unsucessful attempt) in attempts to the synthesis of PEG-ketal-Br initiator.

Scheme B1 illustrates the route (II) that is similar to the above route (I) but differs with the use of an ester bond between PEG and AC4. This route began with the carboxylation of PEG with succinic anhydride to PEG-COOH, followed by the activation of COOH groups with n-hydroxysuccinimide (NHS). The resulting PEG-NHS then reacted with AC4 to form AC8 through the formation of an amide bond. ^{1}H-NMR analysis was used to follow the synthesis of PEG-COOH, PEG-NHS, and AC8 (Figure S8, S9, and S10). The following step was the treatment of AC8 with K_2CO_3. However, no peak at 4.2 ppm corresponding to methylene protons adjacent to the ester bond was found in the ^{1}H-NMR spectrum (data is not shown), suggesting the unexpected cleavage of the ester bonds under this condition. Thus, the further steps could not be explored.

Route (III)

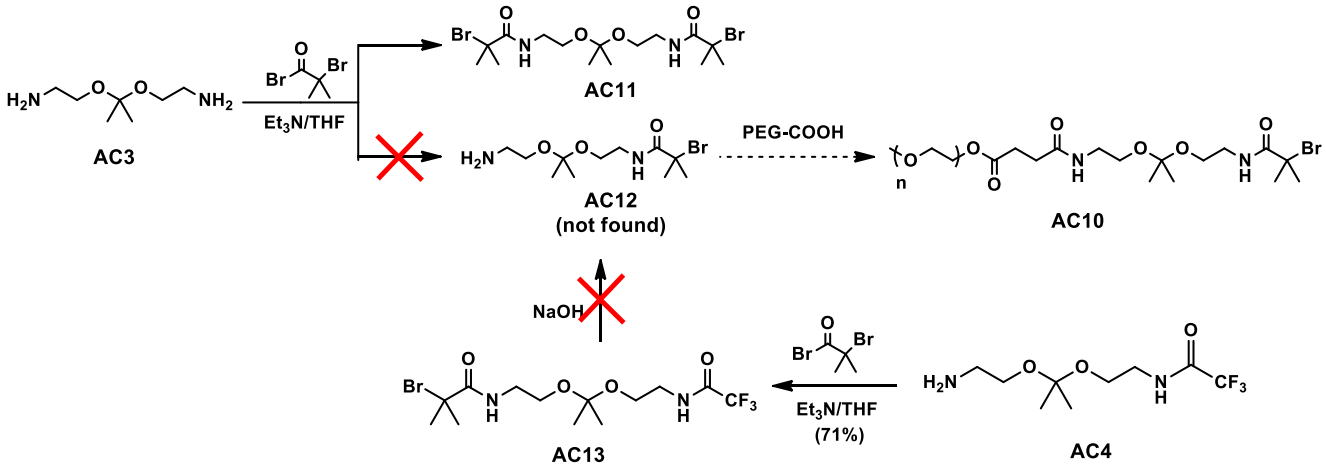

Scheme B2. Illustration of our synthetic route (III) (unsuccessful attempt) in attempts to the synthesis of PEG-ketal-Br initiator.

Scheme B2 illustrates the route (III) that centers on the synthesis of AC12 functionalized with both amine and bromo groups, which could yield a PEG-ketal-Br by its direct coupling with PEG-COOH. One strategy is the coupling reaction of AC3 with Br-iBuBr. Excess AC3 (4 moles equivalent) was designed to minimize the formation of AC11 (a dibromide). Further, excess Et_3N should be used as a base to minimize the unexpected cleavage of acidic pH-labile ketal linkages due to HBr (a strong acid) generated from the coupling reaction. After careful purification by thin layer chromatography and column chromatography, however, the targeted AC7 was not found, but the AC11 byproduct was isolated (^{1}H-NMR spectrum of AC11 in Figure S11). The plausible reason is the high reactivity of the amine group of AC3 toward an acyl bromide to yield only disubstituted AC11, not mono-substituted AC12. A control reaction examined with ethylene diamine under similar conditions also yielded a dibromo-product only (^{1}H-NMR spectrum in Figure B12).

Another strategy is illustrated in Scheme 4, in which the first step is the coupling reaction of AC4 with Br-iBuBr. Excess Et_3N (15 mole equivalent to AC4) and reaction time as short as <3 hrs at room temperature were used to minimize unexpected cleavage of ketal linkages during the coupling reaction. ^{1}H- and ^{13}C-NMR analysis confirms the successful synthesis of AC13 at 70% yield (Figure S13). Then, basic hydrolysis of AC13 was examined in the presence of NaOH; this step was aimed at the cleavage of the trifluoroacetamide group to yield AC12. However, no peak

at 1.9 ppm corresponding to two methyl groups in Br initiating moieties was found in the ^{1}H-NMR spectrum, suggesting no formation of AC12 in a basic condition.

Figure B8. ^{1}H-NMR spectrum of PEG-COOH in $CDCl_3$.

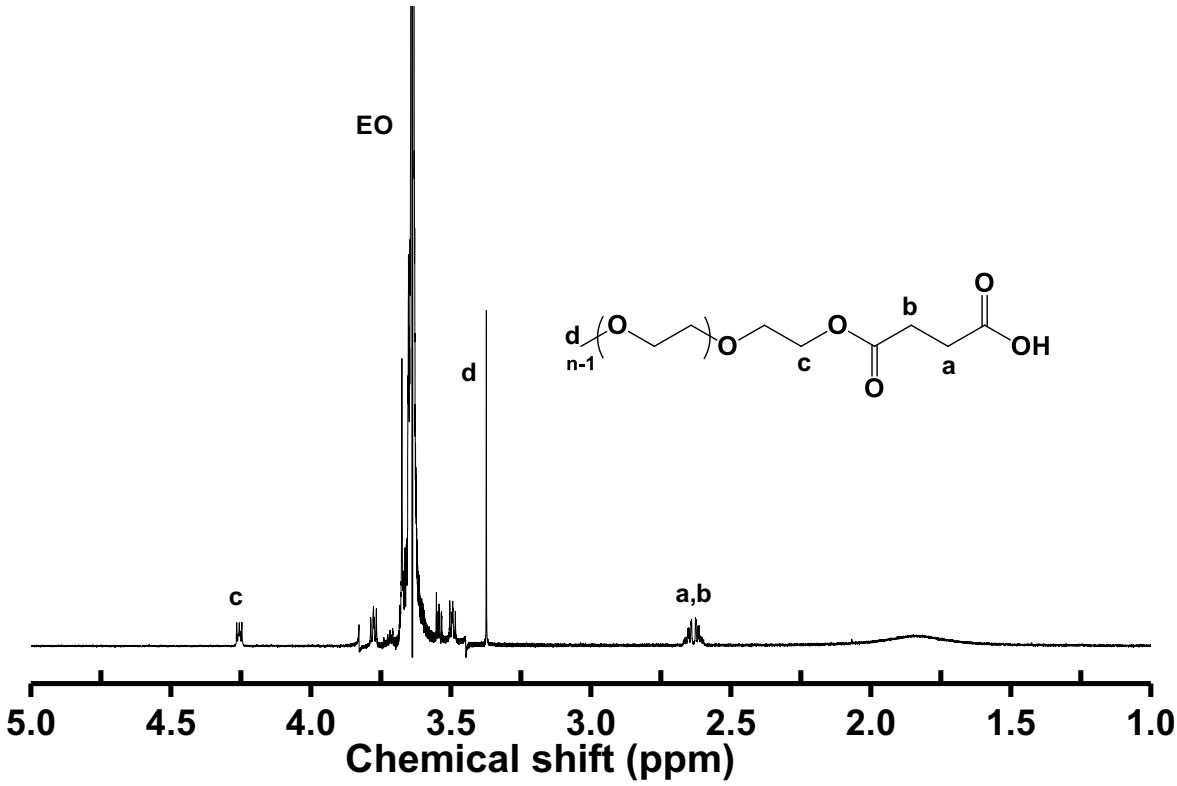

Figure B9. ^{1}H-NMR spectrum of PEG-NHS in $CDCl_3$.X denotes impurities including water.

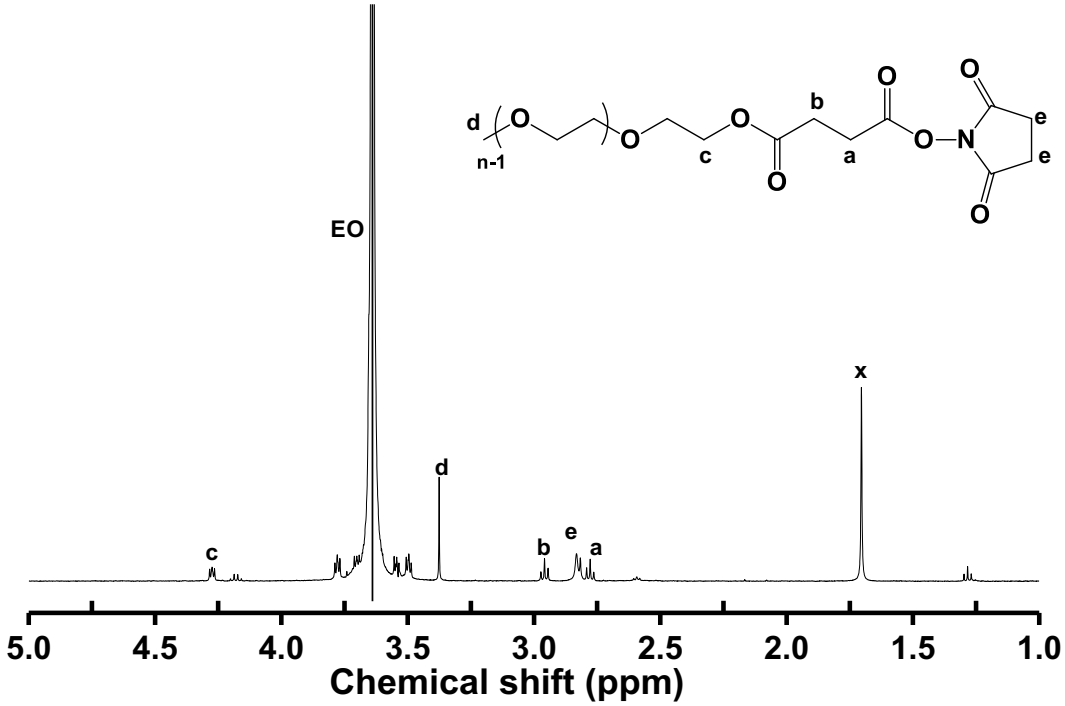

Figure B10. ^{1}H-NMR spectrum of AC8 in $CDCl_3$.

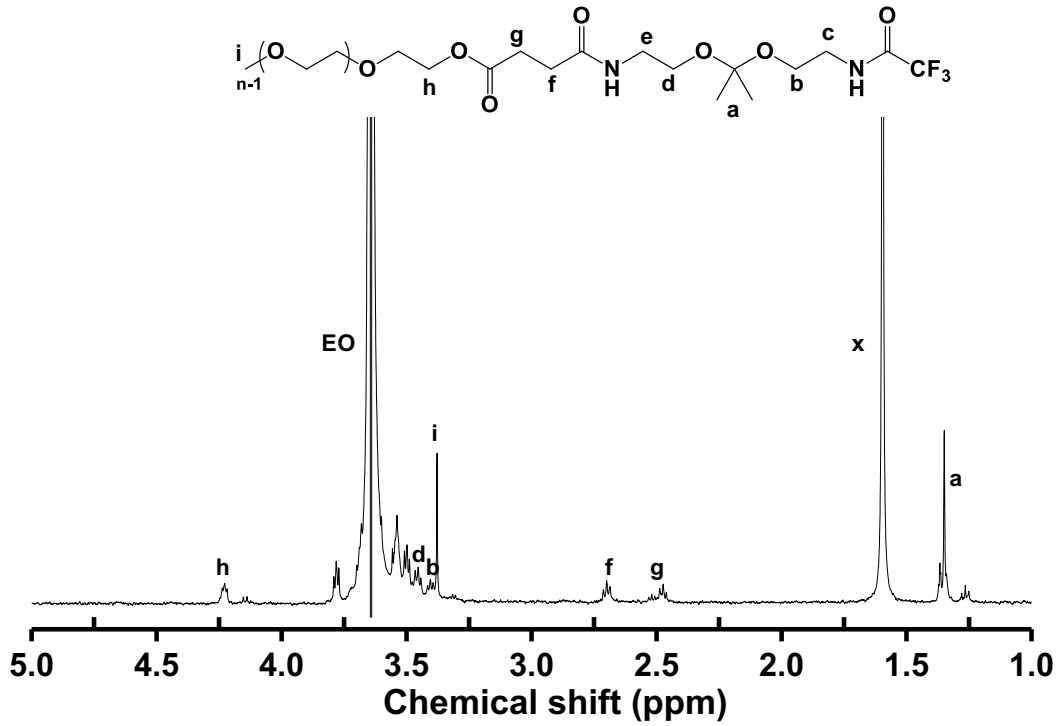

Figure B11. ^{1}H-NMR spectrum of AC11 in $CDCl_3$.

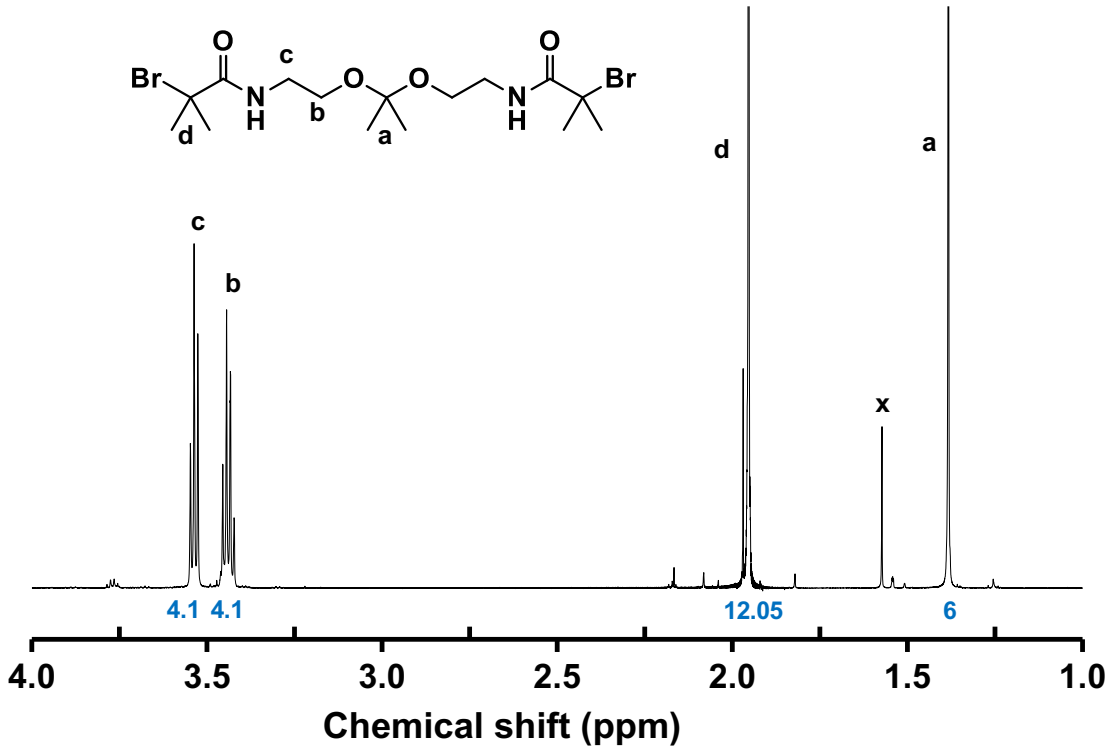

Figure B12. Reaction scheme and ^{1}H-NMR spectrum of a dibromo compound in $CDCl_3$.

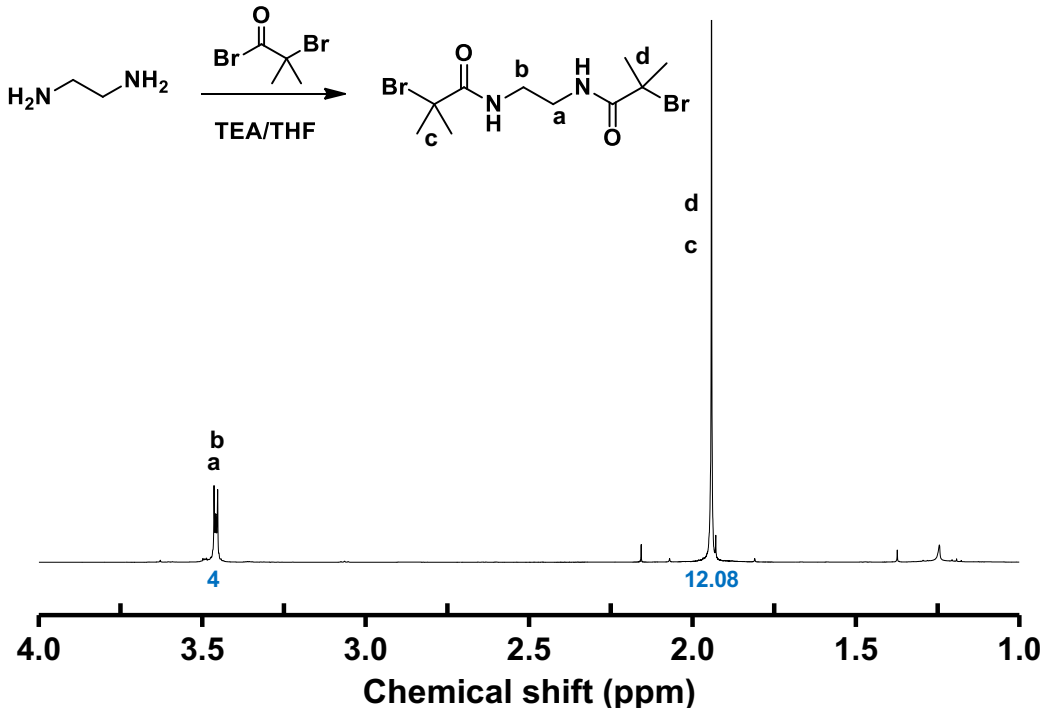

Figure B13. ^{1}H- and ^{13}C-NMR spectra of AC13 in $CDCl_3$.

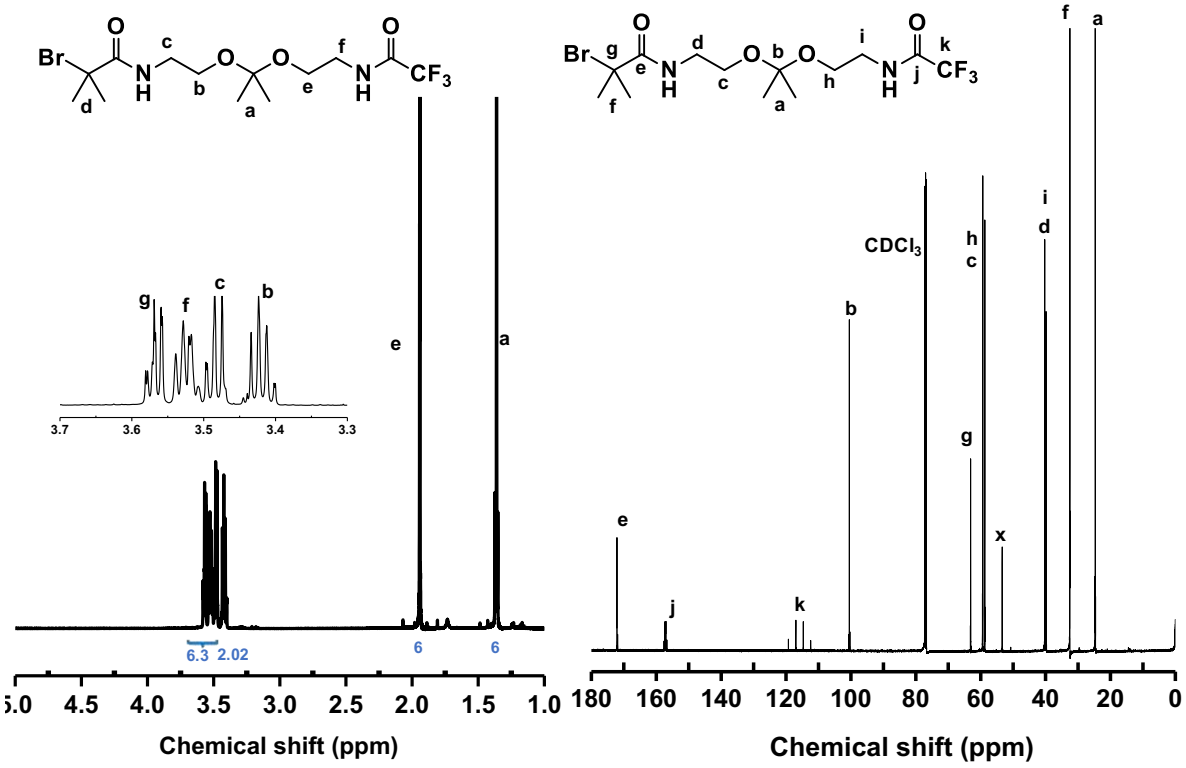

III) Investigation of ketal cleavage during ATRP

Figure B14. GPC diagrams of DLDSRD-1 before and after filtration with basic alumina during purification process after precipitation, compared with that of PEG-ketal-Br.

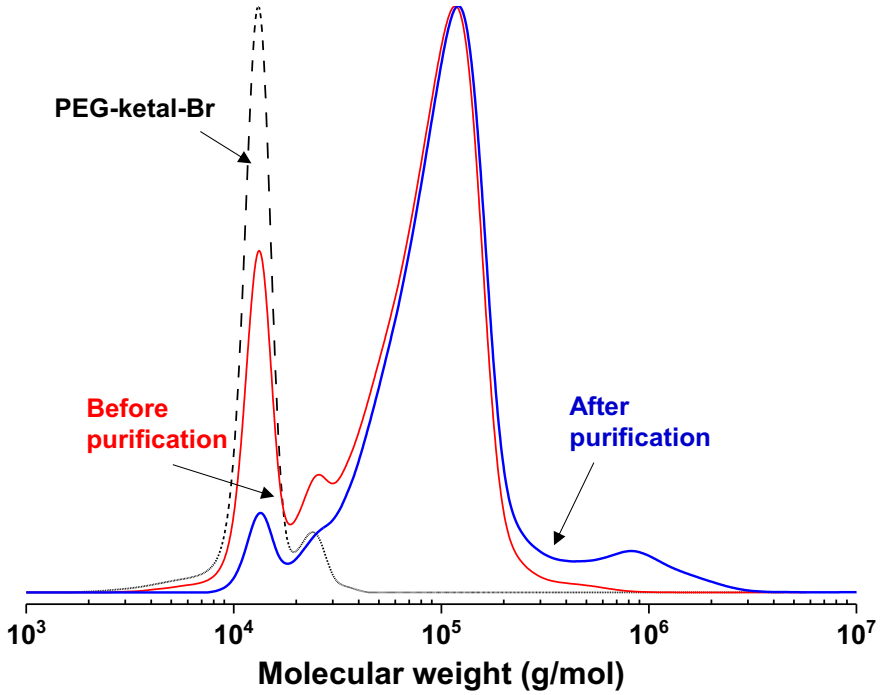

Figure B15. For DLDSRD-2, ^{1}H-NMR spectrum (a) and GPC diagram (b) of residues dissolved in supernatant (hexane) .

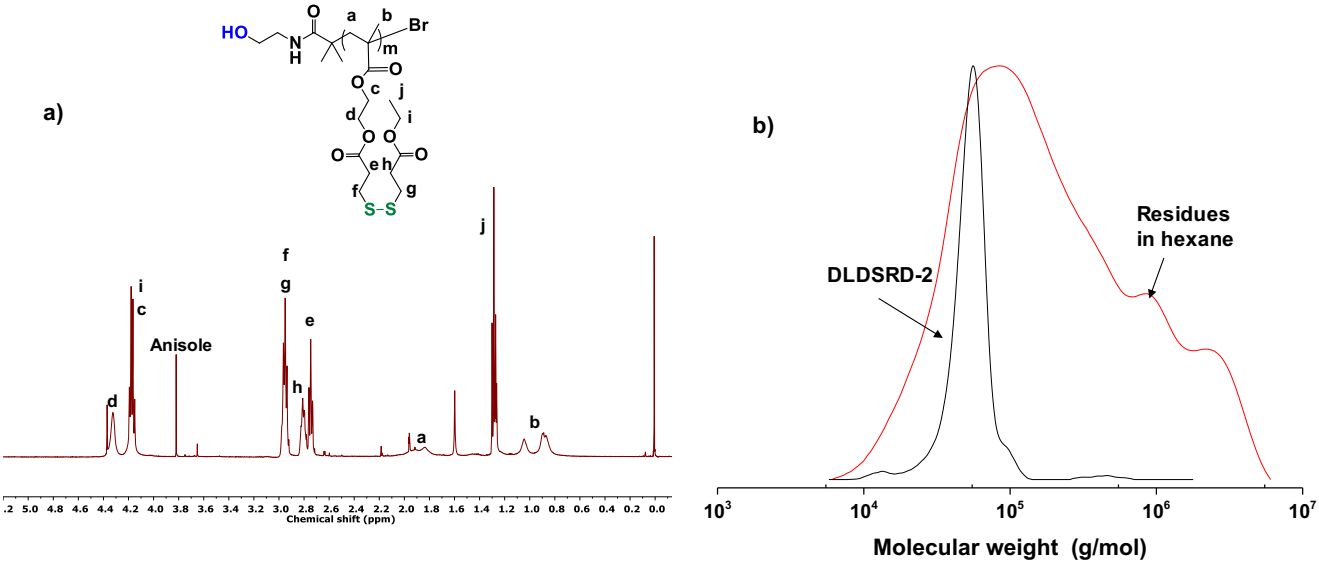

Figure B16. Schematic illustration of synthesis and ^{1}H-NMR spectrum of the purified PEG-b-PHMssEt copolymer in $CDCl_3$.

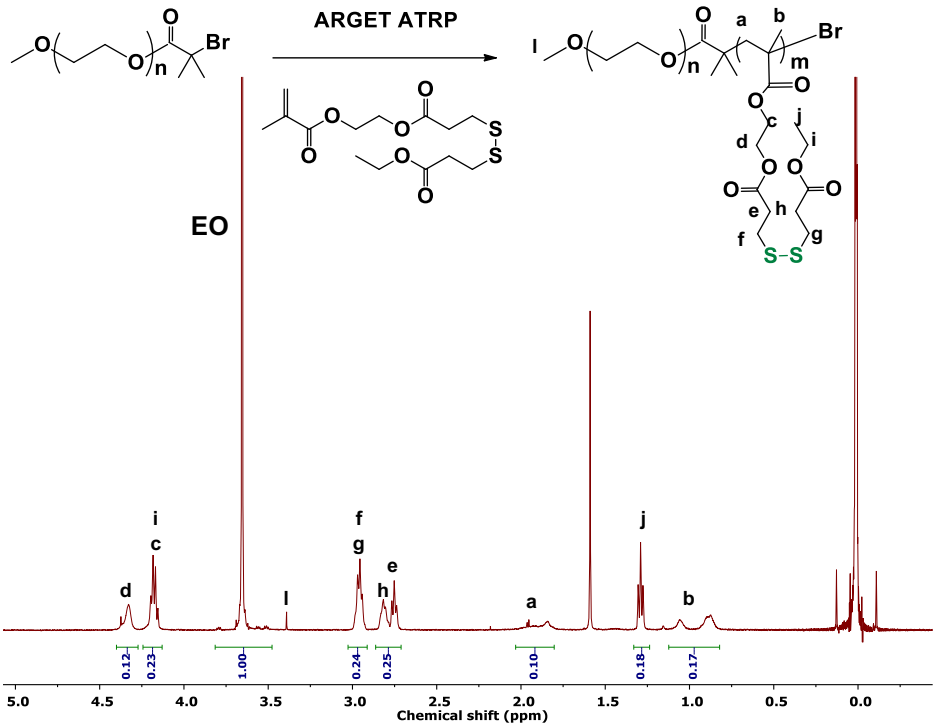

IV) Aqueous micellization and dual stimuli degradation

Figure B17. DLS diagram of micellar aggregates formed through self-assembly of PEG-ketal-PHMssEt in aqueous solution.

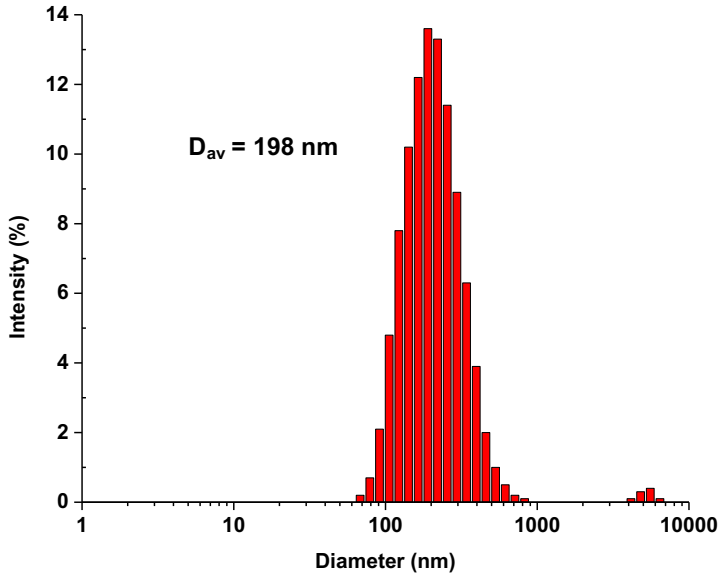

Figure B18. ^{1}H-NMR spectra of PEG-ketal-Br before (a) and after (b) treatment with acid in DMSO-d_6.

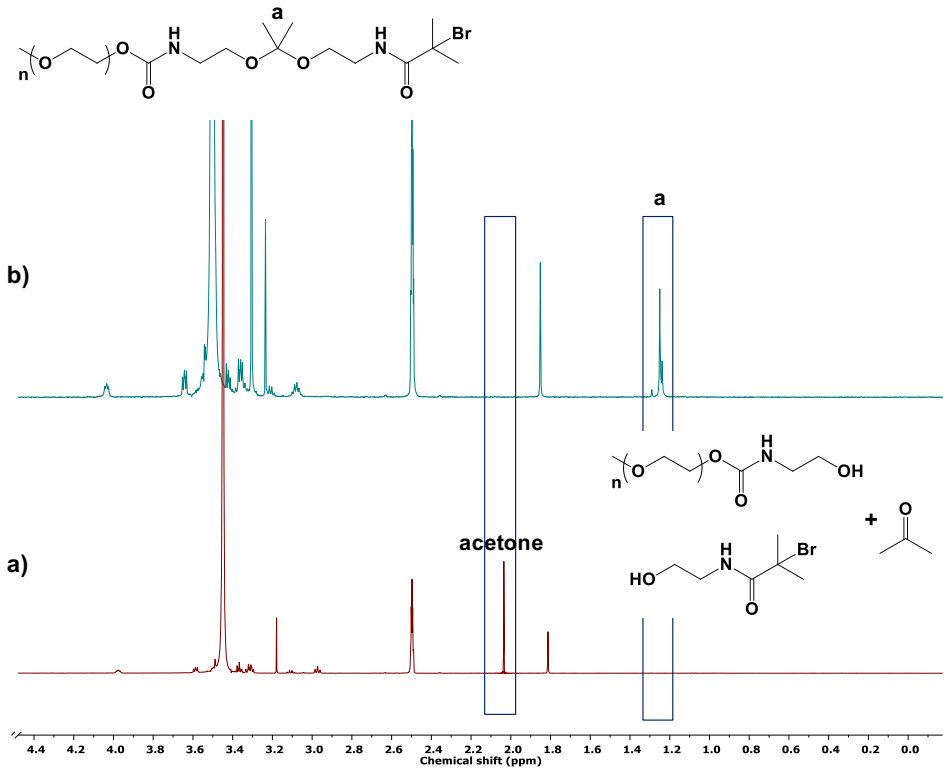

Appendix C

Supporting information and figures for chapter 5

Figure C1. First-order kinetic plot over time (a), evolution of molecular weight and molecular weight distribution (b), and overlaid GPC traces over conversion (c) for RAFT polymerization of HMssEt in the presence of P4 macro-RAFT agent. Conditions: $[HMssEt]_o/[P4]_o/[AMBN]_o$ = 50/1/0.3 in anisole at 73 °C, HMssEt/anisole = 0.6 wt/wt.

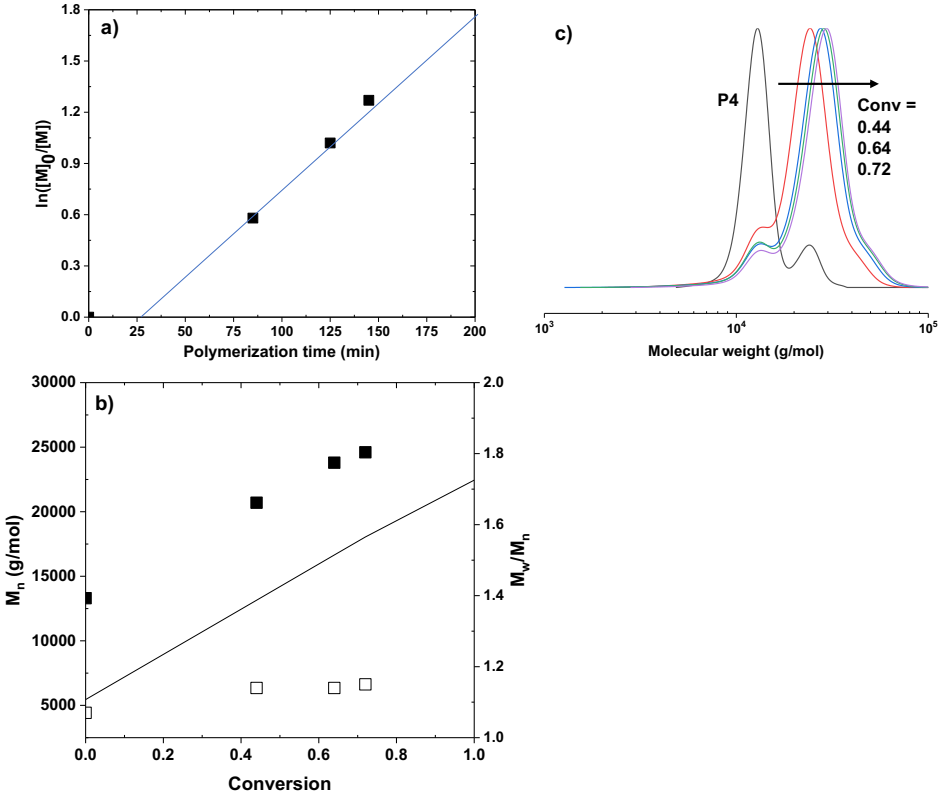

Figure C2. GPC trace of P5 diblock copolymer, compared with P4 macro-RAFT agent.

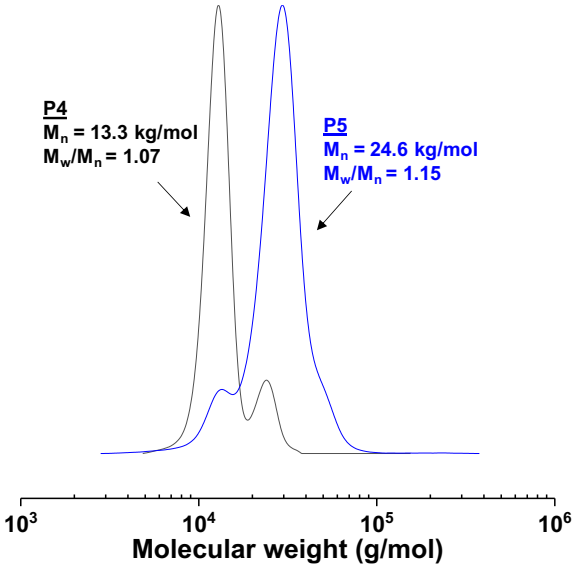

Figure C3. DLS diagram of aqueous micelles self-assembled from P5 at 1 mg/mL.

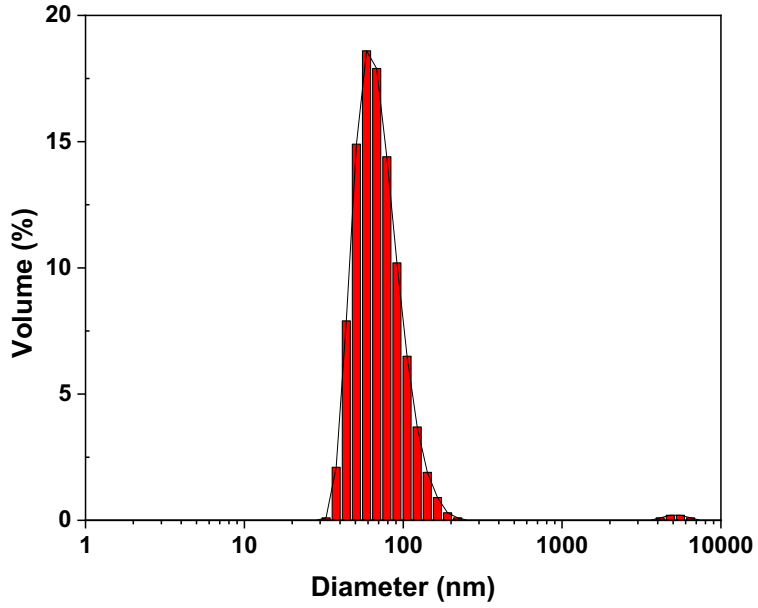

Figure C4. ^{1}H-NMR spectrum of P5 incubated with DCl in $CDCl_3$.

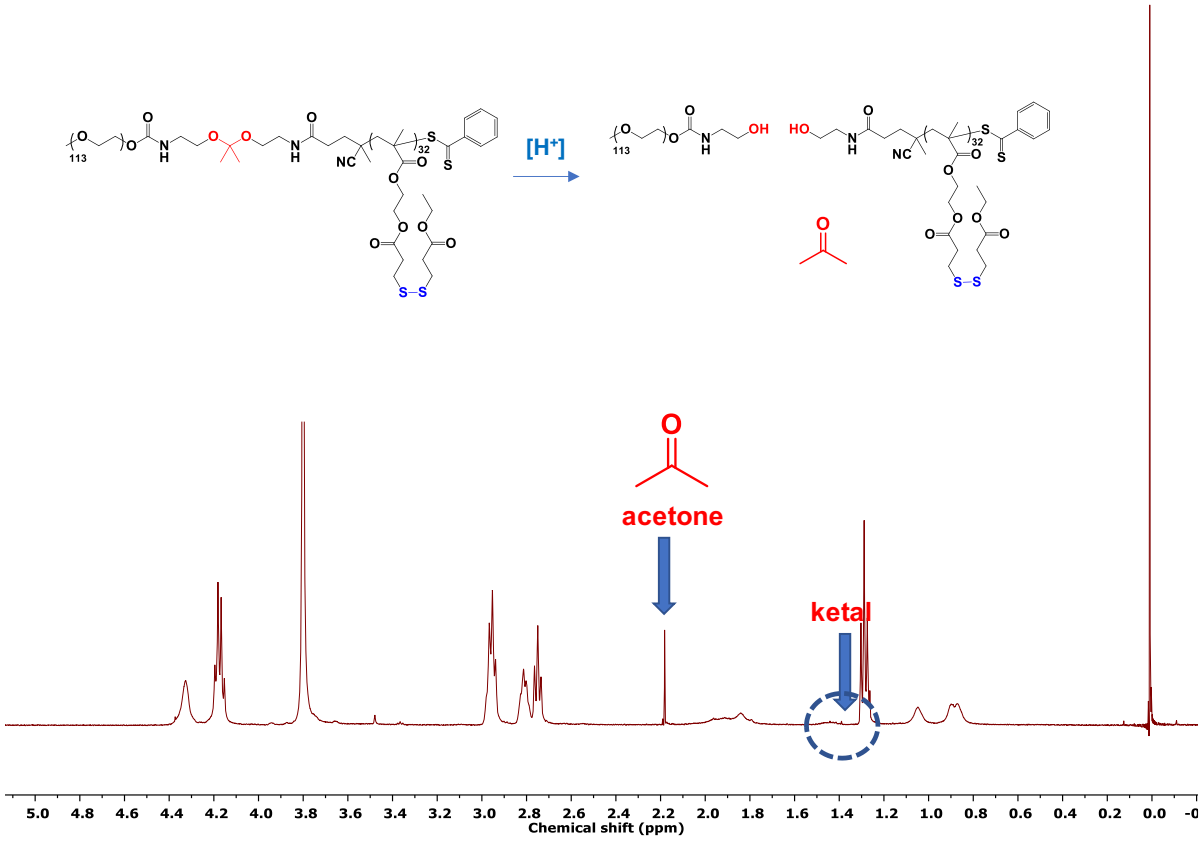

Figure C5. ^{1}H-NMR spectra in $CDCl_3$ for precipitate (a) and supernatant (b) of degraded micelles resulted from the incubation in acidic buffer at pH= 5.4.

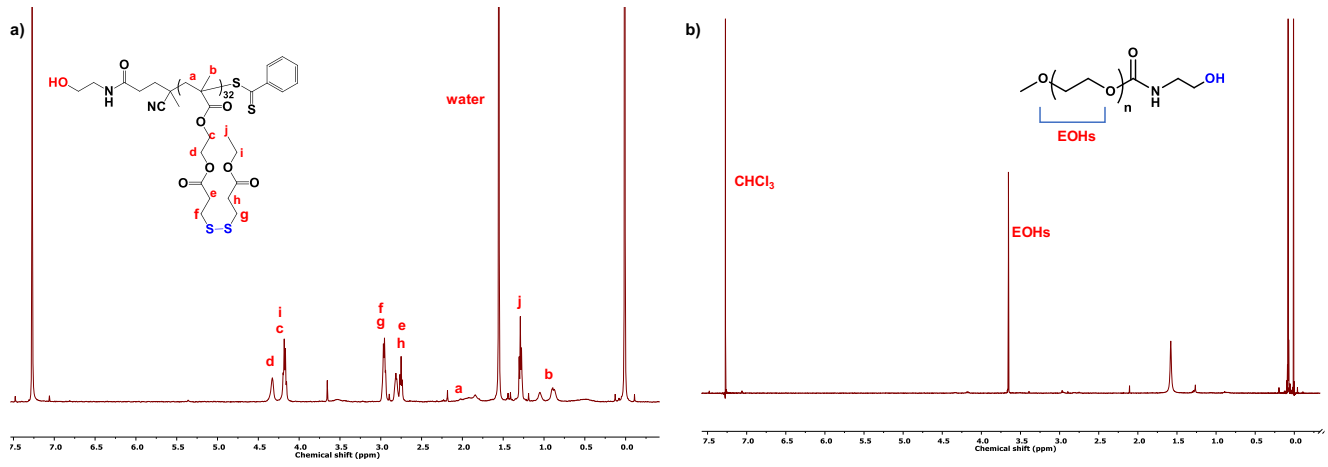

Figure C6. GPC trace of precipitate and supernatant of the degraded micellar dispersion after incubation in acidic buffer pH= 5.4, compared with P4 and P5.

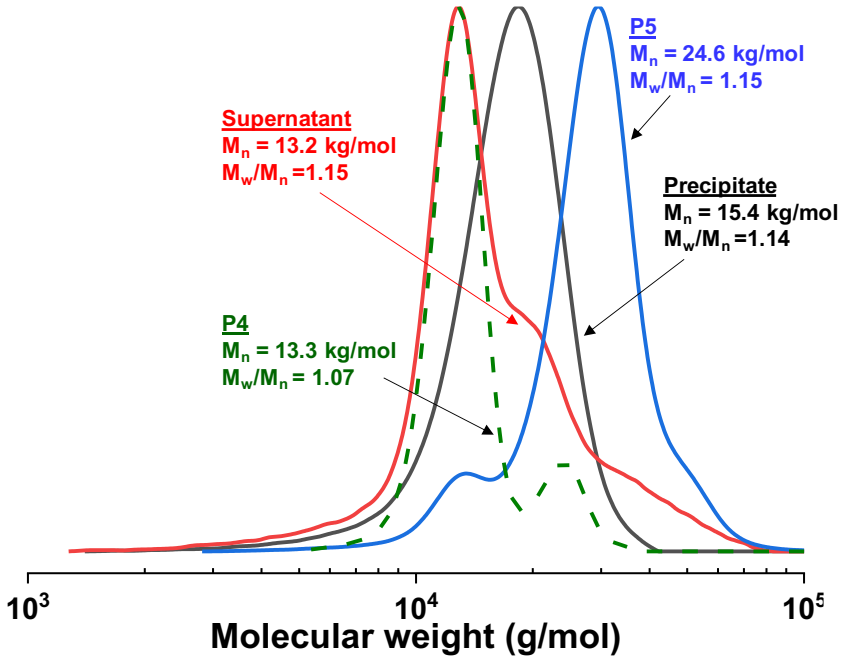

Figure C7. UV/Vis spectrum of a mixture of aqueous Dox-micelles (1 mL) with DMF (5 mL).

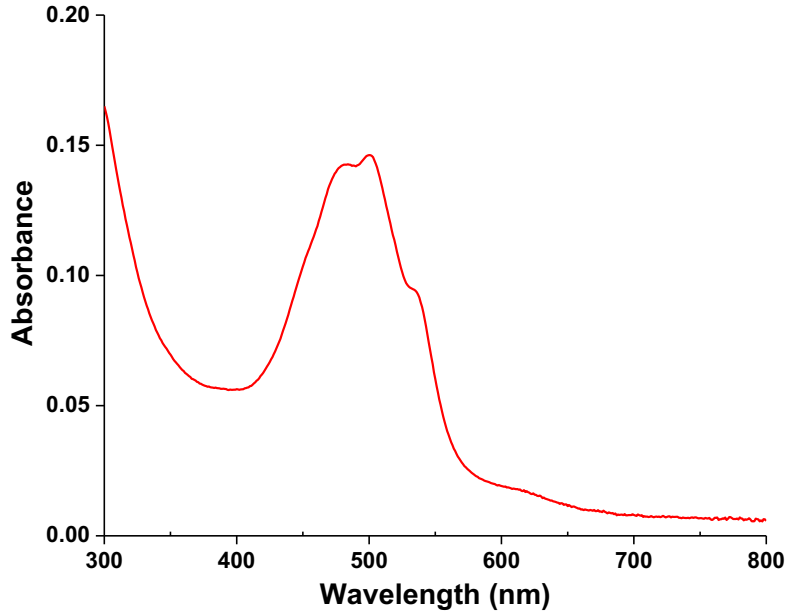

Figure C8. Calibration curves constructed with maximum fluorescence intensity at 593 nm over Dox concentration in buffer solutions at pH = 5.4 and pH = 7.4 with and without 10 mL GSH.

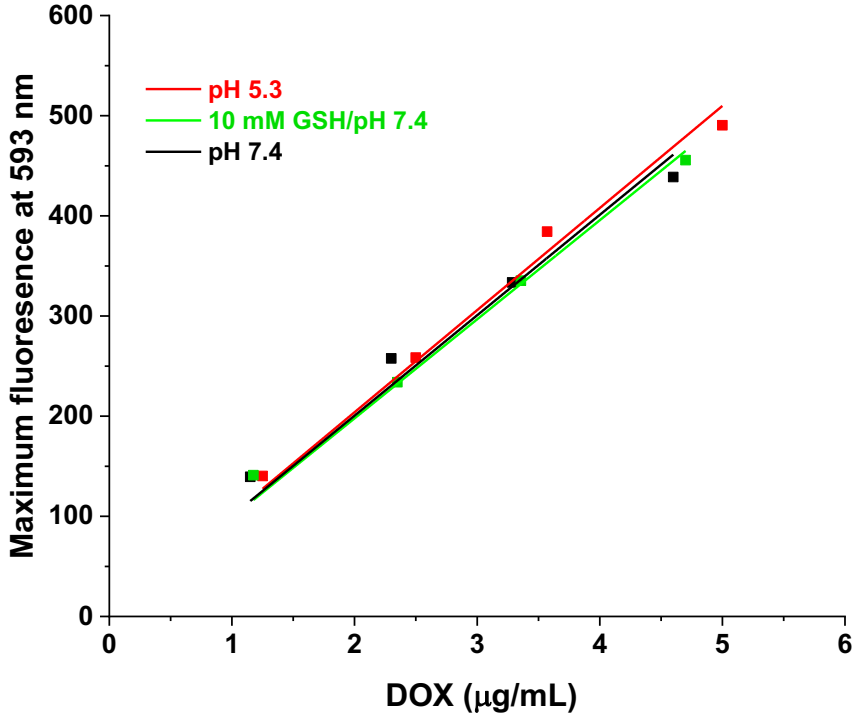

Figure C9. %Dox release from Dox-NPs in triplicate being incubated at pH 7.4 (control with no stimuli).

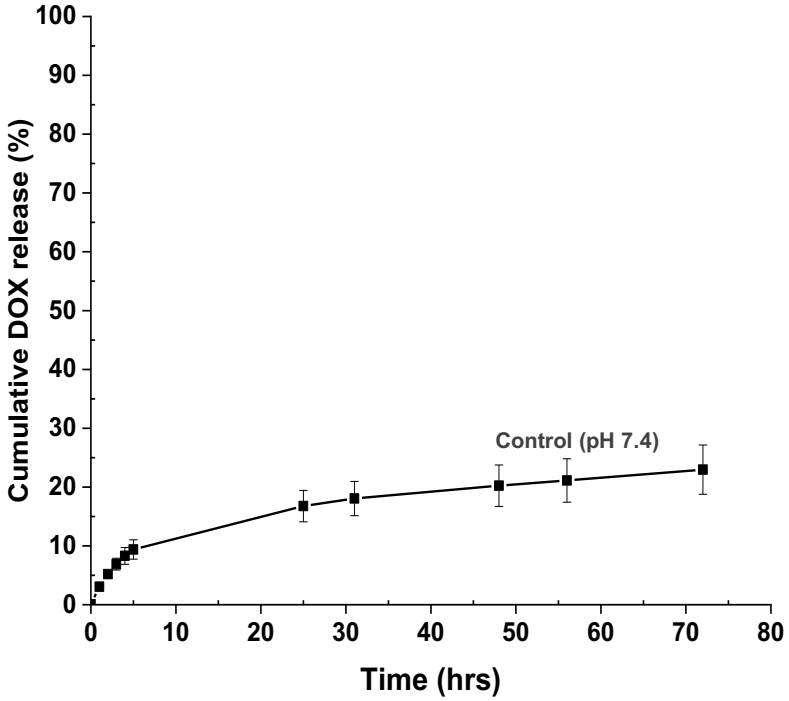

Figure C10. Fluorescence microscopy images of HeLa cells incubated with Dox-NPs (as encapsulated Dox), compared with the control (with not Dox-NPs) at pH = 7.4. Scale bar = 100 um.

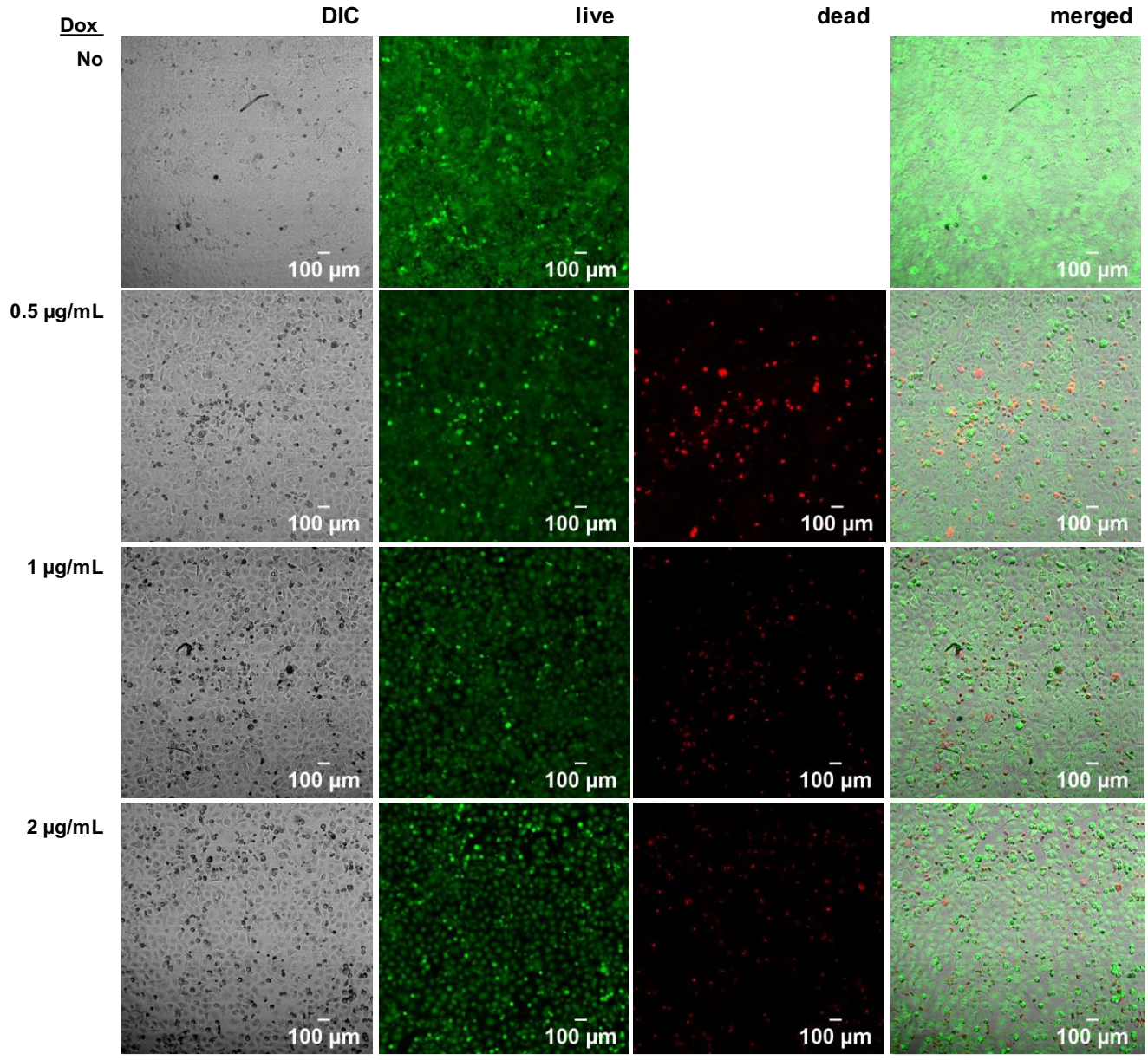

Figure C11. Fluorescence microscopy images of HeLa cells incubated with Dox-NPs (as encapsulated Dox), compared with the control (with not Dox-NPs) at pH = 6.8 with 10 mM GSH-OEt. Scale bar = 100 um.

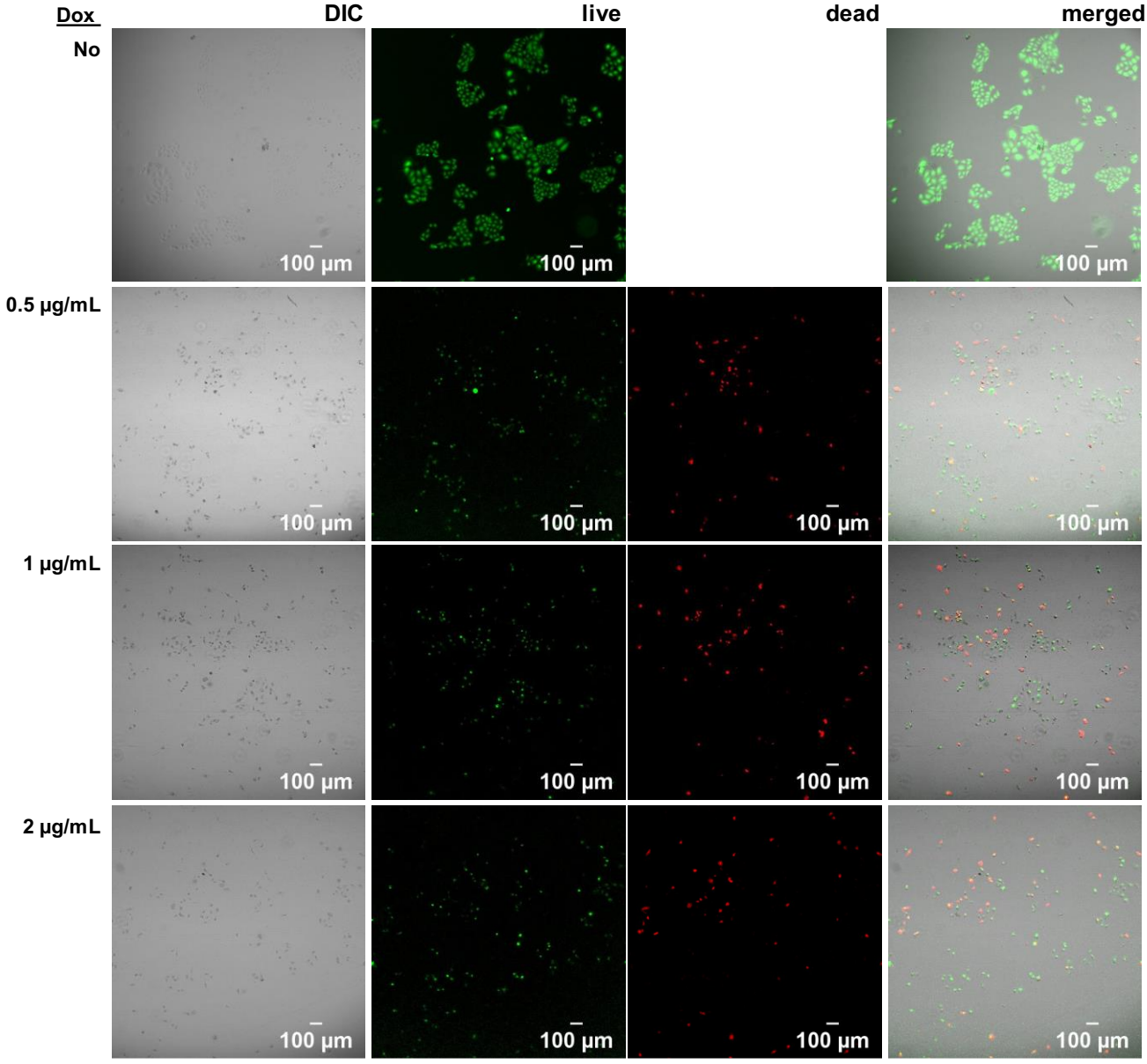

Appendix D

Supporting information and figures for chapter 6

Figure D1. ^{13}C-NMR spectrum of A1 in $CDCl_3$.

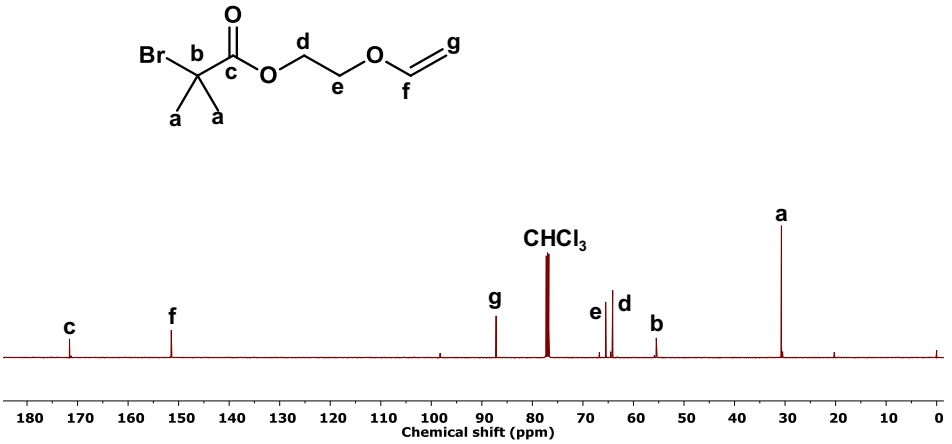

Figure D2. ^{13}C-NMR spectrum of A2 in $CDCl_3$. Note that x denotes impurities including acetone.

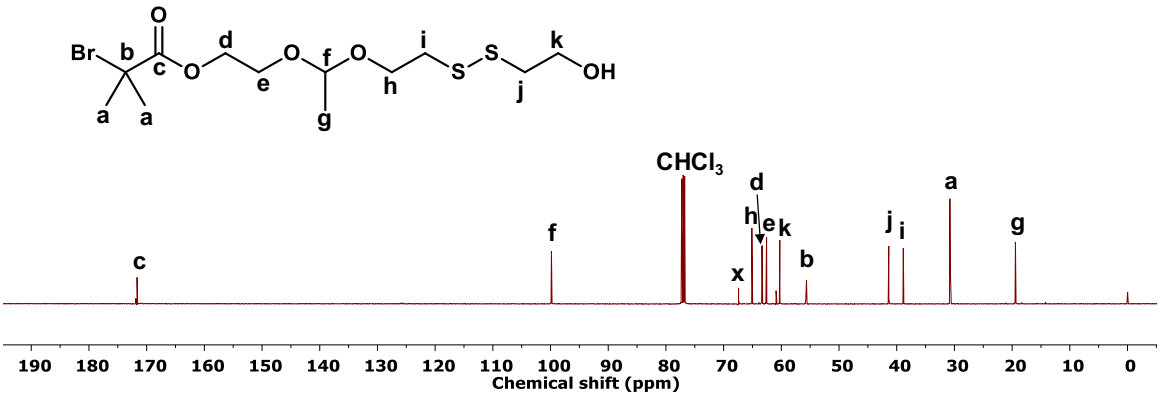

Figure D3. COSY NMR spectrum of A2 in $CDCl_3$.

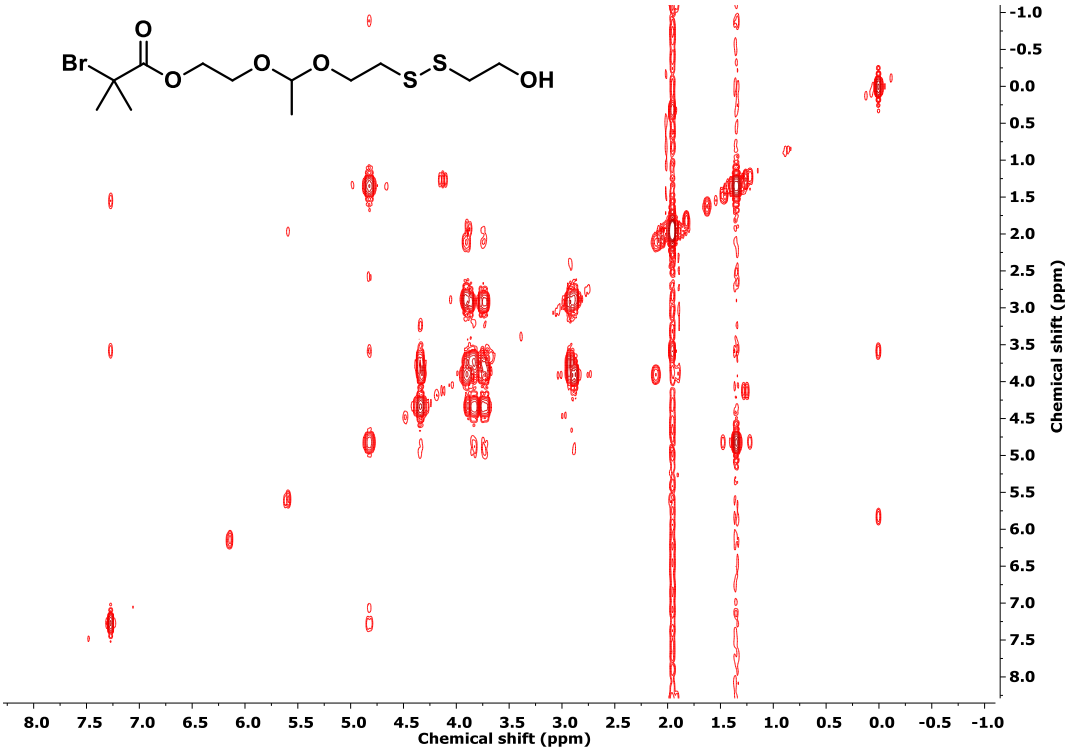

Figure D4. Evolution of GPC traces over conversion for ATRP of OEOMA in the presence of A2 initiator, with various initial mole ratios of $[OEOMA]_o/[A2]_o$ = 20/1 (a), 50/1 (b), and 100/1 (c). Conditions for ATRP: $[A2]_o/[Cu(II)Br_2]_o/[TPMA]_o/[Sn(II)EH_2]_o$ = 1/0.05/0.15/0.4 in anisole at 40 °C, OEOMA/anisole = 0.23 wt/wt.

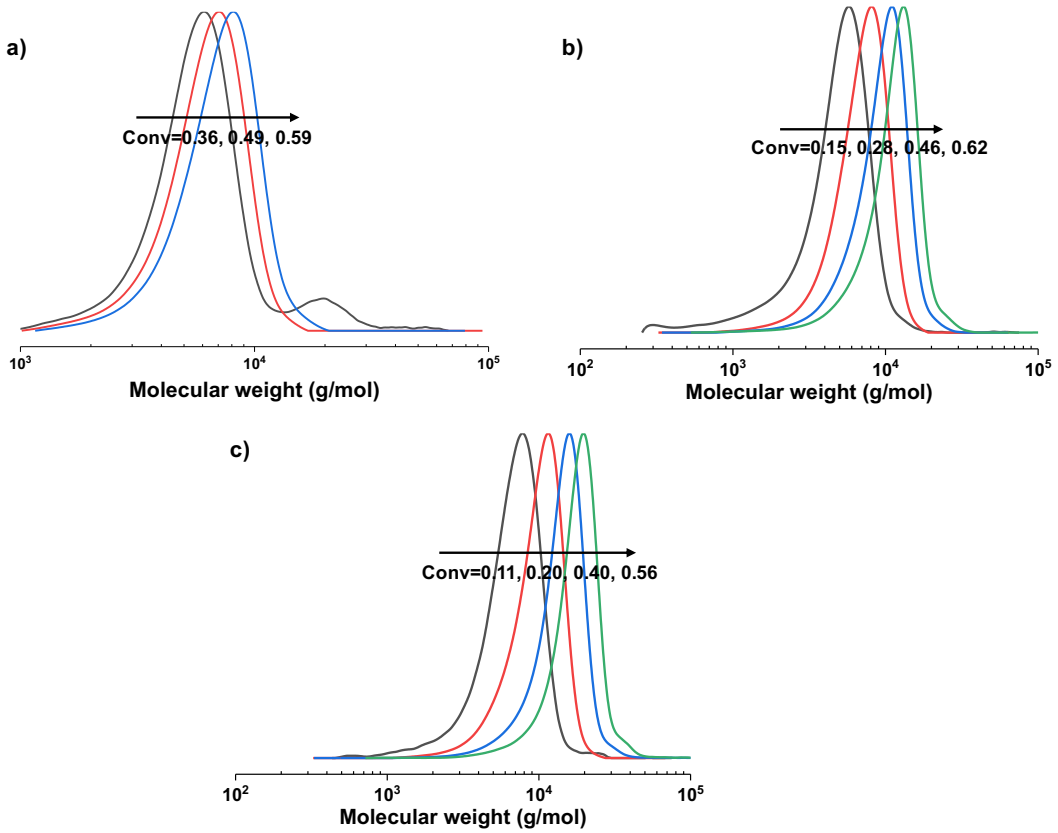

Figure D5. GPC trace of P3, compared with P1-20 precursor.

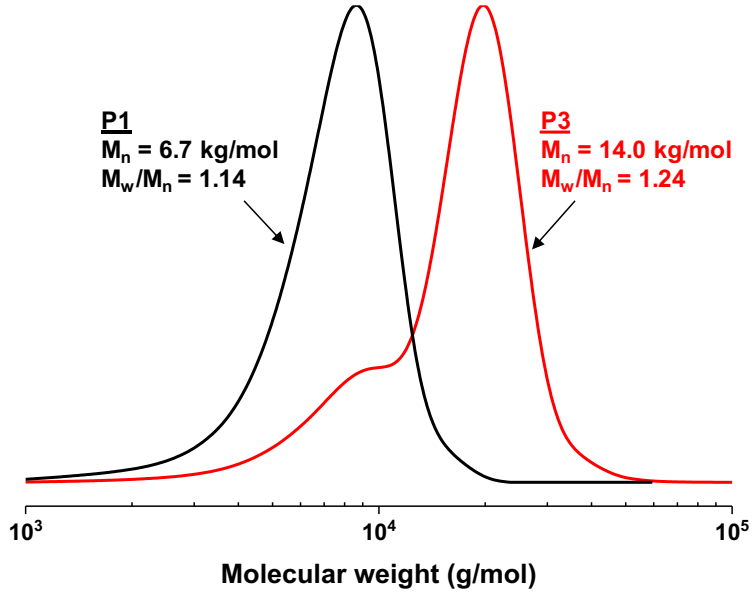

Figure D6. ^{1}H-NMR spectrum of P4 in $CDCl_3$. Note that x denotes impurities including water and acetone.

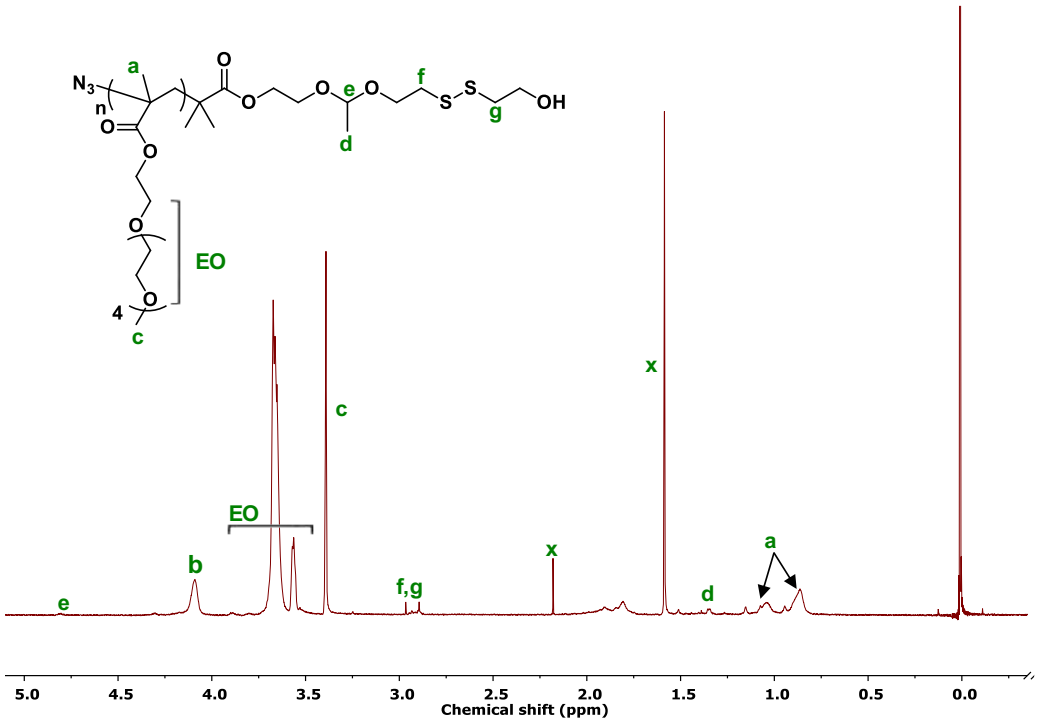

Figure D7. GPC traces of P6, compared with P1-20 and P4 homopolymers.

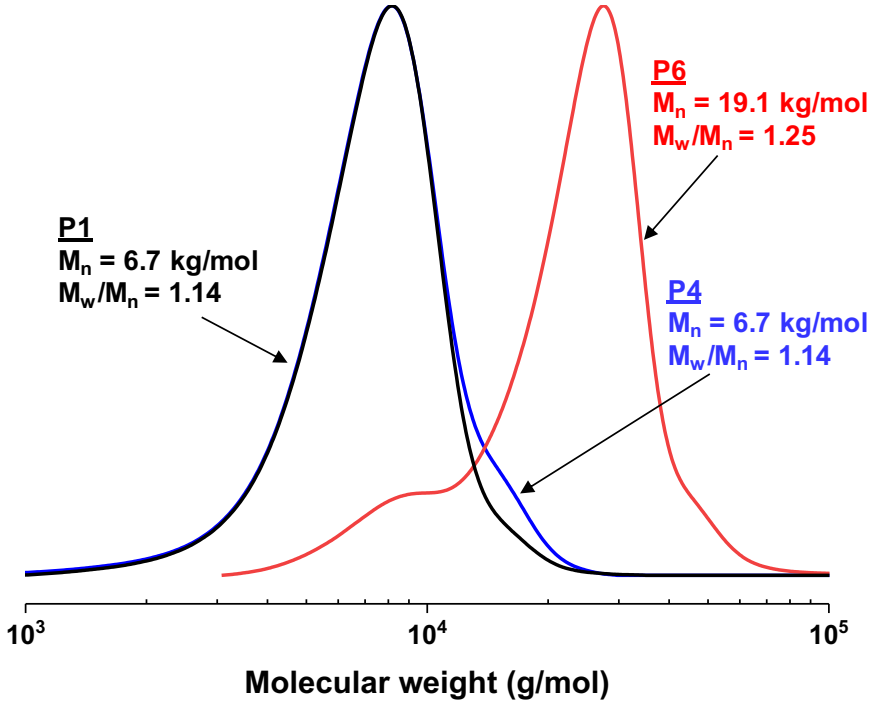

Figure D8. ^{1}H-NMR spectra of P5 (a), and P6 (b) in $CDCl_3$. Note that x denotes impurities including water.

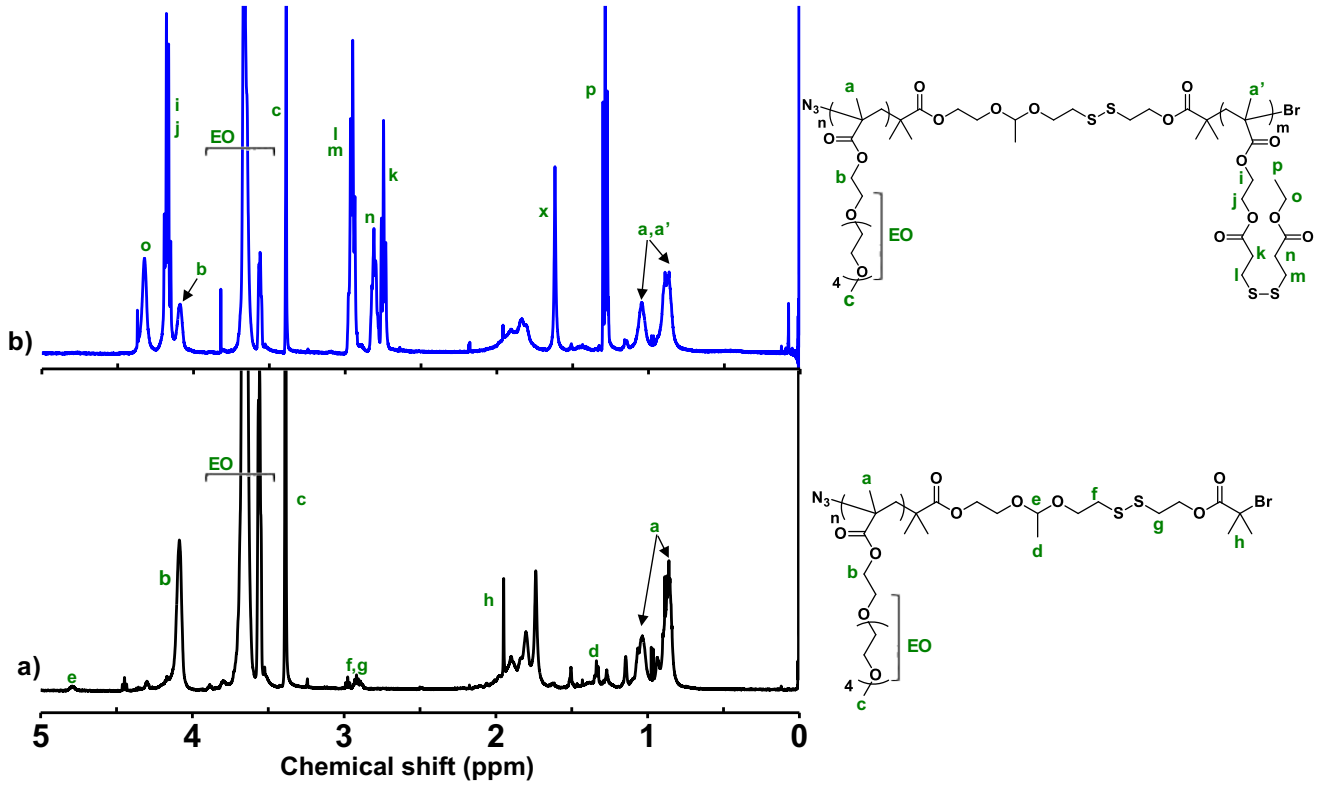

Figure D9. First-order kinetic plot over time (a), evolution of molecular weight and molecular weight distribution (b), and overlaid GPC traces over conversion (c) for ATRP of HMssEt in the presence of P5 macroinitiator. Conditions for ATRP: $[HMssEt]_o/[P5]_o/[Cu(II)Br_2]_o/[TPMA]_o/[Sn(II)EH_2]_o$ = 35/1/0.05/0.15/0.4 in anisole at 40 °C, HMssEt/anisole = 0.18 wt/wt.

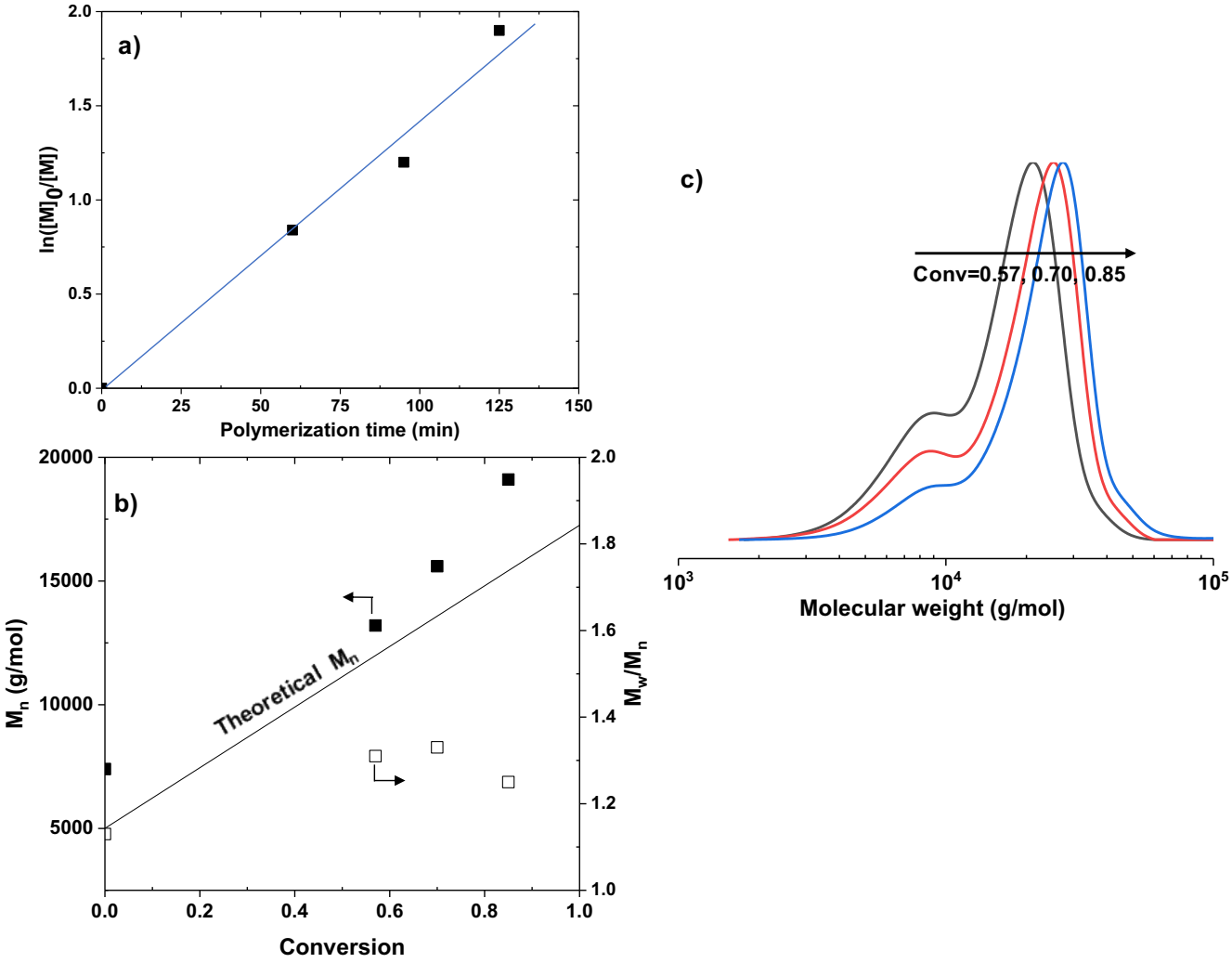

Figure D10. First-order kinetic plot over time (a), evolution of molecular weight and molecular weight distribution (b), and overlaid GPC traces over conversion (c) for RAFT polymerization of OEOMA in the presence of CPTP RAFT agent. Conditions: $[OEOMA]_o/[CPTP]_o/[AMBN]_o$ = 25/1/0.3 in anisole at 70 °C, OEOMA/anisole = 0.6 wt/wt.

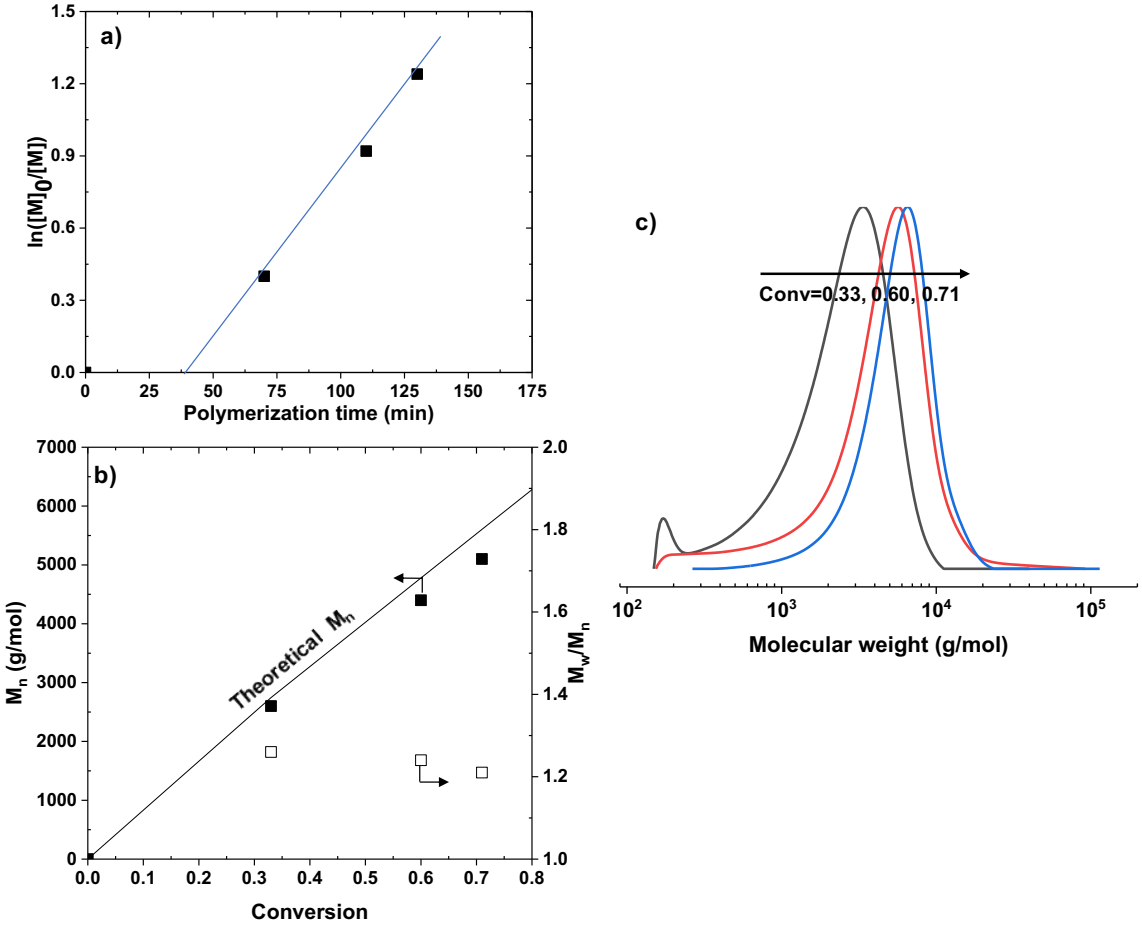

Figure D11. GPC traces of P9, compared with P7 precursor.

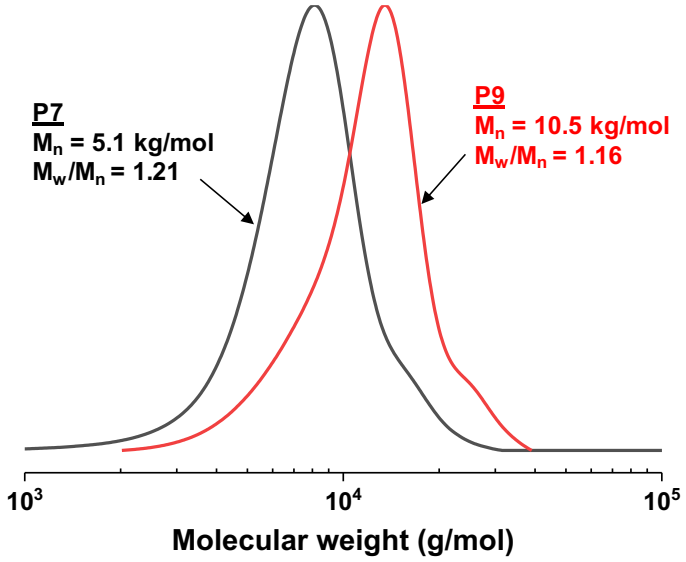

Figure D12. First-order kinetic plot over time (a), evolution of molecular weight and molecular weight distribution (b), and overlaid GPC traces over conversion (c) for ATRP of HMssEt in the presence of P8 macroinitiator. Conditions for ATRP: $[P8]_o/[Cu(II)Br_2]_o/[TPMA]_o/[Sn(II)EH_2]_o$ = 1/0.05/0.15/0.4 in anisole at 40 °C, HMssEt/anisole = 0.18 wt/wt.

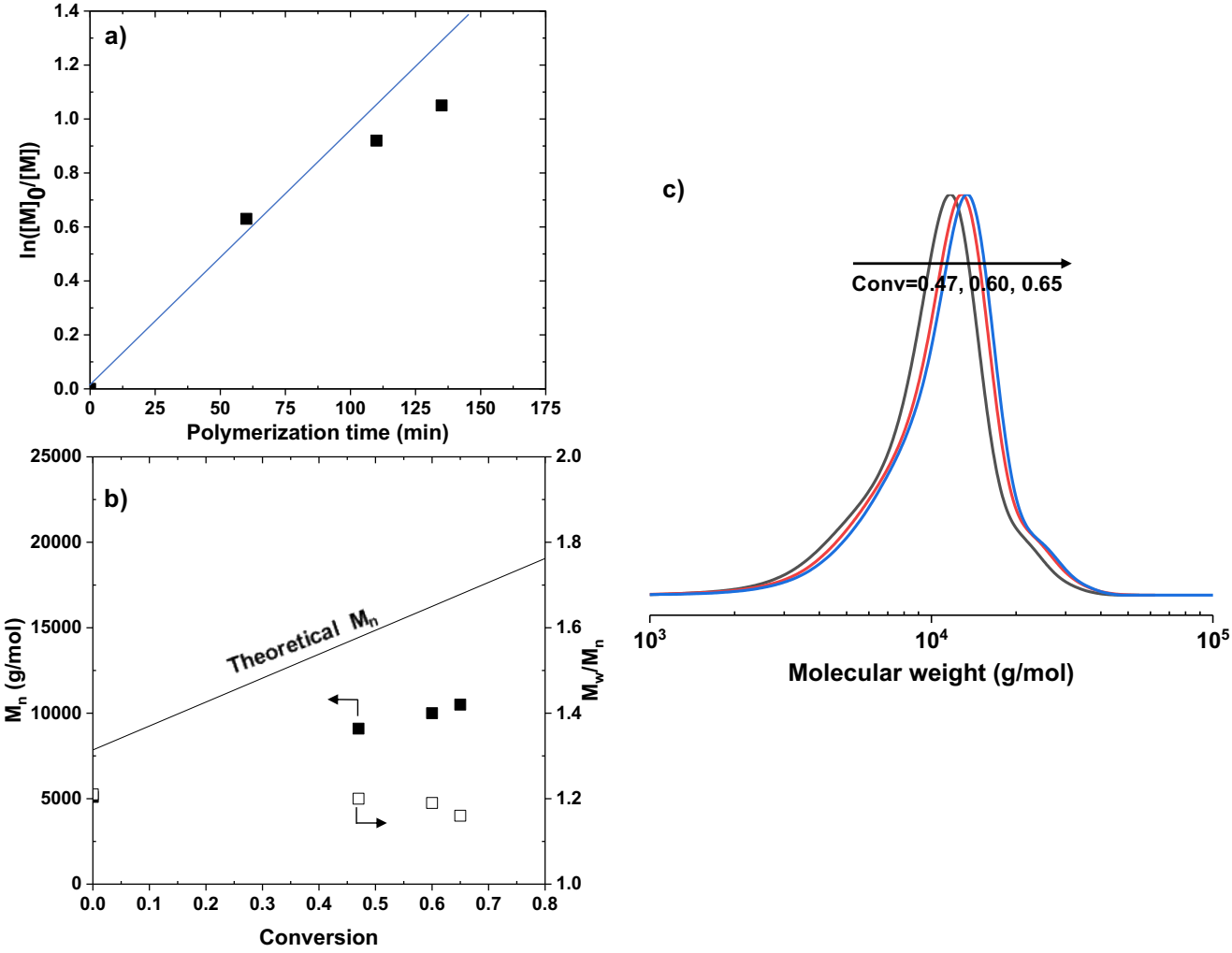

Figure D13. ^{1}H-NMR spectrum in $CDCl_3$ of the precipitate of the degraded solution of P3 after treatment with acid.

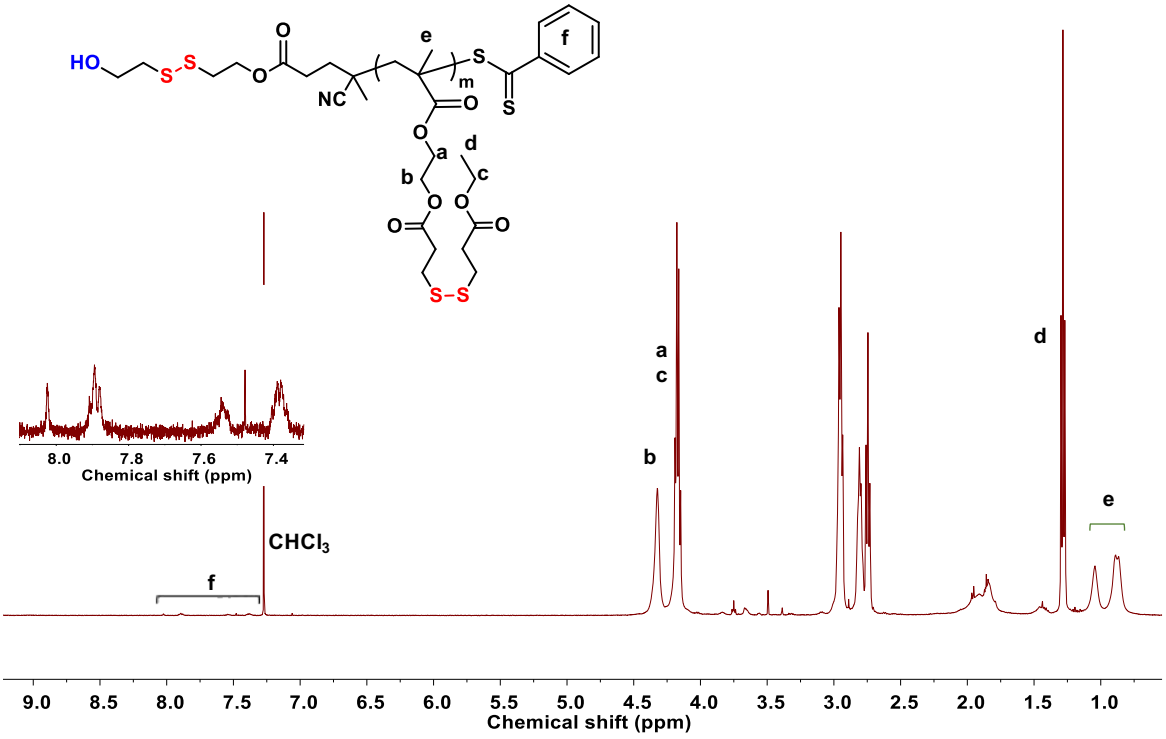

Figure D14. GPC trace of precipitates, compared with degraded products of P3 after treatment with acid and P1 homopolymer.

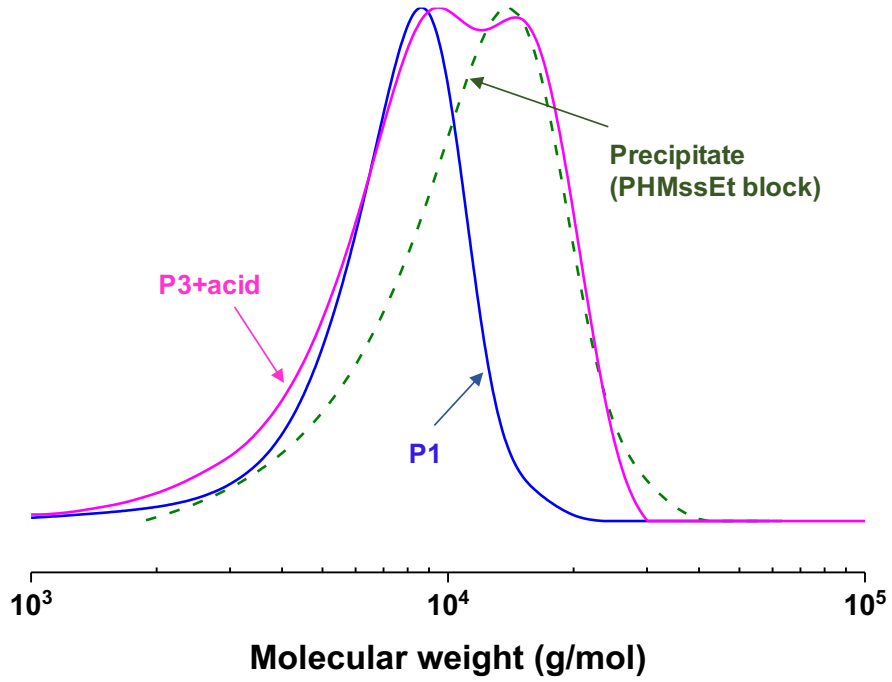

Figure D15. ^{1}H-NMR spectrum of the mixture of P3 with DCl in DMSO-d_6.

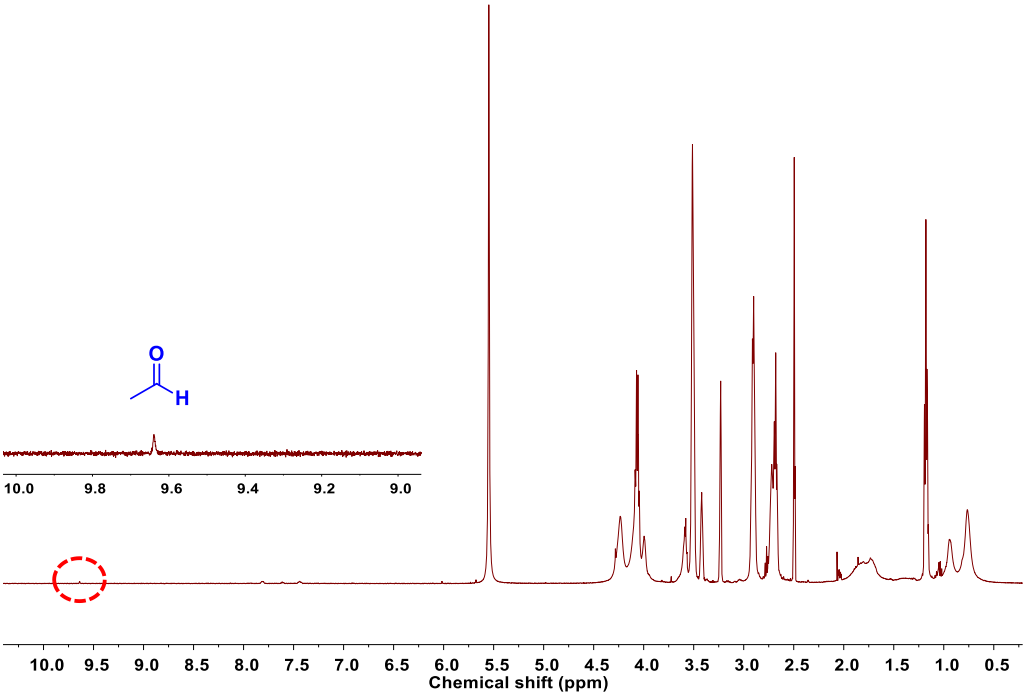

Figure D16. GPC traces of P6 before and after treatment with acid, compared with P1 (POEOMA homopolymer).

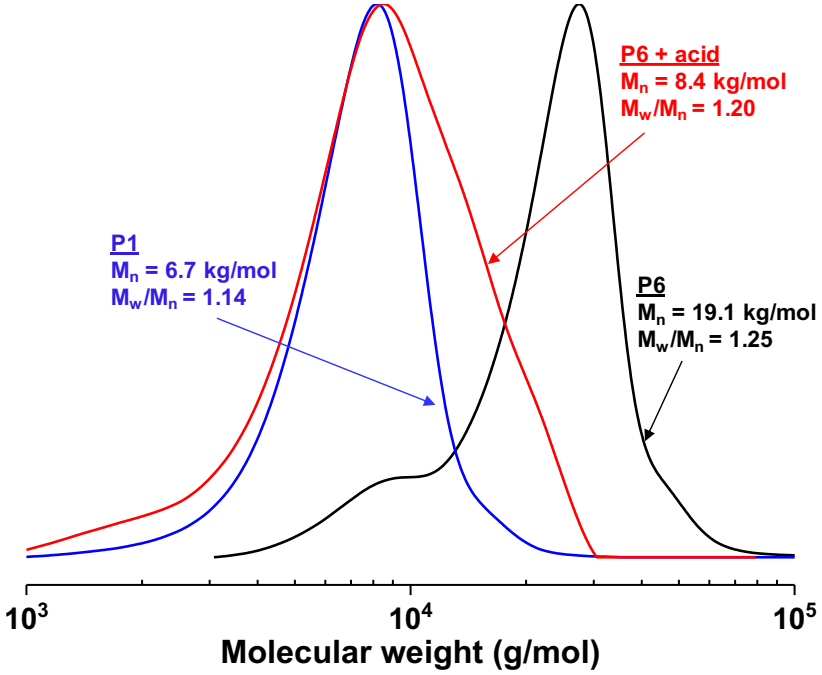

Publications

1. Xiaolei Hu, **Arman Moini Jazani,** and Jung Kwon Oh. Recent advances in development of imine-based acid-degradable polymeric nanoassemblies for intracellular drug delivery, ***Polymer,*** 2020, 230, 124024.

2. Arman Moini Jazani, Chaitra Shetty, Hourieh Movasat, Kamaljeet K. Bawa and Jung Kwon Oh. Imidazole-mediated dual location disassembly of acid-degradable intracellular drug delivery block copolymer nanoassemblies, ***Macromolecular Rapid Communications*****,** 2021, 2100262.

3. Ge Zhang, Twinkal Patel, Pothanagandhi Nellepalli, Shubham Bhagat, Hanees Hase, **Arman Moini Jazani,** Ingo Salzmann, Zhibin Ye and Jung Kwon Oh. Macromolecularly engineered thermoreversible heterogeneous self-healable networks encapsulating reactive multidentate block copolymer-stabilized carbon nanotubes, ***Macromolecular Rapid Communications*****,** 2021, 200514.

4. Yuhang Huang, **Arman Moini Jazani**, Elliot P. Howell, Lisa Reynolds, Jung Kwon Oh and Matthew G. Moffitt. Microfluidic shear processing control of biological reduction stimuli-responsive polymer nanoparticles for drug delivery, ***ACS Biomaterials Science & Engineering*****,** 2020, 6, 9, 5069-5083.

5. Arman Moini Jazani and Jung Kwon Oh. Development and disassembly of single and multiple acid-cleavable block copolymer nanoassemblies for drug delivery, ***Polymer Chemistry*****,** 2020, 11, 2934-2954.

6. Kamaljeet K. Bawa, **Arman Moini Jazani**, Zhibin Ye, Jung Kwon Oh. Synthesis of degradable PLA-based diblock copolymers with dual acid/reduction-cleavable junction, ***Polymer*****,** 2020, 194, 122391.

7. Keaton Maruya-Li, Chaitra Shetty, **Arman Moini Jazani**, Newsha Arezi, Jung Kwon Oh. Dual reduction/acid-responsive disassembly and thermoresponsive tunability of degradable double hydrophilic block copolymer*, **ACS Omega*****,** 2020, 5, 3734–3742.

8. Yuhang Huang, **Arman Moini Jazani**, Elliot P. Howell, Jung Kwon Oh, Matthew G. Moffitt. Controlled microfluidic synthesis of biological stimuli-responsive polymer nanoparticles. ***ACS Applied Materials and Interface*****,** 2020, 12, 1, 177-190.

9. Arman Moini Jazani, Newsha Arezi, Chaitra Shetty, Sunghwa Hong, Haowen Li, Xiangtao Wang, Jung Kwon Oh. Tumor-targeting intracellular drug delivery based on dual acid/reduction-degradable nanoassemblies with ketal interface and disulfide core locations. ***Polymer Chemistry*****,** 2019, 10, 2840-2853.

10. Kamaljeet K. Bawa, **Arman Moini Jazani**, Chaitra Shetty and Jung Kwon Oh. PLA-based triblock copolymer micelles exhibiting dual acidic pH/reduction responses at dual core and core/corona interface location. ***Macromolecular Rapid Communications*****,** 2018, 39, 1800477.

11. Arman Moini Jazani, Newsha Arezi, Keaton Maruya-Li, Sungmin Jung, Jung Kwon Oh. Facile strategies to synthesize dual location dual acidic pH/ reduction-responsive degradable block copolymers bearing acetal/disulfide block junctions and disulfide pendants. ***ACS Omega*****,** 2018, 3, 8980- 8991.

12. Arman Moini Jazani and Jung Kwon Oh. Dual location, dual acidic pH/reduction-responsive degradable block copolymer: synthesis and investigation of ketal linkage instability under ATRP conditions. ***Macromolecules*****,** 2017, 50, 9427-9436.

Oral and Poster Presentations

1. Arman Moini Jazani. Development and disassembly of dual location acid-degradable intracellular rug delivery block copolymer nanoassemblies. Macromolecular Science and Engineering Division (MSED) of Canadian Society of Chemistry (CSC), February 25th, 2021. **(Invited talk)**

2. Arman Moini Jazani and Jung Kwon Oh. Dual acidic pH- and glutathione-responsive degradable polymeric micelles for anti-cancer drug delivery. Worlds Biomaterial Congress (WBC, Online), Glasgow, Scotland, December 11-15th 2020. **(oral)**

3. Arman Moini Jazani and Jung Kwon Oh. Synthesis of PEG-disulfide-PLA block copolymers. Advance polymeric materials. Montreal, QC, Canada, July 3rd, 2019. **(oral for industry)**

4. Yuhang Huang, **Arman Moini Jazani**, Jung Kwon Oh, Mathew Moffitt. Microfluidic control of structure and drug delivery properties of biological stimuli-responsive block copolymer nanoparticles. 102nd Canadian Chemistry Conference (CSC), Quebec City, QC, Canada, June 3-7th 2019. **(oral)**

5. Arman Moini Jazani and Jung Kwon Oh. Dual location acid-degradable polymeric micelles with self-accelerating hydrolysis properties. 102nd Canadian Chemistry Conference (CSC), Quebec, Canada, June 3-7th 2019. **(oral)**

6. Arman Moini Jazani and Jung Kwon Oh. Reactive copolymer-stabilized aluminum oxide nanoparticles: a proof-of-concept for development of robust self-healable heterogeneous crosslinked networks. Dural Inc. Montreal, QC, Canada, December 17th, 2018. **(oral for industry)**

7. Arman Moini Jazani and Jung Kwon Oh. Synthesis of well-defined, multi stimuli responsive degradable amphiphilic block copolymer via combining ATRP and RAFT polymerization: Toward dual reduction and acidic pH labile shell-sheddable micelles. 2nd Annual symposium of Quebec Center for Advanced Materials (QCAM-CQMF), Montreal, QC, Canada, May 3-4th, 2018. **(oral)**

8. Arman Moini Jazani and Jung Kwon Oh. DL-DSRD Platform of Block Copolymer Nanoassemblies for Tumor-targeting Intracellular Delivery. NorthernChem Inc. Niagara Falls, ON, Canada, March 13th, 2018. **(oral for industry)**

9. Arman Moini Jazani and Jung Kwon Oh. Smart nanomedicines with dual location dual stimuli-responsive polymeric nanoassemblies exhibiting location-specific degradation and enhanced drug release. 1st Annual symposium of Quebec Center for Advanced Materials (QCAM), Sherbrooke, QC, Canada, October 23-24th, 2017. **(oral)**

10. Arman Moini Jazani, Keaton Maryu-Li and Jung Kwon Oh. Exploration of a new strategy utilizing ATRP to synthesize dual location dual acidic pH/reduction-responsive degradable block

copolymer. 1st Annual symposium of Quebec Center for Advanced Materials (QCAM), Sherbrooke, QC, Canada, October 23-24th, 2017. **(poster)**

11. Arman Moini Jazani and Jung Kwon Oh. Dual location dual acidic pH/glutathione-responsive block copolymer strategy for precise control of drug release and cellular uptake. 100th Canadian Chemistry Conference (CSC), Toronto, Canada, May28-June 1st, 2017. **(poster)**

12. Arman Moini Jazani and Jung Kwon Oh. Dual reduction/acidic pH-responsive block copolymer micelles: synthesis, self-assembly and stimuli responsive enhanced release. Canadian Society for Pharmaceutical Science/Canadian Chapter of the Controlled Release Society (CSPS/CC-CRS) Conference, Montreal, Canada, May 10-12th, 2017. **(poster)**

13. Arman Moini Jazani and Jung Kwon Oh. Dual Iocation dual reduction/pH-responsive degradable block copolymer micelles for enhanced cellular uptake and drug-controlled release. 37th Canadian High Polymer Forum (CHPF), Gananoque, ON, Canada, August 9-11th, 2016. **(poster)**

14. Arman Moini Jazani and Jung Kwon Oh. Multi-location multiple stimuli-responsive degradation (ML-MSRD) of block copolymer-based micelles for rapid and controlled release. CSCAS/CQMF Advanced Materials Annual Meeting, Montreal, QC, Canada, May 3-4th, 2016. **(poster)**

Award and Honours

1. B3X postdoctoral research scholarship ($ 110,000), Fonds de Recherche du Québec (FRQNT), QC, Canada (2021-2023).

2. Concordia conference and exposition award ($ 920.2), Concordia University, QC, Canada (2021).

3. Concordia accelerator award ($ 5,000), Concordia University, QC, Canada (2021).

4. Concordia conference and exposition award ($ 981.44), Concordia University, QC, Canada (2019).

5. Oral presentation award in Macromolecular Science and Engineering Division (MSED) ($ 300), Canadian Chemistry Conference and Exhibition (CSCE), QC, Canada (2019).

6. B2X doctoral research scholarship ($ 77,000), Fonds de Recherche du Québec (FRQNT), QC, Canada (2019-2023).

7. Alexander graham bell postgraduate scholarships-doctoral program ($ 105,000), Natural Science and Engineering Council of Canada (NSERC), QC, Canada (2019-2022).

8. Mitacs Globalink research award ($ 6,000), Mitacs Canada, Beijing, China (2018).

9. Faculty of arts and science graduate fellowship ($ 24,000), Concordia University, QC, Canada (2018-2021).

10. Outstanding poster award ($ 500), Canadian Society of Pharmaceutical Science (CSPS), QC, Canada (2017).

11. Outstanding poster award, Canadian High Polymer Forum (CHPF), ON, Canada (2016).

12. Triskelion fellowship in chemistry ($ 5,000), Concordia University, QC, Canada (2016-2017).

13. Concordia conference and exposition award ($ 626.88), Concordia University, QC, Canada (2016).

14. Trent international student scholarship ($1,000), Trent University, ON, Canada (2011).

15. Member of Dean's honour roll, Trent University, ON, Canada (2011-2012).